UC Riverside

UC Riverside Electronic Theses and Dissertations

Title

Understanding Vibrio cholerae Pathogenesis: Insights From Bile Acid Metabolism and Microbial Interactions

Permalink

https://escholarship.org/uc/item/8k90256f

Author

Ge, Siyi

Publication Date

2024

Peer reviewed|Thesis/dissertation

eScholarship.org Powered by the California Digital Library
University of California

UNIVERSITY OF CALIFORNIA
RIVERSIDE

Understanding *Vibrio cholerae* Pathogenesis: Insights From Bile Acid Metabolism and Microbial Interactions

A Dissertation submitted in partial satisfaction
of the requirements for the degree of

Doctor of Philosophy

in

Microbiology

by

Siyi Ge

September 2024

Dissertation Committee:
Dr. Ansel Hsiao, Chairperson
Dr. Patrick Degnan
Dr. James Borneman

Copyright by
Siyi Ge
2024

The Dissertation of Siyi Ge is approved:

_____

_____

_____

Committee Chairperson

University of California, Riverside

Acknowledgments

Since 2019, when I began my PhD journey at UCR, I often imagined what it would feel like to write this acknowledgment section five years later. Now that the moment is here, I can hardly believe it. I have so many thoughts and feelings, but they all boil down to one word: Thank you.

I remember the day when I first met with my PI Dr. Ansel Hsiao during the recruitment day, we had a delightful talk about the research, even though at that point I had no experience with bacteria. I was very lucky to find a lab I like and joined without much effort. Thank you so much for providing the research opportunities and your guidance. I wouldn't have made it without you, and I am trying to become a scientist like you.

I would like to express my deepest gratitude to my thesis committee members, Dr. Patrick Degnan and Dr. James Borneman, for your invaluable guidance and support throughout my PhD journey. Patrick, thank you especially for your help with the bioinformatics analysis and for creating the beautiful graphs for my VBH study. I look forward to learning those skills from you in the future.

I also want to extend my heartfelt thanks to all the lab members who have been part of my life during this time, previous and current. Special thanks to Katia and Leda– even though you could not accompany me for the entire PhD journey, I cherish the time we spent together inside and outside the lab. Your friendship has been a source of strength and joy for me. Many thanks to Yue (Laurie) Zhang, I am happy working with you. You are smart and talented, and you will be successful in science.

Special thanks to the mice that contributed to this research. A total of 353 suckling mice and 372 adult mice were recorded, though this may not include all individuals used.

I am grateful to many friends. Dr. Zi Gao, Dr. Wenxin Zhao, and Oxy, you are my best friends at UCR, and you have brightened my life immeasurably. Yannan, Jinli, Shiyang, Qiong, and Yufei, I still remember the day we had the international student orientation. I am thankful that over the past five years, we have been there for each other, sharing both sadness and happiness.

Special thanks to Zhou Shen. You have been a constant source of light in my life.

Lastly, I want to thank my family. My dear parents, thanks for introducing me to the idea of home. Thank you, my dear grandma, the most industrious and courageous woman in the world. Thank you, my dear twin sister, Dr. Siyuan Ge, my best friend since birth, and my brother-in-law, Dr. Ruikang Huang, for listening to my whining, sadness, and happiness. Thank you, my dear husband, Dr. Zhisheng Hu, for all the things you have done for me, for wiping away my tears, and for sharing countless laughs. Thank you Jiumi, you are the most handsome creature in the world. And thank you to my dearest, cutest cat, Enigma. I love you, and you know it.

The *vbh* phylogenetic analysis in Chapter 2 and gene comparison in Chapter 4 was conducted and analyzed by Dr. Patrick Degnan. The animal experiments related to Figure 3.1-1 in Chapter 3-1 were performed by Jennifer Cho and analyzed by Rui Liu. The LuxS expressing *E. coli* strains used in Chapter 3-1 and 3-2 were constructed by Jennifer Cho. The experiments and analysis related to Chapter 3-2 were performed and

analyzed by Siyi Ge, Jennfier Cho, and Katia Salgado. TagA related strains in Chapter 4 were provided by Zhu Lab, UPenn.

ABSTRACT OF THE DISSERTATION

Understanding *Vibrio cholerae* Pathogenesis: Insights From Bile Acid Metabolism and Microbial Interactions

by

Siyi Ge

Doctor of Philosophy, Graduate Program in Microbiology
University of California, Riverside, September 2024
Dr. Ansel Hsiao, Chairperson

Vibrio cholerae is a Gram-negative bacterium responsible for cholera, a highly contagious diarrheal disease posing a significant global public health threat, particularly in developing countries. To successfully colonize and cause disease in the host, *V. cholerae* must travel through the stomach's harsh conditions and withstand fluctuations in oxygen levels, pH, and encounter bile and antimicrobial peptides in the intestines. Bile acids, prominent components of bile, play pivotal roles in regulating *V. cholerae*'s virulence gene expression and influencing disease progression. Bacterial bile salt hydrolases (BSH) facilitate bile acid modification by cleaving amino acids from bile acid molecules, thereby altering the composition of bile acid pool.

In this study, we identified a novel Vibrio Bile Salt Hydrolase (VBH) capable of deconjugating taurodeoxycholic acid (TDCA) to deoxycholic acid (DCA) and converting taurochenodeoxycholic acid (TCDCA) to chenodeoxycholic acid (CDCA). Our findings demonstrate that VBH activity influences *V. cholerae* growth and colonization dynamics,

as well as interactions with other gut microbes such as *Blautia obeum* through bile acid processing. Additionally, we uncovered a novel regulatory pathway where autoinducer-2 (AI-2) modulates secondary bile acid metabolism in *Clostridium scindens*, highlighting bile acids' broader impact on gut commensals.

Furthermore, we explored how *V. cholerae*'s disease outcomes are shaped by interactions with gut commensals, their ability to degrade mucin, and induce mucin production. Lastly, we propose the application of single-cell RNA sequencing (scRANseq) techniques to deepen our understanding of host-microbe interactions involving *V. cholerae*. These insights promise to inform novel therapeutic strategies combating *V. cholerae* infections and other enteric diseases.

Table of Content

Chapter 1 Introduction **1**
Cholera and *Vibrio cholerae* 1
Quorum sensing 6
Quorum sensing regulation in the gut 12
Bile acids 16
Bile acid synthesis and circulation 17
Antimicrobial effects of BAs 21
Microbial effects on BAs 23
Bile acid variations between human and animal models 26
BAs effects on *V. cholerae* 33
Chapter 2 Dual-function bile salt hydrolase in *Vibrio cholerae* modulates virulence and fitness through host-specific bile acid metabolism **35**
Abstract 35
Introduction 36
Methods 39
Results 51
Discussion 73
Supplements 78
Chapter 3.1 AI-2 signals affect microbiome through modulating secondary bile acid synthesis **84**
Abstract 84
Introduction 85
Materials and Methods 87
Results 95
Discussion 109
Supplements 113
Chapter 3.2 Commensal dependent promotion of *Akkermansia muciniphila* via AI-2 ..... **114**
Introduction 114
Method 115

Result 118
Discussion 122
Chapter 4 Diverse infection outcomes in *V. cholerae* driven by virulence-regulated bifunctional protease TagA interacting with personalized microbiota 124
Abstract 124
Introduction 125
Methods 128
Result 130
Discussion 150
Chapter 5 A review on single-cell RNA sequencing in bacteria and possible applications on *V. cholerae* studies 153
Introduction 153
ScRNA-seq vs bulk-RNAseq 155
Challenges in scRNA-seq applications 156
Challenges in scRNA-seq application in prokaryotes 158
Existing ScRNA-seq applications on bacteria 159
Possible applications on *V. cholerae* and gut microbiota studies 181
Chapter 6 Conclusion and Future Directions 185
Conclusion 185
Future directions 188
References 191

List of Figures

Chapter 1 Introduction..... 1

Figure 1-1. Virulence gene regulation in *V. cholerae* and interactions between *V. cholerae* and gut microbiota. 11

Figure 1-2. The classic (neutral) and alternative (acidic) pathways of bile acid synthesis. 28

Figure 1-3. BAs synthesis and enterohepatic circulation. 30

Figure 1-4. Human and mice have different BAs compositions. 32

Figure 1-5. Conversion of primary bile acids to secondary bile acids in human and mouse. 32

Figure 1-6. Chemical structure and sources of some common bile acids. 33

Chapter 2 Dual-function bile salt hydrolase in *Vibrio cholerae* modulates virulence and fitness through host-specific bile acid metabolism 35

Figure 2-1 VBH is a predicted phylotype 6 BSH. 55

Figure 2-2. VBH is broadly conserved in *V. cholerae* but likely originated from HGT. 58

Figure 2-3. *vbh* expression has disadvantage effects on *V. cholerae in vitro* growth under 1mM TDCA. 60

Figure 2-4. *vbh* negative regulates *V. cholerae* colonization *in vivo*. 63

Figure 2-5. *aphA* negatively regulates *vbh* expression. 65

Figure 2-6. *aphA*-*vbh* regulation affects *V. cholerae* fitness in mice. 68

Figure 2-7. VBH converts a subset of bile acids into virulence activating forms. 72

Supplement. Figure 2-1. VBH confers resistance to penicillin V *in vitro* 78

Supplement. Figure 2-2. Phylogenetic and syntenic examination of *vbh* loci in *V. cholerae*. 80

Supplement. Figure 2-3. Effects of *vbh* expression on the growth of *V. cholerae* under 125 μM of bile acids at 9 hours incubation. 81

Supplement. Figure 2-4. Effects of addition of various 1 mM and 125 μM BAs on *V. cholerae* strains. 81

Supplement. Figure 2-5. DCA and TDCA induce *vbh* expression *in vitro*. 82

Supplement. Figure 2-6. Growth curve of *B. obeum* under 1mM of CA, DCA or DMSO. 82

Chapter 3.1 AI-2 signals affect microbiome through modulating secondary bile acid synthesis 84

Figure 3.1-1. Pathways and related genes that are regulated by AI-2 signals in the model community. 97

Figure 3.1-2. AI-2 signal detection from *luxS* expressing *E.coli* (BW30045) strains. . 98

Figure 3.1-3. Impact of *B. obeum luxS* on secondary bile acid synthesis in *Clostridium scindens*..... 103

Figure 3.1-4. Effects of *luxS* supernatants on *C. scindens*..... 104

Figure 3.1-5. Effects of 125 μM CA and DCA on *B. obeum* growth. 104

Figure 3.1-6. Effects of CA and DCA on *C. scindens* growth *in vitro*..... 105

Figure 3.1-7. LuxS affect *C. scindens* level and *bai* expressions in mice. 108

Figure 3.1-8. Working model of *B. obeum* AI-2, *C. scindens* and bile acids. 109

Chapter 3.2 Commensal dependent promotion of *Akkermansia muciniphila* via AI-2 114

Figure 3.2-1 Commensal expressed *luxS* modulate gut microbiome structure..... 120

Figure 3.2-2 *luxS* from *B. obeum* alone did not affect *A. muciniphila* levels in suckling mice model. 121

Chapter 4 Diverse infection outcomes in *V. cholerae* driven by virulence-regulated bifunctional protease TagA interacting with personalized microbiota 124

Figure 4-1. *V. cholerae* colonization levels in the small intestines of adult mice at day 4 post-infection..... 131

Figure 4-2. TagA mutants competed with WT in germ-free adult mice. 134

Figure 4-3. Mucin inducing activity of TagA is required for successful *V. cholerae* colonization in defined communities..... 137

Figure 4-5. Impact of TagA Mucinase and Secretagogue Activities on *V. cholerae* Colonization in CR and DS communities..... 140

Figure 4-6. Relative frequency of the strains based on 16S sequencing analysis of the feces and distal small intestines (SI) collected at day 3 post infection. 142

Figure 4-7. Principal coordinates analysis (PCoA) of microbiome 16S sequencing analysis..... 143

Figure 4-8. Relative abundance of *V. cholerae* (A and B), *Blautia obeum* (C), or *Streptococcus* (D) in germ free mice with CR or DS community. 144

Figure 4-9. Total bacterial load in feces or small intestines (SI) collected from germ free mice..... 145

Figure 4-10. *B. obeum* and *Streptococcus* spp. load in feces or small intestines (SI) collected from germ free mice. 146

Chapter 5 A review on single-cell RNA sequencing in bacteria and possible applications on *V. cholerae* studies 153

Figure 5-1. Challenges in scRNA-seq application in prokaryotes. 159

Figure 5-2. The workflow of MATQ-seq. 161

Figure 5-3. The workflow of PETRI-seq/MicroSPLiT. 164

Figure 5-4. The workflow of par-seqFISH. 168

Figure 5-5. The workflow of BacDrop. 172

Figure 5-6. The workflow of ProBac-seq. 175

Figure 5-7. The workflow of M3-seq. 179

Chapter 6 Conclusion and Future Directions 185

References 191

List of Tables

Chapter 2 Dual-function bile salt hydrolase in *Vibrio cholerae* modulates virulence and fitness through host-specific bile acid metabolism 35

Supplement. Table 2-1. List of strains and primers used in this study. 83

Chapter 3.1 AI-2 signals affect microbiome through modulating secondary bile acid synthesis 84

Table 3.1-1 List of bacterial strains in the model community. 96

Supplement table 3.1-1 Primers used in this study. 113

Chapter 3.2 Commensal dependent promotion of *Akkermancia muciniphila* via AI-2 114

Table 3.2-1 List of defined US healthy gut microbiome. 119

Chapter 4 Diverse infection outcomes in *V. cholerae* driven by virulence-regulated bifunctional protease TagA interacting with personalized microbiota 124

Table 4-1. List of bacterial strains in the model community. 131

Table 4-2. Presence of *dnaA, ctxA1/A2, tcpA* and *tagA* in *V. cholerae* strains..... 148

Chapter 5 A review on single-cell RNA sequencing in bacteria and possible applications on *V. cholerae* studies 153

Table 5-1. Comparisons of existing bacterial scRNA-seq methods. 180

List of Abbreviations and Acronyms

(*S*)-3-hydroxytridecan-4-one (*Vibrio cholerae* CAI-1)
(Z)-3-aminoundec-2-en-4-one (*Vibrio harveyi* CAI-1)
11β-hydroxysteroid dehydrogenase 1 (11β-HSD1)
12a-hydroxylase (CYP8B1)
12-epicholic acid (12-ECA)
14-3–oxosteroid−5b-reductase (AKR1D1)
24(S)-hydroxycholesterol (24HC)
25(R)-26-hydroxycholesterol (26HC, also known as 27-hydroxyl cholesterol)
25-Hydroxycholesterol (25HC)
27α -hydroxylase (CYP27A1)
2-amino-3-ketobutyric acid (AKB)
3,5-dimethylpyrazin-2-ol (DPO)
3α-hydroxysteroid dehydrogenase (3αHSD)
3α-hydroxysteroid dehydrogenase (AKR1C4)
3β-hydroxy-Δ5-C27 steroid dehydrogenase (HSD3B7)
4,5-dihydroxy-2,3-pentanedione (DPD)
4-hydroxy-5-methylfuran-3(2H)-one (MHF)
7-oxolithocholic acid (7-oxoLCA)
7-α hydroxylation by oxysterol 7-α hydroxylase (CYP7B1)
7α-hydroxylase (CYP7A1)
Activated methyl cycle (AMC)
Alpha-muricholic acid (α-MCA)
Amino acid (AA)
Apical sodium-dependent bile acid transporter (ASBT)
Autoinducer (AI)
Autoinducer-2 (AI-2)
Bacterial droplet-based single-cell RNA-seq (BacDrop)
Beta-muricholic acid (β-MCA)
Bile acid-CoA:amino acid N-acyl-transferase (BAAT)
Bile acid-inducible operon (*bai* operon)
Bile acids (BAs)
Bile salt hydrolases (BSH)
Blautia obeum (BO)
Case fatality ratio (CFR)
Chenodeoxycholic acid, 3α, 7α-dihydroxy-5β-cholan-24-oic acid (CDCA)
Chloride ions (Cl-)
Cholera resistant (CR)

Cholera toxin (CT)
Cholera toxin phage (CTXφ)
Cholera autoinducer-1 (CAI-1)
Cholic acid, 3α, 7α, 12α-trihydroxy-5β-cholan-24-oic acid (CA)
Colony-forming units (CFUs)
Competitive index (CI)
Cyclic adenosine monophosphate (cAMP)
Cytochrome P450 Family 46 Subfamily A Member 1 (24S-hydroxylase,CYP46A1)
Deoxycholic acid (DCA)
Diffusible signal factors (DSFs)
Dysbiotic (DS)
Endoplasmic reticulum (ER)
Enterohemorrhagic *E. coli* (EHEC)
Extracellular signal-regulated kinase (ERK)
Farnesoid X Receptor (FXR)
Fibronectin type III domain (FN3)
Fluorescence in situ hybridization (FISH)
Fluorescence-activated flow cytometry (FACS)
Gamma-muricholic acid (γ-MCA)
Genomic DNA (gDNA)
Germ-free (GF)
Glucagon-like peptide-1 (GLP-1)
Glycochenodeoxycholic Acid (GCDCA)
Glycocholic Acid (GCA)
Glycodeoxycholic acid (GDCA)
High cell density (HCD)
High-fat diet (HFD)
Homocysteine (HCY)
Hydroxysteroid dehydrogenase (HSDH)
Hyodeoxycholic acid (HDCA)
Inflammatory bowel disease (IBD)
Intestinal Bile Acid–Binding Protein (IBAB–P)
Intestinal epithelial cells (IEC)
Isocholic acid (iCA),
Jun N-terminal kinase (JNK)
Kyoto Encyclopedia of Genes and Genomes (KEGG)
Lithocholic acid (LCA)
Liver receptor homologue-1 (LRH-1)

Low cell density (LCD)
Lysogeny broth (LB)
Messenger RNA (mRNA)
Microbial split-pool ligation transcriptomics (microSPLiT)
Microliter (μL)
Micromolar (μM)
Mililiter (mL)
Mobile genetic element (MGE)
Molar (M)
Multiple annealing and dC-tailing-based quantitative single-cell RNA-seq (MATQ-seq)
Multiple rounds of annealing and looping-based amplification cycles (MALBAC)
Murideoxycholic acid (MDCA)
Musculoaponeurotic fibrosarcoma oncogene homolog G (MAFG)
N-3-oxododecanoyl homoserine lactone (3OC(12)-HSL)
National Center for Biotechnology Information (NCBI)
Omega-muricholic acid (ω-MCA)
Optical density (OD)
Oral cholera vaccines (OCVs)
Organic anion transporting polypeptides (OATPs)
Organic solute transporter α/β (OSTα/OSTβ)
Parallel sequential fluorescence in situ hybridization(par-seqFISH)
Per-ARNT-Sim (PAS)
Poly(A) polymerase I (PAP)
Polymerase chain reaction (PCR)
Probe-based bacterial sequencing (ProBac-seq)
Prokaryotic expression profiling by tagging RNA in situ and sequencing (PETRI-seq)
Quantitative Real-Time PCR (qPCR)
Quorum sensing (QS)
Reverse transcription (RT)
Ribosomal ribonucleic acid (rRNA)
S-adenosyl-L-homocysteine (SAH)
S-adenosyl-L-methionine (SAM)
Secreted protease of C1 esterase inhibitor (StcE)
Single-cell massively-parallel multiplexed microbial sequencing (M3-seq)
Single-cell RNA (ScRNAseq)
Single-molecule RNA fluorescence in situ hybridization (smFISH)
Sodium ions (Na+)
Sodium taurocholate co-transporting polypeptide (NTCP)

Solute carrier family 21A (SLC21A)
specific pathogen free (SPF)
S-ribosylhomocysteine (SRH)
Streptococcus (STR)
Takeda G protein-coupled receptor 5 (TGR5)
Tauro-alpha-muricholic Acid (Tα-MCA)
Tauro-beta-muricholic Acid (Tβ-MCA)
Taurochenodeoxycholic Acid (TCDCA)
Taurocholic Acid (TCA)
Taurodeoxycholic acid (TDCA)
Terminal deoxynucleotidyl transferase (TdT)
Toxin-coregulated pili (TCP)
ToxR-activated gene A (TagA)
Type VI Secretion System (T6SS)
Unique molecular identifiers (UMIs)
Ursodeoxycholic acid (UCA)
Ursodeoxycholic Acid (UDCA)
Vibrio bile acid hydrolase (VBH)
Vibrio cholerae (Vc)
Vibrio pathogenicity island (VPI-1)
β-Klotho complex (KLB)
Δ4-3-oxosteroid 5β-reductase (aldo-keto reductase 1D1, AKR1D1)

Chapter 1 Introduction

Cholera and *Vibrio cholerae*

Vibrio cholerae, a Gram-negative bacterium, stands as the etiological agent of cholera, a severe watery diarrheal disease that continues to pose a global public health challenge. *V. cholerae* naturally resides in aquatic environment and found in zebra fish, plankton and shellfish[1]. Cholera is more common in areas with inadequate sanitation and hygiene practices. As of March 20, 2023, at least 24 countries globally reported ongoing cholera cases[2], underscoring the persistent threat it poses to populations worldwide. Worryingly, the average case fatality ratio (CFR) exhibits a upward trajectory, signaling the pressing need for a deeper understanding of this pathogen, the factors contributing to its resurgence and finding effective strategies for control and prevention.

Since 1817, there have been seven cholera pandemics, with the current seventh pandemic commencing in 1961. Over 200 serogroups have been identified in *V. cholerae* based on their polysaccharide O antigens[3], predominantly represented by nonpathogenic environmental strains, while all pandemic strains have arisen from either serogroup O1 or serogroup O139 variants. Serogroup O1 is further classified into two biotypes: the "Classical" biotype, initially identified as the causative agent of cholera, and the "El Tor" biotype, named after the Egyptian quarantine station, where it was first isolated around

1900[4]. The initial six cholera pandemics were attributed to the Classical biotype of *V. cholerae*, while the ongoing seventh pandemic is attributed to the El Tor biotype[5].

Symptoms and treatments

Cholera-induced diarrhea is distinguishable from other forms due to its pronounced and rapid loss of water and electrolytes, resulting in a characteristic "rice water" stool containing *V. cholerae* cells, mucus, bile, and gastrointestinal tissues. Additional manifestations include vomiting, muscle cramps, dehydration signs. In severe cases, cholera may progress to kidney failure, coma, potentially culminating in death if not promptly treated[6]. Notably, individuals with mild or asymptomatic infections can still excrete the bacteria in their stool, contributing to disease transmission.

Treatment of cholera primarily involved rehydration and administration of antibiotics. In mild to moderate cases, oral rehydration solutions are usually effective for restoring hydration, while in cases of severe dehydration, intravenous rehydration typically required[7]. Antibiotic treatment is recommended for severe patients in conjunction with hydration. Commonly used antibiotics include tetracycline, doxycycline, erythromycin, norfloxacin, azithromycin and ciprofloxacin. However, antibiotic resistance among *V. cholerae* has emerged in endemic and epidemic situations[8]. This resistance can result from accumulated mutation and exchanges of genetic materials. Inappropriate antibiotic usage can significantly contribute to the swift development of antibiotic resistance. Furthermore, there is a lack of sufficient evidence demonstrating the efficacy of

antibiotics in preventing secondary infections and their effectiveness when administered without concurrent rehydration treatment[9]. There are three WHO pre-qualified killed whole-cell Oral Cholera Vaccines (OCVs) (Dukoral, Shanchol, Euvichol/Euvichol-Plus) and one live attenuated vaccine (Vaxchora) recently approved by the European Medicines Agency for use in adults and children older than six[10]. Despite the availability of vaccines and some preventive measures, cholera continues to pose a significant health burden, underscoring the importance of developing better preventive strategies and alternative treatments for this disease.

V. cholerae pathogenesis and virulence factors

V. cholerae naturally inhabit in warm aquatic environments, such as brackish rivers, estuaries, ponds and coastal waters and is commonly found associated with phytoplankton, zooplankton and other additional environmental hosts. *V. cholerae* usually enter human host via contaminated food or water, and the infectious dose in humans can be as low as 10^3 colony forming unit (CFU) [11]. As *V. cholerae* enter the host, they are exposed to environmental changes, such as low pH, temperature, unbalanced osmolarity, low oxygen level, bile stresses. *V. cholerae* have evolved regulatory mechanisms to adapt to these stresses, permitting the successful colonization in the host. Once *V. cholerae* that have survived the initial challenges reach the small intestines, they employ a single polar flagellum to facilitate their movement and penetrate the protective mucus layer by utilizing mucin-degrading proteins. During this step, a specific set of virulence genes becomes activated. Among these genes, Cholera toxin (CT) and toxin-coregulated pili

(TCP) stand out as the two primary virulence determinants. CT is encoded by *ctxAB* genes on the lysogenic Cholera toxin phage (CTXϕ) bacterial phage and is consist of one A subunit surrounded by five identical noncovalently associated B subunits. The A subunit, which is 28 KDa, is located centrally, while the five B subunits each weighing 11 KDa, are located around A subunit forming the holotoxin. The A subunit itself does not have biological activity because it cannot cross the host cell membrane without B subunits[12]. The A subunit consists of two domains, A1 (21.8 KDa) and A2 (5.4 KDa), linked by a disulfide bridge. The A2 domain connects A subunit to B subunits by a single disulfide bridge. The B subunits bind to the high affinity monosialoganglioside GM1 receptors, initiating the toxin action of CT[13] . After entering the host cell via endocytosis and traveling to the endoplasmic reticulum (ER), the A subunit of CT is separated from the B subunits. Subsequently, it relocates from the ER to the cytoplasm, where it activates adenylate cyclase. This activation leads to a significant rise in intracellular cyclic adenosine monophosphate (cAMP) levels. The most consequential outcome of this process is the stimulation of ion transport mechanisms within the intestinal epithelial cells. This stimulation results in an increased secretion of chloride ions (Cl-) into the intestinal lumen and a simultaneous reduction in the absorption of sodium ions (Na+). This imbalance ultimately leads to the prolific secretion of water and electrolytes into the lumen, resulting in the manifestation of profuse diarrhea[14,15].

TCP are Type IV pili that is indispensable in the successful colonization of *V. cholerae* in the small intestines[16–18]. TCP facilitate microcolony formation to protect *V. cholerae* from

host defenses and concentrate CT[16]. TCP also serve as receptors for the CTXϕ bacterial phage and confer virulence to non-pathogenic *V. cholerae* by providing the CT encoding genes[19]. TCP also secret the colonization factor TcpF[20] and mediates attachment to the host cells[21]. The *tcp* operon is located on *Vibrio* pathogenicity island (VPI-1) and contains 12 genes[16], with the first gene *tcpA* encodes the 20 KDa subunit TcpA of TCP, ten genes encode components involved in biogenesis of TCP, and one gene *tcpF* encodes a protein that is required for colonization in infant mice[20].

ToxT, a protein belong to the AraC/XylS-family[22], is the primary transcription regulator of many *V. cholerae* virulence genes, including *ctxAB* and *tcpA* and other genes within the VPI-1. ToxR can affect a set of virulence gene (ToxR regulon) expressions directly. ToxR can directly bind to the promoter and regulate gene expressions, including *ctxAB*, *toxT*, and two genes coding outer membrane porin proteins OmpT and OmpU[23,24]. Another inner membrane protein ToxS is required for ToxR transcriptional activity[25]. The activation of *toxT* required two outer membrane proteins, TcpP and TcpH, in conjunction with ToxR and ToxS. TcpP binds to the central position (-51 to -40) of *toxT* promoter when ToxR is present[26]. The membrane-localized periplasmic effector protein ,TcpH, protects TcpP from degradation by proteases[27,28]. The periplasmic cysteines of TcpP are required for functional interaction with TcpH to stabilize TcpP and TcpH[29]. AphA is a protein with a N-terminal end resemble the helix-turn-helix domain of MarR[30], a multiple antibiotic resistance repressor. AphA binds to the -101 to -71 region relative to the transcriptional start site of *tcpPH* and activate the gene expression[31]. This activation

process crucially depends on the presence of AphB, a regulator belonging to the LysR-type family. Notably, AphB appears to play a central role as the primary activator, as an increased concentration of AphB can compensate for the absence of AphA, but the reverse is not true[32]. Moreover, AphA enhances the binding capacity of AphB to its recognition sites, which are located just 8 bp away from the AphA recognition site[30]. AphB can enhance ToxR transcription[33]. Besides *tcpPH*, AphA also regulates quorum sensing related genes and a gene coding a bile salt hydrolase.

Quorum sensing

Quorum sensing (QS) is a process of cell-to-cell communication that bacteria utilize to orchestrate group behaviors based on population density. Autoinducers (AIs) are extracellular signaling molecules in the QS system that bacteria produce, release and can detect population-wide[34,35]. Upon reaching a critical concentration, these AIs initiate a synchronized response within the bacterial community. These responses include various behaviors such as bioluminescence, production of virulence factors, DNA exchange, and biofilm formation[35–38].

AIs in bacteria

QS can be found in both Gram-positive and Gram-negative bacteria. In gram-positive bacteria, QS usually uses secreted oligopeptides and two-component systems. While in gram-negative bacteria, AIs are synthesized from *S*-adenosylmethionine (SAM)[35]. Acyl-

homoserine lactones (AHLs) are among the most well-studied and common AIs. AHLs can diffuse freely through bacteria membrane, bound by specific receptors in the inner membrane or cytoplasm in the bacteria, and modulate dozens to hundreds of genes that paly roles in the bacterial biological processes[35]. Moreover, AI-induced QS can activate increased autoinducer synthesis, establishing a feed-forward loop proposed to synchronize gene expression within the bacterial population[35]. Small noncoding RNA (sRNA), which are present across a wide range of bacterial species, are often integrated in this feed-forward loop during QS[39].

QS in *Vibrio* spp.

V. harveyi, a model bacterium for studying QS, was the first discovered bacteria to use several autoinducers. *V. harveyi* uses three AIs: AI-1 (3OHC4-homoserine lactone (HSL)), AI-2 ((2S,4S)-2-methyl2,3,3,4-tetrahydroxytetrahydrofuran-borate), and CAI-1 ((Z)-3-aminoundec-2-en-4-one) produced from LuxM, LuxS, and CqsA enzymes, respectively[34,40,41].

V. cholerae has similar QS systems to *V. harveyi*. At high cell density, *V. cholerae* repress virulence genes and biofilm formation through quorum sensing and genes required for host to adapt to environment transitions, such as adhesin related genes, are upregulated. There are three identified QS systems in *V. cholerae*, AI-2, CAI-1 ((*S*)-3-hydroxytridecan-4-one), and DPO (3,5-dimethyl-pyrazin-2-ol), produced from LuxS, CqsA, and Tdh enzymes, respectively[37,42–44]. These autoinducers are detected by the

membrane-bound receptors LuxPQ, CqsS, and the cytoplasmic receptor VqmA, respectively. CAI-1 produced by *V. cholerae* is slightly different from CAI-1 produced by *V. harveyi*.

A**t low cell density (LCD)**, where autoinducers are scarce, the receptors work as kinases and transfer phosphate to LuxU. LuxO is activated via LuxU by phosphorylation and with σ^{54}, four sRNA (Qrr1-4) are produced. These sRNAs with Hfq then activate AphA and repress HapR. Virulence genes and biofilm genes are turned on. *V. cholerare* cells act as individuals. **At high cell density (HCD)**, AI-2 and CAI-1 bind to the receptors and the phosphor-flow reverses. AphA is deactivated and HapR is derepressed. Virulence genes and biofilm genes are turned off. DPO, independent from LuxO pathway, binds to VqmA, activates sRNA VqmR transcription, and subsequently turns off virulence and biofilm genes. Both Apo-VqmA and DPO-bounded VqmA (holo-VqmA) can activate the transcription of VqmR which posttranscriptionally affect gene expressions[44–46].

DPO-VqmA QS pathway in *V. cholerae*

AI-1, AI-2 and CAI-1 are the most well-studied QS systems in *Vibrio*s. With respect to *Vibrio* spp., AI-1 and CAI-1 are thought to work intra-species, while AI-2 is considered inter-species. DPO is primarily considered as an inter-species signgaling molecule, but it also plays a role in intra-species signaling within *Vibrio*s[47]. However, increasing evidence suggests the presence of novel AIs and QS pathways in *Vibrio*s. Liu et al. [45] identified a transcriptional regulator, VqmA that activates HapR expression at LCD by binding to its

promoter region, and this regulation is cell density dependent and bypass the known LuxO-Qrr sRNA regulatory circuits. Papenfort et al.[46] conducted RNA-seq analysis on WT and LCD-locked *V. cholerae* cultures, and identified a regulatory RNA, VqmR, encoded by a gene called *vqmR*, locating at the upstream of *vqmA*. VqmR directly regulates several messenger RNA (mRNA) posttranscriptional, including *rtx*, a major *V. cholerae* toxin, and *vpsT*, a transcriptional regulator that regulates biofilm formation. Tn5 random mutagenization identified a Threonine dehydrogenase (Tdh) that synthesizes a VqmA-activarting AI in *V. cholerae*. Tdh catalyzes L-theronine to 2-amino-3-ketobutyric acid (AKB), which is followed by several steps and finally produces the DPO. Tdh is ubiquitous in bacteria, archae and eukarya[48], and it is highly conserved as Tdh from *E.coli* is also capable of inducing *vqmR* expression[46].

Blautia obeum has been identified as a key contributor to conferring resistance against *V. cholerae* infection in a VqmA-dependent manner[49], potentially through the production of DPO in the small intestines. Furthermore, AI-2 derived from *B. obeum* has demonstrated the ability to suppress *tcpA* expression in *V. cholerae,* bypassing the LuxPQ signaling pathway and acting instead through VqmA[49]. This suggests that, in addition to DPO, other AIs may also play a role in the regulation of *V. cholerae* through the VqmA-VqmR QS pathway. Further investigations are needed to elucidate the comprehensive regulatory pathway involving foreign AI-2 and the VqmA regulatory system.

The crystallographic analysis of the DPO-VqmA quorum sensing pathway in *V. cholerae* revealed that, unlike typical LuxR-type receptors, which bind AHLs and require interaction with LuxI-type autoinducer synthases to activate transcription, the absence of DPO does not halt the VqmA-dependent activation of vqmR. Instead, DPO binding is essential for achieving maximum activation of VqmA[50].

In contrast to Tdh, VqmA is restricted to *Vibrio*s and a vibriophage VP882[51]. VqmA protein has a conversed PAS (Per-ARNT-Sim)-domain[52] at the N-terminus and a DNA-binding domain at the C-terminus. VqmA can bind both the cyclic DPO and the linear Ala-Amino acid (AA) molecules, which is the putative precursor of DPO, the binding pocket of which is located in the same N-terminal PAS domain in VqmA, however DPO is preferred[50].

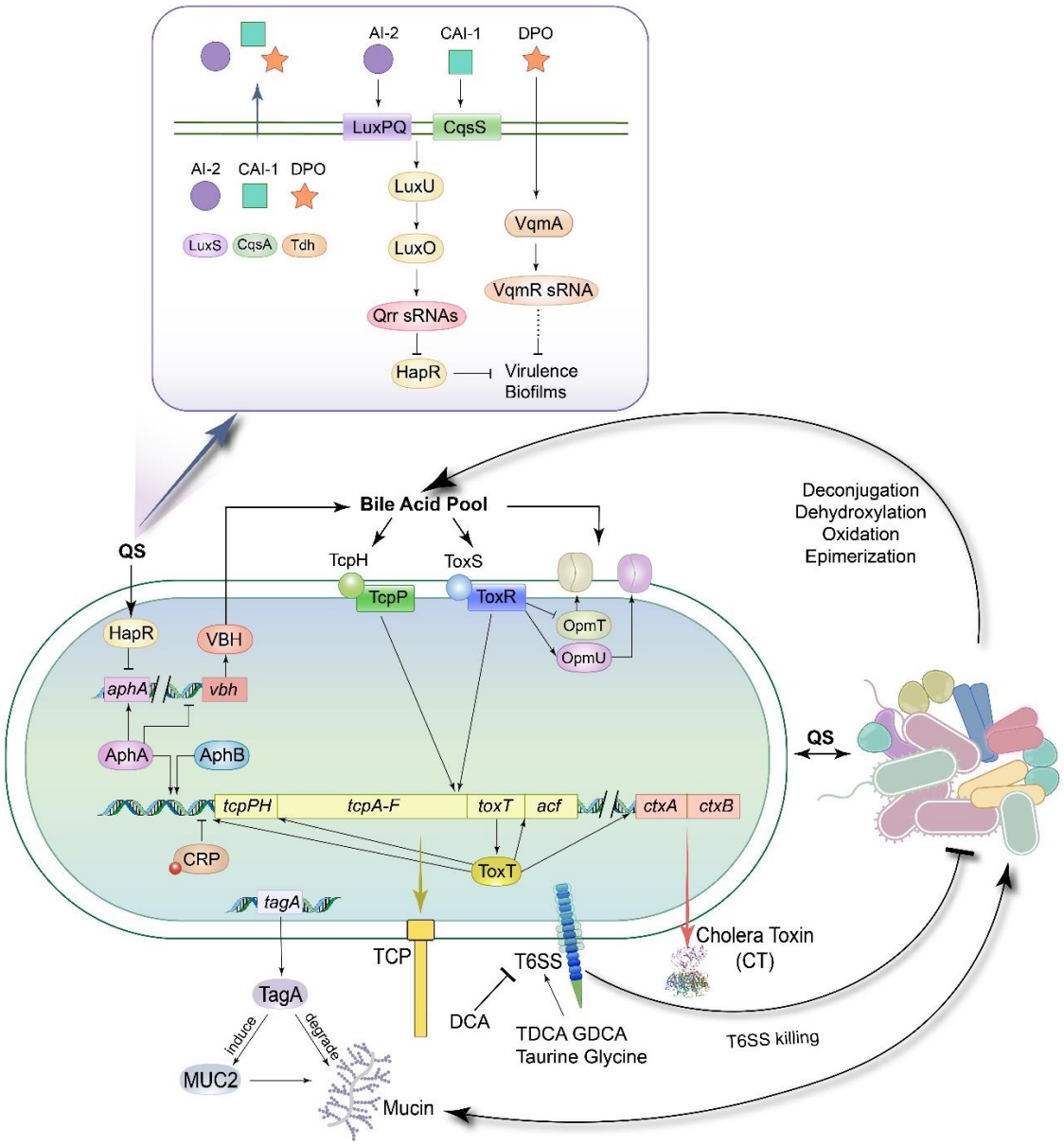


Figure 1-1. Virulence gene regulation in *V. cholerae* and interactions between *V. cholerae* and gut microbiota. The master regulator ToxT activates virulence genes involved in the synthesis of two key virulence determinants, TCP and CT. The expression of *vbh* is negatively regulated by AphA. The total bile acid pool composition is modified by bacterial activities from *V. cholerae* and gut commensals, and in turn, the bile acid pool composition impacts *V. cholerae* gene expression and gut microbiota composition. At LCD, QS systems are active, resulting in the activation of virulence and biofilm genes. QS in *V. cholerae* and the gut microbiota mutually affect each other. The T6SS, which is also regulated by bile acids and QS, directly kills gut microbes. Nutrients such as mucin further complicate the interactions between *V. cholerae* and the gut microbiota.

Quorum sensing regulation in the gut

QS regulates host and intestinal bacteria communication

Many studies showed that QS signals derived from bacteria may influence the host cells in multiple aspects. Tateda et al.[53] showed the autoinducer *N*-3-oxododecanoyl homoserine lactone (3OC(12)-HSL) from *Pseudomonas aeruginosa* accelerates apoptosis in macrophages and neutrophils in mammalian cells. Two independent signal transduction pathway of 3OC(12)-HSL in mammalian cells are identified, one is calcium-dependent and the other one results in modulation of the inflammatory response[54]. The mammalian cells may activate protective mechanisms to get rid of the 3OC(12)-HSL[55]. Zargar et al.[56] found two *E. coli* strains, BL21 and W3110, even though genetically close, but phenotypically different, including flagella, LPS and AI-2 production, exhibit different effects on the human intestinal epithelial cells (IEC) HCT-8, with BL21 appears to cause greater perturbations on human cells. Further investigation revealed that AI-2 activates the NF-κB signaling pathway in IEC and upregulates IL-8 at 6 and 12h but downregulates IL-8 afterwards at 24h, which indicates the involvement of AI-2 as interkingdom signaling molecule on the inflammatory effects on human cells at the early stage. AI-2 can upregulate TNFSF9 gene expression in marcophages[57]. Apart from AI-2, indole, a small molecule produced from tryptophan by tryptophanase, strengthens the barrier functions of IEC via activating many genes involved in multiple biological functions[58,59].

Hosts and microbes produce mimic QS signals to affect gut bacteria

Both hosts and microbes can produce mimic QS signals to regulate gut bacteria in return. Ismail et al.[60] showed that mammalian epithelial cells produce mimic AI-2 molecules in response to bacteria or tight-junction disruption, and this molecule can be detected by the AI-2 receptor LuxP in *V. harveyi* and LsrB in *S. typhimurium,* subsequently activate genes via QS. However, the mimic AI-2 was not identified. Recently, Valastyan et al.[61] identified an AI-2 mimic made by the yeast *Saccharomyces cerevisiae*, 4-hydroxy-5-methylfuran-3(2H)-one (MHF), and they found the production of the mimic molecule requires the CFF1p proteins. In addition to AI-2 mimics, some fatty acids have similar chemical structures with diffusible signal factors (DSFs), one of the quorum sensing signals utilized by some Gram negative bacteria. These fatty acids demonstrated antibiofilm and anti-virulence effects on various microbes (see review[62]). A study showed that treatment with 100 μg/mL of palmitic acid decreases QS-mediated biofilm biomass of *V. harveyi* MTCC 3438, *V. parahaemolyticus* ATCC 17802, *V. vulnificus* MTCC 1145 and *V. alginolyticus* ATCC 17749 without hindering their planktonic growth[63]. Ethanolamine produced by the host targets CqsR, subsequently represses Qrr-sRNA expression and hapR expression, leading to a decreased colonization level of *V. cholerae*[64].

Impact of QS on Gut Microbiome Dynamics

Bacteria within the gut generate a variety of AIs, contributing to the complexity of bacteria-bacteria interactions. The levels of 3-oxo-C12:2, less prevalent in patients with inflammatory bowel disease (IBD), exhibit a positive correlation with increased abundance of *Faecalibacterium prausnitzii*, *Clostridium coccoides*, and *Clostridium Leptum*[65]. An *E. coli* strain lacking the AI-2 kinase gene *lsrK* exhibited a significant increase in the ratio of Firmicutes to Bacteroidetes[66]. This observation underscores the impact of AI-2 levels on shaping the abundance of the major phyla in the gut. A study in rodent model showed the AI-2 signals from *Salmonella typhimurium* can be inhibited by *E. coli* and *Bifidobacterium*, which also produces AI-2 molecules[67]. Similar pattern was also found in weaning swine, AI-2 produced by probiotic bacteria inhibit the virulence of enterohemorrhagic *E. coli* (EHEC)[68].

Many bacteria can produce QS-controlled toxins to compete with other gut microbes. For example, research showed that *Clostridium difficile* may utilize indole-induced QS signals to produce indole and inhibits the growth of the protective gut microbiota during infection[69]. This regulation involves inhibiting the recovery of indole-sensitive taxa, thereby creating a favorable environment for the survival of *C. difficile.* Other examples include bacteriocins in *Streptococcus* species[70,71] and type VI secretion effectors in *Burkholderia thailandensis*[72]. As a vital tool for bacterial competition through contact-dependent killing of rivals, the regulation of the Type VI Secretion System (T6SS) involves multiple mechanisms, including QS. In a *V. cholerae* O1 strain, a gene *hcp*

encoding for a key protein in T6SS is regulated by QS via HapR, and the expression of *hcp* also requires the cAMP receptor protein CRP and an alternative sigma factor RpoN[73]. It is reasonable speculation that as bacteria communicate and coordinate their activities through QS, the competitive abilities against other species are finely tuned, impacting the overall balance and diversity of the gut microbiome.

Phenotypic Heterogeneity in QS

Phenotypic heterogeneity refers to the dynamic cell-to-cell variations in traits or distinct observable characteristics in the same genetic group or environmental conditions[74,75]. Recent studies have demonstrated phenotypic heterogeneity in QS in some bacteria, such as *Pseudomonas* species[76,77], instead of the traditional idea that QS synchronously regulate gene expressions. The term bistability, commonly used in phenotypic heterogeneity, refers to a situation in which a population has two coexisting cell types that exhibit distinct traits[78]. Bet-hedging and division of labor are two of the most recognized benefits of phenotypic heterogeneity. Bet-hedging is a strategy employed by a clonal group of bacteria to survive and proliferate under unpredictable environment without necessitating direct responses to external signals[79]. While division of labor refers to a situation where members of a clonal population interact with each other, simultaneously expressing distinct and often complementary traits[80].

Factors that contribute to the generation of phenotypic heterogeneity in QS system can be complicated. Interestingly, at the early stage of biofilm formation, only a small

population of *Pseudomonas putida* produces AHL, and they can regulate themselves rather than triggering neighboring isogenic cells. In contrast, *P. putida* produce biosurfactants putisolvins to disperse the AHL-producing cells, resulting a delay in biofilm formation[76]. Hence, AIs have the potential to instigate self-directed behavior and play a role in fostering phenotypic heterogeneity.

Despite at LCD, phenotypic heterogeneity is evident in certain bacteria at HCD (see review[75]). For instance, single-cell analysis of *V. harveyi* reveals significant variability in bioluminescence intensity within the same population[81]. Intriguingly, a heterogeneous population of *V. harveyi* exhibits a higher biofilm production compared to a homogeneous one, underscoring the potential advantages of phenotypic diversity.

Bile acids

Bile acids (BAs), one of the key components in bile, are synthesized from cholesterol, stored in the gallbladder, and secreted and released to the small intestines. Bile acids serve critical functions in metabolism, gene regulations, and microbiome composition. There has been increased research on studying the relationship between bile acid pool, microbiome structure and diseases.

Bile acid synthesis and circulation

There are mainly two pathways for BAs synthesis through a series of enzymatic reactions, as depicted in Figure 1-2: the classic or neutral pathway, and the acidic or alternative pathway. The classic pathway is the primary pathway that accounts for 90% of the total BAs synthesis. A total of seventeen enzymes are involved in the conversion of cholesterol to BAs, typically going through hydroxylation, C3 hydroxyl group saturation, epimerization of the C3 hydroxyl group and removal of three carbon units. The synthesis reactions take places in the endoplasmic reticulum, mitochondria, peroxisomes and cytoplasm[82].

The classic/primary pathway

As depicted in Figure 1-2 and Figure 1-3, the classic pathway is initiated by a highly regulated microsomal 7α-hydroxylase (CYP7A1), catalyzing the cholesterol into 7α-hydroxycholesterol[83], which is the determinant step of BAs synthesis rate and pool size. Then, 3β-hydroxy-Δ5-C27 steroid dehydrogenase (HSD3B7) converts 7α-hydroxycholesterol to 7α-hydroxy-4-cholesten-3-one (7α-hydroxy-4-cholesten-3-one, C4). At this step reactions can go two directions: One is after the modification effects of 14-3–oxosteroid−5b-reductase (AKR1D1) and 3a-hydroxysteroid dehydrogenase (AKR1C4, also known as 3α-HSD1) enzymes, the resulting product is then catalyzed by 12α-hydroxylase (CYP8B1) which adds a hydroxyl group to C12 of the steroid ring, after several rounds of enzyme activities, producing the primary BAs cholic acid (3α, 7α, 12α-

trihydroxy-5β-cholan-24-oic acid, CA)[82,84]. The other one is instead of hydroxylation modification of CYP8B1, with the help of sterol 27α -hydroxylase (CYP27A1), chenodeoxycholic acid (3α, 7α-dihydroxy-5β-cholan-24-oic acid, CDCA) is produced[85].

The alternative/acidic pathway

As shown in Figure 1-2 and Figure 1-3, the alternative/acidic pathway only contributes to approximately 10% of total BAs synthesis in human hepatocytes. In specific conditions such as liver disease, when the classic synthesis pathway is suppressed, the alternative one will become the dominant pathway for BAs synthesis and it is also more active during childhood, while the classic pathway becomes predominant with age [86]. The alternative pathway begins with the hydroxylation of the cholesterol by mitochondrial CYP27A1 in inner mitochondrial membrane. This enzyme is widely produced in all the tissues in the body, unlike CYP7A1 only expressed in hepatocytes. CYP27A1 can convert cholesterol into (25R)-26-hydroxycholesterol (26HC, also known as 27-hydroxyl cholesterol, previously known as 26-hydroxycholesterol[87]) and 25-hydroxycholesterol (25HC) and 24(S)-hydroxycholesterol (24HC). Both 25HC and 26HC are involved in cholesterol/lipid homeostasis, with 25HC primarily found in the endoplasmic reticulum and 26HC predominantly found in the brain [88–90]. The factors that contribute to the ratio of these resulting products remains unclear [91]. 26HC can be catalyzed into 3β-Hydroxy-5-cholinic acid, followed by 7-α hydroxylation by oxysterol 7-α hydroxylase (CYP7B1) to produce 3β, 7α -dihydroxy-5-cholinergic acid. Eventually 7α-hydroxy-3-oxo-4-cholesterol acid is produced and this unsaturated acid will be converted to CDCA via Δ^4-

3-oxosteroid 5β-reductase (aldo-keto reductase 1D1, AKR1D1) and 3α-hydroxysteroid dehydrogenase (3αHSD)[82,92]. 24HC and 25HC can be transformed to CDCA in a similar manner[91]. In the human brain, 24HC is produced from cholesterol with the enzyme CYP46A1, which can then exit the brain, enter the bloodstream, and undergo several metabolic steps to eventually be transformed into CDCA in the liver[93]. 24HC can also be converted to CA in human hepatocytes[94].

In the human liver, the primary BAs, CA and CDCA, will be conjugated to glycine or taurine, producing conjugated bile acids TCA, GCA, GCDCA and TCDCA, metabolized by bile acid-CoA:amino acid N-acyl-transferase (BAAT). More than 98% of the BAs secreted are glycine or taurine conjugated. While in mice, CDCA can be epimerized to UDCA metabolized by 7α/β- Hydroxysteroid dehydrogenase (HSDH). CDCA and UDCA can be further hydroxylated to α-muricholic acid (α-MCA) and then subsequently epimerized to β-muricholic acid (β-MCA)[95]. α-MCA and β-MCA can be conjugated by taurine to form Tα-MCA or Tβ-MCA. Then these conjugated BAs will be secreted to the duodenum and pass through small intestines.

Enterohepatic circulation of BAs

As illustrated in Figure 1-3, BAs are synthesized in the liver from cholesterol, stored in the gallbladder and then secreted to the small intestine. 95% of BAs will be reabsorbed in the ileum and only 5% of BAs will exit the body through the feces. A small portion of BAs can be reabsorbed through passive absorption in the jejunum and colon, mostly

unconjugated and uncharged BAs. Most BAs will be actively resorbed in the distal ileum through an apical sodium-dependent bile acid transporter (ASBT) encoded by the slc10a2 gene. Studies conducted on human ileal and renal transporters have indicated that the ASBT exhibits substrate specificity for both unconjugated and conjugated bile acids[96,97]. It was also reported that the interactions of BAs and ASBT may trigger a protection mechanism that stabilize the apical barrier of bicarbonate, and thus protecting cholangiocytes from toxic hydrophobic BAs[98]. Bile acids then exit the lumen through the apical brush border membrane. After binding to intestinal Bile Acid–Binding Protein (IBAB–P), BAs are effluxed to the portal vein by the heterodimeric Organic Solute Transporter α/β (OSTα/OSTβ) located on the basolateral pole of ileal enterocytes. BAs are subsequently reabsorbed through the action of multiple transporters, including the Sodium Taurocholate Co-transporting Polypeptide (NTCP), Organic Anion Transporting Polypeptides (OATPs), and Solute Carrier Family 21A (SLC21A) transport proteins localized in on the basolateral (sinusoidal) domain of hepatocytes[99,100]. NTCP functions as a sodium-dependent transporter for the transportation of conjugated bile acids, whereas the other two transporters operate as sodium-independent transporters for unconjugated bile acids.

BAs synthesis is primarily negatively regulated by three mechanisms. 1). In the liver cells, FXR is activated by BAs, which lead to induction of SHP expression, and SHP inhibits the transcription of CYP7A1 and CYP8P1, leading to reduced BAs synthesis[101]. 2). In the intestine cells, Farnesoid X Receptor (FXR) activates FGF15/19 expression,

which interact with FGFR4/β-Klotho complex on the plasma membrane of liver cells, and the resulting ERK1/2-JNK signaling pathway reduces the transcription of CYP7A1 and BAs synthesis[102,103]. 3). FXR-mediated transcriptional repressor, V-maf avian musculoaponeurotic fibrosarcoma oncogene homolog G (MAFG), can repress multiple BAs synthesis genes, including CYP27A1, and reduce BAs synthesis[104–106].

Antimicrobial effects of BAs

BAs are natural antimicrobial agents, and they can induce various injuries to bacterial cells. Firstly, BAs disrupt the integrity of the bacterial cell membrane. Conjugation of primary bile acids (CA and CDCA) with taurine or glycine enhances their water solubility, facilitating efficient transport. Conjugated BAs, which are fully ionized at physiological pH, remain on the outer leaflet of the membrane, while unconjugated BAs can passively penetrate the membrane and cause damages[107–109]. BAs with high concentration can dissolve the membrane lipids and directly lead to cell leakage and death[110]. DCA is more toxic than CA because of its hydrophobic and detergent like properties[111]. Secondly, BAs can induce DNA damages, trigger SOS response in *E. coli*, increase the likelihood of mutation, and induce curing in virulence plasmids within bacterial cells[112–114]. Moreover, BAs can cause protein misfolding or denaturation, hampering bacterial proliferation, and can also sequester iron and calcium, limiting their availability to bacteria[82].

BAs alter gut microbiome community structure

BAs is one of the major factors that alter the gut microbiome community structure. Since BAs are derived from cholesterol, diet can modify gut microbiome community structure through BAs metabolism. 16sS rRNA sequences revealed that obese people who took high-fat diet (HFD) displayed increased Firmicutes and decreased Bacteroidetes[115]. A HFD with varying cholesterol content exhibited varying levels of resistance to diet-induced obesity in germ-free (GF) mice. Specifically, a high-cholesterol HFD demonstrated resistance to obesity, whereas a low-cholesterol HFD did not[116]. Altered diet-induced gut microbiome modification can occur as early as one day in mice[117] and within four days in humans[118]. Particularly, the animal based diet increases the abundance of bile-tolerant bacteria and decreases the plant polysaccharide metabolizing bacteria in human[118]. Addition of BAs directly changes the gut microbiome as well. Islam et al.[119] demonstrated that administration of CA to rats alter the gut microbiome structure at phylum level, with Firmicutes dominate the microbiome, and the total BAs in feces amount is very likely to the BAs amount in human feces on a HFD. Feeding mice CA also expands the level of DCA producing[119] and 7α-dehydroxylating bacteria[120]. Collectively, reduction of BAs level in the gut is advantageous for gram-negative bacteria while enhanced BAs favors gram-positive and 7α-dehydroxylating bacteria.

Microbial effects on BAs

Bacteria in the gut play a crucial role in transforming bile acids, which significantly impacts their function and availability. These microbial transformations occur mainly in four distinct ways: deconjugation, dehydroxylation at C7, oxidation, and epimerization.

Deconjugation

Deconjugation, considered as the "gateway reaction" to further modification, refers to the enzymatic process by which the conjugated form of BAs, typically with taurine or glycine, is cleaved or hydrolyzed by bile salt hydrolases (BSH, classified as EC 3.5.1.24 in Kyoto Encyclopedia of Genes and Genomes (KEGG)) produced by the gut microbes. The resulting deconjugated primary BAs, CA and CDCA, can serve as signaling molecules and regulate BAs pool. Moreover, increased concentration of CA and CDCA, which are antimicrobial BAs, may modify the gut community structure. Genes encoding BSH are commonly found across all major bacterial phyla and archaeal species in the gut, with 591 of identified bacterial strains in human gut[121]. In the study conducted by Song et al.[121], the authors classified BSHs into eight distinct phylotypes through phylogenetic analysis. They observed that BSHs belonging to different phylotypes displayed substrate specificity, indicating that they have preferences for bile salt substrates. Notably, BSH-T3 demonstrated the highest enzyme activity among the identified phylotypes and is only found in *Lactobacillus*. The enzyme activity may also vary *in vitro* and *in silico*. They also found significant differences in BSH patterns among healthy and diseased cohorts,

indicating that BSH may have impact on the disease development. Approximately 27% of the BSH encoding strains in human gut harbor more than one *bsh* genes. For example, *Blautia obeum* has two identified *bsh* genes, *RUMOBE_00028* and *RUMOBE_ 03454*, and the proteins are both classified as BSH-T1 through sequence alignments. *Bacillus*, *Bacteroides*, and *Enterococcus* exhibit the highest number of strains that possess BSH paralogs[121].

Dehydroxylation

Dehydroxylation is a key transformation of BAs through microbes. By removing hydroxyl (-OH) groups from the BAs, dihydroxylation can lead to formation of different BAs with altered physiological functions and varying effects on lipid metabolism and signaling pathways. Specifically, enzymes convert CA to DCA and UDCA to LCA through 7-α and 7-β dehydroxylation respectively. Compared to deconjugation, only a limited number of 7-α dehydroxylation bacterial strains have been characterized. In *Clostriduium scindens*, the 7-α dehydroxylation pathway requires seven proteins encoded by a bile-acid-induced (*bai*) operon (BaiB, BaiA2, BaiCD, BaiF, BaiE, BaiN, BaiO or BaiA2 in order) to convert CA to DCA[122]. 7-β dehydroxylation pathway is very similar, but BaiH catalyzes the C4 oxidation instead of BaiCD in 7-α dehydroxylation pathway[123]. Activities of dehydroxylation may confer advantage for competition, because DCA and LCA are generally more toxic to microbes, and it may eventually impact the gut community structure.

Oxidation and epimerization

Oxidation is the pre-step for epimerization of BAs. BAs first undergo oxidation of the hydroxyl group at C3, C7 or C12 positions by α-HSDH, followed by a subsequent reduction step facilitated β-HSDH. These reactions can take place in co-cultures, where different species of microorganisms interact and contribute to the overall metabolism of BAs. CA can undergo epimerization to form isocholic acid (iCA), ursodeoxycholic acid (UCA), or 12-epicholic acid (12-ECA) through the action of 3α/β-HSDH, 7α/β-HSDH, or 12α/β-HSDH, respectively. Similarly, CDCA can be converted into UDCA or iCDCA by the enzymatic activity of 7α/β-HSDH or 3α/β-HSDH, respectively[124]. UDCA is considered as protective BA. It is known to exhibit reduced toxicity compared to CDCA concerning the growth of *Clostridium absonum*[125]. The ability of *Ruminococcus gnavus* to efficiently convert 7-oxo-LCA to UDCA further suggests the potential role of *R. gnavus* as a probiotic. Intestinal bacteria play a significant role in performing another important epimerization reaction, known as 6β-epimerization, on murine β-MCA, resulting in the formation of ω-MCA. Additionally, ω-MCA can undergo further transformations, such as 7β-epimerization, leading to the production of γ-MCA, or 7β-dehydroxylation, resulting in the formation of hyodeoxycholic acid (HDCA)[126]. Oxidation and epimerization allow microbes to modify the chemical structure of BAs, resulting in reduced toxicity, and therefore create a more favorable environment for their growth and survival.

Bile acid variations between human and animal models

Human and mice have different BAs compositions (Figure 1-4 and 1-5). **In humans**, primary BAs, CA and CDCA, are synthesized from cholesterol in the hepatocytes via two classical and alternative pathways. However, **in mice**, synthesized primary BAs in hepatocytes include CA, CDCA, UDCA and MCA. UDCA is considered as secondary BAs in humans because it is generated from CDCA via the enzymes (7α-HSDH and 7β-HSDH) produced from the gut microbes, or via hepatic reduction of 7-oxoLCA (7-oxolithocholic acid) by human 11β-HSD1 (11β-hydroxysteroid dehydrogenase 1)[127]. While UDCA is detected in germ-free mice, indicating UDCA is a primary BAs in mice[128]. In both cases, UDCA only accounts for a small component of the BAs pool[129,130]. In contrast to humans, CDCA only accounts for a small portion of the bile acid pool in mice (Figure 1-4). Additionally, there is a notable disparity in the concentration of 6-hydroxylated BAs between humans and mice. In mice, the pool of BAs predominantly comprises 6-hydroxylated BAs, specifically muricholic acid (MCA), which accounts for over half of the total BAs[129,130]. Conversely, in humans, the concentration of 6-hydroxylated BAs is significantly lower[129,130].

In addition to the differences in UDCA and 6-hydroxylated BAs between various models, the selection of glycine or taurine for bile acid conjugation also varies. The enzyme responsible for this process, BAAT, plays a crucial role in determining the preference for glycine or taurine conjugation. In humans and rats, BAAT efficiently utilizes both glycine and taurine, with a taurine-to-glycine ratio of approximately 1 to 3[131]. However, in mice,

BAAT exhibits inefficiency in utilizing glycine, resulting in nearly exclusive conjugation of bile acids with taurine[132]. Different animal species exhibit distinct preferences for conjugation partners. Rabbits and guinea pigs predominantly rely on glycine for bile acid conjugation, while sheep and dogs exclusively utilize taurine[130]. It is worth noting that taurine-conjugated bile acids have enhanced water solubility and lower pKa compared to glycine-conjugated ones. They are primarily actively transported rather than passively diffused[133]. Studies suggest that taurine-conjugated bile acids are less toxic than glycine-conjugated and unconjugated bile acids, potentially explaining the reduced occurrence of certain human diseases in mouse models[134,135]. Furthermore, in humans, CA and CDCA can be 7α-dehydroxylzed to form DCA and LCA, while mice can generate DCA from CA, HDCA and MDCA from α-MCA and β-MCA (Figure 1-5). HDCA and MDCA are C7 hydroxylated secondary BAs with only difference in the C6 position (Figure 1-6). Overall BAs pool in mice are more hydrophilic than BAs pool in humans[136].

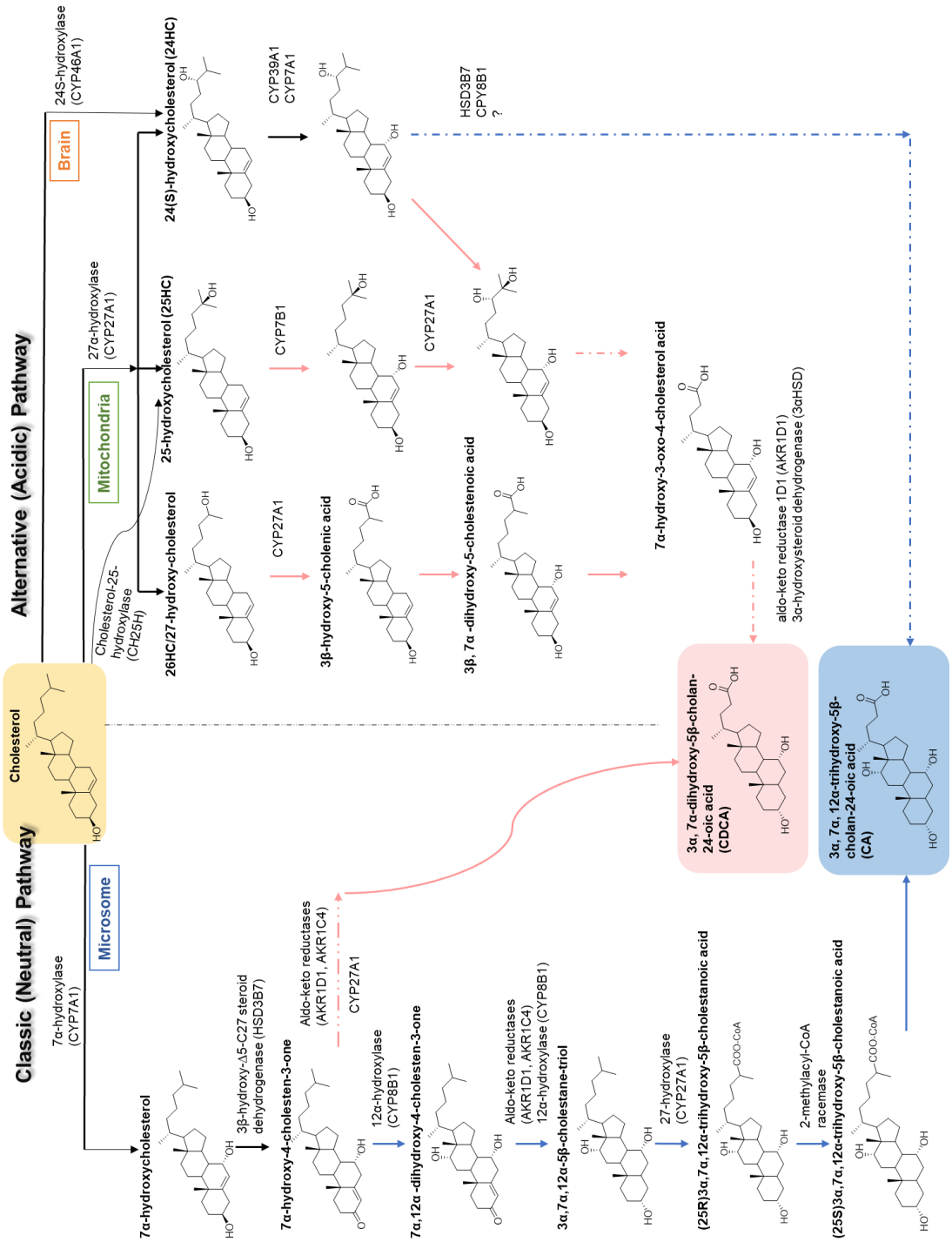


Figure 1-2. The classic (neutral) and alternative (acidic) pathways of bile acid synthesis.

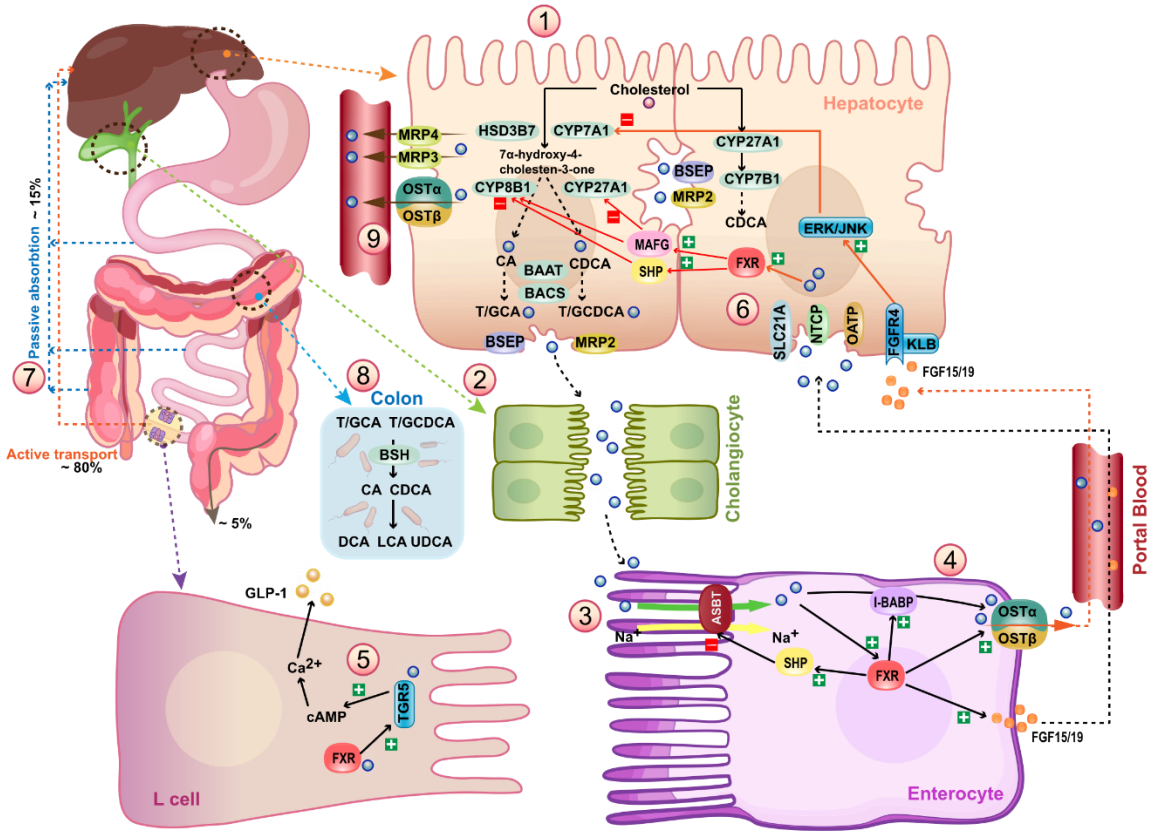

1
Hepatocyte
Cholesterol
HSD3B7
CYP7A1
7α-hydroxy-4-cholesten-3-one
CYP8B1
CYP27A1
CA
CDCA
BAAT
BACS
T/GCA
T/GCDCA
CYP27A1
CYP7B1
CDCA
BSEP
MRP2
MAFG
SHP
FXR
ERK/JNK
6
SLC21A
NTCP
OATP
FGFR4
KLB
FGF15/19
MRP4
MRP3
OSTα
OSTβ
9
BSEP
MRP2
2
Cholangiocyte
Portal Blood
Passive absorption ~ 15%
7
Active transport ~ 80%
~ 5%
8
Colon
T/GCA T/GCDCA
BSH
CA CDCA
DCA LCA UDCA
GLP-1
Ca2+
cAMP
5
TGR5
FXR
L cell
3
4
ASBT
Na+
Na+
I-BABP
SHP
FXR
OSTα
OSTβ
FGF15/19
Enterocyte

Figure 1-3. BAs synthesis and enterohepatic circulation.

1. In the liver, primary BAs CA and CDCA are synthesized from cholesterol by a series of enzymes, such as CYP7A1, HSD3B7, CYP8B1 and CYP27A1 via "classical pathway". CYP7A1 is the rate limiting enzyme. In alternative pathway, CDCA is synthesized by the rate limiting enzyme CYP27A1 and by CYP7B1 at a later step. Primary BAs are then conjugated to glycine or taurine by BA CoA synthase (BACS) and BA-CoA-amino acid N-acetyltransferase (BAAT) to form conjugated BAs. Then conjugated BAs are secreted to the gallbladder by the bile salt export pump (BSEP) and the multidrug resistance-associated protein (MRP2).
2. BAs are stored in the gallbladder and secreted into the duodenum.
3. Around 95% of the bile acids (BAs) undergo reabsorption in the terminal ileum. The primary mode of reabsorption is through active transportation (~80%) in the ileum, facilitated by the Na+ dependent apical sodium-dependent bile acid transporter (ASBT) in the enterocytes. Generally conjugated BAs favors ASBT for active reabsorption. Additionally, a minor fraction of bile acids (~15%) is reabsorbed through passive transportation.
4. In enterocytes, bile acids (BAs) activate the farnesoid X receptor (FXR) and serve multiple functions. Firstly, FXR reduces the uptake of BAs by downregulating the apical sodium-dependent bile acid transporter (ASBT) in a small heterodimer partner (SHP) dependent manner. Secondly, FXR induces the expression of two important proteins: the cellular intestinal BA binding protein (I-BABP) and the organic solute transporter (OSTα/β). These proteins are responsible for the intracellular transport of BAs and the efflux system within the portal blood circulation, respectively. Thirdly, FXR also induces the enterokine fibroblast growth factor 19/15 (FGF19 in human and FGF15 in mice), which enters the portal blood circulation and binds to hepatic FGF receptor 4 (FGFR4) and β-Klotho complex (KLB) in the liver cell membrane to activate Jun N-terminal kinase (JNK) or extracellular signal-regulated kinase (ERK) signaling pathways, which inhibit CYP7A1 and CYP8B1 genes transcription[137,138].
5. In enteroendocrine L cells, BAs induce the expression of FXR and Takeda G protein-coupled receptor 5 (TGR5). FXR in return induces TGR5 to activate cAMP and Ca2+ to secrete the insulin stimulating glucagon-like peptide-1 (GLP-1) in the pancreatic cells.
6. BAs in the portal blood enter the liver cells via sodium taurocholate cotransporting polypeptide (NTCP), organic anion transporting polypeptide (OATP) and solute carrier family 21A (SLC21A) transporters. BAs induce FXR, which increases the transcription of SHP. SHP in return binds with liver receptor homologue-1 (LRH-1), which downregulates the CYP8B1 gene expression and inhibits BAs synthesis. BAs can also induce a transcriptional repressor V-maf avian musculoaponeurotic fibrosarcoma oncogene homolog G (MAFG), which inhibits multiple BAs synthesis genes , including *Cyp8b1* and *Cyp27a1*[106].
7. Passive transportation accounts for approximately 15% of BAs reabsorption and occurs in the entire small intestine and colon. Because of the protonated features, unconjugated BAs have the highest likelihood of being reabsorbed through nonionic diffusion, followed by the glycine-conjugated bile acids, and lastly, the taurine-

conjugated bile acids. Among unconjugated BAs, CDCA and DCA, which are more hydrophobic, have a higher diffusion rate than hydrophilic BAs.

8. The unabsorbed fraction is then shunted to the colon and undergoes modification by microbes: BSHs from the commensal microbes convert conjugated BAs to unconjugated BAs. CA and CDCA can be subsequently metabolized by bacterial 7α-dehydroxylase removes a 7-HO group to form the secondary BAs, DCA and LCA, respectively. CDCA can also form the secondary BAs UDCA by 7α-epimerization. These deconjugated secondary BAs may undergo passive absorption in the colon. Approximately 50% of DCA is reabsorbed in the colon[139], while LCA and UDCA are barely absorbed. Eventually around 5% total BAs are excreted in the feces.
9. BAs in the hepatocytes enter the portal blood circulation via the multidrug resistance protein 3 and 4 and OSTα/β. BAs are then released from the portal blood into the small intestines, reabsorbed in the ileum and returned to the liver for recycling.

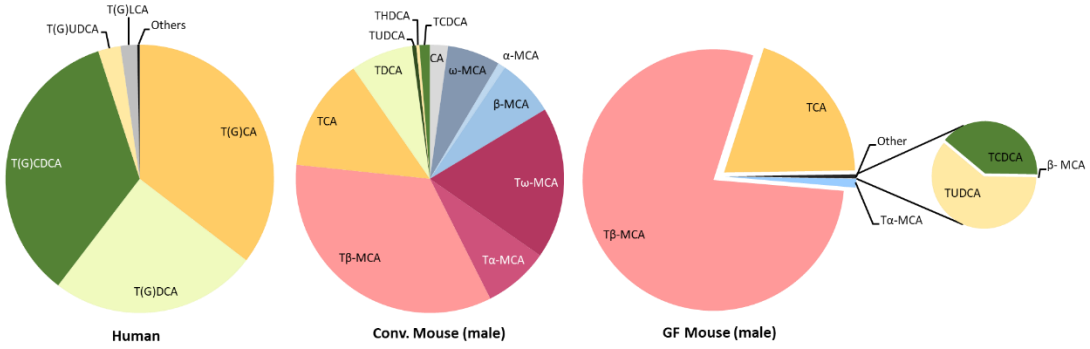


Figure 1-4. Human and mice have different BAs compositions.
Bile acids composition in healthy human biliary bile (left), male conventional mouse biliary bile (middle) and male Germ-free mouse biliary bile (right). Data were obtained from Wahlström et al.[129], Ahmad et al.[140], Honda et al. [141].

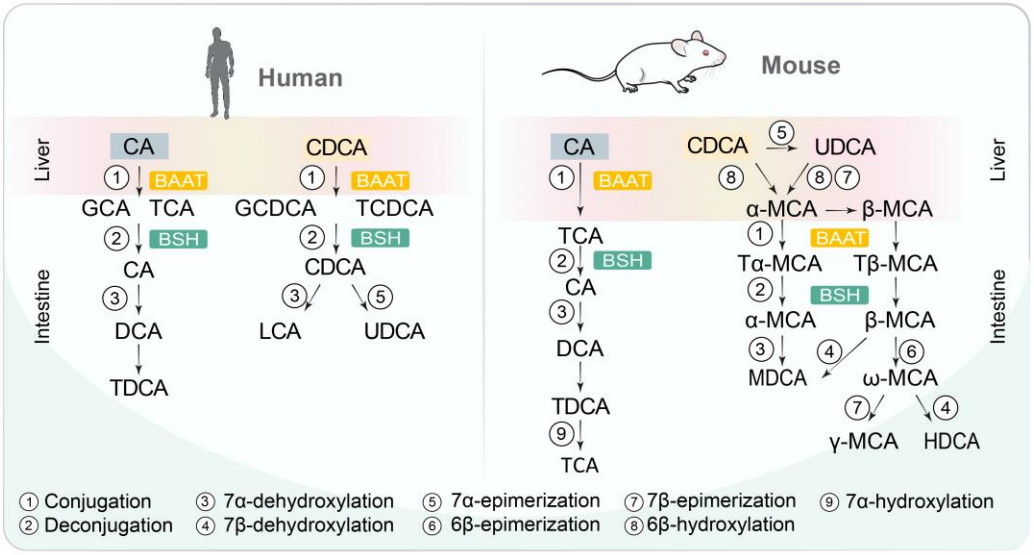
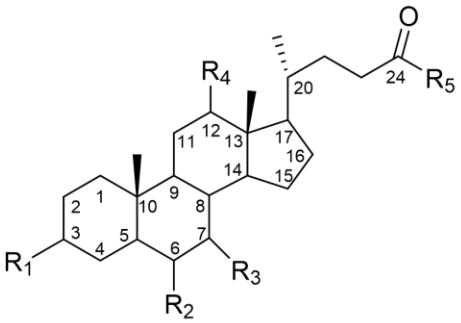


Figure 1-5. Conversion of primary bile acids to secondary bile acids in human and mouse.



Compound name	Abbrev.	R1	R2	R3	R4	R5	Present in
Taurocholate	TCA	α-OH	H	α-OH	α-OH	NHCH2CH2SO3H	Human, murine
Taurochenodeoxycholate	TCDCA	α-OH	H	α-OH	H	NHCH2CH2SO3H	Human, murine
Taurodeoxycholic acid	TDCA	α-OH	H	H	α-OH	NHCH2CH2SO3H	Human, murine
Glycocholate	GCA	α-OH	H	α-OH	α-OH	NHCH2CO2H	Human, murine, vely less in mice
Glycochenodeoxycholate	GCDCA	α-OH	H	α-OH	H	NHCH2CO2H	Human, murine, vely less in mice
Glycodeoxycholic acid	GDCA	α-OH	H	H	α-OH	NHCH2CO2H	Human, murine, vely less in mice
ω-muricholic acid	ω-MCA	α-OH	α-OH	β-OH	H	OH	murine
α-muricholic acid	α-MCA	α-OH	β-OH	α-OH	H	OH	murine
β-muricholic acid	β-MCA	α-OH	β-OH	β-OH	H	OH	murine
Murideoxycholic acid	MDCA	α-OH	β-OH	H	H	OH	murine
Ursodeoxycholic Acid	UDCA	α-OH	H	β-OH	H	OH	Human, murine
Hyodeoxycholic acid	HDCA	α-OH	α-OH	H	H	OH	Human, murine
Cholic acid	CA	α-OH	H	α-OH	α-OH	OH	Human, murine
Chenodeoxycholic acid	CDCA	α-OH	H	α-OH	H	OH	Human, murine
Deoxycholic acid	DCA	α-OH	H	H	α-OH	OH	Human, murine
Lithocholic acid	LCA	α-OH	H	H	H	OH	Human, murine

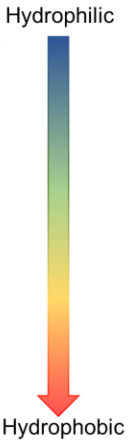


Figure 1-6. Chemical structure and sources of some common bile acids. Free bile acids, and glycine/taurine-conjugated bile acids are included. Primary BAs are highlighted in yellow.

BAs effects on *V. cholerae*

Like many other bacteria, BAs have toxic effects on *V. cholerae* and *V. cholerae* in turn must overcome the stresses via evolved resistance mechanisms such as biofilm formation. Studies confirmed that crude biles and sodium cholate induce *V. cholerae* biofilm formation in a vpsR-dependent way [142]. The mobility of *V. cholerae*, a crucial element for a successful gut infection, saw a notable rise in the presence of bile. A single type of bile salt, TCA, was shown to facilitate *V. cholerae* dispersal from biofilm [143,144], indicating that *V. cholerae* has utilized the signal from bile salts derived from the host to

detach from the biofilm and initiate the activation of its virulent properties. Of utmost significance, BAs play a pivotal role in regulating the expression of *V. cholerae* virulence genes. Specifically, TCA enhances the functioning of the transmembrane transcription factor TcpP, which typically exists in an inactive monomeric state. This enhancement is achieved through the promotion of the creation of an intermolecular disulfide bond between C^{207} residues and the epimerization of TcpP, ultimately leading to the activation of ToxT [145]. DsbA, a periplasmic oxidoreductase, can trigger TcpP dimerization when primary BAs present, but BAs also inhibit DsbA by forming disulfide bonds in the proteins. It has been demonstrated that BAs control proteolysis of ToxR[146], stimulate ToxRS complex interaction[147], and toxin production[148]. Alavi et al.[149] evaluated different BAs for their virulence-inducing potential using a *tcpA* reporter strain. Primary BAs showed higher virulence induction than secondary BAs. Additionally, glycine-conjugated BAs triggered higher *tcpA* induction rates compared to taurine-conjugated BAs, possibly due to the 3 : 1 of glycine-to-taurine ratio in humans. Nevertheless, an opposite discovery emerged when examining the impact of crude ox bile on cholera toxin production[143,148]. This phenomenon's divergence could potentially be elucidated by variations in the composition of BAs and the intricate nature of bile constituents among diverse animal models. For example, unsaturated fatty acids can inhibit toxT transcription by binding to it [150].

Chapter 2 Dual-function bile salt hydrolase in *Vibrio cholerae* modulates virulence and fitness through host-specific bile acid metabolism

Abstract

Vibrio cholerae is the etiologic agent of the severe diarrheal disease cholera, which represents a major burden on global health. *V. cholerae* uses gut-specific biochemical signals, especially bile acids, to fine-tune the timing and levels of expression of virulence genes to maximize fitness during infection. Bile acid metabolism by commensal-encoded enzymes such as bile salt hydrolases that deconjugate amino acids from bile acids is a major contributor to chemical diversity in the bile acid pool and thus virulence gene expression and infection outcome. However, how pathogen-encoded bile salt hydrolases interact with the bile acids that are abundant in humans to affect pathogen and commensal fitness is poorly understood. Here, we show that *V. cholerae* encodes a bile salt hydrolase that has dual functions depending on the substrate, which in turn depends on the host. This enzyme converts taurodeoxycholic acid (TDCA) found in humans and mice to deoxycholic acid (DCA), and converting taurochenodeoycholic acid (TCDCA), highly abundant in humans, into chenodeoxycholic acid (CDCA). We find that CDCA is a potent activator of virulence gene expression in *V. cholerae*, while DCA inhibits *V. cholerae* growth. We show that the expression of this enzymatic function can be suppressed by a major activator of virulence genes in *V. cholerae*. Taken together, our work suggests that the ability of pathogens to balance virulence-activating and growth-suppressive bile acids depending on host bile availability and composition is key to the

relative fitness of commensal and pathogenic bacterial fitness *in vivo*, and that the bile acid pool variability seen in humans may be a key contributor to individualized infection outcome.

Introduction

Vibrio cholerae is the etiologic agent of the severe human diarrheal disease, cholera. Despite much work on the pathogenesis of *V. cholerae* and improved treatment strategies, cholera remains a global health problem[151]; in 2022 alone, reports of cholera cases or outbreaks surfaced in no fewer than 30 countries. *V. cholerae* preferentially colonizes the small intestine, where it produces virulence factors including the colonization factor toxin co-regulated pilus (TCP) and cholera toxin (CT) responsible for diarrhea [18,152]. Virulence gene expression sits within a tightly controlled regulatory cascade. AphA and AphB are transcriptional activators of production of the upstream TcpPH complex that senses environmental signals such as bile that characterize the preferred colonization environment *in vivo*[30–32]. TcpPH signaling leads ultimately to the production of the master virulence regulator ToxT that activates the genes of the *tcp* operon and *ctx* genes responsible for generation of TCP and CT respectively[153–155]. While considerable data exists for the ability of *V. cholerae* to respond to changes in temperature, oxygen levels, gastric and bile acids as it infiltrates the gut[156], less is understood about the capacity of *V. cholerae* to modify the gut biochemical environment, thus modulating its ability to colonize and infect the host.

Bile is a complex digestive fluid stored in the gall bladder and a key environmental determinant of commensal microbial fitness in the gut, and can act a critical modulator of virulence in *V. cholerae*[157]. Bile acids, the major component of bile, are a family of steroidal acids synthesized in the liver from cholesterol and secreted into the proximal portion of the small intestine to aid in the absorption of dietary fats. Primary bile acids comprise cholic acids (CA) and chenodeoxycholic acids (CDCA), which are often conjugated to taurine in mice and humans, or glycine in humans. CDCAs are abundant in the human gut but largely absent in mice[140,128,129,141], and the balance of CA to CDCA derivatives can vary dramatically from individual to individual[158–160]. In the gut, microbial enzymes encoded by diverse commensals can transform bile acid/salt molecules through the action of bile salt hydrolases (BSH) that remove or modify conjugated amino acids, leaving free bile acids.Recent studies also suggest that BSH enzymes can change the conjugated amino acids on bile acid backbones[161,162], contributing to a diverse, microbe-driven pool of molecules whose differential effects on gut associated microbes and overall gut health are not fully elucidated.

Bile acids have multiple physiological effects on *V. cholerae* in the gut, including modulation of biofilm formation[142], pathogen dispersion[143,144], and virulence gene expression[145,148,163]. Many of these effects are bile molecule specific; for example, TCA and GCA primary bile acids are potent activators of virulence in *V. cholerae* via TcpPH[157], in contrast to deconjugated CA [164,165], while DCA is growth inhibitory[166]. The composition of the *in vivo* bile pool is thus critical for determining the outcome of *V. cholerae* infection.

Here, we show *V. cholerae*, like many gut symbionts, encodes a bile salt hydrolase in the AphA-repressed gene *VCA0877*[167], and that the resulting enzyme displays activity in deconjugating deoxycholic acids (DCA) and chenodeoxycholic acids (CDCA). We therefore renamed this gene *vbh* for *Vibrio* Bile Salt Hydrolase. In this study, we show that VBH interacts with host bile to modulate pathogen fitness during infection. We find that the *vbh* gene is highly conserved among pathogenic *V. cholerae* isolates. Using mass spectrometry, and *in vitro* and *in vivo* fitness assays, we find that VBH confers multiple functions on *V. cholerae* depending on available bile substrates. In environments with high levels of CA derivates, including the mouse and some individual human guts, VBH accumulates DCA leading to growth inhibition, which is controlled by the repression of *vbh* via AphA. However, in environments with higher levels of CDCA derivatives, such as the human gut, VBH can generate CDCA, which we find for the first time to be a highly potent stimulator of *tcp* gene expression. Thus, depending on the individual host CA/CDCA ratio, and the activities of gut commensal microorganisms that generate downstream bile metabolites, VBH may allow for *V. cholerae* to optimize virulence gene expression in high CDCA individuals, while using AphA regulation as a hedge against accumulation of growth inhibitory bile substrates in less accommodating host bile compositions. The host-type specificity of this bile metabolite in *V. cholerae* gene regulation suggests that the most common mammalian animal models for *V. cholerae* pathogenesis studies may miss some of the complexities of *in vivo* human infection.

Methods

Bacterial strains and growth conditions

All *V. cholerae* strains were derived from the C6706 El Tor pandemic isolates and grown in LB medium with appropriate antibiotic at 37°C. To construct E*vbh*^{c} a *E. coli* strain constitutively expressing *vbh*, a *vbh* fragment was PCR-amplified from *V. cholerae* using primers (5'-GAGGTCGACGGTATCGATATCACCAAAGAGGAATCAGAG-3') and (5' –GCTGCAGGAATTCGATATCATATCCTGATCATTCTGCC-3'). A pZE21 vector for barboring *vbh* was generated using primers (5'-TGATATCGAATTCCTGCAGC-3') and (5'- TATCGATACCGTCGACCTC-3'). The *vbh* amplicons were then cloned downstream of the constitutively $P_{Ltet-O1}$ promoter of plasmid pZE21 through Gibson Assembly (New England Biolabs). The resulting plasmids were then electroporated at 2.5kV into *E. coli* DH5**αλ**pir to generate E*vbh*^{c}. The plasmids with *vbh* were then electroporated at 1.8kV into *V. cholerae* C6706 to generate a strain *vbh*^{c}.

A Δ*vbh* and a Δ*aphA*Δ*vbh* strain were constructed from *V. cholerae* C6706 (WT) and *V. cholerae* C6706 Δ*aphA* mutant strain respectfully with natural transformation based on the published method with slight modification[168]. Fragments of flanking genomic DNA upstream and downstream of Δ*vbh* and Δ*aphA*Δ*vbh* were generated using primers listed in Supplement. Table 2-1. Fragments of flanking genomic DNA upstream and downstream of Δ*aphA*Δ*vbh* were generated using primers indicated in supplementary table 2-1. A spectinomycin resistance (Spec^{R}) cassette was amplified from SAD033

genomic DNA using primers ABD123 (5'-ATTCCGGGGATCCGTCGA-3') and ABD124 (5'-TGTAGGCTGGAGCTGCTTC-3'). Amplicons were joined by overlapping PCR using Phusion High-Fidelity PCR Master Mix (Thermo Fisher Scientific, Waltham, MA, USA). An Equimolar of a *vbh* upstream fragment, a *vbh* downstream fragment and a SpecR cassette amplicon were mixed for PCR with the following conditions: 98°C for 30 s, followed by 15 cycles (94°C for 10 s, 50°C for 30 s, 72°C for 4min), and 72°C for 10 min. A *vbh* upstream fragment forward primer and a *vbh* downstream fragment reverse primer were added to the PCR reaction continued with 15 more PCR cycles described above. The final PCR product was then gel-purified ready for use. Appropriate *V. cholerae* cultures were initiated by inoculating LB broth and incubating overnight at 37°C with continuous shaking. Subsequently, 13 µL of the overnight culture was subcultured to 3 mL of fresh LB medium and incubated at 37°C with shaking until reaching an OD_{600} between 0.5 and 1.0. Cells were harvested by centrifugation at 18000 rcf for 1 minute and resuspended in 0.5X IO solution (7 g/L of instant ocean sea salts) to achieve an OD_{600} of 1.0. For each transformation reaction, 150 µL of chitin slurry (prepared by mixing 8g of chitin powder from shrimp shells, Fisher J6120622, with 150mL of 0.5X IO solution and autoclaving for sterilization) was dispensed into a sterile 2.0mL Eppendorf tube. To this, 750 µL of 0.5X IO solution and 100 µL of washed cells were added, followed by brief vortexing to ensure thorough mixing. The tubes were then placed at 30°C for static incubation for 16-24 hours. Afterward, approximately 550µL of supernatant was carefully removed without disturbing the settled chitin. Subsequently, 5-10µL of gel-purified PCR product was added to each tube and gently inverted 2-3 times

to facilitate mixing. The reactions were returned to 30°C and allowed to incubate for an additional 16-24 hours. Following incubation, transformation reactions were vigorously vortexed and 50 to 200 μL was directly plated onto LB agar plates supplemented with appropriate antibiotics. Resistant colonies were subsequently selected and confirmed via PCR analysis and sanger sequencing.

A *V. cholerae* strain overexpressing *vbh* gene was constructed using natural cotransformation using similar method described above. Unselected fragments were generated as follows: A constitutively $P_{Ltet\text{-}O1}$ promoter was amplified from plasmid pZE21. Fragments of flanking genomic DNA upstream and downstream of *vbh*'s original promoter were generated via PCR. Amplicons were joined by overlapping PCR described above. Selected fragments were generated as follows: A SpecR cassette was amplified from SAD033 using primers described above and fragments of flanking genomic DNA upstream and downstream of a neutral gene *VC1807* were generated. Amplicons were then joined by overlapping PCR described above. Primers are listed in Table 2-1. Both unselected and selected PCR products were gel-purified and incorporated into *V. cholerae* WT as described above. Resistant colonies were then selected on spectinomycin-containing LB agar (200 μg/ml) and confirmed via PCR and sanger sequencing.

The AphA-binding site mutation of *vbh* was achieved by deleting the 6 bp "TATGCA" on *vbh* promoter, or by replacing it with a random 6 bp sequence "CGGTAC" in WT *V.*

cholerae. For each mutation, an upstream fragment and a downstream fragment of aphA binding site was generated and joined via PCR. Similarly, a 7kb product containing a SpecR cassette and fragments of flanking genomic DNA upstream and downstream of a neutral gene *VC1807* was used for antibiotic selection. Both unselected and selected PCR products were gel-purified and incorporated into *V. cholerae* WT, and colonies were selected as described above. Primers are listed in Supplemtary Table 2-1.

Preparation of bacteria for animal studies

All *V. cholerae* strains were grown from glycerol stocks in LB media with appropriate antibiotics as overnight culture. For inoculation into CD-1 suckling mice, overnight cultures were diluted at 1:100 in fresh LB with appropriate antibiotic and grown in a shaker at 37°C for until OD_{600} = 0.3 to 0.4. 100 µL of *V. cholerae* cultures were pelleted and resuspended in fresh LB with antibiotic and diluted at 1:1000 in fresh LB with antibiotic. 50 µL of *V. cholerae* ($1x10^4$ – $1x10^5$ CFU) was gavaged into each suckling mouse. For inoculation into CD-1 adult mice, overnight cultures were diluted at 1:100 in fresh LB with appropriate antibiotics, grown for ~4.5 hours in a shaker at 37°C for until OD600 = 0.4 to 0.5, pellet and concentrated at 10:1 in fresh LB with appropriate antibiotic. 100 µL *V. cholerae* ($1x10^9$ – $1x10^{10}$ CFU) was gavaged into each adult mouse.

Animal studies

All animal experiments were approved by the Institutional Animal Care and Use Committee of the University of California, Riverside (UCR) and followed NIH guidelines. All CD-1 suckling and adult Swiss-Webster germfree mice were reared at the UCR gnotobiotic facility. Adult mice were used at 4 to 6 weeks of age.

For the CD-1 suckling mouse model, 4-day old suckling CD-1 animals were fasted for 1.5 hours, and then orally gavaged with 50 μL of 75 mg/mL spectinomycin solutions using plastic tubing, after which the animals were placed back to lactating dams. After 24 hours, suckling animals were then fasted for 1.5 hours, gavaged with 50 μL of *V. cholerae* strains prepared as described above using plastic tubing. At 18 hours post-infection, animals were sacrificed, intestinal tissue were dissected and homogenized in 5 mL sterile 1x PBS for numeration.

For the CD-1 adult mouse model, 4 to 6-week-old adult CD-1 animals were provided with sterile water containing 3.5 g/L spectinomycin sulfate and 5 g/L Splenda for 3 days. Mice were fasted for 30 minutes prior to the introduction of bacteria. 100 μL 1M $NaHCO_3$ was then gavaged to each mouse to buffer stomach pH, followed by gavage with 100 μL of *V. cholerae* strains prepared as described above. Animals were sacrificed at 24 hours post-infection. Fecal samples were collected in 500 μL sterile 1x PBS for numeration. Intestinal tissue was dissected and homogenized in 5 mL sterile 1x PBS for numeration.

Fecal pellet collection

Fecal pellets were collected from adult CD-1 mice, weighted and resuspended in 500 µL of PBS in a 2.0 mL screw cap tube. The pellets were then disrupted by agitation using a bead beater (BioSpec) at 1400 rpm for 30 seconds. The resulting slurry was serial diluted and plated on LB with appropriate antibiotics for *V. cholerae* numeration.

V. cholerae in vitro **Penicillin V resistance assays**

Overnight *V. cholerea* cultures were 1:100 inoculated into fresh LB liquid media containing appropriate antibiotics at 37°C with agitation for 4 hours (OD_{600}≈0.35). 80 µL of the resulting cultures were then mixed with 40 µL LB liquid media supplemented with or without 2% (v/v) *Penicillin V* Potassium (pv, final concentration was 1%) in a 96-well plate at room temperature statically for 1 hour. The resulting slurry was serial diluted and plated on LB with appropriate antibiotics to determine survival rates.

VBH structure comparisons

The potential 3D structure models of proteins were constructed by Phyre2[169] by aligning amino acid sequences to known protein structure models in the database. The 3D structure comparison and root-mean-square distance (RMSD) per-column spatial variation among structures were calculated using UCSF developed Chimera (V1.14).

Effects of *vbh* expression on the growth of *V. cholerae* under bile acids *in vitro*

All *V. cholerae* strains were grown as overnight culture from glycerol stocks in LB media with appropriate antibiotics, sub-cultured 1:100 in LB media with appropriate antibiotics for ~5 hours at 37°C. Growth was measured by OD_{600} and cultures were diluted 1:1000 using LB media with appropriate antibiotic. 100 mM and 125 μM bile acids in DMSO were added to diluted *V. cholerae* cultures to a final concentration of 10 mM and 125 μM. 150 μL of each sample was loaded to a 96-well incubation plate in a plate reader (BioTek Synergy HTX multi-mode reader) shaking at 250 rpm at 37°C for 11 hours. Growth was measured by OD_{600} every 30 minutes. Each sample had three replicates.

***In vitro* preparation of samples for quantification of bile salts**

Evbh^{c} and the corresponding vector strain were grown overnight, sub-cultured at 1:100 in fresh LB with kanamycin for 48 hours. Growth was measured by OD_{600} and normalized to 1.5 mL of OD600=0.4 culture. All cultures were then centrifuged, aqueous layer removed, pellets washed twice with 1 volume of 1xPBS, and then resuspended in 1 volume of 1xPBS with different bile acids to a final concentration of 125 μM. Samples were then incubated for 48 hours at 37°C, centrifuged, supernatant filter-sterilized using a 0.22 μM filter. The resulting sample was desiccated using a SpeedVac Concentrator (ThermalFisher Scientific) and resuspended in one-fifth volume of sterile water. Four volumes of acetonitrile were then added, and samples were briefly vortexed and incubated at room temperature for 20 min for deproteinization. The aqueous layer was

desiccated using SpeedVac and resuspended in one and a half volume of methanol, incubated at 65°C for 10 min to assist dissolution, filtered as described above, and stored at -80°C for quantification of bile salts.

LC-MS measurements of bile acids

Standards for nine bile salts (TCA, GCA, TCDCA, TDCA, CA, GCDCA, GDCA, CDCA, and DCA) were used to determine retention times and fragmentation patterns for each compound. Chromatographic separations were conducted in a Waters I-class UPLC system using an Acquity UPLC BEH C18 column (2.1 × 100 mm, 1.7 μM; Waters). Water with 0.1% formic acid (A) and acetonitrile with 0.1% formic acid (B) were used as mobile phases. Sample separation was conducted after 1 uL injections with the column kept at 40 °C, with a flow rate of 0.4 mL/min under the following gradient: 0 min, 10% B; 1 min, 10% B; 1.5 min, 25% B; 8 min, 45% B, 10 min, 90% B; 16 min, 90% B, 17 min, 45% B, 19 min, 25% B; 21 min, 10% B; 26 min, 10% B.

Mass spectrometry measurements were conducted in a Synapt G2-Si quadrupole time-of-flight mass spectrometer (Waters). The instrument was operated in negative ion mode under MS/MS conditions with a source capillary voltage of 2.5 kV, source temperature of 150 °C, desolvation temperature of 600 °C and desolvation gas at 600 L/hr. Leucine enkephalin was used as lock spray standard for mass correction. The following retentions times and mass transitions (m/z) produced by the indicated collision energies (trap and transfer) were used for signal identification and relative quantitation of each bile acid: TCA, 5.09 min, 79.95 and 124.00 (CE 40 V); GCA, 6.13 min, 74.02 and 402.29 (CE 25

V); TCDCA, 6.72 min, 79.95 and 124.00 (CE 40 V); TDCA, 7.14 min, 79.95 and 124.00 (CE 40 V); CA, 7.81 min, 343.26 and 407.28 (CE 25 V), GCDCA, 8.15 min, 74.02 and 448.30 (CE 25 V); GDCA, 8.56 min, 404.30 and 448.30 (CE 25 V); CDCA, 9.57 min, 373.27 and 391.28 (CE 25 V); DCA, 9.68 min, 343.26 and 391.28 (CE 25 V). The Quanlynx software (Waters) was used for peak integration. The peak area for both monitored transitions were included for relative abundance calculations. A quality control sample for the experiment was produced by pooling equal amounts of sample and used to monitor system stability and reproducibility.

Quantification of *vbh* expression by qPCR

Overnight *V. cholerae* strains were sub-cultured at 1:100 in either LB or AKI and grown in a shaker at 37°C, and then cultures were collected at 6h and 24h. Total RNAs were then extracted by Trizol (Ambion) extraction, followed by cDNA synthesis with the SuperScript IV First-Strand Synthesis (Invotrogen) following manufactures' instructions. Reactions comprised 2 µL of cDNA as a template, 12.5 µL SYBR Green Master Mix (BioRad), 10 µL PCR-grade water, and 0.25 µL of forward and reverse primers of *vbh* at 10 µM (5'-GCCTCCTTCAGATACAGCATGT -3' and 5'-GGAACGGTTGGTGACAATCCA-3') and of reference gene *recA* at 10 µM (5'-ATTGAAGGCGAAATGGGCGATAG-3' and 5'-TACACATACAGTTGGATTGCTTGAGG-3'). Cycle conditions were 95°C for 3 min, followed by 39 cycles (95°C for 10 sec, 55°C for 30 sec, 95°C for 10 sec, 65°C for 5 sec, 95°C for 5 sec).

Construction of *E. coli* strains producing various BSH

The *bsh* genes from *V. cholerae* and *B. obeum* were codon-optimized for *E. coli* and placed downstream of the $P_{Ltet-O1}$ promoter derived from the plasmid vector pZE21. The constructs were cloned into PMK vector by the GeneArt Subcloning & Express Cloning Service (ThermoFisher). Then the constructs composed of a $P_{Ltet-O1}$ promoter, a codon optimized *bsh*, and a kan^R cassette were integrated into the *lacZ* gene in *E. coli* using Lambda Red recombineering system.

Preparation of BSH processed bile acids supernatants for *in vitro tcpA* induction

E. coli HS^{170} strains (expressing *bsh* or vector) were cultured overnight in LB supplemented with 50 μg/ml kanamycin and subcultured at 1 to 100 in fresh LB with 50 μg/ml kanamycin until OD_{600} reaches 0.3 to 0.5. Cultures were then normalized to 1.5 mL of OD600=0.4, centrifuged, aqueous layer removed, pellets washed twice with 1 volume of 1xPBS, and then resuspended in 1 volume of 1xPBS with different bile acids to a final concentration of 125 μM. Samples were then incubated at 37°C statically for 48 hours, and the supernatants were then collected via centrifugation and filtration using a 0.22 μM filter.

***In vitro tcpA* induction**

The $P_{tcpA\text{-}sh\text{-}ble}$ strain was cultured overnight, then diluted 1:1000 in fresh LB medium and incubated for 2 hours at 37°C. Each reaction was set up in 40 mL of 0.5X LB medium

adjusted to pH 8.5, supplemented with various bile acids including sodium taurocholate hydrate (TCA, Sigma-Aldrich), sodium glycocholate hydrate (GCA, Sigma Aldrich), cholic acid (CA, Alfa Aesar), sodium taurodeoxycholate hydrate (TCDCA, Sigma-Aldrich), sodium glycodeoxycholate (GCDCA, Sigma Aldrich), deoxycholic acid (DCA, MB Biomedicals), chenodeoxycholic acid (CDCA) and BSH producing *E.coli* HS incubated bile acids, to a final concentration of 125 μM. Subsequently, 2 μL of subcultured reporter strain was added, and the samples were incubated anaerobically at 37°C for 4 hours.

After incubation, 2 mL of each reaction was combined with 200 μL of 0.5X LB adjusted to pH 8.5 and supplemented with 10 mg/ml of zeocin (Sigma Aldrich). The mixture was then incubated aerobically at 37°C with agitation for 30 minutes, followed by serial dilution and plating onto LB agar plates containing streptomycin to determine survival rates.

Induction was calculated as the percentage of surviving $P_{tcpA\text{-}sh\text{-}ble}$ reporter cells after treatment with zeocin, relative to the average survival of control samples without zeocin and expressed as (zeocin-treated sample survival/average of no-zeocin controls) x 100. Survival rates were normalized to those induced by 125 μM taurocholate (CA).

Taxonomic characterization, BSH phylotype assignment, secretion prediction

425 amino acid sequences were obtained from the Kyoto Encyclopedia of Genes and Genomes (KEGG) using the EC designation "3.5.1.24". In addition to that, two *bsh* amino acid sequences from *Blautia obeum*, a *bsh* amino acid sequence of *Vibrio vulnificus*, a putative *bsh* amino acid sequence of *V. cholerae* were added to the list. Taxonomic information was obtained from the National Center of Biotechnology Information (NCBI). The final 428 BSH sequences were aligned with eight representing reference sequences[121] using BLASTP. The phylotype of each BSH was then assigned based on the highest sequence identity. Signal peptides of each BSH were predicted using SignalP (v 6.0).

Complete *V. cholerae* genomes present in NCBI NT database (downloaded 21 Sept. 2023) were screened for the presence or absence of *dnaA, vbh, ctxA,* and *tcpA* by BlastN v 2.14.1+ (-evalue 1e-30 -taxids 666). Further, the synteny of the ~15kb region surrounding *vbh* was examined using a combination of blastn and Mauve v2015-02-25 [171]. Strains without O-antigen predictions were analyzed and assigned to known or putative O-antigen groups with VicPred[172]. A core set of 291 *V. cholerae* genes [173] were then searched for in the complete *V. cholerae* genome assemblies in NT using BlastN. Sets of orthologous genes were individually extracted and aligned with Muscle v3.8.1551 [174] prior to being concatenated into a single multigene alignment. All gaps and invariant sites were removed leaving only SNP positions. This alignment was then used to reconstruct a maximum likelihood phylogeny using Fasttree v2.1.11[175] and RAxML

v8.2.12 on the CIPRES server [176,177]. The GTR substitution matrix was used, and bootstrapping was allowed to be automatically stopped. An identical process was used to identify, align, and generate a phylogeny for *vbh* homologs, except that invariant sites were retained after trimming. This included finding all *bsh* homologs in the KEGG database, identifying the top 26 homologs in the NR database, and all of the *vbh* homologs among the panel of *V. cholerae* genomes. The *vbh* alignment was also subjected to pairwise dN/dS estimates with PAML[178].

Quantification and statistical analysis

Statistical analyses were performed using GraphPad Prism Software (v9). Student's t-test was performed if data were deemed normally distributed. Mann-Whitney U test was performed if data were deemed not normally distributed. Comparisons where $P < 0.05$ were considered statistically significant. Results are representative of independent repeated experiments.

Results

VCA0877 Gene from *V. cholerae* encodes a bile salt hydrolase enzyme

Our previous studies indicated a role for commensal-encoded BSH enzymes in modulating gut bile acid pool composition and thus *V. cholerae* virulence gene activation. Since the action of commensal encoded BSH enzymes is critical for *V. cholerae* virulence regulation

and fitness, we wanted to examine possible contributions of *V. cholerae* to bile metabolism in the gut. Previous studies grouped different Bile Salt Hydrolase (BSH) enzymes in the gut microbiome into eight phylotypes based on sequence similarities and specific deconjugation activity against different types of target primary amino acid conjugated bile acids[121]. Using sequence comparisons to these BSH phylotypes, we found that *V. cholerae VCA0877* encodes a putative BSH homolog (Figure 2-1). We compared the amino acid sequences and predicted structures of VCA0877 with a representative type 6 BSH enzyme[121], and found 45.5% identity and 74.4% similarity of the amino acid sequences using ClustalW, accompanied by highly similar predicted structures using Chimera (Figure 2-1A to D), with a root-mean-square distance (RMSD) of 1.287 angstroms (Figure 2-1C).

To confirm the enzymatic activity of VCA0877 against amino acid conjugated bile acids, we constitutively expressed *VCA0877* in *E. coli DH5λpir* by cloning this locus downstream of a constitutive $P_{Ltet\text{-}O1}$ promoter in the pZE21 plasmid ($P_{Ltet\text{-}O1}$-*vbh*). We then incubated this strain with different forms of amino acid conjugated bile acids, including TCA and TDCA, but also glycine conjugated variants of these more commonly found in humans, as well as taurine and glycine-conjugated CDCA molecules much more abundantly found in humans compared to mice[128,129,140,141]. We then used mass spectrometry to determine the ratio of conjugated bile acids after incubation with *VCA0877*-expressing strains (Figure 2-1E), and found that this strain does not exhibit activity against previously-known virulence-activating bile acids like TCA and GCA, but that it is able to convert TDCA to DCA (Figure 2-1F).This aligns with Song et al.'s observations that type 6 phylotype BSH enzymes have

limited activity against TCA and glycocholic acid (GCA) but are more active against other less common bile acids[121]. This finding also suggests a potential preference of VCA0877 in deconjugating taurine-conjugated bile acids over glycine-conjugated ones. Strikingly, we also found that expression of the enzyme led to a substantially stronger deconjugation activity against CDCA derivatives that are common in humans but rare in mice (Figure 2-1E). However, the impact of conjugated vs deconjugated CDCA on *V. cholerae* remains largely unexplored. Taken together, our findings support the classification of VCA0877 as a type 6 VBH and thus we propose to name *VCA0877* as *vbh* (*Vibrio cholerae* bile salt hydrolase). Interestingly, *VCA0877* was previously characterized as a gene encoding a penicillin amidase under the direct negative control of the upstream virulence gene activator AphA[167]. While we demonstrate BSH activity for this gene product, our *in vitro* findings corroborate a role for VBH in penicillin response, with WT *V. cholerae* C6706 and a constitutive vbh^{C} generated by transferring our $P_{Ltet\text{-}O1}$-*vbh* constitutive expression plasmid into WT C6706 *V. cholerae* both showing significantly higher survival rates at 1% PV compared to a *Δvbh* strain generated by replacing the coding region of *vbh* with a spectinomycin-resistant cassette (Supplement. Figure 2-1).

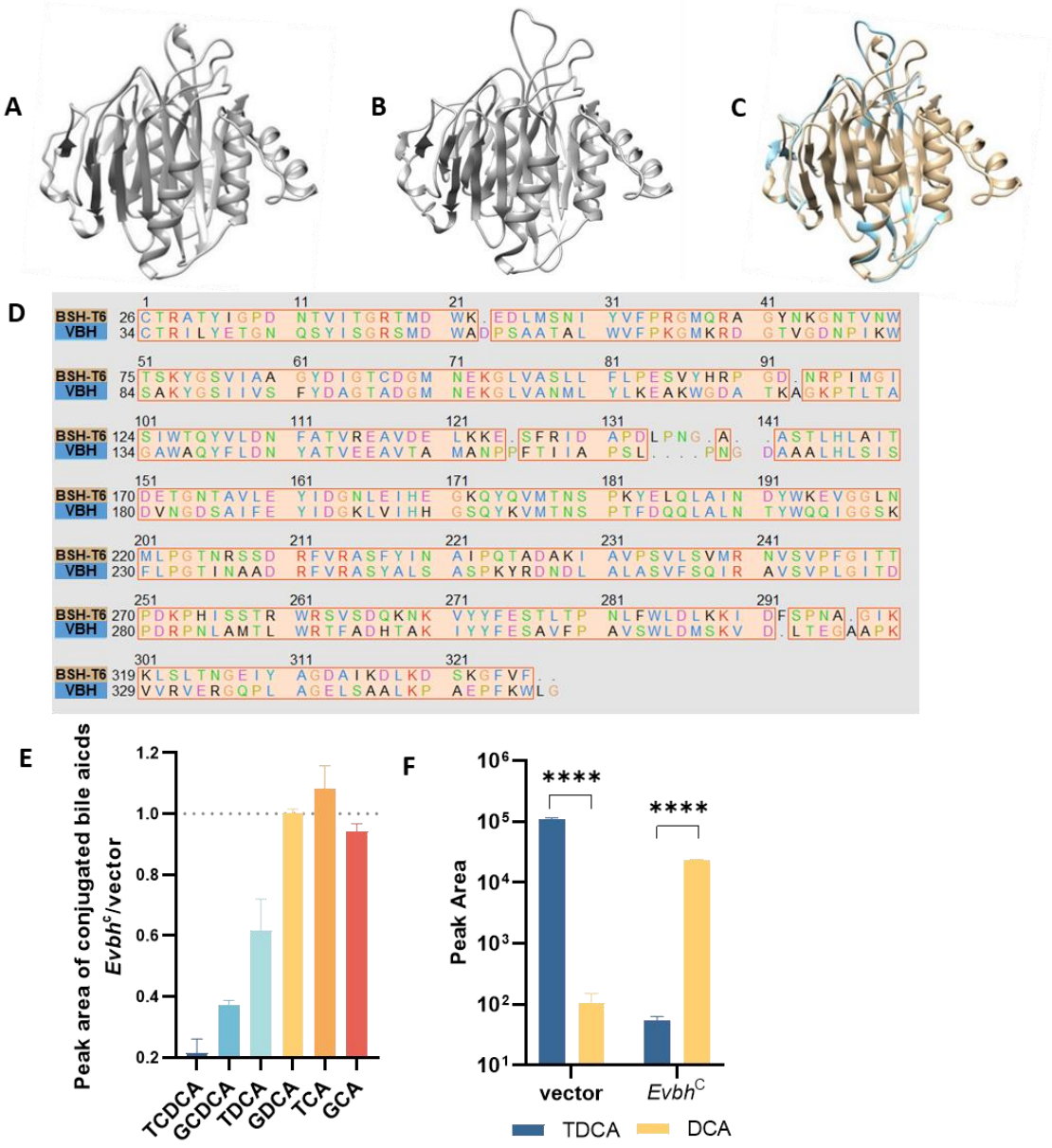

A
B
C
D
BSH-T6
VBH
E
Peak area of conjugated bile aicds
Evbh^c/vector
1.2
1.0
0.8
0.6
0.4
0.2
TCDCA
GCDCA
TDCA
GDCA
TCA
GCA
F
Peak Area
10^6
10^5
10^4
10^3
10^2
10^1
****
****
vector
Evbh^C
TDCA
DCA

Figure 2-1 VBH is a predicted phylotype 6 BSH.

(A) Predicted structure of consensus phylotype 6 BSH from song et al[121].

(B) Predicted structure of *V. cholerae* bile salt hydrolase VBH.

(C) Overlapping of predicted consensus phylotype 6 BSH and *V. cholerae* VBH. The root-mean-square deviation (RMSD) of atomic positions between phylotype 6 BSH and VBH. RMSD between 319 atom pairs is 1.287 angstroms. The blue ribbon indicates the part of VBH which does not match with the representing BSH-T6. There is a 45.5% identity and 74.4% similarity in 347 aa overlaps.

(D) Amino acid alignment of VBH and phylotype 6 BSH using ClustalW.

(E) Mass spectrometry of the deconjugation efficiency of $Evbh^{C}$ against the indicated of bile substrates (conjugated bile remaining in constitutive expressing strain / vector strain).

(F) Mass spectrometry measurements of bile acid levels in 125μM solutions of TDCA incubated with vector *E. coli* or $Evbh^{C}$. (n = 3, t test, *P < 0.05; **P < 0.01; ***P < 0.001; ****P < 0.0001; ns, not significant. Error bars represent mean ± SEM)

VBH is conserved across numerous pathogenic isolates

To begin to determine the potential importance of this locus to *V. cholerae* pathogenicity we evaluated 104 additional *V. cholerae* strains with complete genomes including 50 O1/O139 strains and 54 non-O1/O139 strains for the presence of *vbh*. The overwhelming majority of both groups encode an intact copy of *vbh,* 90% and 76% respectively (Figure 2-2A, Supplementary. Figure 2-2A). Notably, the five O1/O139 strains without *vbh* are also non-toxigenic and at least four were isolated from environmental sources (Figure 2-2A). Despite the widespread prevalence of *vbh* among *V. cholerae* strains, closely related orthologs were not detected in other *Vibrio* species. Phylogenetic reconstructions of genome encoded BSHs retrieved from KEGG (EC:3.5.1.24, KO:K01442) place VBH from *V. cholerae* far from those from marine vibrios (Figure 2-2B). Instead, it exhibits a greater similarity to the putative BSH of the human pathogen *V. vulnificus.* However, closer examination of homologs identified in NCBI NR database identifies the most closely related *vbh*-like homologs are in fact detected in a number of freshwater microbes including *Pseudomonas sp., Candidatus* Thiodictyon and *Cyanobium* sp. genomes (77 – 87% amino acid identity) (Figure 2-2C). This suggests that *vbh* may have been horizontally acquired by *V. cholerae* from an environmental microbe.

To further evaluate the possibility of HGT of *vbh*, we mapped the presence of *vbh* and the extent of synteny surrounding this locus on a core gene phylogeny for all 105 *V. cholerae* strains (Figure 2-2A). This analysis supports a single *vbh* acquisition by an ancestral *V. cholerae* strain, only to have been subsequently lost at least 7 times. This hypothesis is

further supported by broad concordance between the *vbh* phylogeny and that of the species tree (Supplementary. Figure 2-2A). We note that the region flanking the *vbh* locus shows evidence of both deletions and rearrangements, even among those strains that have retained *vbh* (Supplementary. Figure 2-2B). We speculate that this is exacerbated by the hypothetical gene cluster immediately downstream of *vbh* (VC_RS17510-VC_RS17540) with at least one ORF that has a partial match to IS3 family transposase (supplement Fig. 2B). Despite the volatility of this genomic region we observe evidence of purifying (negative) selection acting on *vbh* alleles. All but one of the O1/O139 strains' *vbh* alleles (45/46) are invariant, having estimates of 0 nonsynonymous changes per nonsynonymous sites (dN) and synonymous changes per synonymous sites (dS) compared to *V. cholerae* N16961 O1 El Tor. And among non-O1/O139 strains the pairwise dN/dS when compared to *V. cholerae* N16961 O1 El Tor is much less than 1 indicating purifying selection (0.160 ± 0.02 SE, *n*=40) is likely maintaining VBH function.

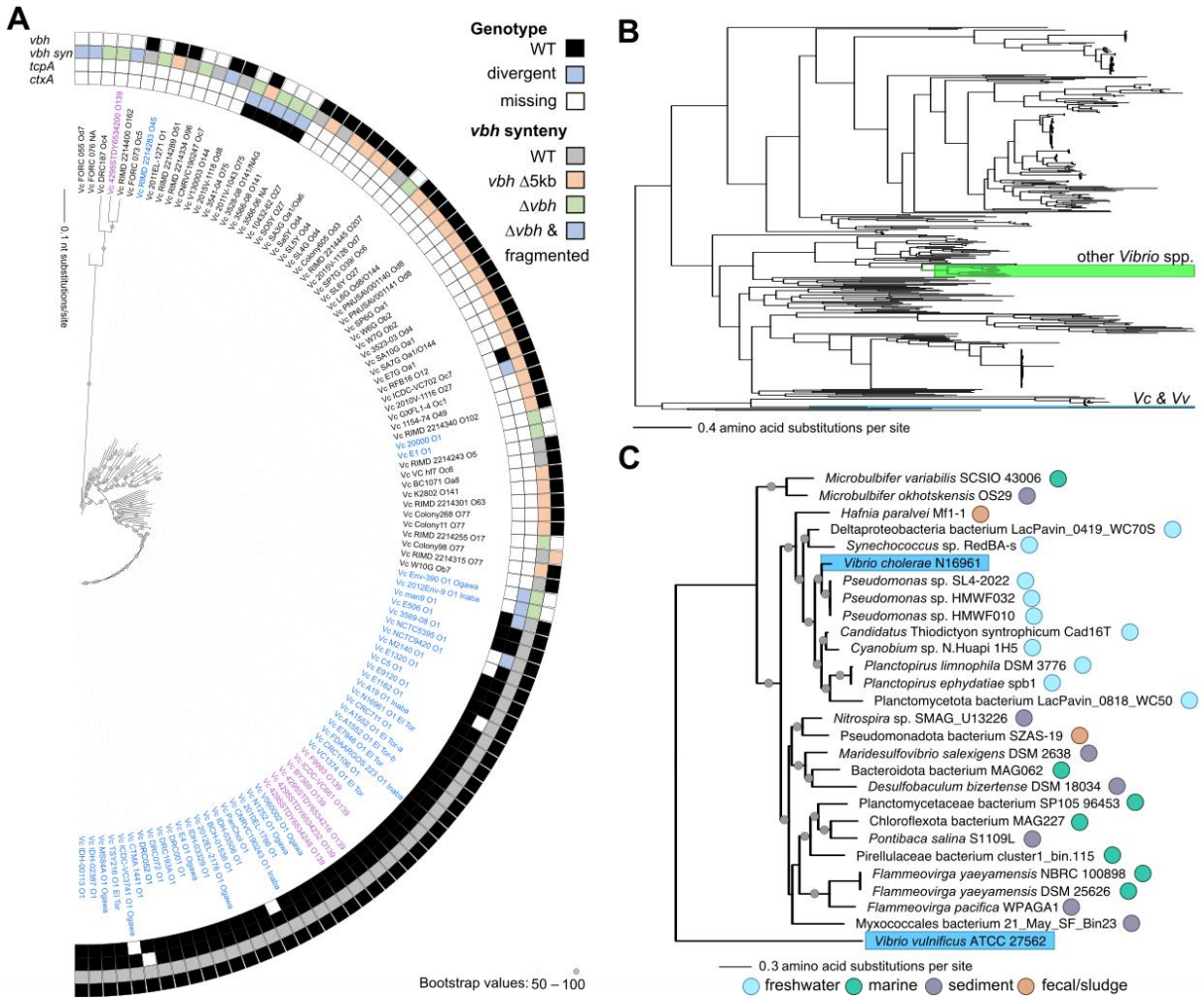


Figure 2-2. VBH is broadly conserved in *V. cholerae* but likely originated from HGT. **(A)** Core gene species phylogeny for 105 *V. cholerae* strains with their *vbh*, *tcpA* and *ctxA* character states indicated by the colored boxes according to the key. Strain names include known or predicted serotypes with O1 strains in blue font, and O139 strains shown in purple fonts. Bootstrap values ≥75% are shown as grey circles at the relevant node. (**B**) BSH phylogeny of proteins annotated by KEGG. Marine Vibrios are highlighted in green and the lineage representing *V. cholerae* and *V. vulnificus* is highlighted blue. (**C**) BSH phylogeny of *V. cholerae* and *V. vulnificus* BSH genes from **B** along with the top 26 non-Vibrio best blastp matches in NCBI NR database. Bootstrap values ≥75% are shown as grey circles at the relevant node.

Constitutive expression of *vbh* alters *V. cholerae* growth under bile acids

To investigate the effect of *vbh* expression on *V. cholerae* growth in the presence of bile acids, we manipulated *vbh* expression by generating a *V. cholerae* strain (vbh^c) that constitutively expressed *vbh* from a $P_{Ltet\text{-}O1}$ promoter on a plasmid in C6706 *V. cholerae* WT and created a *Δvbh* strain by replacing the coding region of *vbh* with a spectinomycin-resistant cassette. We inoculated 1:100 with overnight cultures of WT, vbh^C, and *Δvbh* at 1:100 vol/vol into LB supplemented with 1 mM or 125 μM of various bile acids dissolved in DMSO and measured the OD_{600} over 11h to access the impact of bile acids on the growth. The presence of 1 mM DCA significantly reduced the growth of all three *V. cholerae* strains after 1.5 ~ 2h incubation, but 1mM TDCA or GDCA did not strongly affect the growth of either WT or *Δvbh*, but strongly inhibited the growth of vbh^C (Figure 2-3A, supplement Figure 2-4). Additionally, the Area Under the Curve (AUC) of vbh^C under TDCA and DCA was significantly lower than under DMSO control conditions (Figure 2-3B). These data suggested that expression of VBH leads to deconjugation of T/GDCA and resulting growth inhibition in *V. cholerae* but that this gene is negatively regulated during *in vitro* growth in WT background.

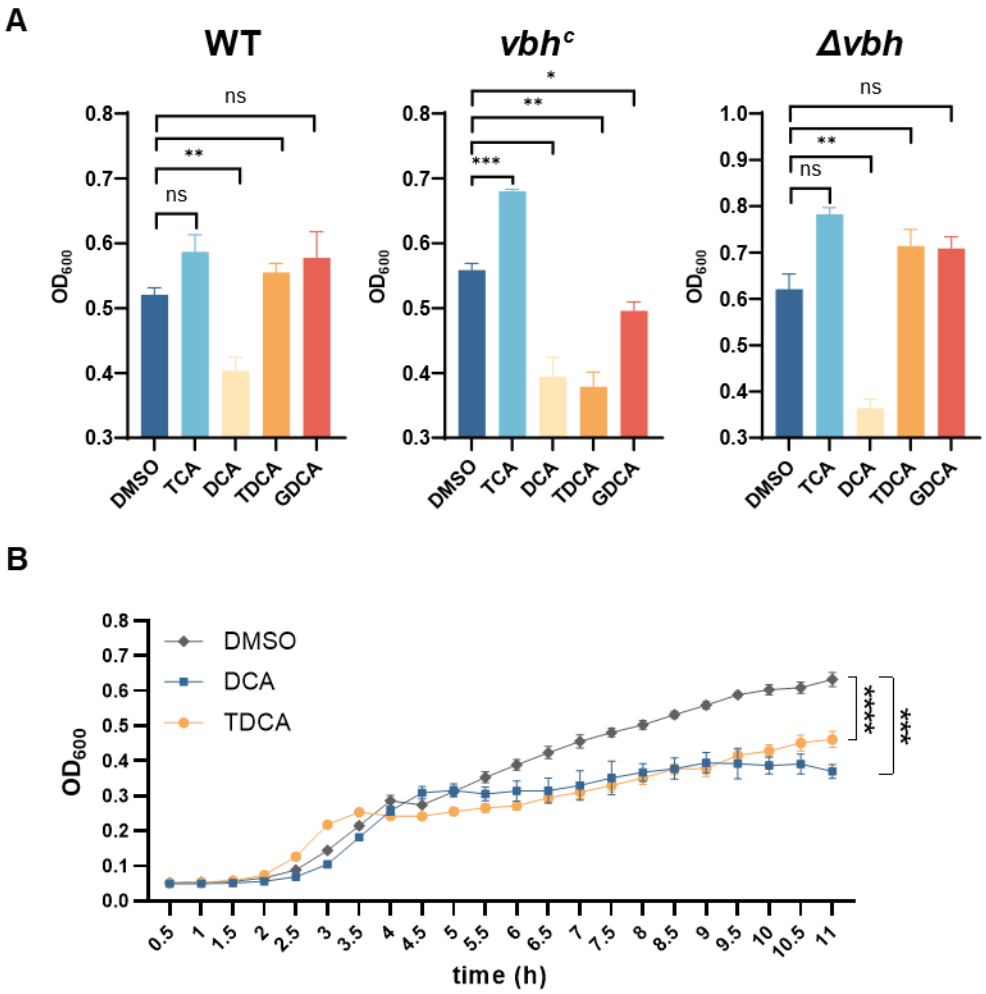


Figure 2-3. *vbh* expression has disadvantage effects on *V. cholerae in vitro* growth under 1mM TDCA.

(A) Effects of *vbh* expression on the growth of *V. cholerae* under 1mM of bile acids at 9 hours incubation.

(B) Growth curve of *vbh*^{c} under 1mM of DCA and TDCA or DMSO. Statistical analysis was tested based on Area Under the Curve (AUC). (n = 3, t test, *P < 0.05; **P < 0.01; ***P < 0.001; ****P < 0.0001; ns, not significant. Error bars represent mean ± SEM)

Constitutive *vbh* expression limits *V. cholerae* colonization in both suckling and adult mice

To further investigate the impact of *vbh* expression on *V. cholerae* colonization, we constructed two *vbh* constitutively expressing *V. cholerae* strains and tested their colonizations in animal models. In addition to *vbh*^{c} and Δ*vbh*, we replaced the native promoter of *vbh* with $P_{Ltet\text{-}O1}$, originated from plasmid vector pZE21, generating strain $P_{Ltet\text{-}O1}$-*vbh.* 4-day old SPF CD-1 suckling mice were provided with water supplemented with 3.5g/L streptinomycin and 5g/L Splenda for 4 days and then replaced with pure water 3 days beofore bacterial inoculation. Mice were buffered with $NaHCO_3$, and then gavaged with WT, $P_{Ltet\text{-}O1}$-*vbh*, or *vbh*^{c}. After 18 hours of infection, we collected and homogenized the intestines for enumerating colony-forming units (CFUs). Both strains that overexpress *vbh* showed significantly lower *V. cholerae* colonization levels in the whole intestines of suckling mice compared to WT *V. cholerae* (Figure 2-4A). In the case of *Δvbh*, we observed an enhanced colonization in the large intestine of suckling mice compared to WT (Figure 2-4B), underscoring the contribution of *vbh* repression to *V. cholerae* colonization. Given the higher bile concentration levels in adult mice[129,130] which could lead to more pronounced effects, we further investigated these outcomes in conventional adult mice. Both the WT and *Δvbh* strains displayed comparable colonization levels in the large intestines and feces 18 hours post-inoculation (Figure 2-4D and E). In the distal third of the small intestine, *Δvbh* exhibited a significantly higher colonization level (Figure 2-4C). This suggests that *vbh* needs to be repressed during

colonization for maximum *V. cholerae* fitness, and is consistent with prior reports of direct repression by AphA, which would be active during infection[167].

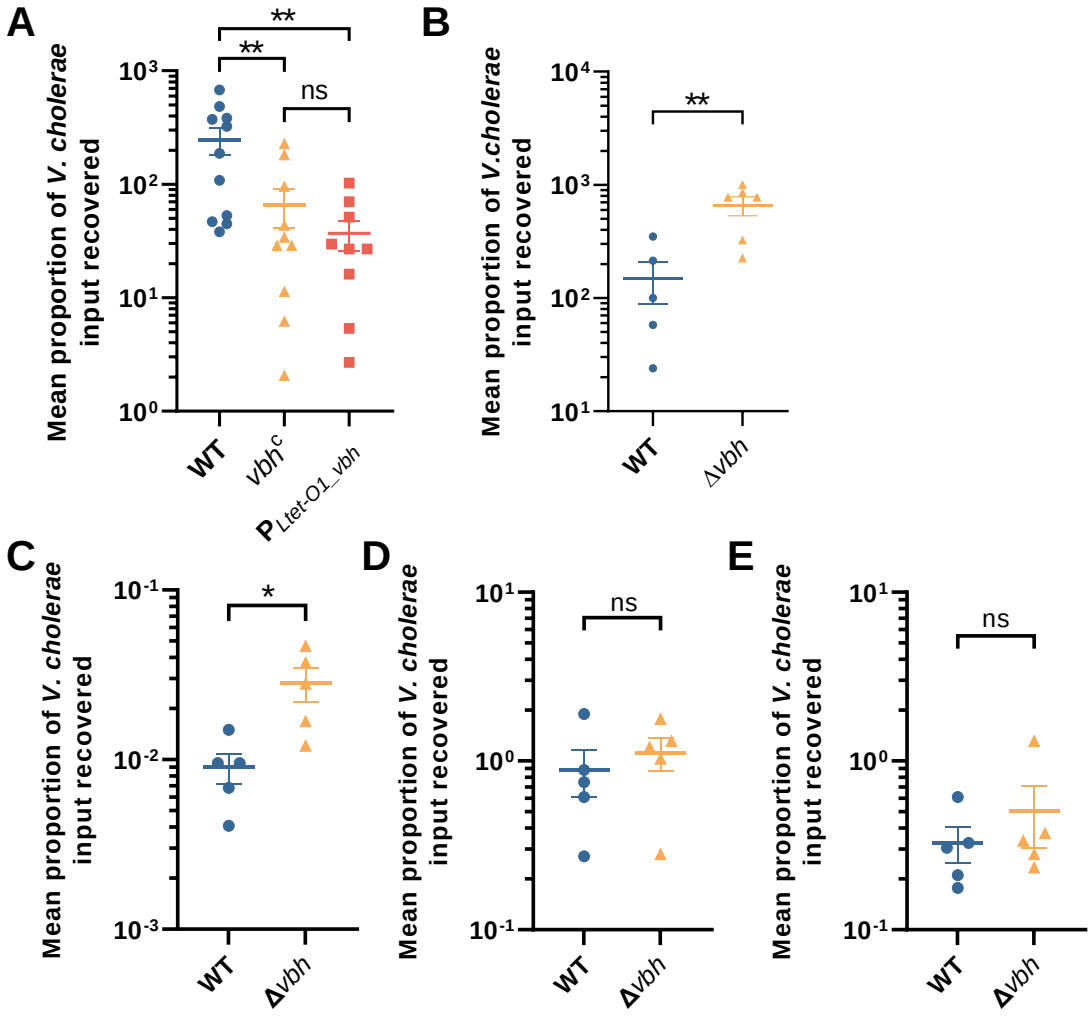


Figure 2-4. *vbh* negative regulates *V. cholerae* colonization *in vivo*.

(A) Mean *V. cholerae* (WT, vbh^c and $P_{Ltet\text{-}O1_vbh}$) colonization in suckling mice.

(B) Mean *V. cholerae* (WT and Δ*vbh*) colonization in the large intestine of suckling mice.

(C) Mean *V. cholerae* (WT and Δ*vbh*) colonization in adult mice (3rd distal small intestines) at day 1.

(D) Mean *V. cholerae* (WT and Δ*vbh*) colonization in adult mice (large intestines) at day 1.

(E) Mean *V. cholerae* (WT and Δ*vbh*) colonization in adult mice (feces) at day 1.

n = 5 to 11, Mann-Whitney U-test., *P < 0.05; **P < 0.01; ***P < 0.001; ****P < 0.0001; ns, not significant. Error bars represent mean ± SEM.

Regulation of *vbh* by AphA affects *V. cholerae* growth *in vitro*

We examined whether *vbh* expression was influenced by the presence of different bile acids. Using quantitative real-time reverse-transcriptase PCR (qRT-PCR), we found significantly increased levels of *vbh* transcript after incubation with 1mM DCA and TDCA for 4hrs compared to *recA* control transcripts (Supplement. Figure 2-5), suggesting that *vbh* was positively regulated by the presence of bile. To elucidate the regulatory relationship between *vbh* and AphA, we first conducted *in vitro* growth experiments using overnight cultures of both the WT and Δ*aphA* strains. Strains were sub-cultured at a 1:100 ratio in LB. Samples were collected at log (6-hour) and stationary (24-hour) time points, and *vbh* expression levels were quantified through real-time qRT-PCR. After 6 hours of incubation, we observed increased *vbh* expression in the Δ*aphA* strain in LB growth compared to WT (Figure 2-5A). After 24 hours of growth, even though the expression levels dropped, *vbh* expression remained higher in the *ΔaphA* strain (Figure 2-5A).

Based on our *vbh* expression analysis, we hypothesized that AphA repression would maintain *V. cholerae* fitness as it enters the virulence-activating and bile-rich environment of the small intestines by preventing accumulation of DCA from TDCA. To test this hypothesis, we assessed the OD_{600} of multiple *V. cholerae* strains cultivated in LB supplemented with 1mM TDCA. After 6.5 hours of incubation in LB medium, as anticipated, *Δvbh* displayed the most robust growth, whereas the growth of an *ΔaphA* strain, which we expect to be unable to repress *vbh* expression, was notably

impaired (Figure. 2-5B). A *ΔaphAΔvbh* double mutant exhibited significantly higher growth than *ΔaphA*, at levels almost identical to WT, further suggesting that AphA-mediated *vbh* repression was important to *V. cholerae* fitness in the presence of TDCA (Figure. 2-5B). In contrast, also as expected, the strain overexpressing *vbh* had the lowest growth under these conditions (Figure. 2-5B). Taken together these data aligns with previous reports that AphA, a crucial positive regulator of virulence, directly represses *vbh* transcription[167], maintaining *V. cholerae* fitness in high T/GDCA environments.

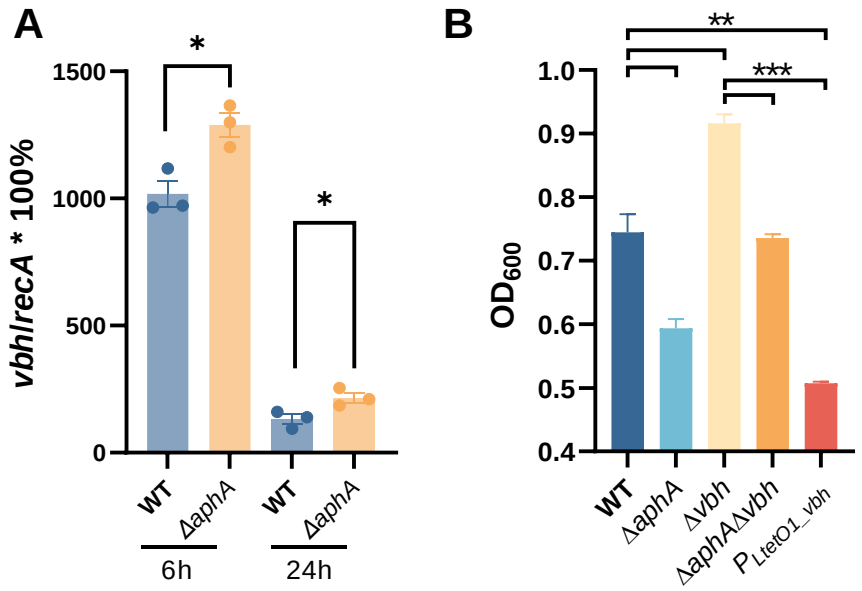


Figure 2-5. *aphA* negatively regulates *vbh* expression.

(A) *vbh* expression in *V. cholerae* WT and Δ*aphA* in LB at 6 and 24 hour-post incubation (hpi).

(B) OD_{600} of *V. cholerae* strains in LB with 1mM TDCA at 6.5 hpi.

n = 3, t test, *P < 0.05; **P < 0.01; ***P < 0.001; ****P < 0.0001; ns, not significant. Error bars represent mean ± SEM.

Regulation of *vbh* by AphA drives improved *V. cholerae* fitness *in vivo*

After establishing that *vbh* negatively impacts *V. cholerae* growth in the presence of TDCA, and that this effect can be controlled by AphA-dependent regulation, we sought to assess whether these effects similarly manifested *in vivo*. To investigate this, we examined the colonization levels of Δ*aphA* and Δ*aphA*Δ*vbh* in both suckling and adult CD-1 conventional mice. Since deletion of *aphA* would be expected to have non *vbh*-dependent colonization effects due to the critical role for AphA in colonization factor regulation, checking for the effects of deletion or expression of *vbh* in *ΔaphA* background allows for a direct examination of the role of this bile salt hydrolase in colonization. We found that deletion of *vbh* in Δ*aphA* significantly increased the colonization in the small intestines of suckling mice (Figure 2-6A), even though no difference in the large intestines (Figure 2-6B). To confirm that direct regulation of *vbh* by AphA was responsible for increased colonization, we compared the colonization of WT *V. cholerae* with strains where the putative AphA binding site in the *vbh* promoter was either randomized ($vbh^{P\text{-}Ran}$) or deleted completely($vbh^{P\text{-}Del}$). We found that interruption of AphA repression by either method inhibited *V. cholerae* colonization (Figure 2-6C). Notably, we observed no discernible differences in colonization levels in the large intestines and feces of adult mice one day post-inoculation, but significant better colonization in the distal small intestines (Figure 2-5C), consistent with the higher levels of bile acids to be expected in the proximal gut[179].

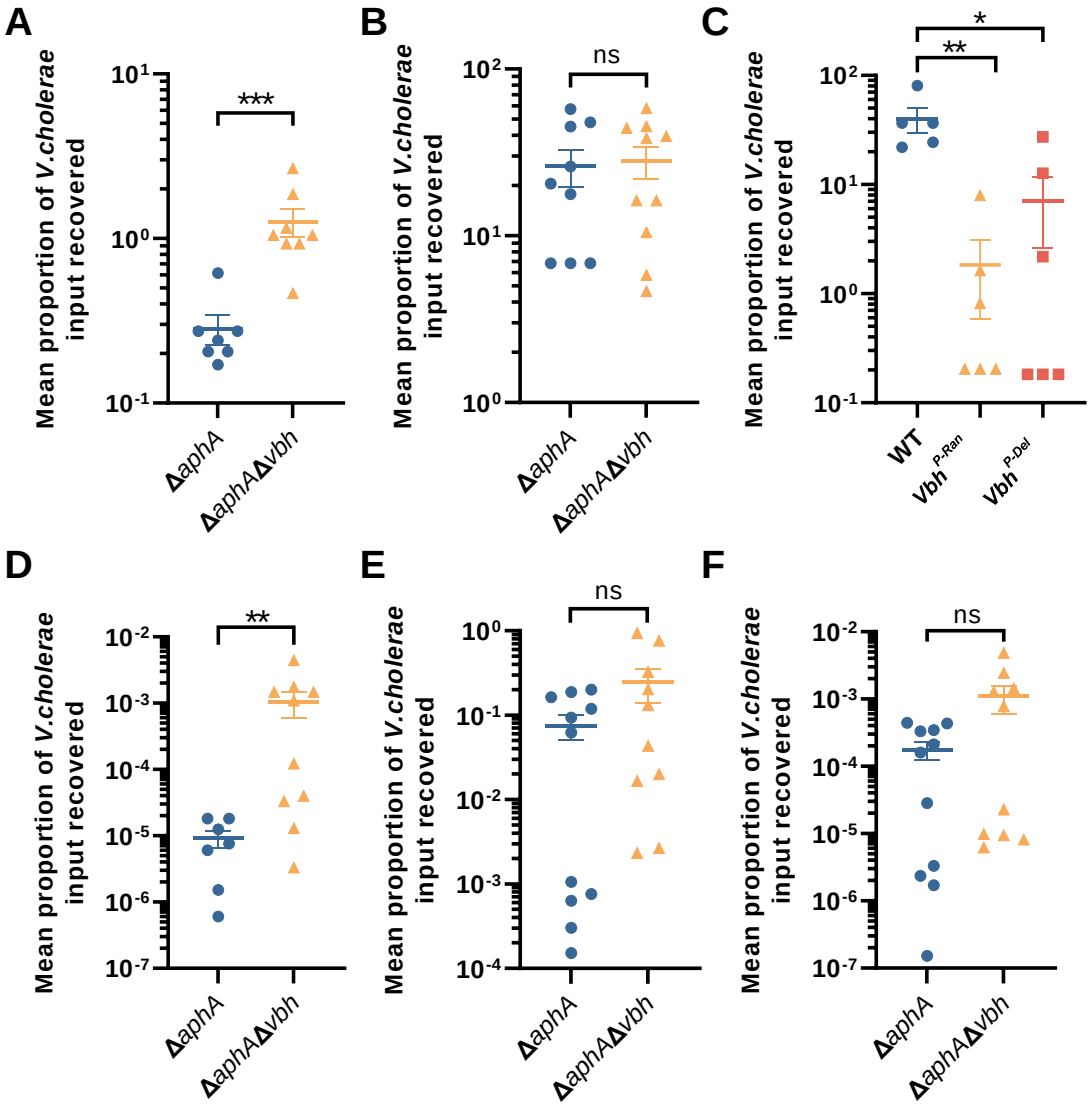

A
B
C
D
E
F
Mean proportion of V.cholerae input recovered
***
ns
*
**
ΔaphA
ΔaphAΔvbh
WT
Vbh P-Ran
Vbh P-Del

Figure 2-6. *aphA-vbh* regulation affects *V. cholerae* fitness in mice.

- **(A)** Mean *V. cholerae* (Δ*aphA* and Δ*aphA*Δ*vbh*) colonization in suckling mice (small intestines) at day 1.
- **(B)** Mean *V. cholerae* (Δ*aphA* and Δ*aphA*Δ*vbh*) colonization in suckling mice (large intestines) at day 1.
- **(C)** Mean *V. cholerae* (WT and *aphA* binding site mutants i) $vbh^{P\text{-}Ran}$, randomized mutation in *vbh* promoter ii) $vbh^{P\text{-}Del}$, deletion in *vbh* promoter) colonization in suckling mice at day 1.
- **(D)** Mean *V. cholerae* (Δ*aphA* and Δ*aphA*Δ*vbh*) colonization in adult mice (3rd distal small intestines) at day 1.
- **(E)** Mean *V. cholerae* (Δ*aphA* and Δ*aphA*Δ*vbh*) colonization in adult mice (large intestines) at day 1.
- **(F)** Mean *V. cholerae* (Δ*aphA* and Δ*aphA*Δ*vbh*) colonization in adult mice (feces) at day 1.

n = 6 to 11, Mann-Whitney U-test., *P < 0.05; **P < 0.01; ***P < 0.001; ****P < 0.0001; ns, not significant. Error bars represent mean ± SEM.

VBH converts a subset of bile acids into virulence activating forms

Given the importance of *vbh* regulation for optimal fitness of *V. cholerae in vitro* in the presence of TDCA and *in vivo*, we wanted to examine why this enzyme has been retained. Bile acids in humans are highly complex through cycles of microbial action, reabsorption by host, reconjugation to amino acids and re-secretion. We have examined TCA and TDCA effects on virulence and *in vitro* growth, but the effects on *V. cholerae* of the other substrate predicted by our mass spectrometry analyses (Figure 2-1E), conjugated chenodeoxycholic acids (CDCA), has not been extensively studied. CDCAs are abundant in the human gut[140] but largely absent from mice[128,129,141].

We used *E. coli* strains constitutively expressing BSH enzymes from *V. cholerae* and *B. obeum* via a $P_{Ltet\text{-}O1}$ promoter, with the expression construct integrated into the chromosomal *lacZ*. Using a *V. cholerae lacZ:*$P_{tcpA\text{-}sh\ ble}$ zeocin resistance *tcp* expression reporter, we examined the ability of products of BSH activity on TCA, TDCA, TCDCA to affect *V. cholerae* virulence gene expression. We observed that TCA, and TCA incubated with both *vbh* expressing *E. coli* and the isogenic parent strain were able to strongly induce *tcpA* gene expression (Figure 2-7A) compared to deconjugated or solvent control. In contrast, *B. obeum* BSH was able to ablate the ability of TCA to activate virulence (Figure 2-7A), as reported previously[149]. Strikingly, when we examined the role of CDCA derivatives, common in humans but not mice, in activating *tcpA*, we observed that taurine-conjugated TCDCA did not strongly induce virulence, but deconjugated CDCA was a potent activator of *tcpA* (Figure 2-7A). Since our mass spectrometry studies

suggested that VBH was an effective de-conjugating enzyme for T/GCDCA (Figure 2-1E), we examined whether constitutive expression of *vbh* was able to allow generation of virulence-activating molecules from TCDCA. When TCDCA was pre-incubated with VBH producing *E.coli* , the resulting supernatant induced significantly increased *tcpA* expression compared to TCDCA alone, or TCDCA incubated with *E. coli* isogenic vector strain (Figure 2-7B). We therefore speculated that VBH converts TCDCA to CDCA, thus promoting *V. cholerae* virulence gene expression.

To confirm this, we incubated VBH producing *E. coli* or vector with pure solutions of TCDCA in 1xPBS and incubated for 24h. The supernatant was collected, filtered sterilized, and used for mass spectrometry analysis. The result confirmed that VBH converts TCDCA to CDCA *in vitro* (Figure 2-7C and D), while CDCA was not detectable in the vector control (Figure 2-7D). This suggests that *V. cholerae* can convert TCDCA to CDCA via VBH, which may allow for fine tuning virulence expression in complex bile mixtures, depending on the relative abundance of TCA, TDCA, and TCDCA.

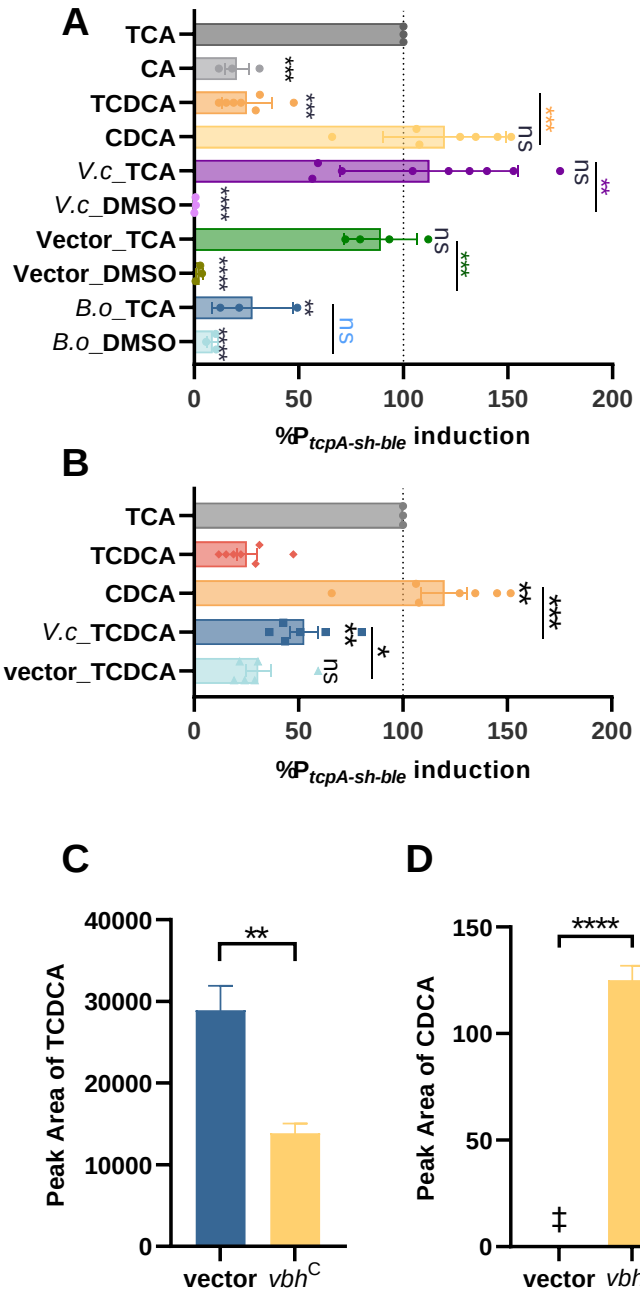

A
TCA
CA
TCDCA
CDCA
V.c_TCA
V.c_DMSO
Vector_TCA
Vector_DMSO
B.o_TCA
B.o_DMSO
0
50
100
150
200
%P tcpA-sh-ble induction
B
TCA
TCDCA
CDCA
V.c_TCDCA
vector_TCDCA
0
50
100
150
200
%P tcpA-sh-ble induction
C
Peak Area of TCDCA
40000
30000
20000
10000
0
vector
vbhC
D
Peak Area of CDCA
150
100
50
0
vector
vbhC

Figure 2-7. VBH converts a subset of bile acids into virulence activating forms.

(A) Effects of 125 μM pure bile acids or BSH producing *E. coli* treated bile acids on *V. cholerae tcpA* expression *in vitro*. Black asterisks or "ns" at the top of bars: Significance compared to 125 μM TCA. Colored asterisks or "ns": Significance between groups indicated by black lines. (n= 3 to 9, t test, *P < 0.05; **P < 0.01; ***P < 0.001; ****P < 0.0001; ns, not significant. Error bars represent mean ± SEM)

(B) VBH processed TCDCA induces *V. cholerae tcpA* expression *in vitro*. Black asterisks or "ns" at the top of bars signify significance compared to 125 μM TCDCA. Significance between groups is indicated by black lines. (n = 3 to 8, t test, *P < 0.05; **P < 0.01; ***P < 0.001; ****P < 0.0001; ns, not significant. Error bars represent mean ± SEM)

(C) TCDCA and **(D)** CDCA levels after 24-hour incubation of 125 μM TCDCA with *E. coli* vector and *Evbh*^{C} strains as measured by mass spectrometry. "‡" indicates no detectable targets. (n = 3, t test, **P < 0.01; ****P < 0.0001. Error bars represent mean ± SEM)

Discussion

In this study, we show that *V. cholerae* expresses a BSH, VBH, capable of deconjugating TDCA to DCA and TCDCA to CDCA, and that this has divergent substrate-specific effects on *V. cholerae* behavior *in vivo* and *in vitro*. We have also shown a novel role for CDCA as a potent activator of *V. cholerae* virulence gene expression; the ability of VBH to generate this metabolite from high CDCA environments such as the human gut is consistent with the high level of conservation of this enzyme among pathogenic *V. cholerae* isolates, alongside a role for the enzyme in resistance to pencillin[171] (Supplement. Figure 2-1) by hydrolyzing it to 6-aminopenicillanic acid (6-APA)[167]. In contrast, in TDCA rich environments, for example the mouse gut or in the gut of humans with high CA/CDCA ratios and commensals able to mediate 7α-dehydroxylation, VBH accumulates DCA that can inhibit *V. cholerae* colonization; *vbh* expression can be repressed by AphA to prevent severe effects on fitness during early infection until diarrhea can reduce the local concentration of bile. These findings are consistent with a model in which *V. cholerae* retains the VBH enzyme to modulate bile metabolism for optimal fitness depending on the specific microbial bile metabolism and thus bile acid pool composition of a given human host. Despite the general belief that bile acids are toxic to microbes, our findings show that lower doses of certain bile acids can promote the growth of *V. cholerae* (see Supplement. Figure 2-3). 125 μM DCA has minimal inhibition effects on *V. cholerae in vitro*. Nonetheless, the findings here suggest that the preferred rodent models for *V. cholerae* may not fully reveal the complexities of pathogen gene regulation in response to host-specific metabolites.

Bile is a key environmental factor of the mammalian gastrointestinal tract, regulate gut composition, and in turn the composition of the bile acid pool, generated by combined microbial and host metabolism, plays important roles in host processes such as immune cell development[180], influencing the colonization of gastric pathogens and the development of gastric diseases[181]. One key contributor to this to the diversity and ultimate function of bile is the activity of microbial bile salt hydrolases[182]. Studies have shown that DCA supplementation in mice leads to a decrease in BSH activity and alterations in the abundance of microbial taxa, with a decrease in Firmicutes and an increase in Bacteroidetes, specifically Parabacteroides and Bacteroides[183], indicating BSH may be capable of modulating the gut composition via its deconjugation activity of TDCA to DCA.

BSH's primary function involves removing amino acids conjugated to bile acids, facilitating bile acid recycling and modulating the composition of the bile acid pool. Bile acids are predominantly synthesized in the liver through two main pathways: the classical pathway and the alternative pathway, and both pathways give rise to CA and CDCA, albeit with differing proportions. Both CA and CDCA can be conjugated to amino acids and then secreted into the gut. The enzyme CYP8B1 appears to be crucial in regulating the ratio of CA to CDCA under normal physiological conditions[184,185]. In mice, CDCA is largely converted to muricholic acids, which we and others have shown to have little effect on virulence gene expression[149], but in humans, CDCA is retained, and the

CA/CDCA ratio varies heavily in human individuals[158–160]. Bile acids also exhibit varying concentrations along the gastrointestinal tract[128]. The small intestines, notably, host a high concentration of conjugated bile acids, with the majority of these being reabsorbed in the ileum and transported back to the liver through portal blood circulation, reducing availability in the colon[179]. The diversity of commensals leads to further diversification of the bile acid pool via BSH and 7α-dehydroxylation activity, followed by reabsorption, conjugation to new amino acids, and re-secretion, leading to highly complex and individual-specific collections of bile metabolites.

Conjugated bile acids, especially T/GCA, are believed to play a crucial role in driving intermolecular disulfide bond formation in TcpP[157], a process critical for activation of *toxT* transcription, ultimately leading to the induction of TCP and CT expression. While DCA is believed to enhance the interaction between ToxR and ToxS[148], thereby influencing TCP and CT expression in a manner that does not rely on ToxT[148,186], such activation is not very strong[163] (Supplement. Figure. 2-5). DCA also induces biofilm formation and confers resistance to stress in *V. cholerae*[187], but is inhibitory to *V. cholerae* growth *in vitro* and colonization (Figure 2-3 & 2-4). The precise mechanism of CDCA-dependent virulence gene regulation remains unclear though it may, similarly to TCA, induce post-translational changes in TcpP. The scarcity of CDCA in mice and the difficulty in introducing high levels of novel bile metabolites also complicates *in vivo* studies of this process.

It is increasingly evident that the structure of the gut microbiota plays a pivotal role in both host defense mechanisms[188] and *V. cholerae* fitness[149,49,189]. One mechanism by which this occurs is through adjusting BSH activities in the commensal microbiota. For example, *B. obeum* BSH deconjugates primary molecules TCA, TDCA to CA and DCA, respectively, leading to inhibition of *V. cholerae* colonization via virulence gene repression and reduced fitness from DCA activity [149,187]. Similarly, *Bifidobacterium bifidum* can prevent *V. cholerae* virulence activity via inhibiting the type VI protein secretion system (T6SS) from metabolism of GDCA, TDCA and CA into DCA[190]. However, while DCA accumulation can have broadly inhibitory effects on *V. cholerae*, VBH activity in high D/CA environments may confer advantages by locally inhibiting commensal competitors in the gut, while *V. cholerae* employs multiple strategies to resist bile acids. These mechanisms including regulating of expression of outer membrane porin genes (*ompU* and *ompT*) via ToxR[191,192], utilizing efflux pumps[193–196], and promoting bile resistance through quorum sensing and biofilm formation[142,187]. Among commensals, Studies have shown that DCA supplementation in mice decreases BSH activity and drives alterations in microbial taxa, with a decrease in Firmicutes and an increase in Bacteroidota, specifically *Parabacteroides* and *Bacteroides*[183]. *B. obeum* (Supplementary. Figure 2-6) and *Bifidobacterium longum*[183] are both highly DCA sensitive[149].

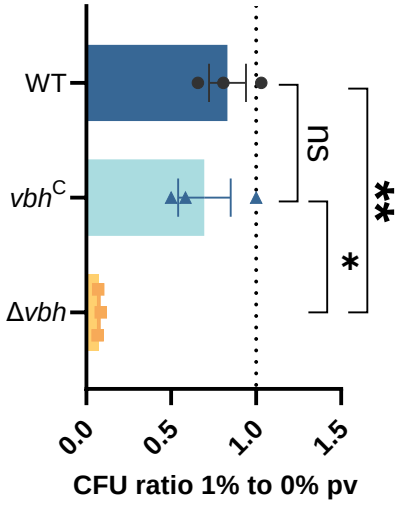
VCA0877 was previously characterized as a gene encoding a penicillin amidase under the direct negative control of the upstream virulence gene activator AphA [167]. Although we demonstrate *VCA0877* has BSH activity we were able to corroborate a role for VBH in *in*

vitro penicillin resistance (Supplement. Figure 2-1). Wildtype *V. cholerae* C6706 and a constitutive *vbh*^{C} generated by transferring our $P_{Ltet\text{-}O1}$-*vbh* constitutive expression plasmid into WT C6706 *V. cholerae* both exhibited significantly higher survival rates at 1% penicillin V compared to a *Δvbh* strain generated by replacing the coding region of *vbh* with a spectinomycin-resistant cassette (Supplement. Figure 2-1).We note that this dual functionality is reflected in motif predictions with overlapping matches to PFAM domains for choloylglycine hydrolases (PF02275) and 6-aminopenicillanic acid acyl-transferases (PF03417). While it is possible that VCA0877 acts as a multi-functional enzyme using penicillin as a substrate, the activity of this enzyme might contribute to penicillin resistance; indeed, penicillin susceptibility has long been known to be modulated by bile acids[200].

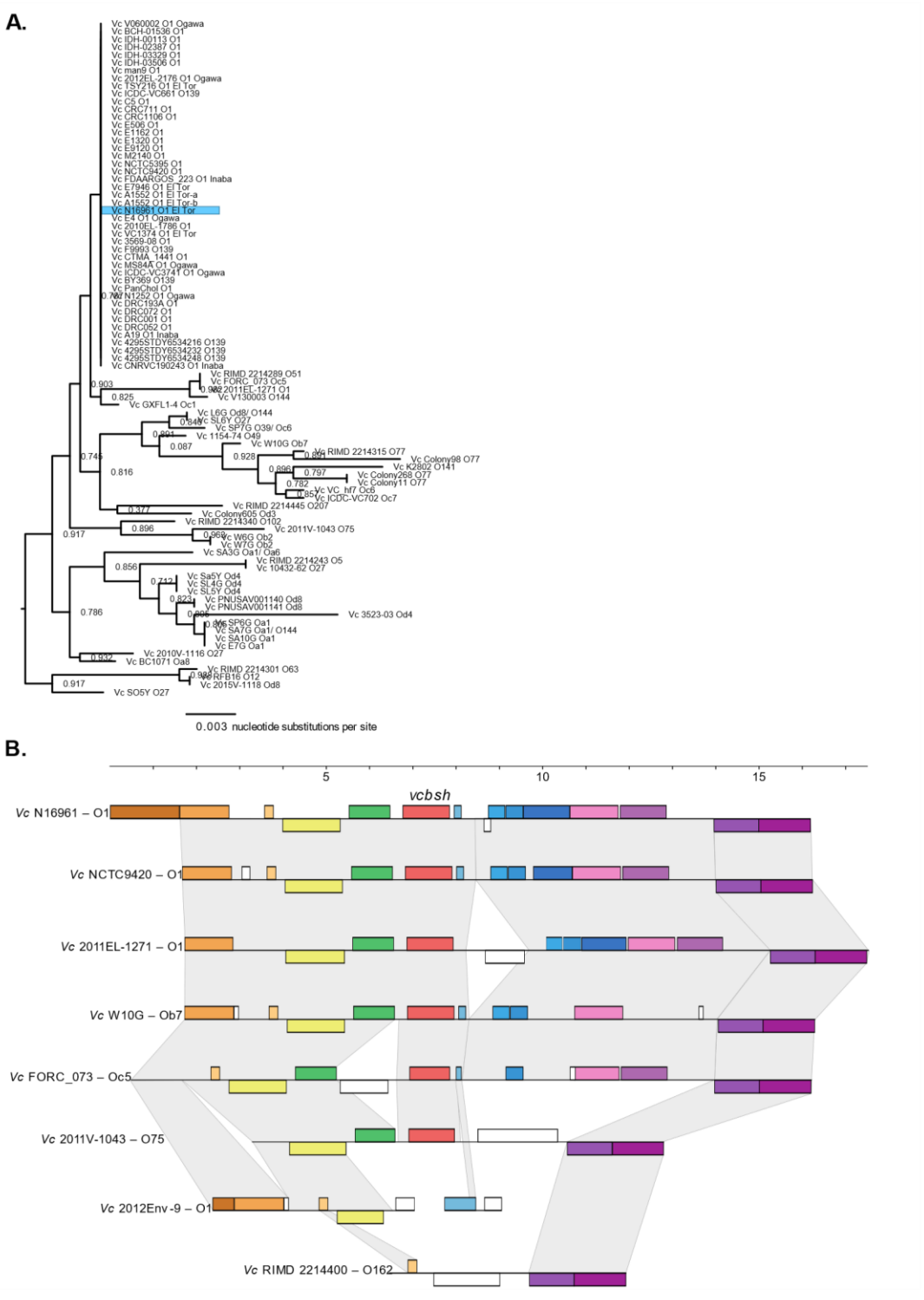
Future research can explore the diversity of BSH enzyme function in other gut microbes, *V. cholerae* strains and *Vibrio* species. Investigating how the expression and function of these enzymes within both pathogens and commensals influences relative competitive advantage of the microbes resident in and invading the gut may offer insights into how gut microbes have adapted to their host niche. Further, the presence of VBH homologs in numerous environmental strains raises intriguing questions about their importance in these contexts. The regulation of *vbh* in *V. cholerae* and the role of CDCA in *tcp* gene expression are also open areas of investigation. Since *aphA* is negatively regulated by multiple quorum sensing mechanisms, and *V. cholerae* virulence gene expression can be regulated by commensal autoinducers[49], including that of *B. obeum*, quorum sensing and

de-repression of *vbh* in high TDCA environments may synergize to promote infection resistance. Host diet is both able to induce bile acid secretion[197], and potently drive microbiome structure[198] , as well as playing a role in *V. cholerae* infection[150,199], and may also be a vector for future therapeutic approaches targeting commensals, bile, and personalized resistance to disease.

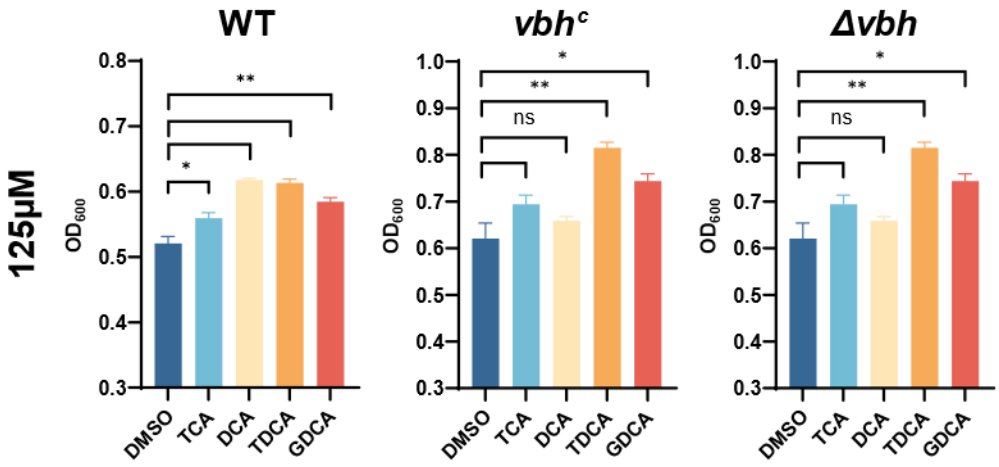
Supplements



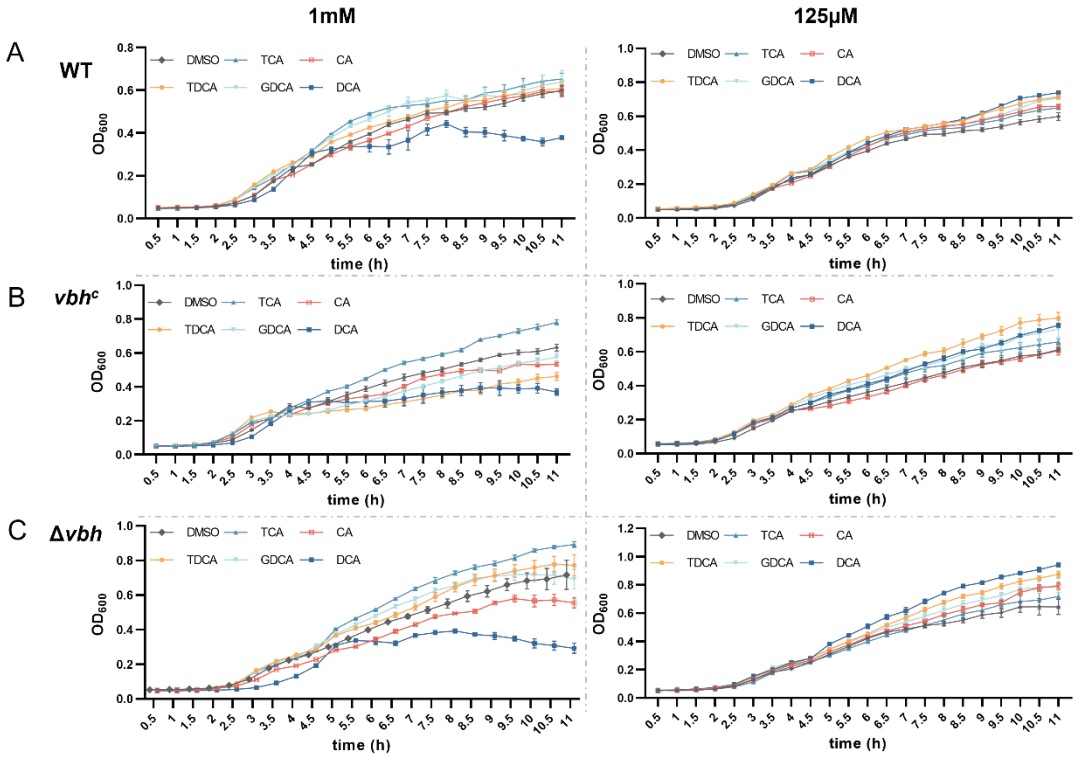
Supplement. Figure 2-1. VBH confers resistance to penicillin V *in vitro*. Ratio of V. cholerae CFU after 1 hour incubation with 1% and 0% PV *in vitro*. n = 3, t test, *P < 0.05; **P < 0.01; ***P < 0.001; ****P < 0.0001; ns, not significant. Error bars represent mean ± SEM.


A.
Vc V060002 O1 Ogawa
Vc BCH-01536 O1
Vc IDH-00113 O1
Vc IDH-02387 O1
Vc IDH-03329 O1
Vc IDH-03506 O1
Vc man9 O1
Vc 2012EL-2176 O1 Ogawa
Vc TSY216 O1 El Tor
Vc ICDC-VC661 O139
Vc C5 O1
Vc CRC711 O1
Vc CRC1106 O1
Vc E506 O1
Vc E1162 O1
Vc E1320 O1
Vc E9120 O1
Vc M2140 O1
Vc NCTC5395 O1
Vc NCTC9420 O1
Vc FDAARGOS_223 O1 Inaba
Vc E7946 O1 El Tor
Vc A1552 O1 El Tor-a
Vc A1552 O1 El Tor-b
Vc N16961 O1 El Tor
Vc E4 O1 Ogawa
Vc 2010EL-1786 O1
Vc VC1374 O1 El Tor
Vc 3569-08 O1
Vc F9993 O139
Vc CTMA_1441 O1
Vc MS84A O1 Ogawa
Vc ICDC-VC3741 O1 Ogawa
Vc BY369 O139
Vc PanChol O1
Vc N1252 O1 Ogawa
Vc DRC193A O1
Vc DRC072 O1
Vc DRC001 O1
Vc DRC052 O1
Vc A19 O1 Inaba
Vc 4295STDY6534216 O139
Vc 4295STDY6534232 O139
Vc 4295STDY6534248 O139
Vc CNRVC190243 O1 Inaba
Vc RIMD 2214289 O51
Vc FORC_073 Oc5
Vc 2011EL-1271 O1
Vc V130003 O144
Vc GXFL1-4 Oc1
Vc L6G Od8/ O144
Vc SL6Y O27
Vc SP7G O39/ Oc6
Vc 1154-74 O49
Vc W10G Ob7
Vc RIMD 2214315 O77
Vc Colony98 O77
Vc K2802 O141
Vc Colony268 O77
Vc Colony11 O77
Vc VC_hf7 Oc6
Vc ICDC-VC702 Oc7
Vc RIMD 2214445 O207
Vc Colony605 Od3
Vc RIMD 2214340 O102
Vc 2011V-1043 O75
Vc W6G Ob2
Vc W7G Ob2
Vc SA3G Oa1/ Oa6
Vc RIMD 2214243 O5
Vc 10432-62 O27
Vc Sa5Y Od4
Vc SL4G Od4
Vc SL5Y Od4
Vc PNUSAV001140 Od8
Vc PNUSAV001141 Od8
Vc 3523-03 Od4
Vc SP6G Oa1
Vc SA7G Oa1/ O144
Vc SA10G Oa1
Vc E7G Oa1
Vc 2010V-1116 O27
Vc BC1071 Oa8
Vc RIMD 2214301 O63
Vc RFB16 O12
Vc 2015V-1118 Od8
Vc SO5Y O27
0.003 nucleotide substitutions per site
B.
5
10
15
vcbsh
Vc N16961 – O1
Vc NCTC9420 – O1
Vc 2011EL-1271 – O1
Vc W10G – Ob7
Vc FORC_073 – Oc5
Vc 2011V-1043 – O75
Vc 2012Env-9 – O1
Vc RIMD 2214400 – O162

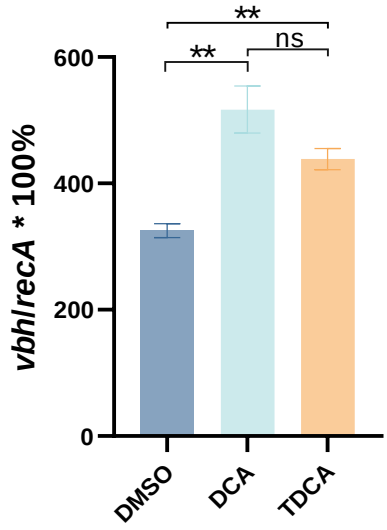
Supplement. Figure 2-2. Phylogenetic and syntenic examination of *vbh* loci in *V. cholerae*. (**A**) Phylogenetic reconstruction of 87 *V. cholerae vbh* alleles highlights the ~100% sequence identity among O1/O139 strains and broad similarity of the phylogeny with the species phylogeny. Bootstrap values above 75% are labeled adjacent to relevant node. **(B)** Representative alignment of *vbh* genomic locus in *Vc* N16961 with homologous regions of strains with and without *vbh* orthologs. Regions from representative strains were recovered based on Blastn results of the ~16kb region surrounding *vbh* in Vc N16961 and were then aligned with Mauve. Homologous gene predictions are shown with similar colors and are connected by grey shaded bars. Unique or hypothetical ORFs are shown in white. Note, genome Vc 2012Env-9 is a fragmented assembly and the only matching contigs are shown.



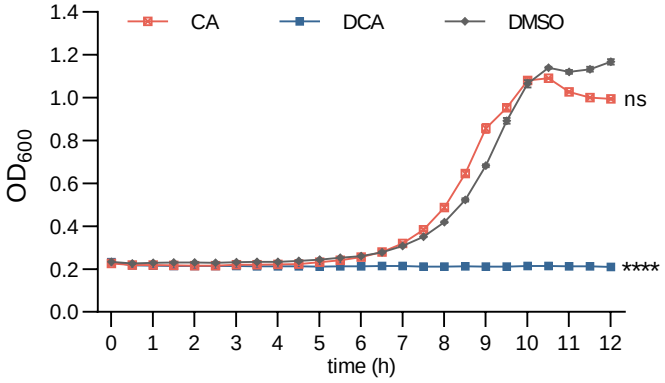
Supplement. Figure 2-3. Effects of *vbh* expression on the growth of *V. cholerae* under 125 μM of bile acids at 9 hours incubation.
(n = 3, t test, *P < 0.05; **P < 0.01; ***P < 0.001; ****P < 0.0001; ns, not significant. Error bars represent mean ± SEM)



Supplement. Figure 2-4. Effects of addition of various 1 mM and 125 μM BAs on *V. cholerae* strains. **(A)** WT, **(B)** *vbh*^{c}, **(C)** Δ*vbh* growth *in vitro*. n=3, error bars represent mean ± SEM.



Supplement. Figure 2-5. DCA and TDCA induce *vbh* expression *in vitro*.
n = 3, t test, *P < 0.05; **P < 0.01; ***P < 0.001; ****P < 0.0001; ns, not significant. Error bars represent mean ± SEM)



Supplement. Figure 2-6. Growth curve of *B. obeum* under 1mM of CA, DCA or DMSO. Area Under Curve (AUC) was used for statistical analysis. Comparisons were made between DMSO and bile acids. n = 3, **** P < 0.0001; ns, not significant. Error bars represent mean ± SEM.

Supplement. Table 2-1. List of strains and primers used in this study.

Strain/Plasmid	Genotype/sequence	Source
Bacterial strains		
Vibrio cholerae		
Wild type	C6706 El TorWild type SmR	Hsiao Lab stock
Δ*aphA*	C6706 El Tor Δ*aphA* SmR	Zhu Lab stock
Δ*vbh*	C6706 El Tor Δ*vbh* ::SpecR	This study
Δ*aphA* Δ*vbh*	C6706 El Tor Δ*aphA* Δ*vbh* ::SpecR	This study
$vbh^{P\text{-}Ran}$	aphA binding site 6 bp mutation on *vbh* promoter	This study
$vbh^{P\text{-}Del}$	aphA binding site 6bp deletion on vbh promoter	This study
P_{LtetO1_vbh}	C6706 El Tor with PLtetO1 promoter intergrated to upstream of *vbh* SpecR	This study
$P_{tcpA\text{-}sh\text{-}ble}$	zeocin resistance reporter *V. cholerae* C6706 El Tor strain	Liu et al. 2008
Escherichia coli		
$Evbh^{c}$	*E. coli* constitutively expressing *V. cholerae vbh* : *E. coli* DH5α-λpir pZE21- *vbh* , KmR	This study
E. coli	DH5α-λpir	Hsiao Lab stock
E. coli HS	A human isolate	DuPont et al. 1971
Plasmids		
pZE21	Vector used for *vbh* gene expression, donor of P_{ltet_O1} promoter	Kunjapur et al. 2018
pMK	Vector used for harboring *bsh* s from different bacteria	
pKD46	Vector used for intergrating bshs into the genome of *E.coli* HS	Datsenko and Wanner, 2000
Oligonucleotide primers (5′→3′)		
qRT-PCR		
aphA -F	GCAGAACCTTACCGTCTGCAA	Vikram et al. 2014
aphA -R	GCGTAATAAGCGGCTTCGATT	Vikram et al. 2014
vbh -F	GCCTCCTTCAGATACAGCATGT	This Study
vbh -R	GGAACGGTTGGTGACAATCCA	This Study
recA -F	ATTGAAGGCGAAATGGGCGATAG	Amin Marashi et al., 2013
recA -R	TACACATACAGTTGGATTGCTTGAGG	Amin Marashi et al., 2013
tcpA -F	GAAGAAGTTTGTAAAAGAAGAACACG	Fykse et al. 2007
tcpA -R	CGCTGAGACCACACCCATA	Alavi et al. 2020
Cloning		
vbh -F cloning primer	GAGGTCGACGGTATCGATATCACCAAAGAGGAATCAGAG	This Study
vbh -R cloning primer	GCTGCAGGAATTCGATATCATATCCTGATCATTCTGCC	This Study
pZE21 vector for *V. cholerae vbh* insertion by Gibson -F	TGATATCGAATTCCTGCAGC	This Study
pZE21 vector for *V. cholerae vbh* insertion by Gibson -R	TATCGATACCGTCGACCTC	This Study
PLtet-O1 cloning from pZE21 -F	AGACAATCAACGACAGGCTTTACTTTGCAGGGCTTCCC	This Study
PLtet-O1 cloning from pZE21 -R	CATGTGTTTCATCTTCATTGCGTTATCCCCTGATTCTG	This Study
PLtet-O1 insertion upstream fragment -F	GGCTCTGAAGAGTACACTG	This Study
PLtet-O1 insertion upstream fragment -R	GGGAAGCCCTGCAAAGTAAAGCCTGTCGTTGATTGTCT	This Study
PLtet-O1 insertion downstream fragment -F	CAGAATCA GGGATAACGCAATGAAGATGAAACACATG	This Study
PLtet-O1 insertion downstream fragment -R	AACGATGTAATAATTTGCGC	This Study
vbh deletion uppstream fragment -F	CGTAAATTGTGTGTGTTTAAAATGGC	This Study
vbh deletion upstream fragment -R	GTCGACGGATCCCCGGAATTGATCAGGATATTGCGGTGA	This Study
vbh deletion Downstream fragment -F	GAAGCAGCTCCAGCCTACATCAGGATATTGCGGTGACTA	This Study
vbh deletion Downstream fragment -R	TCAATAACCAAACTTATTAATAAGCCTAATG	This Study
Spectinomycin resitance cassette replacement -F (ABD123)	ATTCCGGGGATCCGTCGA	This Study
Spectinomycin resitance cassette replacement -R(ABD124)	TGTAGGCTGGAGCTGCTTC	This Study
aphA binding site mutation upstream fragment -F	GAGTATCATAGCGCCCAAGC	This Study
aphA binding site mutation upstream fragment -R	GTGTACCGTTTGCTTTATACAGAACTGTATTGAGAGGCGC	This Study
aphA binding site mutation downstream fragment -F	GTATAAAGCAAACGGTACACAAATTACACATGTGTTGTAT	This Study
aphA binding site mutation downstream fragment -R	GCGGTATCAACATTTGGGCT	This Study
aphA binding site deletion upstream fragment -F	GAGTATCATAGCGCCCAAGC	This Study
aphA binding site deletion upstream fragment -R	ACAACACATGTGTAATTTGTTTTGCTTTATACAGAACTGT	This Study
aphA binding site deletion downstream fragment -F	ACAGTTCTGTATAAAGCAAAACAAATTACACATGTGTTGT	This Study
aphA binding site deletion downstream fragment -R	GCGGTATCAACATTTGGGCT	This Study

Chapter 3.1 AI-2 signals affect microbiome through modulating secondary bile acid synthesis

Abstract

Quorum sensing (QS) plays a crucial role in bacterial communication and coordination of population-wide behaviors. This study investigates the impact of Autoinducer-2 (AI-2), a universal QS signaling molecule, on the gut microbiome. Specifically, we investigated how AI-2 produced by *Blautia obeum* and *Streptococcus* impacts the colonization of *Vibrio cholerae* and the commensal microbiota compositions and functions. We demonstrated that AI-2 produced by *Blautia obeum* significantly downregulates the expression of bile acid inducible (*bai*) genes in *Clostridium scindens*, a key player in secondary bile acid synthesis. This downregulation leads to reduced conversion of primary bile acid cholic acid (CA) to the more toxic secondary bile acid deoxycholic acid (DCA).

Our findings suggest a novel mechanism where AI-2 signaling modulates gut microbiome composition by regulating bile acid metabolism. This interplay between quorum sensing and bile acid transformation offers new insights into microbial community dynamics. Further research is needed to fully elucidate the molecular pathways involved.

Introduction

Quorum sensing (QS) is a biological process through which bacteria communicate with each other by releasing and detecting signaling molecules called autoinducers (AIs), and enable them to collectively regulate gene expression and coordinate behavior based on the density of the bacterial population on a community-wide scale, such as bioluminescence, production of virulence factors, DNA exchange, and biofilm formation[35–38]. QS mechanisms exist in both Gram-positive and Gram-negative bacteria, but they differ in their signal molecules and regulatory pathways. In Gram-positive bacteria, small peptides or modified oligopeptides serve as signaling molecules, while in Gram-negative bacteria, QS typically involves the production and detection of acyl-homoserine lactones (AHLs). Autoinducer-2 (AI-2), catalyzed by the LuxS enzyme, is a universal signaling molecule in both Gram-positive and Gram-negative bacteria. Bacteria within the gut generate a variety of AIs, contributing to the complexity of bacteria-bacteria interactions. Studies found that the expression of *Blautia obeum luxS* gene alone is capable of lowering *V. cholerae* colonization in germ-free mouse model[49]. An *E. coli* strain lacking the AI-2 kinase gene *lsrK* exhibited a significant increase in the ratio of Firmicutes to Bacteroidetes[66]. These observations underscore the impact of AI-2 levels on shaping the abundance of the major phyla in the gut.

Bile is a mixture of fluid produced by the liver and stored in the gallbladder, comprising bile acids, cholesterol, bilirubin, electrolytes, and water. Bile acids serve critical functions in metabolism, gene regulations, and microbiome composition. Microbes in the gut can

transform bile acids in different ways, which can lead to formation of different bile acids with altered physiological functions.

Clostridium scindens is a prevalent bacterium inhabiting the human gut and is recognized as one of the primary anaerobic microorganisms responsible for bile acid 7-dehydroxylation. This enzymatic process involves the removal of a hydroxyl group at the C7 position of primary bile acids, leading to the formation of 7-dehydroxylated bile acids. These metabolites constitute a significant proportion of the secondary bile acid pool within the gut ecosystem. The 7-α dehydroxylation pathway requires seven proteins encoded by a bile-acid-induced (*bai*) operon (BaiB, BaiA2, BaiCD, BaiF, BaiE, BaiN, BaiO or BaiA2 in order) to convert primary bile acid cholic acid (CA) to secondary bile acid deoxycholic acid (DCA)[122], which is considered one of the most toxic bile acids because of its hydrophobic and detergent like properties[111]. Studies have found that *C. scindens* can resist *C. difficile* infection in mice in a secondary bile acid synthesis dependent manner[201,202]. Thus, the bile acid pool composition may eventually impact the gut community structure and disease development.

Our investigation delves into the intersection of these phenomena, revealing novel insights into the interplay between AI-2 signaling and bile acid metabolism within the gut microsystem. Through *in vitro* and *in vivo* analyses, we demonstrate that AI-2 signals produced by *B. obeum* inhibit *V. cholerae* colonization and gut microbiome composition. Furthermore, our study uncovers a regulatory link whereby AI-2 signals from *B. obeum*

downregulate *bai* gene expression in *C. scindens*, attenuating DCA production and highlighting a previously unexplored facet of AI-2-mediated microbial interactions.

Materials and Methods

Integration of AI-2 expression genes into *E. coli*

The *luxS* genes from *B. obeum* (from genome position 33,305 to 33,784) and *S. infantarius* (from genome position 414,476 to 414,994) were codon-optimized for *E. coli* BW30045 (Δ*luxS*) and placed downstream of the $P_{Ltet-O1}$ promoter derived from the plasmid vector pZE21. The constructs were cloned into PMK vector by the GeneArt Subcloning & Express Cloning Service (ThermoFisher). Then the constructs composed of a $P_{Ltet-O1}$ promoter, a codon optimized *luxS*, and a kan^R cassette were integrated into the *endA* gene in *E. coli* BW30045 using Lambda Red recombineering system using primers listed in the supplementary table 3.1-1.

AI-2 signal production

AI-2 expressing *E. coli* BW30045 or vector *E. coli* BW30045 (Δ*luxS*) strains started from glycerol stocks in LB media with appropriate antibiotics at 37°C shaking at 250 rpm overnight, and then were subcultured with a ratio of 1:100 into fresh LB media without antibiotics. OD_{600} was monitored constantly until it reached 0.20 to 0.22. Cultures were then centrifuged, and supernatants were filtered with 0.22 μM filters.

Bioluminescence assay of AI-2 signal

AI-2 activity was accessed using a previously published method[203]. Briefly, BB170 (a *Vibrio harveyi* AI-2 reporter strain) was grown in Luria-marine (LM) medium at 30°C overnight and then was diluted at 1:1000 into AI bioassay (AB) medium[204]. 90 µL of the diluted BB170 was mixed with 10 µL of filtered AI-2 supernatants in a 96-well plate, and the plate was incubated at 30°C with shaking at 175 rpm for 3h. Luminescence and OD_{600} were then measured immediately. AI-2 signal activity was calculated as Luminescence/OD_{600}. All AI-2 signals were conducted in triplicates.

RNA extraction from *C. scindens* cultures supplemented with CA and AI-2 signals.

C. scindens ATCC 35704 was started from glycerol stocks in LYH-BHI media in anaerobic chamber (5% H_2, 20% CO_2, balance N_2) at 37°C without agitation for 14h, subcultured 1: 6 in fresh LYH-BHI medium for 5h. Growth was measured by OD_{600} and normalized to 3 mL of OD_{600}=0.3 culture for each reaction. All cultures were then centrifuged, aqueous layer removed, and then resuspended in 3 mL of LYH-BHI supplemented with 3 mM CA dissolved in DMSO and 2 mL of AI-2 signals from *E. coli* BW30045 expressing *B. obeum luxS* or 2 mL of supernatants collected from *E. coli* BW30045(Δ*luxS*). Samples were then incubated in anaerobic chamber (5%H_2, 20% CO_2, balance N_2) at 37°C without agitation for 5h. 2 mL culture was centrifuged at 12,000 rpm for 3 min at 4°C. The supernatant was discarded and resuspended in 1 mL TRIzol to

extract total RNA according to manufacturer's instruction. DNA was removed and total RNA was cleaned up and concentrated using RNA Clean & Concentrator Kits (catalog no. R1013; Zymo).

Reverse transcription and quantitative of *bai* operon expression

Concentration and purity of DNA-depleted RNA was measured with a plate reader (BioTek Synergy HTX multi-mode reader). 800 ng of RNA was reverse transcribed into cDNA with the SuperScript IV First-Strand Synthesis (catalog no. 18091050, Invitrogen) following manufacturers' instructions. RT-qPCR Reactions comprised 2 µL of 1:5 diluted cDNA as a template, 12.5 µL SYBR Green Master Mix (BioRad), 10 µL PCR-grade water, and 0.25 µL of forward and reverse primers (supplementary table) at 10 µM. All runs were performed with the following program: 95°C for 3 min, followed by 39 cycles (95°C for 10 sec, 55°C for 30 sec, 95°C for 10 sec, 65°C for 5 sec, 95°C for 5 sec).

Growth curve testing

B. obeum and *C. scindens* ATCC 35704 started from glycerol stocks in LYH-BHI media in anaerobic chamber (5%H_2, 20% CO_2, balance N_2) at 37°C without agitation for 14h and was subcultured with the ratio of 1:100 and 1:20 into fresh LYH-BHI medium until they reached the early stationary phase. For testing the effect of pure bile acids on *C. scindens* and *B. obeum*, growth was measured by OD_{600}, and cultures were normalized and diluted to OD_{600}=0.004 using LYH-BHI media supplemented with bile acids to a final

concentration of 1 mM and 125 μM. 150 μL of each sample was loaded to a 96-well incubation plate in a plate reader without agitation for 24h. For testing the effect of CA incubated with *C. scindens* and AI-2 on *B. obeum* growth, 100 μL of *B. obeum* at OD_{600}=0.004 in LYH-BHI medium and 50 μL of the filtered supernatants from *C. scindens* incubated with 3 mM CA and AI-2 signals were mixed in each well. For testing the effects of AI-2 signals on *C. scindens* and *B. obeum*, 100 μL of the bacterial culture at OD_{600}=0.004 in LYH-BHI medium and 50 μL of the AI-2 supernatants were mixed in each well. Growth was measured by OD_{600} every 30 minutes. Each experimental group was performed with three biological replicates.

In vitro preparation of samples for quantification of bile acids

C. scindens ATCC 35704 was started from glycerol stocks in LYH-BHI media in anaerobic chamber (5% H_2, 20% CO_2, balance N_2) at 37°C without agitation for 14h, subcultured 1: 6 in fresh LYH-BHI medium for 5h. Growth was measured by OD_{600} and normalized to 3 mL of OD_{600}=0.5 culture for each reaction. All cultures were then centrifuged, aqueous layer removed, and then resuspended in 3 mL of LYH-BHI supplemented with 125 μM CA dissolved in DMSO and 2 mL of LuxS supernatants from *Blautia Obeum* or 2 mL of supernatants collected from *E. coli* Δ*luxS*. Samples were then incubated in anaerobic chamber (5% H_2, 20% CO_2, balance N_2) at 37°C without agitation for 12h. 2 mL LuxS supernatants were added and mixed by pipetting, and incubated for another 12h. Samples were then centrifuged, supernatant filter-sterilized using a 0.22 μM filter. For each reaction, 500 μL of the resulting sample was desiccated using a SpeedVac Concentrator (Thermal

Fisher Scientific) and resuspended in 100 µL sterile water. 400 µL of acetonitrile were then added, and the sample was briefly vortexed and incubated at room temperature for 20 min for deproteinization. The aqueous layer was desiccated using SpeedVac and resuspended in 800 µL of methanol, incubated at 65°C for 10 min to assist dissolution, filtered as described above, and stored at -80°C for quantification of bile acids.

LC-MS measurements of bile acids

Standards for CA and DCA were used to determine retention times and fragmentation patterns for each compound. Chromatographic separations were conducted in a Waters I-class UPLC system using an Acquity UPLC BEH C18 column (2.1 × 100 mm, 1.7 µM; Waters). Water with 0.1% formic acid (A) and acetonitrile with 0.1% formic acid (B) were used as mobile phases. Sample separation was conducted after 1 µL injections with the column kept at 40°C, with a flow rate of 0.4 mL/min under the following gradient: 0 min, 10% B; 1 min, 10% B; 1.5 min, 25% B; 8 min, 45% B, 10 min, 90% B; 16 min, 90% B, 17 min, 45% B, 19 min, 25% B; 21 min, 10% B; 26 min, 10% B.

Mass spectrometry measurements were conducted in a Synapt G2-Si quadrupole time-of-flight mass spectrometer (Waters). The instrument was operated in negative ion mode under MS/MS conditions with a source capillary voltage of 2.5 kV, source temperature of 150°C, desolvation temperature of 600°C and desolvation gas at 600 L/hr. Leucine enkephalin was used as lock spray standard for mass correction. The following retentions times and mass transitions (m/z) produced by the indicated collision energies (trap and

transfer) were used for signal identification and relative quantitation of each bile acid: CA, 7.81 min, 343.26 and 407.28 (CE 25 V), GCDCA, 8.15 min, 74.02 and 448.30 (CE 25 V); DCA, 9.68 min, 343.26 and 391.28 (CE 25 V). The Quanlynx software (Waters) was used for peak integration. The peak area for both monitored transitions were included for relative abundance calculations. A quality control sample for the experiment was produced by pooling equal amounts of sample and used to monitor system stability and reproducibility.

Preparation of bacteria strains for testing AI-2 effects on *C. scindens* colonization in conventional CD-1 mice

C. scindens ATCC 35704 was started from glycerol stocks in LYH-BHI media in anaerobic chamber (5% H_2, 20% CO_2, balance N_2) at 37°C without agitation overnight and subcultured with the ratio of 1:100 into fresh LYH-BHI media for 16-20h. All *E. coli* BW30045 *luxS* expressing strains were started from glycerol stocks in LB media at 37°C shaking at 250rpm overnight and then was subcultured with the ratio of 1:100 into fresh LB at 37°C shaking at 250 rpm for ~4h until OD_{600} reached 0.4. *C. scindens* and *E. coli* BW30045 *luxS* expressing strains were normalized to OD=0.4, and each mouse received a mixture of 300 μL of that mass of *C. scindens* and 300 μL of that mass of *E. coli* BW30045. For each gavage volume, the 600 μL mixed cultures were pelleted and concentrated to 200 μL in fresh LYH-BHI under anaerobic conditions. The resulting mixed cultures were sealed in vials for gavage.

In vivo testing on *C. scindens* and *E. coli* co-colonization in conventional CD-1 mice

5- to 8-week-old specific pathogen free (SPF) CD-1 female mice were purchased from Charles River Laboratories. Mice were given an antibiotic cocktail *ad libidum* in drinking water (1 g/L ampicillin, 1 g/L neomycin, and 125 mg/L vancomycin) supplemented with 5 g/L for seven days and then the cocktail was replaced by autoclaved pure water for 3 days. Mice were fasted for 30min and were subsequently gavaged with 100 μL of 1M $NaHCO_3$ 20 min prior to bacterial inoculation. Fecal pellets were collected and half of the pellets were homogenized in 500 μL 1xPBS by agitation (BioSpec bead beater without beads) at 1400rpm for 30s, followed by serial dilution of resulting suspensions and spotting on LB agar containing appropriate antibiotics for CFU enumeration of *E. coli* BW30045 and DNA extraction, and the other half of the pellets were homogenized in 1mL TRIzol using a similar method as described above for RNA extraction. Mice were sacrificed at 2 day-post inoculation. The 3rd distal small intestines, cecum and large intestines were collected separately and homogenized in 5 mL 1xPBS for CFU counts of *E. coli* BW30045 and DNA and total RNA extraction.

DNA/RNA extraction from fecal, intestinal and cecum samples from *C. scindens* and *E. coli* co-colonized CD-1 mice

500 μL homogenates of fecal, intestinal and cecum samples were used for DNA extraction. Briefly, 500 μL homogenates, 210 μL 20% SDS, and 500 μL phenol:chloroform:isoamyl-alcohol (24:24:1, pH 6.9, Fisher Scientific) were added to bead-beating tubes with 0.1mm

glass beads (BioSpec) and shaking at 2400 rpm for 5 min. DNA were purified and precipitated as described previously[49].

For fecal samples, homogenates in 1 mL TRIzol were used for total RNA extraction according to manufacturer's instruction. DNA was removed and total RNA was cleaned up and concentrated using RNA Clean & Concentrator Kits (catalog no. R1013; Zymo).
For intestinal and cecum samples, 500 µL homogenates in 1xPBS were centrifuged at 12,000g for 3min at 4°C and resuspended in 1 mL TRIzol in bead-beating tubes without beads, followed by agitation (BioSpec bead beater) at 1400 rpm for 30s. DNA was removed and total RNA was cleaned up and concentrated using the same method as fecal samples.

qPCR Quantification of *C. scindens* in *C. scindens* and *E. coli* co-colonized CD-1 mice

Colonization levels of *C. scindens* in CD-1 mice was determined by quantitative PCR using DNA extracted from the fecal and intestinal samples as templates. All DNA samples were diluted at 1:100 to 1:1000. qPCR Reactions comprised 2 µL of diluted DNA as templates, 12.5 µL SYBR Green Master Mix (BioRad), 10 µL PCR-grade water, and 0.25 µL of *C. scindens* specific *recA* forward and reverse primers (supplementary table 3.1-1) at 10 µM. All runs were performed with the following program: 95°C for 3 min, followed by 39 cycles (95°C for 10 sec, 55°C for 30 sec, 95°C for 10 sec, 65°C for 5sec, 95°C for 5 sec).

Statistical Analysis

Statistical analyses were performed using GraphPad Prism Software (v9). Generally, Student's t-test was performed if data were deemed normally distributed. Mann-Whitney U test was performed if data were deemed not normally distributed. Specifically, for comparing OD_{600} of *B. obeum* at specific time point, one-way ANOVA test was used to assess overall differences among treatments, followed by a Dunnett multiple comparison test for specific group disparities. Student's t-test was used to analyze qRT-PCR results and Mass Spectrometry results. Comparisons where $P < 0.05$ were considered statistically significant. Results are representative of independent repeated experiments.

Results

RNA seq results reveal downregulation of secondary bile acids biosynthesis related genes regulated by *B. obeum* AI-2

In a previous study, we co-inoculated the defined resistant and susceptible human model microbial communities (Table 3.1-1) with the constructed *E. coli* that overexpresses *B. obeum* or *S. infantarius* AI-2 synthase LuxS in a gnotobiotic mouse model. RNAseq analysis of the mouse feces collected at day 3 post-inoculation revealed a down-regulation of the secondary bile acid biosynthesis in *C. scindens* in the presence of overexpressed *B. obeum luxS* (Figure 3.1-2A), but not differential expressed in the *S. infantatius luxS* expressing group (Figure 3.1-2B). The *bai* operon is responsible for the 7α -dehydroxylation of the primary bile acids to the relatively more toxic secondary bile

acids[9]. In this case, genes that were detected in the *bai* operon (baiA-F, H) were down-regulated in *B. obeum luxS* expressing group (Figure 3.1-3A).

Table 3.1-1 List of bacterial strains in the model community. Species that contain *luxS* gene are boldly highlighted.

Resistant	Susceptible
Dorea longicatena	***Escherichia coli (luxS-, B. obeum luxS, S. infantarius luxS)***
Bacteroides caccae	***Streptococcus infantarius***
Bacteroides vulgatus	***Enterococcus faecalis***
Dorea formicigenerans	***Streptococcus salivarius***
Collinsella aerofaciens	***Streptococcus thermophilus***
Ruminococcus torques	
Eubacterium rectale	
Faecalibacterium prausnitzii	
Bacteroides thetaiotaomicron	
Blautia obeum	
Clostridium scindens	
Bactreroides uniformis	
Bifidobacterium longum	

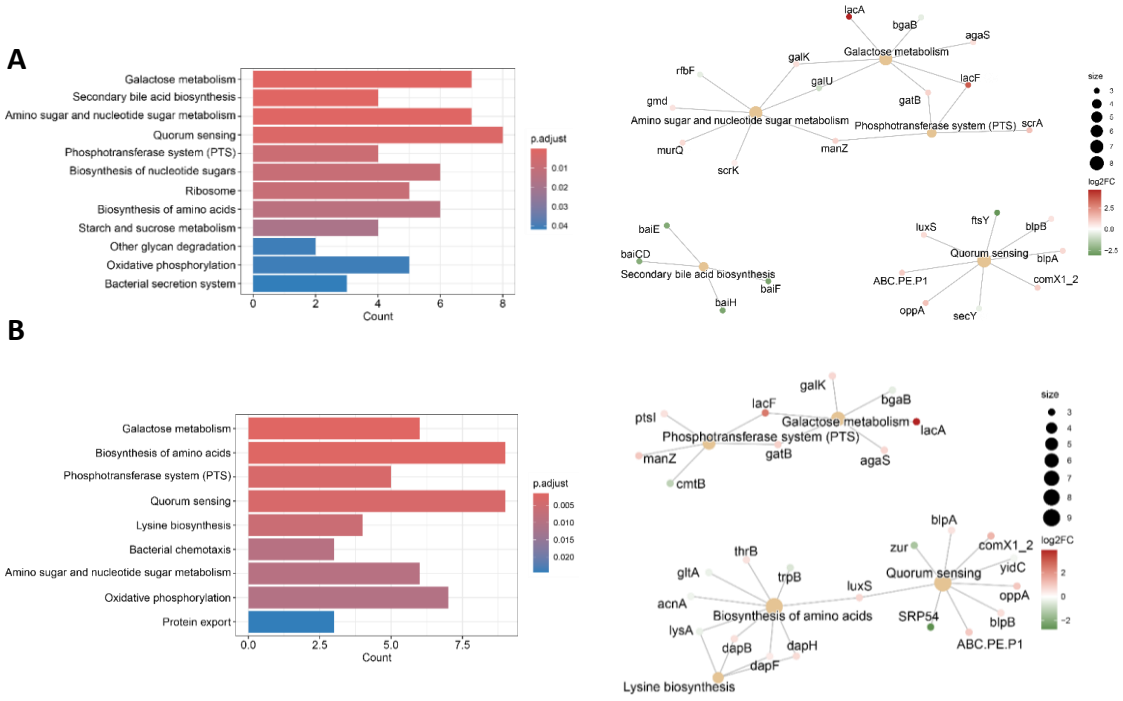


Figure 3.1-1. Pathways and related genes that are regulated by AI-2 signals in the model community. (A) enriched pathways by significantly differential expressed genes (DEGs, FDR<0.05, |Fold Change|≥2) regulated by *B. obeum* AI-2 signal produced in E. coli vector at day 3 in adult germ-free mice fecal pellets (left). Network of the top 5 enriched pathways with DEGs (right). **(B)** enriched pathways by significantly differential expressed genes (DEGs, FDR<0.05, |Fold Change|≥2) regulated by S. infantarius AI-2 signal produced in *E. coli* vector at day 3 in adult germ-free mice fecal pellets (left). Network of the top 5 enriched pathways with DEGs (right).

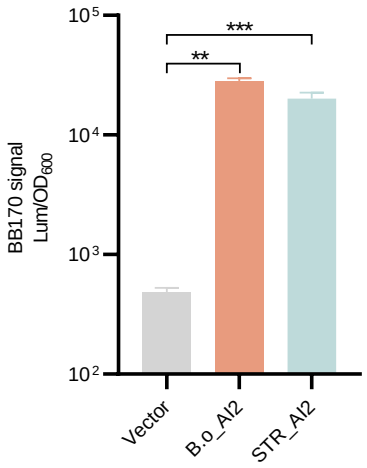


Figure 3.1-2. AI-2 signal detection from *luxS* expressing *E.coli* (BW30045) strains. n =3, t test, ** p<0.01, *** p<0.001. Error bars represent mean ± SEM.

In vitro validation of *B. obeum* AI-2 effects on *bai* genes expression

Based on the described RNA-seq results, we aimed to elucidate whether the observed downregulation of *bai* genes *in vivo* was specific or if it could be triggered solely by expressing *B. obeum luxS*. To address this, we conducted an incubation experiment wherein *C. scindens* was exposed to 3 mM CA in fresh LYH-BHI medium supplemented with either supernatant harvested from an *E. coli* strain expressing *B. obeum luxS*, or control supernatants obtained from an *E. coli ΔluxS* strain, over a duration of 5h. We detected strong AI-2 signals of *B. obeum* and *S. infantarius* compared to the vector control strain using BB170 (*V. harveyi* AI-2 reporter) method (Figure 3.1-2), indicating the strains are producing functional LuxS enzyme that producing detectable AI-2 signals. The qRT-PCR results revealed a significant decrease in the expression of *baiE* and *baiF*, which encode the rate-limiting enzyme bile acid 7-α dehydratase and bile acid-CoA

hydrolase, respectively, upon addition of *B. obeum luxS* supernatants (Figure 3.1-3B). Conversely, no significant expression differences were observed for *baiH* and *baiCD*, despite a trend towards reduced expression following the addition of *B. obeum luxS* supernatants (Figure 3.1-3B). While addition of *S. infantarius luxS* supernatants did not change *baiE* and *baiF* expressions (Figure 3.1-4B). This suggests that *B. obeum luxS* supernatants alone are sufficient to downregulate the expressions of *baiE* and *baiF* in *C. scindens in vitro*. However, it appears that a more substantial reduction in the expression of these *bai* genes may require an *in vivo* environment.

B. obeum AI-2 alleviate the negative effects from bile acids by downregulating _bai_ gene expression in _C. scindens_

We proceeded to examine the influence of host bile acids on *B. obeum* growth and investigated how *B. obeum luxS* supernatants might counteract these effects. When incubated with 1 mM or 125 μM pure CA or DCA in fresh LYH-BHI media, it became evident that 1 mM DCA significantly hindered *B. obeum* growth, while CA did not notably impact growth (Figure 3.1-3C and D). However, at a concentration of 125 μM, the inhibitory effect of DCA diminished, and notably, 125 μM CA significantly enhanced *B. obeum* growth compared to the DMSO control (Figure 3.1-5A and B). In contrast, for *C. scindens*, both 1 mM CA and DCA suppressed its growth, with DCA exerting a more pronounced effect (Figure 3.1-6A). Notably, 125 μM CA and DCA exhibited mitigated suppressive effects on *C. scindens* growth (Figure 3.1-6B). These observations suggest

that *B. obeum* could potentially serve as an indicator for assessing the conversion of CA to DCA by *C. scindens*.

To further elucidate the role of *B. obeum* AI-2 in this context, we incubated *C. scindens* with 3mM CA in fresh LYH-BHI medium supplemented with either *B. obeum luxS* supernatants or control supernatants over a 12-hour period. These supernatants, harvested from an *E. coli* strain expressing either *B. obeum luxS* or a *ΔluxS* strain, were subsequently filtered and added to *B. obeum* cultures to a final concentration of 1 mM total bile acids. The OD_{600} was measured every 30 minutes to assess *B. obeum* growth. Remarkably, we observed enhanced *B. obeum* growth when supplemented with *C. scindens*-incubated CA in the presence of *B. obeum luxS* supernatants (Figure 3.1-3E). While when *B. obeum* was incubated with supernatants only, neither *luxS* supernatants change its growth (Figure 3.1-3F). These results suggest that the better growth observed in Figure 3.1-3E was not due to the addition of *B. obeum* signals. Worth mentioning, *B. obeum luxS* supernatants did not change *C. scindens* growth as well, but *S. infantarius luxS* supernatants boosted *C. scindens* growth (Figure 3.1-4A).

To corroborate these growth observations, we conducted Mass spectrometry analysis on the supernatants of 125 μM CA incubated with *B. obeum luxS* supernatants or vector supernatants to quantify CA and DCA levels. The results revealed a lower DCA/CA ratio in cultures supplemented with *B. obeum luxS* supernatants (Figure 3.1-3G). These collective findings suggest that *B. obeum* produces LuxS that reduce the conversion rate

of CA to DCA and alleviate the negative effects associated with the 7-α dehydroxylation of CA to DCA via the *bai* operon in *C. scindens*.

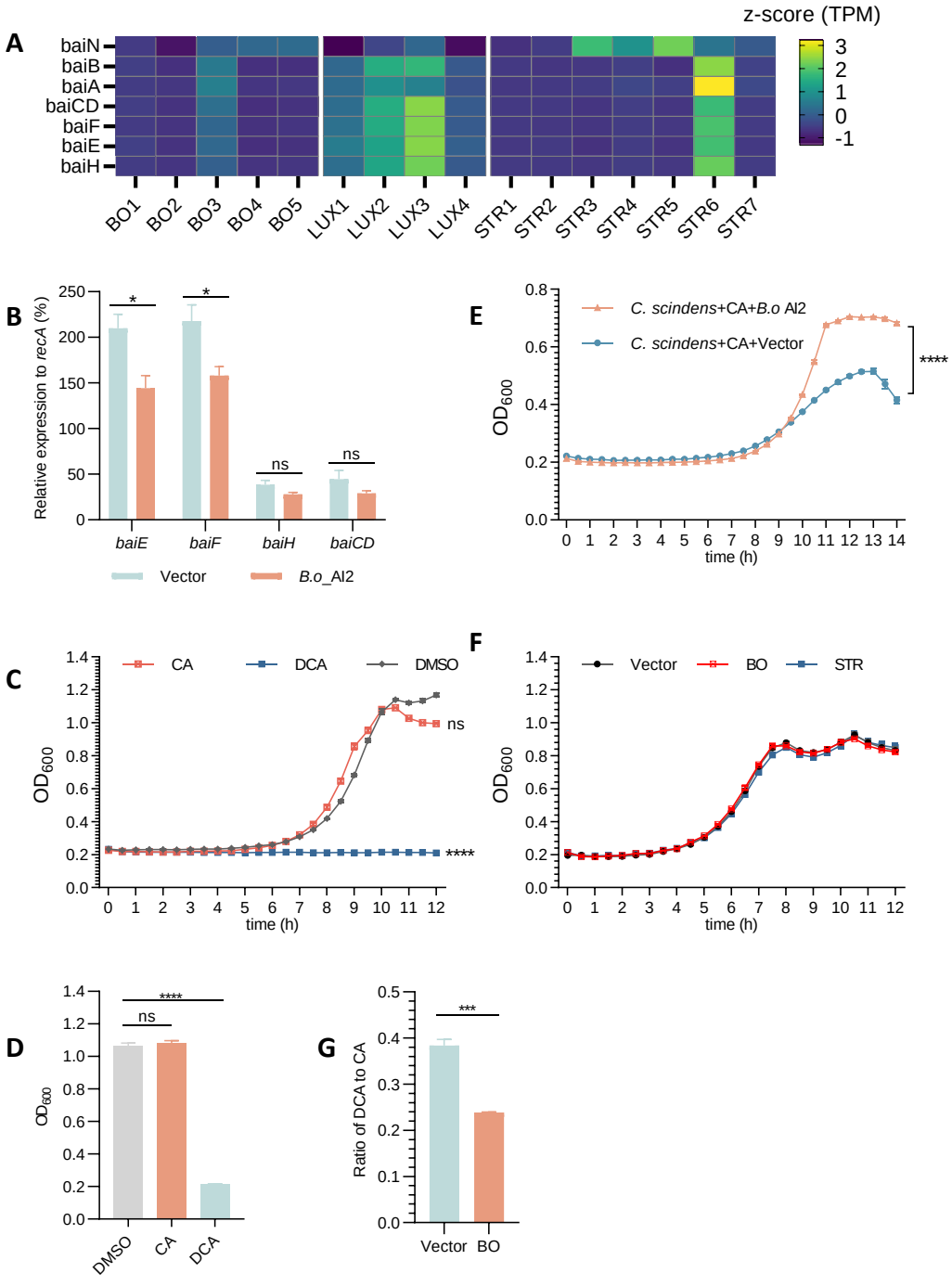

A
z-score (TPM)
3
2
1
0
-1
baiN
baiB
baiA
baiCD
baiF
baiE
baiH
BO1
BO2
BO3
BO4
BO5
LUX1
LUX2
LUX3
LUX4
STR1
STR2
STR3
STR4
STR5
STR6
STR7
B
Relative expression to recA (%)
baiE
baiF
baiH
baiCD
Vector
B.o_AI2
ns
E
C. scindens+CA+B.o AI2
C. scindens+CA+Vector
OD600
time (h)
C
CA
DCA
DMSO
F
Vector
BO
STR
D
DMSO
CA
DCA
G
Ratio of DCA to CA
Vector
BO

Figure 3.1-3. Impact of *B. obeum luxS* on secondary bile acid synthesis in *Clostridium scindens*.
(A) *bai* gene expressions induced by different signals in *C. scindens*. BO: *B. obeum luxS*, STR: *S. infantarius luxS*, LUX: *luxS*- control.
(B) *B. obeum luxS* supernatants downregulate *bai* genes expressions *in vitro*. n = 3, t test, *P < 0.05; ns, not significant. Error bars represent mean ± SEM.
(C) The growth curve of *B. obeum* under DMSO control or pure 1 mM CA and DCA. Area Under Curve (AUC) was used for statistical analysis. Comparisons were made between DMSO and bile acids. n = 3, **** P < 0.0001; ns, not significant. Error bars represent mean ± SEM.
(D) Effects of 1 mM CA and DCA on the growth of *B. obeum* at 10 hours post incubation. n = 3, t test, ****P < 0.0001; ns, not significant. Error bars represent mean ± SEM.
(E) The growth curve of *B. obeum* supplemented with CA processed by *C. scindens* supplemented with *B. obeum luxS* supernatants or vector supernatants. The total molar of bile acids in each testing sample was 1mM. Area Under Curve (AUC) was used for statistical analysis. n = 3, **** P < 0.0001; ns, not significant. Error bars represent mean ± SEM.
(F) The growth curve of *B. obeum* supplemented with *B. obeum luxS* supernatants, *S. infantarius luxS* supernatants or vector supernatants. BO: *B. obeum luxS*, STR: *S. infantarius luxS*, Vector: *luxS*- control.
(G) The ratio of mass spectrometry measurement of DCA to CA in 125 μM CA incubated with *C. scindens* supplemented with indicated *luxS* supernatants. BO: *B. obeum luxS*, Vector: *luxS*- control. n = 3, t test, *** P < 0.001. Error bars represent mean ± SEM.

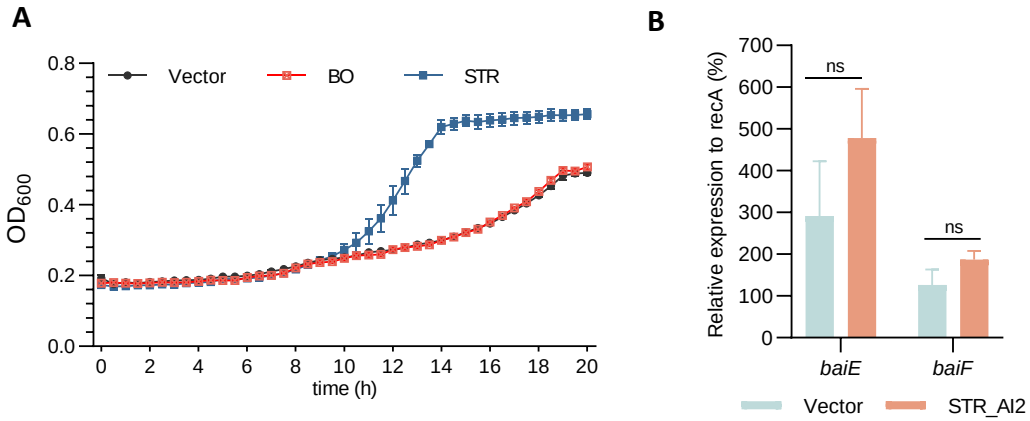


Figure 3.1-4. Effects of *luxS* supernatants on *C. scindens*. (A) The growth curve of *C. scindens* under *luxS* supernatants. **(B)** *S. infantarius luxS* supernatant does not affect *bai* genes expressions *in vitro*.

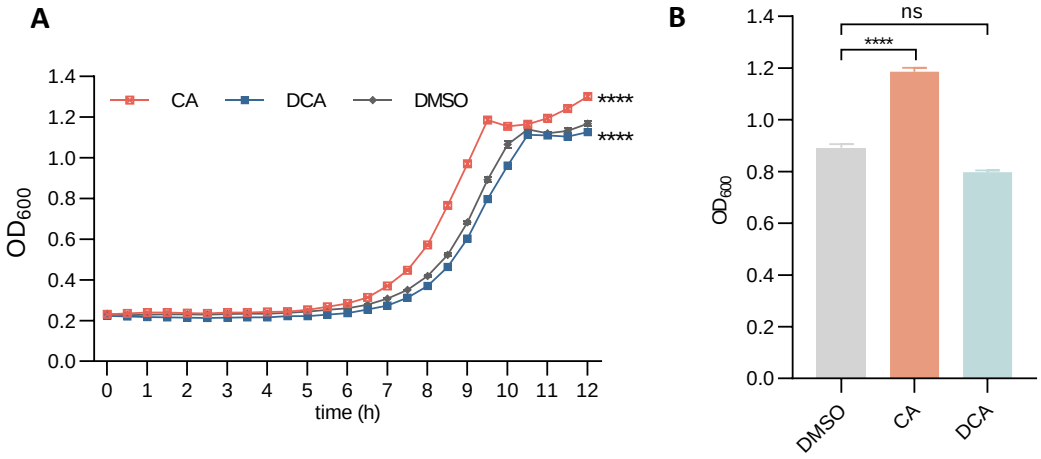


Figure 3.1-5. Effects of 125 µM CA and DCA on *B. obeum* growth. (A) The growth curve of *B. obeum* under DMSO control or pure 125 µM CA and DCA. Area Under Curve (AUC) was used for statistical analysis. Comparisons were made between DMSO and bile acids. n = 3, ****P < 0.0001. Error bars represent mean ± SEM. **(B)** Effects of 125µM CA and DCA on the growth of *B. obeum* at 9.5 hours post incubation. n = 3, t test, ****P < 0.0001; ns, not significant. Error bars represent mean ± SEM.

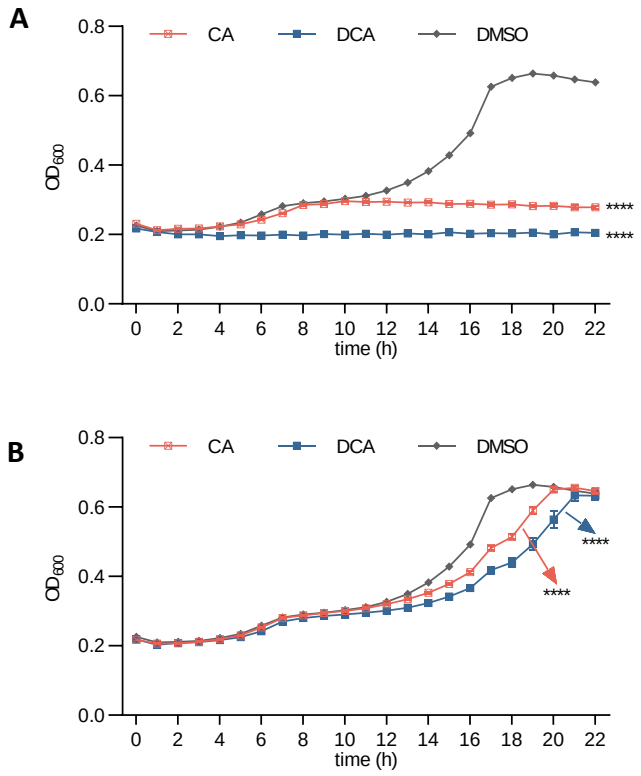


Figure 3.1-6. Effects of CA and DCA on *C. scindens* growth *in vitro*. (A) The growth curve of *C. scindens* under DMSO control or pure 1 mM CA and DCA. **(B)** The growth curve of *C. scindens* under DMSO control or pure 125 µM CA and DCA. Area Under Curve (AUC) was used for statistical analysis. Comparisons were made between DMSO and bile acids. n = 3, t test, ****P < 0.0001. Error bars represent mean ± SEM.

B. obeum luxS affect *C. scindens* level and *bai* expressions in mice

Having demonstrated that *B. obeum luxS* supernatant downregulates the *bai* gene expression of *C. scindens in vitro*, resulting in reduced DCA production, we aimed to determine if this effect is also observed in a mouse model and to assess its impact on *C. scindens* levels. We co-inoculated adult CD-1 mice with *C. scindens* and *E. coli* Δ*luxS* or

E. coli strains expressing *B. obeum luxS* or *S. infantarius luxS*. We measured total bacterial abundance and *C. scindens* abundance in feces and large intestines at day 2 after inoculation using qPCR targeting the 16S rRNA. Our results indicated that expressing *luxS* did not alter the total bacterial biomass in feces and large intestines (Figure 3.1-7A, left). However, expressing either *B. obeum* or *S. infantarius luxS* resulted in approximately 50-fold higher *C. scindens* biomass in feces at day 2 post-inoculation compared to the vector group (Figure 3.1-7B). Additionally, in the large intesteines, an increase in *C. scindens* biomass was observed in the *B. obeum luxS* expressing group but this increase was not statistically significant when expressing *S. infantarius luxS* (Figure 3.1-7B, right). *E. coli* levels were not significantly different in feces collected at day 1 post-inoculation (Figure 3.1-7C). However, on day 2 post-inoculation, a lower colonization level of *E. coli* was observed in feces, large intestines, and cecum when *B. obeum luxS* was expressed, while *S. infantarius luxS* did not significantly affect *E. coli* colonization (Figure 3.1-7D). These results contradict the previous 16S results, which showed that expressing both *luxS* gave *E. coli* strains an advantage against other community members (Data not shown). This discrepancy could be due to differences in the experimental setup, with one experiment involving a more complex community and the other including only two strains.

Because *C. scindens* colonization levels were low (Figure 3.1-7B) and *bai* expression was undetectable, we compared *bai* gene expressions between *B. obeum* and *S. infantarius luxS* expressing groups. We found decreased *baiF* expression in the *B. obeum luxS*

expressing group compared to the *S. infantarius luxS* expressing group in the large intestines on day 2 post-inoculation, but no significant difference in the feces (Figure 3.1-7E). These findings suggest that *B. obeum luxS* plays a role in modulating gut microbial composition by downregulating *bai* gene expression in *C. scindens*, thereby reducing DCA production. The reduced DCA levels likely create a less hostile environment for *C. scindens*, allowing for its increased colonization. In contrast, *S. infantarius luxS* did not exhibit the same effect on *E. coli* colonization or *bai* gene expression, indicating a possible specificity in the interaction between *B. obeum luxS* and *C. scindens*.

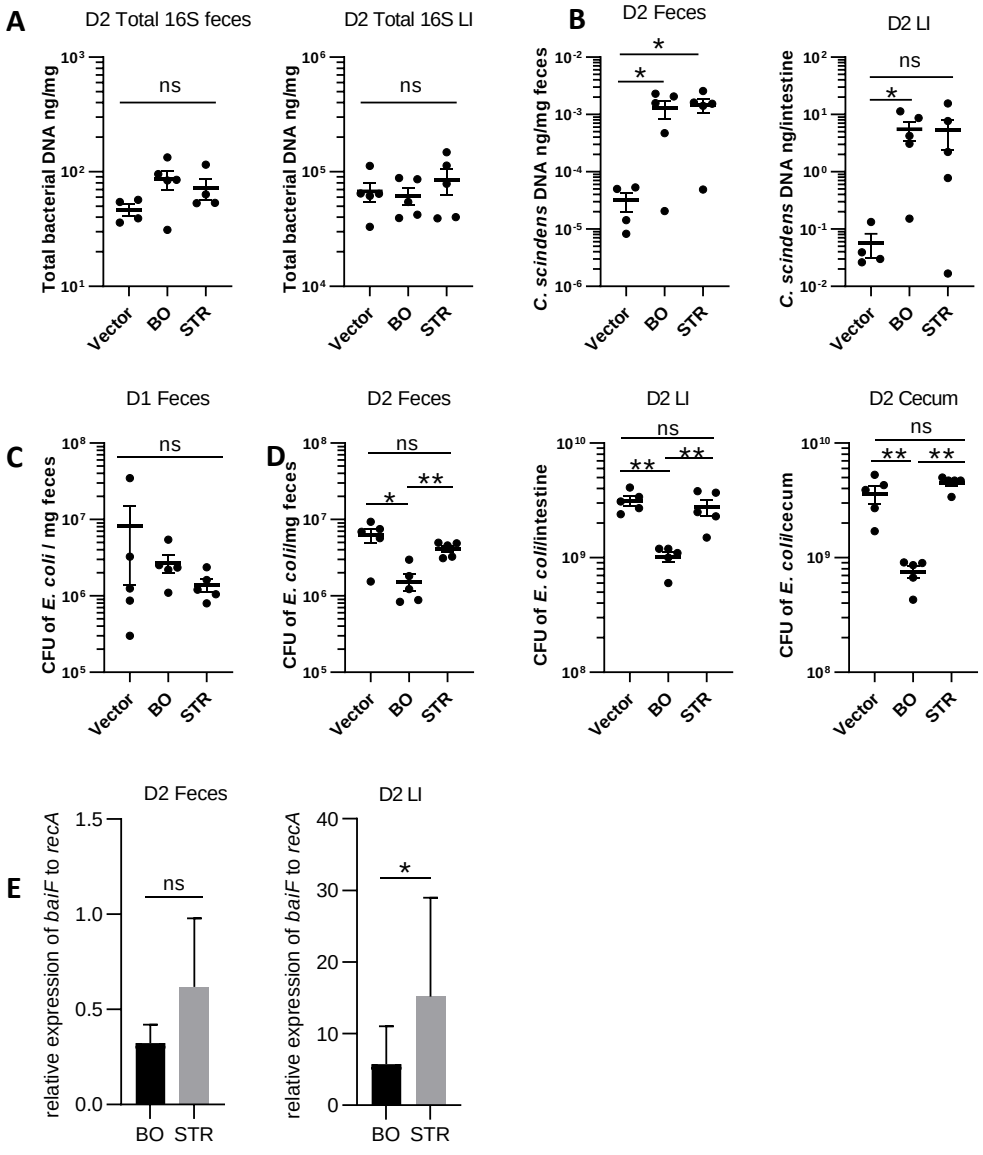


Figure 3.1-7. LuxS affect *C. scindens* level and *bai* expressions in mice. (A) Total bacterial 16S DNA load in fecal pellets and large intestines at day2. **(B)** *C. scindens* load in fecal pellets and large intestines at day2. **(C)** CFU of LuxS producing *E. coli* in fecal pellets at day1. **(D)** CFU of AI-2 producing *E. coli* in fecal pellets, large intestines and cecum at day2. **(E)** *bai* gene expression in fecal pellets and large intestines at day2. Mann-Whitney U-test, * $p<0.05$, ** $p<0.01$, ns: not significant. BO: *B. obeum luxS*, STR: *S. infantarius luxS*, LUX: *luxS*- control.

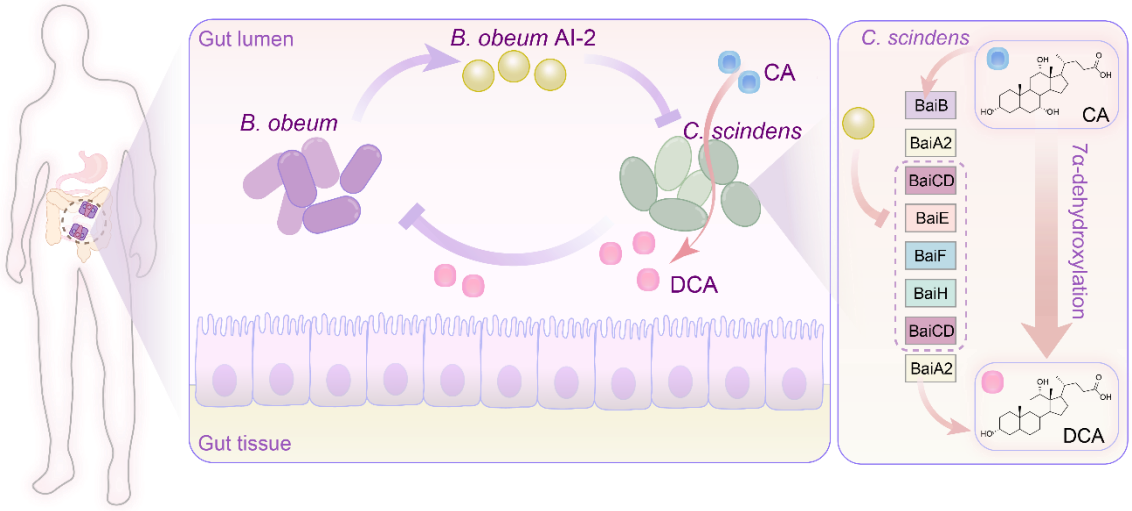


Figure 3.1-8. Working model of *B. obeum* AI-2, *C. scindens* and bile acids.

Discussion

Studies have illustrated the importance of gut microbiome in affecting gut microbial diseases and regulating host responses[49,149]. QS has been demonstrated to be one of the mechanisms that can alter gut microbiome structure, gene transcriptions and host immune responses. This study provides insight into the interaction of QS and gut microbiome via modulating bile acid pool. First, we generated two different *luxS* expressing *E. coli* strains by cloning *luxS* gene from *B. obeum* and *S. infantarius*, which are representatives from a previously defined *Vibrio* resistant and *Vibrio* susceptible community respectively. RNAseq results revealed that adding *luxS* expressing *E. coli* shifted the overall gene expression of model communities (Figure 3.1-1). Specifically, we found that secondary bile acid synthesis related genes, *baiE*, *baiCD*, *baiF*, *baiH*, from *C. scindens*, were downregulated in *B. obeum luxS* expressing group, but they were not differentially

expressed in *S. infantarius luxS* expressing group. We further showed that supernatants from *E. coli* producing *B. obeum* LuxS can downregulated *bai* gene expressions in *C. scindens* and hinder the 7-dehydroxylation of CA to DCA, which attenuates the defect of DCA on *B. obeum* growth. Moreover, Mass Spectometry analysis confirmed the decreased production of DCA when *C. scindens* incubated with *E. coli* producing *B. obeum* LuxS. Finally, investigation of *luxS* expressing *E. coli* and *C. scindens* competition *in vivo* revealed that *LuxS* from *B. obeum* and *LuxS* from *S. infantarius* affect the *C. scindens* colonization differently: In large intestines, expressing *B. obeum luxS* showed increased *C. scindens* colonization level, and reduced *E. coli* colonization levels, while *S. infantarius luxS* did not. Decreased *baiF* expression of *C. scindens* when express *B. obeum luxS* suggest that such increase in *C. scindens* colonization is linked to decreased DCA production.

Here we proposed a working model (Figure 3.1-8): The model proposes that primary bile acid CA, synthesized in the liver, undergoes transformation by *C. scindens* into DCA via the *bai* operon. DCA exerts inhibitory effects on *B. obeum* growth, yet *B. obeum* counters this toxicity by producing AI-2 signals that downregulate key genes in the *bai* operon, thereby reducing DCA production. Moreover, *B. obeum* plays a crucial role in attenuating virulence induction in *Vibrio cholerae* by converting taurocholic acid (TCA) into non-virulence-inducing CA via bile salt hydrolase (BSH) activity.

The results of this study have provided new insights into AI-2 and microbiome regulation. However, several questions remain unanswered, highlighting areas for further investigation. One major question is how AI-2 and *C. scindens* regulation occurs. Specifically, while it is known that *C. scindens* possesses the *lsr* operon, including the identified *lsrF* gene, which suggests the potential for detecting and transporting extracellular AI-2 molecules, the exact mechanisms remain unclear. It is possible that *C. scindens* senses AI-2 via some other, yet undefined, signaling and transportation pathways. These uncertainties are significant in the context of previous studies, where *B. obeum* AI-2 impact *V. cholerae* infection via VqmA-dependent manner[49] instead of via AI-2 detector, LuxPQ. Future research should aim to elucidate the precise molecular pathways involved in AI-2 sensing and transportation in *C. scindens*. Investigating whether alternative signaling pathways are at play could provide deeper insights into the regulatory networks of the microbiome.

Furthermore, it is unexplored whether AI-2 affects the metabolism of other bile acids beyond 7α-dehydroxylation, including bile conjugation and deconjugation. Understanding how AI-2 influences these bile acid metabolic processes is essential, as it could significantly impact the composition and functionality of the microbial community. The gut microbiome is a highly complex and dynamic community of microorganisms that can vary significantly between individuals. Different microbial species may interpret and react to AI-2 signals in unique ways, contributing to the overall diversity and variability of the gut microbiome. Even if we showed that the changes in *bai* expressions in *C.*

scindens is one possible factor that modulate gut microbiota composition, it is possible that other pathways are also involved, such as galactose metabolism, amino sugar and nucleotide sugar metabolism. Further research is needed to elucidate the extent to which AI-2 influences these additional metabolic pathways and to determine their combined effects on the gut microbiota.

AI-2 is produced through the activated methyl cycle (AMC), which recycles S-adenosyl-L-methionine (SAM). During this process, SAM is converted to S-adenosyl-L-homocysteine (SAH), and then to S-ribosylhomocysteine (SRH), the substrate of LuxS, with the assistance of Pfs enzymes. LuxS catalyzes the production of 4,5-dihydroxy-2,3-pentanedione (DPD) from SRH, leading to AI-2 activity and the formation of homocysteine (HCY) [205,206]. Furanone derivatives, particularly 4-hydroxy-5-methyl-3(2H)-furanone (MHF), which can be derived from DPD, are known to induce bioluminescence in *Vibrio harveyi* [43,206]. Our results confirmed that *E. coli* strains expressing *B. obeum* and *S. infantarius luxS* induce detectable luminescence in *V. harveyi* BB170, indicating the production of DPD by both LuxS enzymes. Specifically, *B. obeum* LuxS did not affect *C. scindens* growth *in vitro* but altered its function by downregulating *bai* gene expression. Conversely, *S. infantarius* LuxS negatively impacted *C. scindens* growth *in vitro* without affecting its function. The differing results may be attributed to the distinct chemicals produced by the LuxS enzymes of *B. obeum* and *S. infantarius*. Studies have indicated the presence of other molecules produced by LuxS that exhibit higher AI-2 activity than MHF *in vitro* [43,206,207]. Whether LuxS generates multiple

derivatives of DPD, and the potential ratio of these derivatives, remains unknown. This variability may also contribute to the different outcomes observed in this study.

Supplements

Supplement Table 3.1-1 Primers used in this study.

qRT-PCR primers for *bai* operons	
	Primers (5' -3')
*recA**	F-ATTGAAGGCGAAATGGGCGATAG
	R-TACACATACAGTTGGATTGCTTGAGG
baiE	F-CTGCCTGGACGGAAAGATGT
	R-TGTCAATGGTGATCTCCGGC
baiF	F-CTATGACGCAGTAGGCCAGG
	R-AGCCCAGCATGTGGTAAGTC
baiH	F-CCGTATGGGAGGCTGATGAC
	R-TCTTCTGCCGTCGCTTCTTT
baiCD	F-AGCAGGGCAAGGTTCACTAC
	R-TTGCCTTCAGTCCATCGCTT

*Indicates housekeeping gene.

Primers for inserting P_{LtetO1}+*luxS* into *endA* gene of the *E. coli* BW30045 genome	
	Primers (5' to 3')
Forward	CCAAAACAGTTTCGCTACGTTGCTGGCTCGTTTTAACACGGAGT AAGTGTTAGAAAAATTCATCCAGCA
Reverse	GGTTGTACGCGTGGGGTAGGGGTTAACAAAAAGAATCCCGCTA GTGTAGGCGGGCAGTGAAAGGAAGGCC

Chapter 3.2 Commensal dependent promotion of *Akkermansia muciniphila* via AI-2

Introduction

Akkermansia muciniphila is a Gram-negative anaerobic commonly found in the human gut microbiota and accounts for 1 to 4% of bacterial population in human colon. *A. muciniphila* is a mucin-degrading specialist found predominantly in the mucus layer and is the only representative of the Verrucomicrobia phylum in the human gut. In recent years, extensive research has elucidated the multifaceted roles of *A. muciniphila* in maintaining gut barrier integrity, modulating immune responses, regulating host metabolism[208]. Research have demonstrated negative correlations between the abundance of *A. muciniphila* and some disease progressions, such as obesity, diabetes and microbiota related diseases, such as Inflammatory bowel disease (IBD) and colitis[208].

The gut microbiota plays important roles in the pathogenesis of many diseases. Many bacteria in the gut can produce quorum sensing signals to regulate gene expression and later bacterial behaviors at the population level, such as bioluminescence, biofilm formation, virulence gene expression, which can modulate the entire gut microbiota structure and affect disease development. *Blautia obeum* and *Streptocuccus infantarius*, which are members from a previously described US healthy human gut microbiota and dysbiotic gut microbiota, respectively, can produce LuxS enzyme that catalyzes the production of the quorum sensing (QS) signals autoinducer-2 (AI-2). It has been shown

that the *B. obeum luxS* gene alone can inhibit *Vibrio cholerae* colonization in a germ-free mice model[49]. However, research on studying the role of QS signaling molecules in modulating gut microbiome and the probiotic bacterium *A. muciniphila* is limited.

In this study, we employed a controlled model community consisting of the probiotic bacterium *A. muciniphila* and genetically modified *E. coli* strains engineered to produce LuxS. Our aim was to investigate the impact of various QS signaling molecules on the structure of the gut microbiota. Intriguingly, despite *A. muciniphila* lacking a canonical AI-2 receptor, its abundance increased in the presence of LuxS-producing strains within the community. Subsequent analysis revealed that these effects were mediated indirectly.

Method

Preparation of bacteria for animal studies

All anaerobic bacteria were started from glycerol stocks in LYH-BHI media in anaerobic chamber (5% H_2, 20% CO_2, balance N_2) at 37°C without agitation overnight and subcultured with the ratio of 1:100 into fresh LYH-BHI media for 16-20h. All *E. coli* BW30045 *luxS* expressing strains were started from glycerol stocks in LB media at 37°C shaking at 250 rpm overnight and then was subcultured with the ratio of 1:100 into fresh LB at 37°C shaking at 250 rpm for 16-20h. Strains were normalized to OD=0.4, and the bacterial mixture were mixed in a total volume of 300 µL per mouse, with the ratio of a) 45% microbial community, 20% *E. coli* BW30045 expressing *luxS* from either

Streptococcus infantarius, *Blautia obeum*, or empty expression vector, and 35% of *A. muciniphila.* Or b) equal quantities of *E. coli* strains and *A. muciniphila.*

Infant mouse studies

All animal experiments were approved by the Institutional Animal Care and Use Committee of the University of California, Riverside (UCR) and followed NIH guidelines. All CD-1 suckling mice were purchased from Charles River Laboratories. Suckling and adult mice were reared at the UCR gnotobiotic facility. Four-day old suckling CD-1 animals were fasted for 1.5 hours, and then orally gavaged with 50 μL of 75 mg/mL spectinomycin solutions using plastic tubing, after which the animals were placed back to lactating dams. After 24 hours, suckling animals were then fasted for 1.5 hours, gavaged with 50 μL of bacteria mix prepared as described above using plastic tubing. At 18 hours post-infection, animals were sacrificed, intestinal tissue were dissected and homogenized in 5 mL sterile 1x PBS for numeration.

Fecal pellet collection

Fecal pellets were collected from adult CD-1 mice, weighted and resuspended in 500 μL of PBS in a 2.0 mL screw cap tube. The pellets were then disrupted by agitation using a bead beater (BioSpec) at 1400 rmp for 30 seconds. The resulting slurry was serial diluted and plated on LB with appropriate antibiotics for *V. cholerae* numeration.

DNA/RNA extraction from fecal and intestinal samples

500 μL homogenates of fecal and intestinal samples were used for DNA extraction. Briefly, 500 μL homogenates, 210 μL 20% SDS, and 500 μL phenol:chloroform:isoamyl-alcohol (24:24:1, pH 6.9, Fisher Scientific) were added to bead-beating tubes with 0.1 mm glass beads (BioSpec) and shaking at 2400 rpm for 5 min. DNA were purified and precipitated as described previously[49].

qPCR Quantification of *C. scindens* colonization in CD-1 mice

Colonization levels of *A. muciniphila* in CD-1 suckling mice were determined by quantitative PCR using DNA extracted from the fecal and intestinal samples as templates. All DNA samples were homogenized with nuclease free water to a concentration of 500 ng/μL. qPCR Reactions comprised 2 μL of 1:100 diluted as templates, 12.5 μL SYBR Green Master Mix (BioRad), 10 μL PCR-grade water, and 0.25 μL of forward and reverse primers at 10 μM: primers specific to *A. muciniphila* (Forward: 5'-CAGCACGTGAAGGTGGGGA-3', reverse: 5'-CCTTGCGGTTGGCTTCAGATC-3') and primers targeting the total bacterial load (Forward: 5'-CTCCTACGGGAGGCAGCAG-3', reverse: 5'-TTACCGCGGCTGCTGGCAC-3'), primers specific to *B. longum* (Forward: 5'-GTTCCCGACGGTCGTAGAG-3', reverse: 5'-GTGAGTTCCCGGCATAATCC-3'), and primers specific to *F. prausnitzii* (Forward: 5'-GATGGCCTCGCGTCCGATTAG-3', reverse: 5'-CCGAAGACCTTCTTCCTCC-3').

Statistical Analysis

Statistical analyses were performed using GraphPad Prism Software (v9). Generally, Student's t-test was performed if data were deemed normally distributed. Mann-Whitney U test was performed if data were deemed not normally distributed. Results are representative of independent repeated experiments.

Result

AI-2 signals modulate gut microbiome compositions in mouse model

Previous studies have shown that some immunogenic bacteria in the gut may impact host immune responses. We designed a model community based on US healthy gut microbiomes (Table 3.2-1), including *B. obeum* and *A. muciniphila*. We introduced three groups of suckling mice with model communities and i) Δ*luxS E. coli*, or *E. coli* expressing the *luxS* of two different human gut commensals, (ii) *B. obeum* and (iii) *S. infantarius*. Total 16s abundance of small intestines measured by qPCR showed higher bacterial load in the *S. infantarius luxS* group, but no statistically significant differences between vector group and either *luxS* groups (Figure 3.2-1A). While in the large intestines, total bacterial load was lower in the *infantarius luxS* group compared to vector group, but no significant difference among other groups (Figure 3.2-1B).

We then investigated the relative abundance of specific bacterial strains by qPCR using strain specific primers. We found that the relative abundance of *A. muciniphila* was significantly increased in both groups with *E. coli* expressing the *luxS* in either

compartment of intestines (Figure 3.2-1C&D). However, *B. longum* only increased in the presence of *S. infantarius luxS* in the large intestines (Figure 3.2-1E) and no significant difference was found *F. prausnitzii* (Figure 3.2-1F). Taken together, it suggested that AI-2 signals can modulate gut community structures, especially affect *A. muciniphila* relative abundance.

Table 3.2-1 List of defined US healthy gut microbiome.

Bacterium	Strain Name
Bacteroides vulgatus	ATCC 8482
Bifidobacterium longum subsp. Longum	ATCC 25986
Blautia obeum	ATCC 29174
Colinsella aerofaciens	ATCC 25986
Clostridium scindens	ATCC 35704
Dorea formicigenerans	ATCC 27755
Eubacterium rectate	ATCC 33656
Faecalibacterium prausnitzii	DSM 17677
Akkermancia muciniphila	ATCC BAA-835

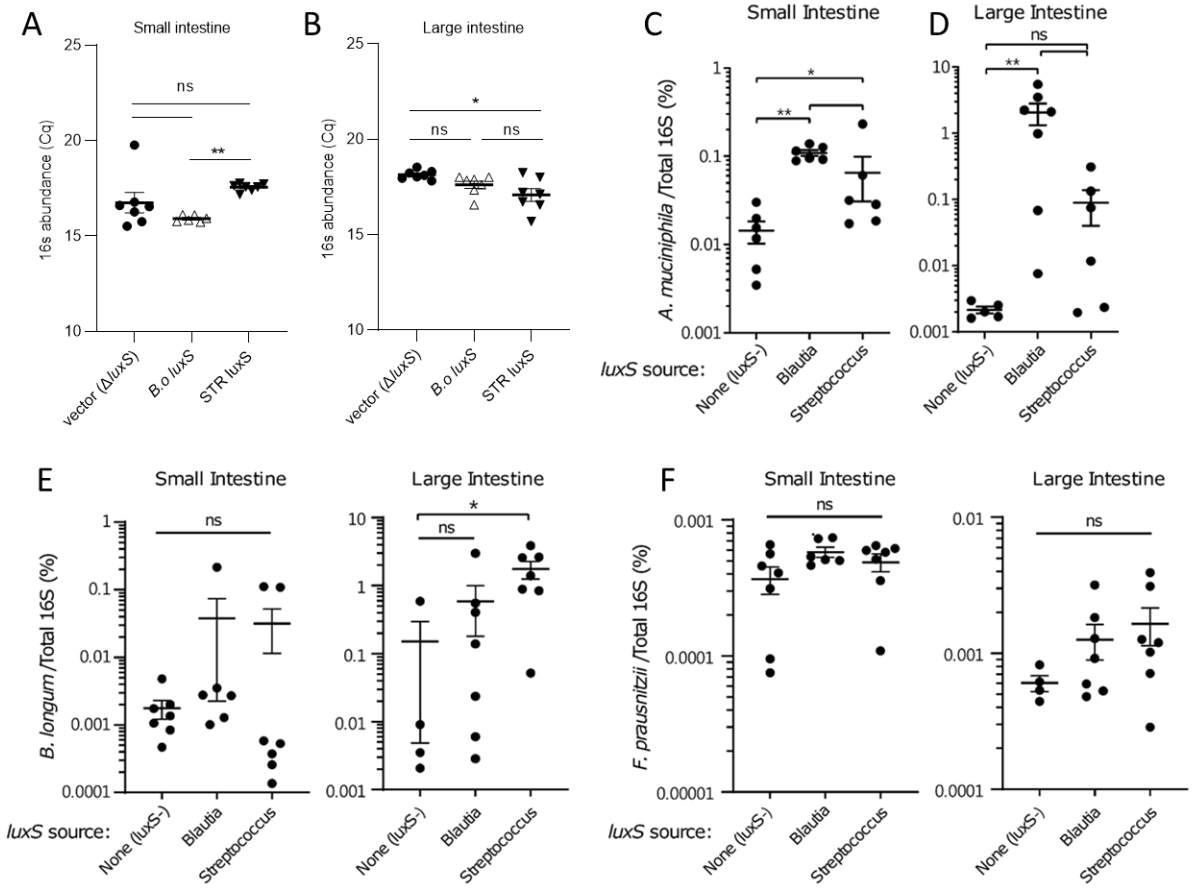


Figure 3.2-1 Commensal expressed *luxS* modulate gut microbiome structure.

(A) Overall 16S levels in the small intestines of suckling mice measured by quantitative PCR.

(B) Overall 16S levels in the large intestines of suckling mice measured by quantitative PCR.

(C) Colonization levels of *A. muciniphila* with defined model community and *E. coli* expressing *luxS* from *B. obeum* or *S. infantarius* in the small intestines of suckling mice measured by quantitative PCR.

(D) Colonization levels of *A. muciniphila* with defined model community and *E. coli* expressing *luxS* from *B. obeum* or *S. infantarius* in the large intestines of suckling mice measured by quantitative PCR.

(E) Colonization level of *B. longum* with defined model community and *E. coli* expressing *luxS* from *B. obeum* or *S. infantarius* measured by quantitative PCR.

(F) Colonization of *F. prausnitzii* with defined model community and *E. coli* expressing *luxS* from *B. obeum* or *S. infantarius* measured by quantitative PCR.

(G) n = 6 to 7, Mann-Whitney U test, * $P < 0.05$; ** $P < 0.01$; ns, not significant. Error bars represent mean ± SEM.

***A. muciniphila* respond to indirectly effects of AI-2 signals under defined community**

Our hypothesis posited that AI-2 signals modulate community structure by influencing community behaviors rather than directly impacting *A. muciniphila*. To investigate this, we co-inoculated *A. muciniphila* with either Δ*luxS E. coli* or *E. coli* expressing the *B. obeum luxS* alone. The overall bacterial abundance showed no significant difference between the Δ*luxS* and *B. obeum luxS* groups in either intestinal compartment (see Figure 3.2-2A). Consistent with expectations, we did not observe any statistically significant differences in the relative abundance of *A. muciniphila*. Collectively, these findings suggest that AI-2 signals indirectly modulate *A. muciniphila* within a defined community structure.

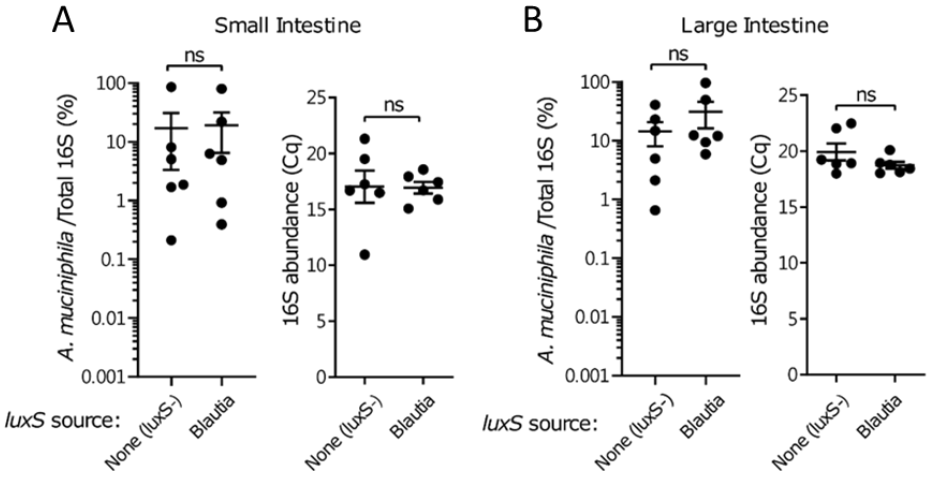


Figure 3.2-2 *luxS* from *B. obeum* alone did not affect *A. muciniphila* levels in suckling mice model. *A. muciniphila* in the **(A)** small intestines and **(B)** large intestines of suckling mice when co-colonized with *E. coli* expressing *luxS* from *B. obeum*. n = 6, Mann-Whitney U test, ns, not significant. Error bars represent mean ± SEM.

Discussion

This study provides novel insights into the interplay between QS signaling molecules and gut microbiome composition, with a focus on the probiotic bacterium *A. muciniphila*. We demonstrated that AI-2 signals, produced by engineered *E. coli* strains expressing LuxS from different commensal bacteria, significantly modulate the structure of a defined gut microbial community. A key finding is the increased relative abundance of *A. muciniphila* in the presence of LuxS-producing strains, despite *A. muciniphila* lacking a known canonical AI-2 receptor. This suggests an indirect mechanism by which AI-2 signaling influences *A. muciniphila* colonization. This effect was observed only in a complex microbial community and not in co-inoculation with LuxS-producing *E. coli* alone, supporting a community-mediated mechanism.

These findings raise important questions for future research: (1) What specific mechanisms enable AI-2 signaling to promote *A. muciniphila* growth in the complex community? Potential explanations include altered nutrient availability, changes in mucin degradation by other community members, or modulation of host factors influencing the mucus layer. (2) How does AI-2 signaling impact *A. muciniphila*'s known benefits for metabolic health and gut barrier function in a simple or complex community? Investigation on these topics will provide novel insight into the interplay between QS and complex microbial community.

Overall, our findings suggest new strategies for microbiome modulation and disease treatment. Modulating QS signaling could selectively promote beneficial bacteria like *A. muciniphila* without direct probiotic administration, potentially leading to novel therapeutic approaches for gut microbiome-related diseases.

Chapter 4 Diverse infection outcomes in *V. cholerae* driven by virulence-regulated bifunctional protease TagA interacting with personalized microbiota

Abstract

Vibrio cholerae (Vc) is a pathogenic bacterium responsible for cholera, a significant global health concern. The virulence master regulator ToxT regulates various factors crucial for Vc pathogenesis, including the upregulation of TagA, a secreted metalloprotease. Here, we elucidate the multifaceted role of TagA in Vc growth within mucin-rich environments. Our findings reveal TagA as a bifunctional protein with both mucinase and mucus secretagogue activities, the latter inducing host mucin production. To dissect TagA's dual functions, we employed a proteolytically inactive TagA mutant ($TagA^{E433D}$) and a TagA variant lacking the fibronectin type III domain ($TagA^{\Delta FN3}$), which retains mucolytic but loses MUC2-inducing activity. Utilizing *ex vivo* tissue culture and *in vivo* gnotobiotic mouse models, we demonstrate distinct impacts of TagA's activities on Vc fitness during infection, modulated by specific human gut microbes. We constructed model gut microbiota resembling healthy (CR) and dysbiotic (DS) states found in cholera endemic regions. TagA mucolytic activity is crucial for CR-mediated Vc infection resistance *in vivo*, potentially via mechanisms inhibiting Vc epithelial adherence. In contrast, the mucin-inducing activity of TagA FN3 is required for DS microbes promoting Vc infection. In vitro investigations suggest DS microbes modulate Vc infection-associated mechanisms, including motility.

In conclusion, our study unveils TagA as a pivotal virulence-regulated protein mediating Vc interactions with diverse resident gut microbes, ultimately shaping the outcome of cholera infections. Understanding these complex interactions sheds light on potential therapeutic strategies targeting Vc pathogenesis within the gut microbiome.

Introduction

Vibrio cholerae is the etiology agent of a severe diarrheal disease, cholera, that remains to be a significant public health challenge. To successfully colonize the human gut, V. cholerae relies on two critical virulence factors: the toxin-coregulated pilus (TCP), encoded by the Vibrio pathogenicity island (VPI), which is essential for colonization in the human intestine[16,18]; and cholera toxin (CT), encoded by the CTXφ bacteriophage, is the primary cause of the profuse watery diarrhea characteristic of cholera[18]. CT is transcriptionally co-regulated with TCP by ToxRST regulon.

The human gut microbiome is a dynamic ecosystem with a high degree of diversity, significantly influencing gastrointestinal health and susceptibility to diseases. It is well-documented that variations in gut microbiota composition can impact the outcome of various infections, including *V. cholerae*. A previous study has shown that different gut microbiota compositions will drive dramatically different *V. cholerae* infection results in a mouse model, suggesting that the microbiota plays a key role in the disease's progression and severity. The mucus layer, a complex structure colonized by a range of

gut microbes including *V. cholerae*, plays a multifaceted role in the gut: it serves as both a nutrient source and a structural anchor for microbiota while also providing a defense mechanism against invasive enteric pathogens. Mucins, which are O-glycosylated glycoproteins, are the primary building blocks of mucus. Research has indicated that the degradation of mucins can disrupt the gut microbiota and contribute to a spectrum of diseases, including obesity, diabetes, colorectal cancer, and inflammatory bowel disease (IBD)[209–211]. Direct visualization has shown that *V. cholerae* preferentially colonize in the gut regions that produce less mucins, suggesting that mucins are a limiting factors for *V. cholerae* colonization in the gut[212]. Additionally, a recent study indicated that mucin-associated O-glycans might suppress the expression of the CTXφ-encoded cholera toxin by disrupting the ToxR/P/T regulatory pathway[213]. Despite these insights, the role of mucin metabolism in metabolic and regulatory interchanges between *V. cholerae* and specific members of gut microbiota, and the resulting impact on personalized *V. cholerae* infection outcomes, remains poorly understood.

TagA (ToxR-activated gene A), encoded by the Vibrio pathogenicity island (VPI), is a putative 115 kDa lipoprotein that shares 35% sequence similarity with StcE (Secreted protease of C1 esterase inhibitor), a mucinase secreted by enterohaemorrhagic *E. coli* (EHEC). Despite this similarity, TagA exhibits distinct proteolytic activity compared to StcE. Previous studies have demonstrated that TagA cleaves mucins found in crude animal samples, human saliva, and those attached to the LS174T human goblet-like cell line, but it does not cleave C1-INH as StcE does[214]. TagA is also less efficient at cleaving

CD43 than StcE. The difference is possible due to the sequence divergences between TagA and StcE. In contrast, the only other identified SLiMe TagA protein from *Aeromonas hydrophila*, which shares 68% sequence similarity with StcE, produces the same-sized product as StcE.

TagA is a bifunctional protein that functions both as a mucinase and a mucus secretagogue, inducing host mucin production. A mutation in TagA, specifically E433D, was shown to inactivate its mucinase activity. Mutation in E433D does not exhibit different protein secretion than active TagA. However, overexpression of $TagA^{E433D}$ increases *Vibrio cholerae* adherence to epithelial cells, likely due to receptor-ligand interactions that active TagA interrupts.[214]. Additionally, deletion of the FN3 (Fibronectin type-III) domain ($TagA^{\Delta FN3}$) abolishes its mucin-inducing activity while retaining its mucolytic activity. In this study, we separately examine the two functions of TagA using $TagA^{E433D}$ and $TagA^{\Delta FN3}$ in gnotobiotic mice. We utilized two distinct developed model gut microbiota representative of different human gut microbiota states: one model community ("CR") mimicking that of healthy individuals, which promotes resistance to *V. cholerae* infection, and another ("DS") resembling the dysbiotic state found in cholera-endemic areas, which is associated with high susceptibility to *V. cholerae* colonization. Our findings indicate that the two functions of TagA play distinct roles in CR and DS communities, driving different disease outcomes.

Methods

Animal experiments

For the gnotobiotic experiments, all 5-7-week Swiss Webster mice were kept in germ-free isolators. For bacteria preparation, wild type or mutant *V. cholerae* O1 El Tor C6706 were started from -80°C glycerol stock in LB broth with appropriate antibiotic at 37°C with agitation overnight, and the strains were sub-cultured at the ratio of 1:100 at 37°C with agitation until it reached the log phase (OD_{600}≈0.4-0.5), and then were concentrated at 10:1 in fresh LB with appropriate antibiotic if needed.. For inoculation without community strains, wild type *V. cholerae* and *TagA* mutant strain were mixed at the ratio of 1 to 1, and 100 μL of the mixed culture ($1x10^9$ – $1x10^{10}$ CFU) was gavaged into each mouse. For inoculation with CR or DS communities, aerobic strains were prepared the same as *V. cholerae.* Anaerobic strains were cultured from glycerol stocks in LYH-BHI media in anaerobic chamber at 37°C for 48 hours, and then were sub-cultured with 1:100 ratio in fresh LYH-BHI for additional 48 hours before gavage. For each mouse, the total volume of a 0.4 OD_{600} culture, amounting to 300 μL, was evenly distributed among different strains by the community. Subsequently, the combined culture was subjected to centrifugation, pelleted, and then resuspended in fresh LYH-BHI along with *V. cholerae* mixture prepared as described above ($1x10^9$ – $1x10^{10}$ CFU). For all mice experiments, mice were gavaged with 100 μL 1M $NaHCO_3$ 30 minutes prior to gavage with bacterial cultures. Mice were sacked at 4 day-post inoculation. Fecal samples were suspended in 500μL PBS and homogenized using bead beater (BioSpec) at 1400 rpm for 30s, followed

by serial dilution and spotting on LB agar containing appropriate antibiotic for CFU enumeration. 3rd distal small intestines were collected and homogenized in 5 mL 1xPBS, followed by spotting on LB agar containing appropriate antibiotic for CFU enumeration.

DNA extraction and 16S library preparation

500 µL homogenates of fecal and intestinal samples were used for DNA extraction. Briefly, 500 µL homogenates, 210 µL 20% SDS, and 500 µL phenol:chloroform:isoamyl-alcohol (24:24:1, pH 6.9, Fisher Scientific) were added to bead-beating tubes with 0.1mm glass beads (BioSpec) and shaking at 2400 rpm for 5min. DNA were purified and precipitated as described previously[49].

The V4 variable region of the bacterial 16S ribosomal RNA gene was amplified using a 25 µl PCR reaction mixture containing 1 µl of 1:100 or 1:1000 diluted DNA as template, 10 µl of Platinum Hot Start PCR Master Mix (ThermoFisher), 13 µl of PCR-grade water, and 0.5 µl each of forward and reverse primers (10 µM). PCR cycling conditions consisted of an initial denaturation step at 94°C for 3 minutes, followed by 30 cycles of denaturation at 94°C for 45 seconds, annealing at 50°C for 60 seconds, and extension at 72°C for 90 seconds, with a final extension step at 72°C for 10 minutes before holding at 4°C. Subsequently, an equal amount of each amplicon was pooled and purified using QIAquick PCR purification columns (Qiagen) before sequencing on the Illumina MiSeq platform.

16s sequencing analysis

The analysis was conducted using QIIME 2 version 2022.2[215]. Sampling depth was set at 1000.

Result

TagA is important for *V. cholerae* colonization in abx-cleared system

Previous study showed that TagA transcripts were detected in stool samples from patients with cholera[216]. However, it is unexplored how TagA and its bifunctions contribute to *V. cholerae* pathogenesis and fitness. To test this, we first performed single strain colonization in an adult mouse model. Mice were treated with antibiotic cocktails for 7 days and subsequent Streptomycin water for 3 days, and were gavaged with TagA mutants (*ΔtagA*, $tagA^{E433D}$, $tagA^{FN3}$) or WT. After 4 days, 3rd distal small intestines were collected and numerated for *V. cholerae* CFU. Results showed that deletion of *tagA* results in ~10-fold lower colonization level than WT **(Figure 4-1A)**. Mutation of E433D also exhibits ~5-fold lower colonization level than WT (**Figure 4-1B)**. However, when FN3 is mutated, *V. cholerae* colonized better than WT **(Figure 4-1C)**. It suggests that MUC-2 inducing activity is disadvantages for *V. cholerae* colonization in an abx-cleared system.

Table 4-1. List of bacterial strains in the model community.

Cholera Resistant (CR)	Dysbiotic (DS)
Dorea longicatena	*Escherichia coli*
Bacteroides caccae	*Streptococcus infantarius*
Bacteroides vulgatus	*Enterococcus faecalis*
Dorea formicigenerans	*Streptococcus salivarius*
Collinsella aerofaciens	*Streptococcus thermophilus*
Ruminococcus torques	
Eubacterium rectale	
Faecalibacterium prausnitzii	
Bacteroides thetaiotaomicron	
Blautia obeum	
Clostridium scindens	
Bactreroides uniformis	
Bifidobacterium longum	

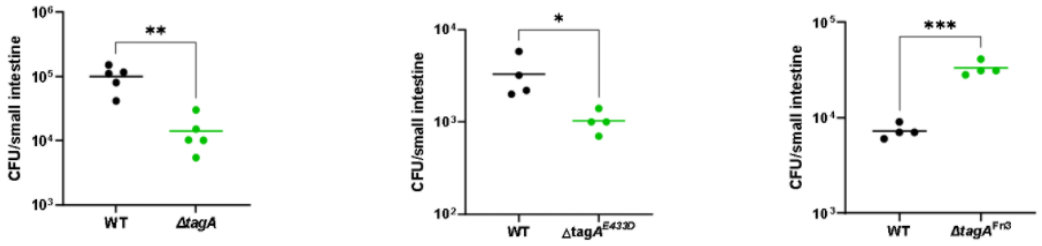


Figure 4-1. *V. cholerae* colonization levels in the small intestines of adult mice at day 4 post-infection. 6-week-old CD-1 mice were single-infected with 10^8 WT, **(A)***ΔtagA*, **(B)***tagA*^{E433D}, or **(C)***tagA*^{FN3}. All analysis were tested with Mann-Whitney, n = 4 to 5, *: P < 0.05, **: P < 0.01, ***: P < 0.001. Error bars represent mean ± SEM.

TagA is essential for *V. cholerae* fitness in germ-free system

To investigate the distinct roles of TagA as a mucinase and mucus secretagogue, we conducted competition assays with WT *V. cholerae*. Germ-free, 6-week-old CD-1 mice were co-infected with 10^8 CFU of WT and 10^8 CFU of either *ΔtagA*, *tagA*^{E433D}, or *tagA*^{FN3}.

Fecal samples were collected daily, and the mice were sacrificed on day 3 post-infection to collect samples from the distal small intestines. The results showed that deletion of tagA (*ΔtagA*) led to a significant reduction in colonization, approximately ninefold lower than WT, indicating that TagA is crucial for effective colonization. This suggests that *in vivo* trans-complementation of TagA is either absent or negligible (Figure 4-2A and B). For the $tagA^{E433D}$ mutant, which lacks functional mucinase activity, we observed that it colonized 4 to 10-fold higher than WT in fecal samples on days 1 and 2. However, this colonization advantage was not evident by day 3 (Figure 4-2C). Similarly, no significant difference in colonization levels was found in the distal small intestines (Figure 4-2D). The $tagA^{FN3}$ mutant, which does not induce MUC-2 production, showed a similar pattern. It colonized approximately 4-fold higher than WT on day 1 in fecal samples (Figure 4-2E), with no significant difference from WT observed on days 2 and 3 or in the distal small intestines (Figure 4-2E and F).

These findings suggest that the absence of TagA negatively impacts *V. cholerae* colonization in germ-free mice. In contrast, mutations that impair TagA's mucinase activity ($tagA^{E433D}$) or its ability to induce mucin production ($tagA^{FN3}$) do not adversely affect colonization. When WT *V. cholerae* is the only other present microbes, losing the functions of mucinase or mucus secretagogue is not crucial for establishing colonization in germ-free mouse model.

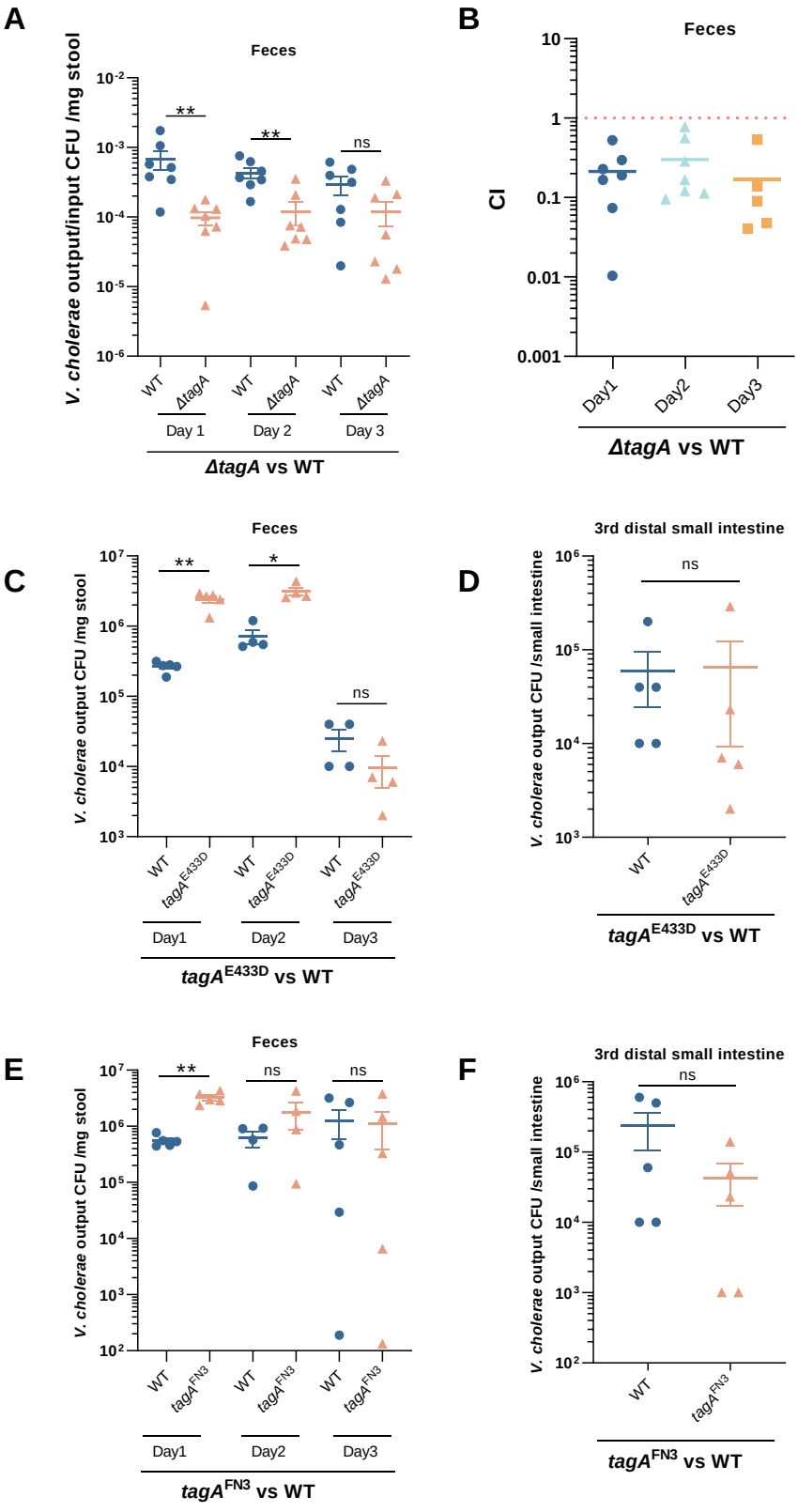

A
Feces
V. cholerae output/input CFU /mg stool
**
**
ns
WT
ΔtagA
Day 1
Day 2
Day 3
ΔtagA vs WT
B
Feces
CI
Day1
Day2
Day3
ΔtagA vs WT
C
Feces
V. cholerae output CFU /mg stool
**
*
ns
tagAE433D
Day1
Day2
Day3
tagAE433D vs WT
D
3rd distal small intestine
V. cholerae output CFU /small intestine
ns
tagAE433D vs WT
E
Feces
V. cholerae output CFU /mg stool
**
ns
ns
tagAFN3
Day1
Day2
Day3
tagAFN3 vs WT
F
3rd distal small intestine
V. cholerae output CFU /small intestine
ns
tagAFN3 vs WT

Figure 4-2. TagA mutants competed with WT in germ-free adult mice. (A) *V. cholerae* recovered in feces from germ-free adult mice co-infected with WT and *ΔtagA*. (B) *V. cholerae* recovered in 3rd distal small intestines from germ-free adult mice co-infected with WT and *ΔtagA* at day 3 post-infection. (C) *V. cholerae* colonization in feces from germ-free adult mice co-infected with WT and $tagA^{E433D}$. (D) *V. cholerae* colonization in 3rd distal small intestines from germ-free adult mice co-infected with WT and $tagA^{E433D}$ at day 3 post-infection. (E) *V. cholerae* colonization in feces from germ-free adult mice co-infected with WT and $tagA^{FN3}$. (D) *V. cholerae* colonization in 3rd distal small intestines from germ-free adult mice co-infected with WT and $tagA^{FN3}$ at day 3 post-infection. All analysis were tested with Mann-Whitney, n = 5 to 7, *: $P < 0.05$, **: $P < 0.01$, ns: not significant. Error bars represent mean ± SEM.

TagA FN3 is important for *V. cholerae* colonization in defined communities

We next examined microbiota specific effects of the mucin degradation and secretagogue activities of TagA. We first competed *tagA*^{E433D} and *tagA*^{FN3} in the presence of CR (Cholera resistant) or DS (Dysbiotic, high susceptibility to *V. cholerae* infection) communities[149]. Feces were collected daily, and mice were sacrificed at day 3 post infection to collect 3rd distal small intestines. In fecal and intestinal samples, *tagA*^{FN3} performed worse than *tagA*^{E433D} in both microbiota communities (Figure 4-3A and B). However, the loss of FN3 was particularly detrimental in the DS community, where the competitive index (CI) values for *tagA*^{FN3} were ~100-fold lower in feces on day 2 and ~10 fold lower in feces and 3rd distal small intestines on day 3 (Figure 4-3A and B). This suggests that the FN3 domain, responsible for the mucin-inducing ability, is critical for *V. cholerae* to effectively invade and establish itself in susceptible microbiomes.

To further contextualize these findings, we incorporated previously published data to compare the *V. cholerae* colonization levels of each strain when co-infected with CR or DS communities in germ-free CD-1 adult mice on day 3 post-infection. Similar to WT, which exhibited ~50-fold higher colonization in DS compared to CR, *tagA*^{E433D} also demonstrated ~10-fold higher colonization in DS versus CR. Worth noticing, *tagA*^{E433D} colonized even better than WT in CR, while no difference in DS (Figure 4-3C). In contrast, *tagA*^{FN3} showed no significant difference in colonization levels between CR and DS communities, maintaining colonization levels similar to the WT strain (Figure 4-3C). This suggests that the FN3 domain's mucin-inducing activity appears to be particularly important in the DS

community, which is more susceptible to *V. cholerae* infection. The FN3 domain's role in inducing mucin degradation likely aids in establishment, proliferation and dissemination of *V. cholerae*. In contrast, the mucin-inducing activity of FN3 may not be as critical in the CR community, where the existing microbiota is robust enough to resist *V. cholerae* colonization. The microbes in CR communities can effectively compete with or inhibit *V. cholerae*, making the mucin-inducing activity less necessary. Interestingly, the absence of mucin degradation (*tagA*^{E433D}) activity seems to reverse *V. cholerae* resistance in the CR community, indicating that the mucinase role might extend beyond mere mucin degradation to include interactions that suppress *V. cholerae* resistance mechanisms in certain microbial contexts.

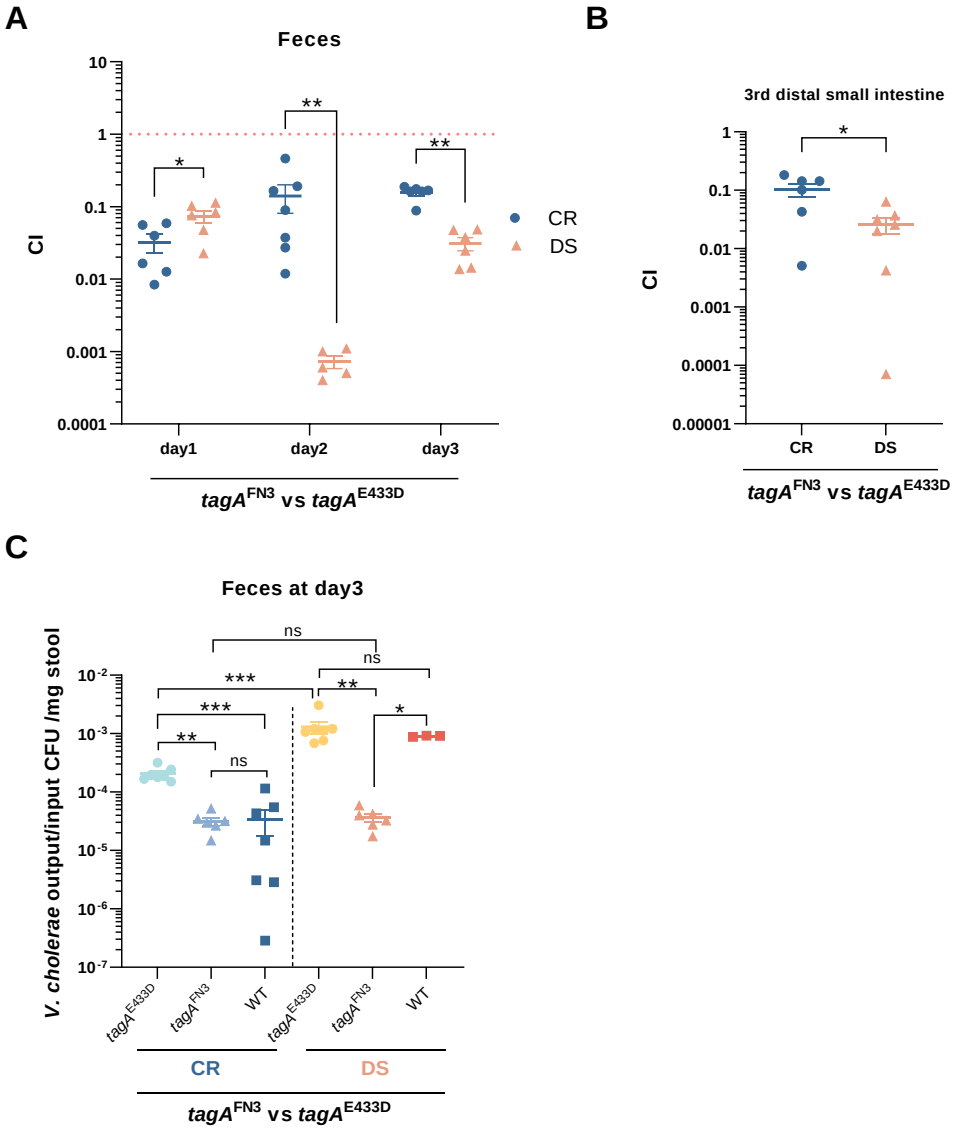


Figure 4-3. Mucin inducing activity of TagA is required for successful *V. cholerae* colonization in defined communities. Germ-free 6-week-old CD-1 mice were co-infected with *tagA*^{FN3} and *tagA*^{E433D}. **(A)** The competition index (CI) of *tagA*^{FN3} vs *tagA*^{E433D} in the feces collected from day 1 to day 3 postinfection. **(B)** The competition index (CI) of *tagA*^{FN3} vs *tagA*^{E433D} in the 3rd distal small intestines collected at day 3 post infection. **(C)** The output *V. cholerae* CFU normalized by input CFU of each strain. The WT data from a previous paper[149] were incorporated into the graph. All analysis were tested with Mann-Whitney, n = 3 to 7, *: $P < 0.05$, **: $P < 0.01$, ***: $P < 0.001$, ns: not significant. Error bars represent mean ± SEM.

The dual activity of TagA drives microbiota-specific differences in *V. cholerae* fitness during colonization

To better evaluate the human microbiota specific effects of mucinase and the mucin degradation and secretagogue activities of TagA separately, we did another competition experiment in germ-free mouse models. We competed Δ*tagA*, *tagA*^{E433D}or *tagA*$^{\Delta FN3}$ with WT *V. cholerae* in CR or DS contexts. Feces were collected daily, and mice were sacrificed at day 4 post infection to collect 3rd distal small intestines. *ΔtagA* colonized equally well as in both communities in feces and the 3rd distal small intestines (Figure 4-4A and C), except for day 2, when *ΔtagA* colonized slightly better in CR in feces (Figure 4-4A). By day 4 post infection, *ΔtagA* colonized ~10 fold lower than WT in the 3rd small intestines without any microbial community (Figure 4-4C). This suggests that the presence of gut microbes compensates for the negative effects of deleting *tagA*, indicating that other microbial factors can partially mitigate the loss of TagA. The *tagA*^{E433D} mutant, which retains mucinase activity but lacks the secretagogue function, performed similarly to WT in DS community in feces collected at day 2 to day 4 (Figure 4-4B) and in the 3rd distal small intestines (Figure 4-4D). In contrast, *tagA*^{E433D} colonized ~10 fold better than WT in CR community ((Figure 4-4D), suggesting that mucinase activity of TagA is crucial for the CR community's resistance to *V. cholerae* colonization. This activity likely promotes the growth of CR microbes by providing nutrients from degraded mucin, thereby enhancing the community's competitive edge against *V. cholerae*.

The *tagA*^{FN3} mutant, which lacks the mucin-inducing FN3 domain, colonized equally well

as WT in the absence of human gut microbes or in the presence of the CR community. However, *tagA*^{FN3} exhibited defective colonization in the presence of DS microbes, which are more susceptible to WT *V. cholerae* colonization (Figure 4-3C). This highlights the critical role of the FN3 domain in promoting *V. cholerae* colonization in DS contexts, likely by inducing mucin production and other unidentified mechanisms, which helps *V. cholerae* establish and proliferate in these susceptible environments.

Taken together, these results suggest distinct roles for the mucin-degrading and mucin-inducing activities of TagA in different microbial contexts. The mucin-degrading activity of TagA appears to contribute to the ability of CR microbes to prevent *V. cholerae* colonization, possibly by providing a nutrient source that supports the growth of competitive gut bacteria. On the other hand, the mucin-inducing activity of TagA is crucial for *V. cholerae* to exploit and colonize in dysbiotic microbiomes.

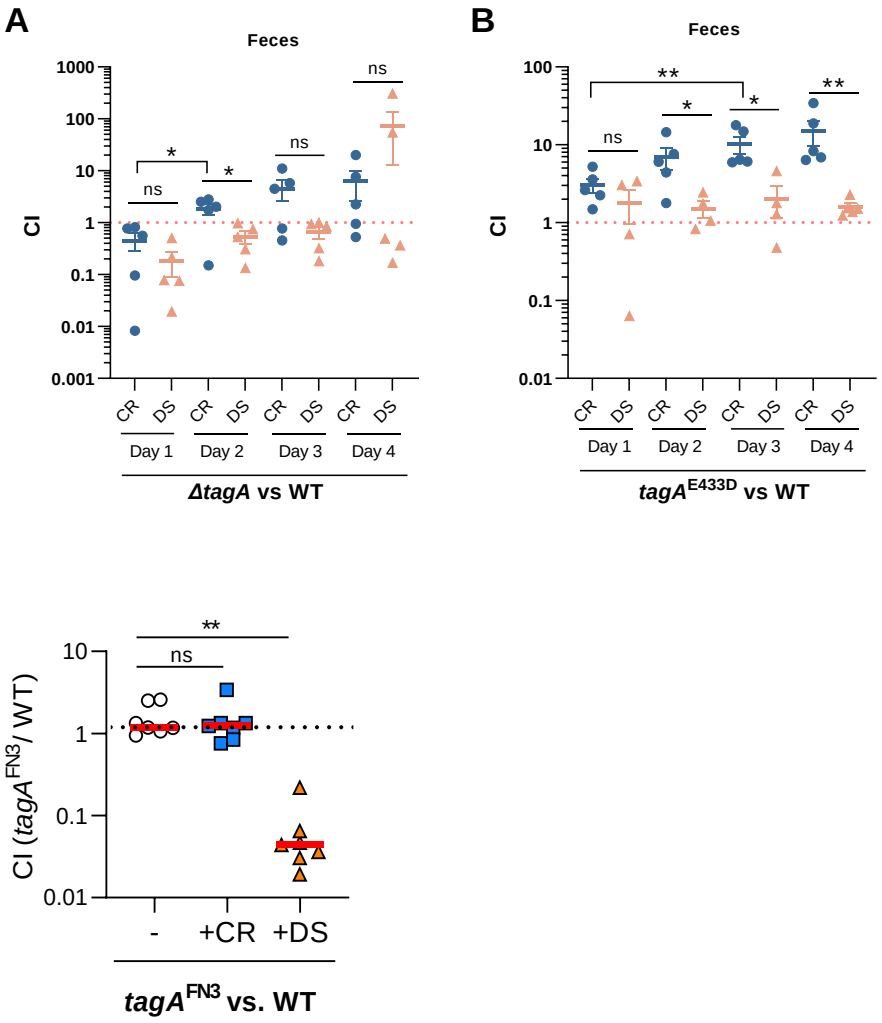


Figure 4-5. Impact of TagA Mucinase and Secretagogue Activities on *V. cholerae* Colonization in CR and DS communities.

(A) The competition index (CI) of *ΔtagA* vs WT withCR or DS communities in the feces collected from day 1 to day 4 post infection.

(B) The competition index (CI) of *tagA*^{E433D} vs WT with CR or DS communities in the feces collected from day 1 to day 4 post infection.

(C) The competition index (CI) of *ΔtagA* vs WT with/without CR or DS communities in the 3rd distal small intestines collected at day 4 post infection.

(D) The competition index (CI) of *tagA*^{E433D} vs WT with/without CR or DS communities in the 3rd distal small intestines collected at day 4 post infection.

(E) The competition index (CI) of *tagA*^{FN3} vs WT with/without CR or DS communities in the 3rd distal small intestines collected at day 4 post infection.

All analysis were tested with Mann-Whitney, n = 5 to 7, *: $P < 0.05$, **: $P < 0.01$, ***: $P < 0.001$, ****: $P < 0.0001$, ns: not significant. Error bars represent mean ± SEM.

16s sequencing analysis of fecal and intestinal samples

We conducted 16s rRNA gene sequencing analysis on fecal and distal small intestinal samples collected on day 3 post-inoculation. In mice with CR communities, *Bacteroides* spp. was the most abundant bacterial genus, followed by *Blautia obeum* (Figure 4-6). *Streptococcus* spp. dominated the microbiome of mice with DS communities, with *Enterococcus* spp. being the next most abundant (Figure 4-6). Although the overall microbial community structures did not exhibit statistically significant differences between groups based on 16s analysis (Figure 4-7), we observed notable variations in the relative abundances of specific bacterial taxa, particularly *V. cholerae*.

Mice harboring the CR community exhibited an inhibitory effect on *V. cholerae* colonization, with relative abundances ranging from ~ 2% in fecal samples to 0-4% in distal small intestinal samples (Figure 4-8A). In contrast, the DS community appeared to promote *V. cholerae* infection, as evidenced by relative abundances of 20-40% in fecal samples and 0-6% in distal small intestinal samples (Figure 4-8B). The relative abundance of *B. obeum* did not differ significantly between groups in both fecal and distal small intestinal samples. However, *Streptococcus* spp. exhibited a higher relative abundance in fecal samples of mice inoculated with the *TagA*^{FN3} strain compared to the WT strain.

To quantify the total bacterial loads in these samples, we performed qRT-PCR analysis. Within each community type (CR or DS), the total bacterial loads did not differ significantly between groups (Figure 4-9C and D). However, we observed substantial

variations in bacterial loads between sample types and community types. In mice harboring either the CR or DS communities, the total bacterial loads were approximately 10- to 100-fold higher in fecal samples compared to distal small intestinal samples (Figure 4-9C and D). Furthermore, fecal samples from mice with CR communities exhibited approximately 10-fold higher bacterial loads than those from mice with DS communities (Figure 4-9A and C). Regarding specific bacterial taxa, the absolute abundance of *B. obeum* was higher in the *TagA*^{FN3} group compared to the *TagA*^{E433D} and WT groups in fecal samples, while the absolute abundance of *Streptococcus* spp. did not differ significantly among groups in both fecal and distal small intestinal samples (Figure 4-10).

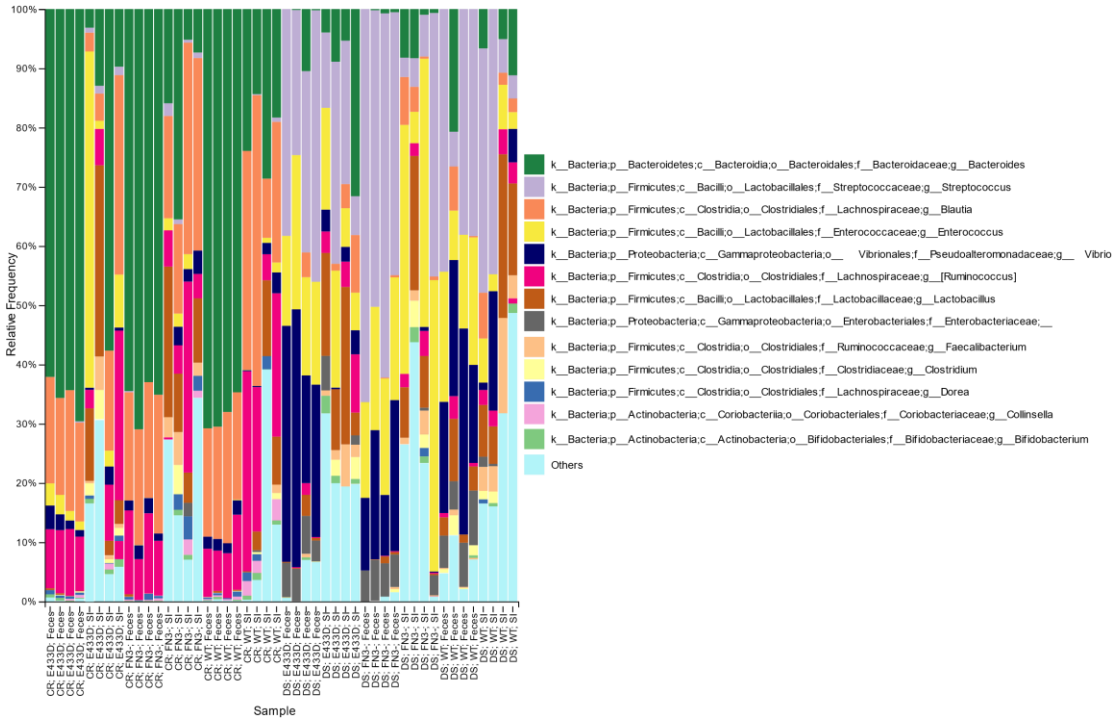


Figure 4-6. Relative frequency of the strains based on 16S sequencing analysis of the feces and distal small intestines (SI) collected at day 3 post infection. E433D: *tagA*^{E433D}; FN3: tagA^{FN3}, WT: WT.

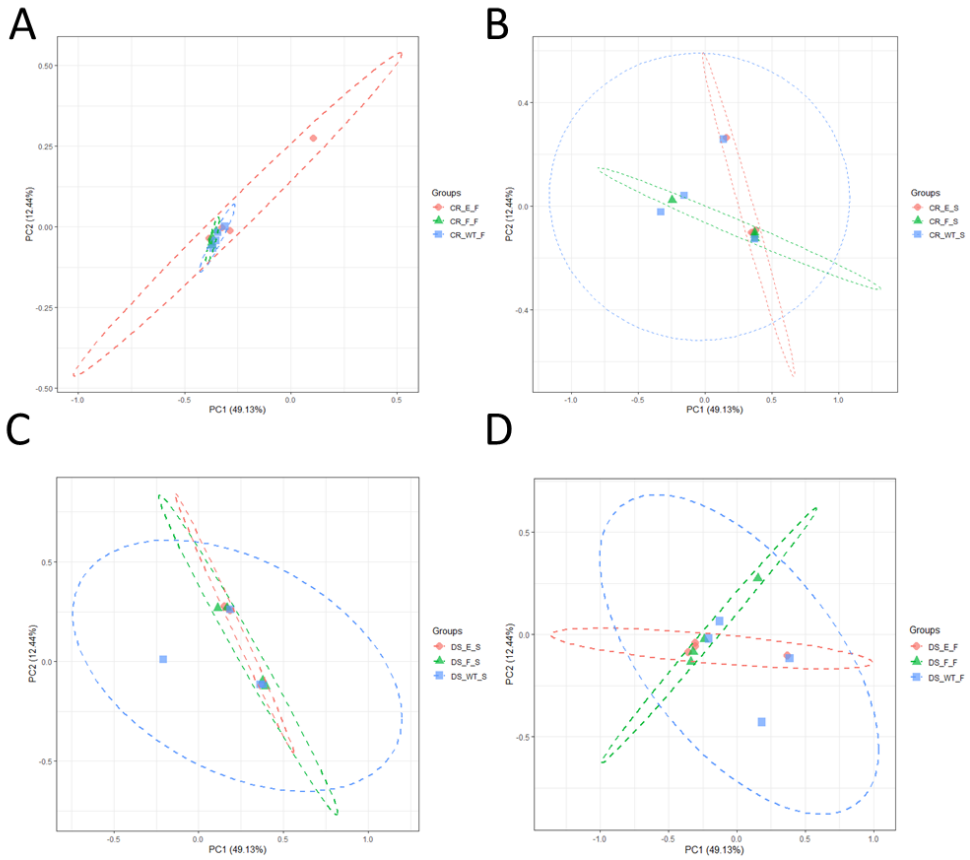


Figure 4-7. Principal coordinates analysis (PCoA) of microbiome 16S sequencing analysis. PCoA of microbiome community diversity based on unweighted UniFrac distance of **(A)** feces or **(B)** the 3rd distal small intestines in mice with CR community collected at day 3 post inoculation, and **(C)** feces or **(D)** the 3rd distal small intestines in mice with DS community collected at day 3 post inoculation. % variance explained shown in each axis. Ellipses show 95% confidence intervals.

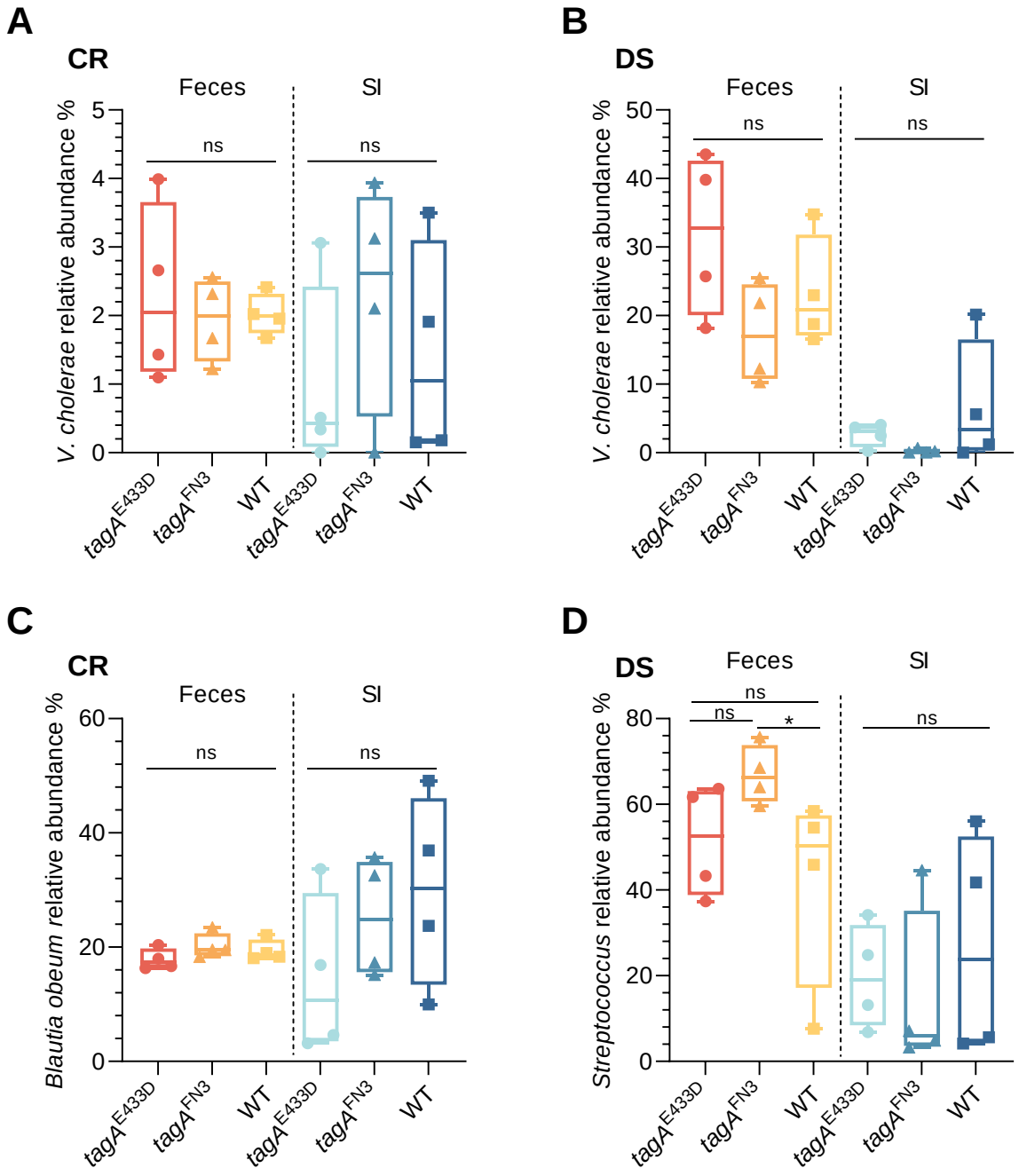


Figure 4-8. Relative abundance of *V. cholerae* (A and B), *Blautia obeum* (C), or *Streptococcus* (D) in germ free mice with CR or DS community.

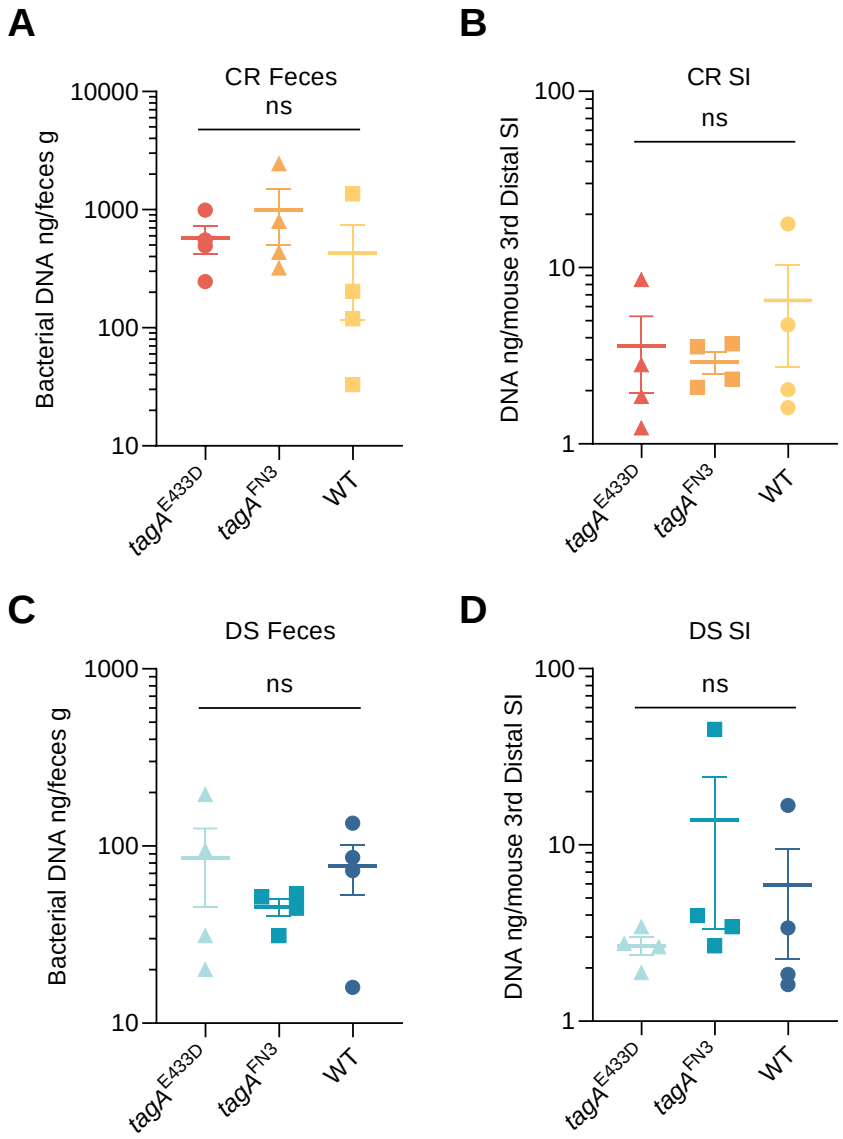


Figure 4-9. Total bacterial load in feces or small intestines (SI) collected from germ free mice. Total bacterial load in **(A)** feces or **(B)** small intestines (SI) collected from germ free mice with CR community; Total bacterial load in **(C)** feces or **(D)** small intestines (SI) collected from germ free mice with DS community. Mann-Whitney U-test, n=4, ns: not significant. Error bars represent mean ± SEM.

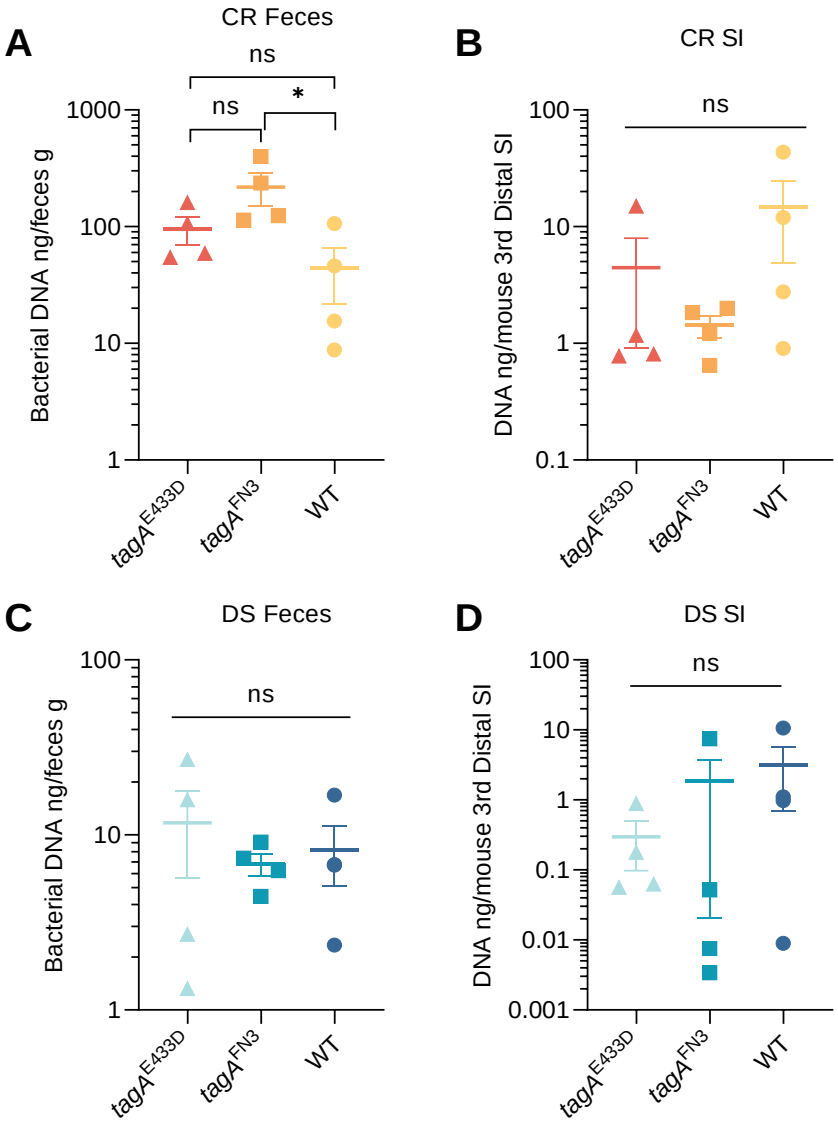


Figure 4-10. *B. obeum* and *Streptococcus* spp. load in feces or small intestines (SI) collected from germ free mice. *B. obeum* load in **(A)** feces or **(B)** small intestines (SI) collected from germ free mice with CR community; and *Streptococcus* spp. load in **(C)** feces or **(D)** small intestines (SI) collected from germ free mice with DS community. Mann-Whitney U-test, n=4, ns: not significant. Error bars represent mean ± SEM.

TagA is commonly found in *V. cholerae* strains process *tcpA*

To further investigate the role of the TagA protein in *V. cholerae*, we compared the presence of five genes (*dnaA*, *ctxA1*/*A2*, *tcpA*, and *tagA*) across a diverse set of *V. cholerae* strains with different serotypes and environmental niches. The *dnaA* gene, encoding an AAA+ ATPase, was present in all examined *V. cholerae* strains, as expected (Table 4-2 and Figure 4-11). The ctxA1 and ctxA2 genes, encoding the major components of cholera toxin, were found in 45 out of the strains analyzed. Notably, 43 of these 45 strains also harbored the *tagA* gene (Table 4-2 and Figure 4-11). All 16 strains possessing *ctxA2* also carried *tagA*. Furthermore, tcpA, encoding the major component of the toxin-coregulated pilus (TCP), a critical virulence factor in *V. cholerae* infections, exhibited a high degree of overlap with *tagA* across the examined strains (Table 4-2 and Figure 4-11). These findings suggest that the *tagA* gene may be preferentially retained by *V. cholerae* strains, potentially due to its functional significance. Further studies are warranted to elucidate the precise mechanisms by which *TagA* influences *V. cholerae* pathogenesis.

Table 4-2. Presence of *dnaA*, *ctxA1/A2*, *tcpA* and *tagA* in *V. cholerae* strains. Blue box indicates the presence of this gene, empty box indicates absence of this gene.

	Strain	Serotype	*dnaA* (VC0012)	*ctxA1* (VC1457)	*ctxA2* (VC1457)	*tcpA* (VC0828)	*tagA* (VC0820)
1	*Vibrio cholerae* strain E7G	environmental	■				
2	*Vibrio cholerae* strain Env-390	environmental	■			■	■
3	*Vibrio cholerae* strain L6G	environmental	■				
4	*Vibrio cholerae* strain PS-4	environmental	■				
5	*Vibrio cholerae* strain RFB16	environmental	■				
6	*Vibrio cholerae* strain SA10G	environmental	■				
7	*Vibrio cholerae* strain SA3G	environmental	■				
8	*Vibrio cholerae* strain Sa5Y	environmental	■				
9	*Vibrio cholerae* strain SA7G	environmental	■				
10	*Vibrio cholerae* strain SL4G	environmental	■				
11	*Vibrio cholerae* strain SL5Y	environmental	■				
12	*Vibrio cholerae* strain SL6Y	environmental	■				
13	*Vibrio cholerae* strain SO5Y	environmental	■				
14	*Vibrio cholerae* strain SP6G	environmental	■				
15	*Vibrio cholerae* strain SP7G	environmental	■				
16	*Vibrio cholerae* strain W10G	environmental	■				
17	*Vibrio cholerae* strain W6G	environmental	■				
18	*Vibrio cholerae* strain W7G	environmental	■				
19	*Vibrio cholerae* strain DRC187	non-O1	■				
20	*Vibrio cholerae* strain CNRVC190247	non-O1/non-O139	■				
21	*Vibrio cholerae* BCH-01536 DNA	O1	■	■		■	■
22	*Vibrio cholerae* IDH-00113 DNA	O1	■	■		■	■
23	*Vibrio cholerae* IDH-02387 DNA	O1	■	■		■	■
24	*Vibrio cholerae* IDH-03329 DNA	O1	■	■		■	■
25	*Vibrio cholerae* IDH-03506 DNA	O1	■	■		■	■
26	*Vibrio cholerae* isolate CTMA_1441	O1	■	■			
27	*Vibrio cholerae* man9 DNA	O1	■	■	■	■	■
28	*Vibrio cholerae* strain 20000	O1	■				
29	*Vibrio cholerae* strain 2010EL-1786	O1	■	■		■	■
30	*Vibrio cholerae* strain 2011EL-1271	O1	■				
31	*Vibrio cholerae* strain 3569-08	O1	■	■	■	■	■
32	*Vibrio cholerae* strain C5	O1	■	■		■	■
33	*Vibrio cholerae* strain CRC1106	O1	■	■		■	■
34	*Vibrio cholerae* strain CRC711	O1	■	■		■	■
35	*Vibrio cholerae* strain DRC001	O1	■	■		■	■
36	*Vibrio cholerae* strain DRC052	O1	■	■		■	■
37	*Vibrio cholerae* strain DRC072	O1	■	■		■	■
38	*Vibrio cholerae* strain DRC193A	O1	■	■		■	■
39	*Vibrio cholerae* strain E1162	O1	■	■	■	■	■
40	*Vibrio cholerae* strain E1320	O1	■	■	■	■	■
41	*Vibrio cholerae* strain E506	O1	■	■	■	■	■
42	*Vibrio cholerae* strain M2140	O1	■	■	■	■	■
43	*Vibrio cholerae* strain NCTC5395	O1	■			■	■
44	*Vibrio cholerae* strain NCTC9420	O1	■			■	■
45	*Vibrio cholerae* strain PanChol	O1	■			■	■
46	*Vibrio cholerae* strain A1552	O1 El Tor	■	■		■	■
47	*Vibrio cholerae* strain A1552	O1 El Tor	■	■		■	■
48	*Vibrio cholerae* strain A1552	O1 El Tor	■	■		■	■
49	*Vibrio cholerae* strain A1552	O1 El Tor	■	■		■	■
50	*Vibrio cholerae* strain E7946	O1 El Tor	■	■		■	■
51	*Vibrio cholerae* strain N16961	O1 El Tor	■	■		■	■
52	*Vibrio cholerae* strain TSY216	O1 El Tor	■	■		■	■
53	*Vibrio cholerae* strain VC1374	O1 El Tor	■	■		■	■
54	*Vibrio cholerae* strain 2012Env-9	O1 Inaba	■			■	■
55	*Vibrio cholerae* strain A19	O1 Inaba	■	■		■	■

	Strain	Serotype	*dnaA* (VC0012)	*ctxA1* (VC1457)	*ctxA2* (VC1457)	*tcpA* (VC0828)	*tagA* (VC0820)
56	*Vibrio cholerae* strain CNRVC190243	O1 Inaba					
57	*Vibrio cholerae* strain 2012EL-2176	O1 Ogawa					
58	*Vibrio cholerae* strain MS84A	O1 Ogawa					
59	*Vibrio cholerae* strain N1252	O1 Ogawa					
60	*Vibrio cholerae* V060002 DNA	O1 Ogawa					
62	*Vibrio cholerae* strain 4295STDY6534200	O139					
63	*Vibrio cholerae* strain 4295STDY6534216	O139					
64	*Vibrio cholerae* strain 4295STDY6534232	O139					
65	*Vibrio cholerae* strain 4295STDY6534248	O139					
66	*Vibrio cholerae* strain F9993	O139					
67	*Vibrio cholerae* strain 3566-08	O141					
68	*Vibrio cholerae* strain K2802	O141					
69	*Vibrio cholerae* strain 3528-08	O141/NAG					
70	*Vibrio cholerae* V130003 DNA	O144					
71	*Vibrio cholerae* O162 RIMD 2214400 DNA	O162					
72	*Vibrio cholerae* O17 RIMD 2214255 DNA	O17					
73	*Vibrio cholerae* O207 RIMD 2214445 DNA	O207					
74	*Vibrio cholerae* strain 10432-62	O27					
75	*Vibrio cholerae* O45 RIMD 2214283 DNA	O45					
76	*Vibrio cholerae* strain 1154-74	O49					
77	*Vibrio cholerae* O5 RIMD 2214243 DNA	O5					
78	*Vibrio cholerae* O51 RIMD 2214289 DNA	O51					
79	*Vibrio cholerae* O63 RIMD 2214301 DNA	O63					
80	*Vibrio cholerae* strain 2011V-1043	O75					
81	*Vibrio cholerae* strain 3541-04	O75					
82	*Vibrio cholerae* O77 RIMD 2214315 DNA	O77					
83	*Vibrio cholerae* O96 RIMD 2214334 DNA	O96					
84	*Vibrio cholerae* isolate Vibrio cholerae str. BC1071	NA					
85	*Vibrio cholerae* strain 2010V-1116	NA					
86	*Vibrio cholerae* strain 2015V-1118	NA					
87	*Vibrio cholerae* strain 2015V-1126	NA					
88	*Vibrio cholerae* strain 3523-03	NA					
89	*Vibrio cholerae* strain 3566-06	NA					
90	*Vibrio cholerae* strain BY369	NA					
91	*Vibrio cholerae* strain CECT 514	NA					
92	*Vibrio cholerae* strain Colony11	NA					
93	*Vibrio cholerae* strain Colony268	NA					
94	*Vibrio cholerae* strain Colony605	NA					
95	*Vibrio cholerae* strain Colony98	NA					
96	*Vibrio cholerae* strain E1	NA					
97	*Vibrio cholerae* strain E4	NA					
98	*Vibrio cholerae* strain FDAARGOS_223	NA					
99	*Vibrio cholerae* strain FORC_055	NA					
100	*Vibrio cholerae* strain FORC_073	NA					
101	*Vibrio cholerae* strain FORC_076	NA					
102	*Vibrio cholerae* strain GXFL1-4	NA					
103	*Vibrio cholerae* strain ICDC-VC3741	NA					
104	*Vibrio cholerae* strain ICDC-VC661	NA					
105	*Vibrio cholerae* strain ICDC-VC702	NA					
106	*Vibrio cholerae* strain PNUSAV001140	NA					
107	*Vibrio cholerae* strain PNUSAV001141	NA					
108	*Vibrio cholerae* strain RFB05	NA					
109	*Vibrio cholerae* strain VC_hf7	NA					

NA: Not applicable

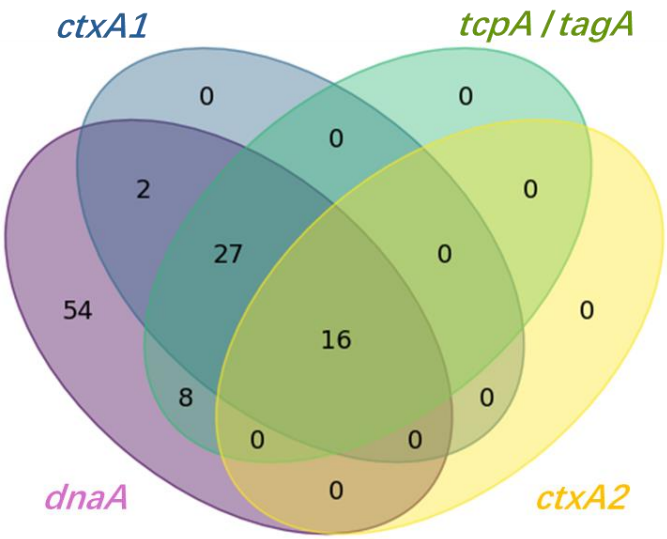


Figure 4-11. Venn diagram of 5 genes from 110 *V. cholerae* strains.

Discussion

Mucins, crucial components of mucus, are glycoproteins produced by epithelial cells. They provide a protective barrier on epithelial surfaces and between microbes, lubricate mucosal surfaces, serve as nutrient sources for microorganisms, facilitate nutrient absorption, regulate the secretion of signaling molecules, influence intercellular communication, affect gene expression and cell physiology, and contribute to the host's defense against invading pathogens[217]. Many microbes can degrade mucin by secreting hydrolytic enzymes and utilizing mucin-derived glycan as a primary carbon source, including pathogenic. This includes pathogenic microbes like *Candida albicans*, which secretes the aspartyl protease Sap2, and *V. cholerae* which secretes the metalloproteas TagA. Symbiotic microbes, such as *Akkermansia muciniphila*, a probiotic bacterium that was found depleted in patients with

diabetes and obesity[214,218–220], also degrade mucin through four relevant mucin-degrading enzymes: sialidases, fucosidases, N-acetyl-β-glucosaminidases and GlcNAc-sulfatases[221]. Additionally, some microbes can bind to mucin. For example, *Helicobacter pylori* used BabA and SabA adhesins to bind to MUC1, triggering "mucin shedding", which protects host epithelial cells from pathogens[222–224]. During infection, *V. cholerae* secretes HapA and TagA via Type 2 secretion system to penetrate the mucus layer. In a mouse model, *V. cholerae* utilizes GbpA to bind N-acetyl-d-glucosamine residues of intestinal mucin, increasing mucin secretion, and in turn inducing GbpA expression[225]. Mucin also activates type VI secretion system (T6SS), a crucial mechanism *V. cholerae* uses to kill other bacteria[190].

The host gut microbiota significantly influences the fitness of invading microorganisms. Research has uncovered various mechanisms by which gut microbes inhibit *V. cholerae* colonization. For example, Lactobacillus species from the feces of cholera patients[226] and healthy children[227] produce diffusible compounds that inhibit *V. cholerae*. *Bautia obeum* generates AI-2 signals that impede *V. cholerae* colonization through unidentified quorum sensing pathways[49]. Furthermore, a commensal *Escherichia coli* strain from a healthy human gut can kill *V. cholerae in vitro*[228], and the probiotic *E. coli* Nissle 1917 reduces *V. cholerae* colonization in zebrafish[229] by lowering pH via glucose catalysis. Additionally, gut microbes produce toxic metabolites to combat *V. cholerae* infection, such as colibactin produced by an *E. coli* isolated from a mouse small intestine (EMS1) [230].

The effects of mucin production and degradation on microbial behavior and community composition are significant. This study explored the dual-function of metalloproteas TagA in *V. cholerae*, including its mucinase and mucin-inducing activities. We found that TagA's dual activity influences *V. cholerae* fitness during colonization in a microbiota-specific manner: mucinase activity helps the CR community resist *V. cholerae* colonization, while mucin-inducing activity aids the DS community in promoting *V. cholerae* colonization. Future studies will elucidate the mechanisms driving mucin-dependent interactions between commensal communities and *V. cholerae*. One key area if focus will be to identify how mucolytic activity contributes to CR resistance to *V. cholerae* and how DS members promote *V. cholerae* colonization through induced mucin production. It is likely that one or a combination of microbial species work together to alter *V. cholerae* adhesion to epithelial cells, modulate its motility, and influence the expression of virulence genes. We will explore how these microbes secrete metabolites and engage in exchanges within the gut environment that favor or hinder *V. cholerae* colonization. Moreover, we plan to extend our research by studying the effects of TagA on more diverse model communities from human samples collected in cholera-endemic areas. This broader investigation will help us understand how environmental factors and varying microbial compositions influence the interaction between *V. cholerae* and the host gut microbiota.

Chapter 5 A review on single-cell RNA sequencing in bacteria and possible applications on *V. cholerae* studies

Introduction

Gut microbiota is a complex and dynamic community of microorganisms (most are non-pathogenic) that are involved in essential processes in human host, such as digestion, nutrient absorption and host immune response to defend against pathogen invasion. Recently, there has been significant focus on studying the composition of the gut microbiome in both healthy and disease states, and how these differences contribute to various disease outcomes. Disruptions in the gut microbiota composition, known as dysbiosis, have been linked to diseases such as inflammatory bowel disease, obesity, diabetes, cancer, and bacterial infections like cholera[49,149,231]. The advent of high-throughput next-generation sequencing (NGS) technologies, such as metagenomics and metatranscriptomics, has significantly advanced our understanding of the microbiome and has become the standard approach for studying microbial communities. However, these methods provide a community-level perspective, which often falls short in capturing the heterogeneity and individual behaviors of microbial cells, potentially masking important variations and interactions at the single-cell level.

Recently, single-cell RNA (scRNAseq) has emerged as a powerful tool for examining gene expression at the individual cell level. The pioneering work of Tang et al. in 2009 marked the inception of single-cell RNA sequencing (scRNA-seq), wherein they sequenced the

transcriptome of individual blastomeres and oomycetes[232]. Since then, a plethora of modified and enhanced scRNA-seq technologies have emerged, such as Smart-seq[233], Smart-Seq2[234], Drop-seq[235], 10xGenomics[236], MATQ-seq[237], Seq-Well[238], CEL-seq[239], MARS-seq[240], inDrop-seq[241], broadening the scope of its applications and facilitating significant discoveries in mammalian systems. This technological advancement has fostered a deeper understanding and appreciation of the transcriptional heterogeneity within cell types and states, thereby unveiling novel insights into cellular biology, elucidating mechanisms of disease progression, improving diagnostic and treatment methods. For example, scRNA-seq has been used to better diagnose and treat gastric cancer (reviewed in [242]) and identify novel mucosal ciliated cell states and CD4+ cell states in healthy and diseased individuals with asthma[243]. Initially developed for eukaryotic cells, scRNA-seq has been adapted to prokaryotic systems, offering unprecedented resolution in studying microbial communities.

In this chapter, we discussed the advantages and disadvantages of scRNA-seq and bulk RNA-seq methods, along with the technical challenges of applying scRNA-seq in bacterial systems. We also compared existing scRNA-seq technologies and experimental protocols for bacterial studies, evaluating the results and limitations of each method. Furthermore, we examined the effectiveness of these approaches in addressing practical problems and their prospects for solving complex microbiome issues. Lastly, we proposed future applications for studying *V. cholerae* and other gut microbes, highlighting the questions that scRNA-seq approaches may help us answer.

ScRNA-seq vs bulk-RNAseq

While bulk RNA-seq captures average gene expression across a population of cells, scRNA seq unveils transcriptomic landscape with single-cell resolution. The advantages of scRNA seq compared to bulk RNA seq reflects on several aspects:

a. **Resolution of cellular heterogeneity and identification of rare cell types.** ScRNA allows discern of the presence of heterogeneity within a cell population, such as rare cell types, transitional states, and different stress responses, which are masked by traditional bulk RNA seq. Especially when studying complex tissues and diseases in human, animals and plants, scRNA enables identification, classification and discovery of new or rare cells types, providing more profound information about health and disease development[244].

b. **Identification of novel cell types and states.** ScRNA-seq has the capability to reveal previously undiscovered cell types or transitional states, thereby potentially expanding our comprehension of cellular diversity and developmental processes.

c. **Dynamic insights into gene regulation:** scRNA-seq allows for the examination of gene expression dynamics at a single-cell resolution, providing insights into the regulation of gene expression patterns during cellular processes such as differentiation, development, and response to stimuli.

d. Unveiling the transient and cell to cell direct response. ScRNA-seq may be helpful in discovering transcriptional bursts and pulses[245,246], which may generate some novel and uncommon behaviors. ScRNA-seq also enables the direct measurement of transcriptomic profiles during specific cell interactions, particularly when coupled with technologies aiding cell localization. This capability proves invaluable in studying transient responses occurring only when cells are in close contact, whether between identical cell types or heterogeneous populations.

Challenges in scRNA-seq applications

a. Technical variability and noise: scRNA-seq workflows involve multiple steps that may introduce technical variability and noise, leading to biases in gene expression quantification. For example, Brink et al. found that protease dissociation strongly induce the expression of stress genes in a subpopulation of muscle stem cells[247].

b. Challenges in understanding cell-to-cell interactions. While numerous scRNA-seq studies have shed light on the cellular composition and heterogeneity, such as within tumors[244], understanding the specific biological functions of individual cell types and deciphering the communication networks between cells remains a significant challenge.

c. Data analysis complexity: Analyzing scRNA-seq data requires specialized computational methods to handle the high-dimensional, sparse data generated from

individual cells. It is important and challenging to correctly identify cell types and filtering noises.

d. Undeveloped pipelines and tools for application in plants and prokaryotes. The realm of scRNA-seq has predominantly centered around studies involving humans and animals, leaving a significant gap in its application within plant and prokaryotic systems. The pipelines and tools available for generating scRNA-seq library and analyzing scRNA-seq data in plants and prokaryotes remain underdeveloped and less mature compared to those tailored for human studies, which limits its applicability of scRNA-seq in plants and prokaryotes.

e. Problem of detection of lowly expressed genes: scRNA-seq may struggle to detect genes with low expression levels, especially in samples with limited RNA content or technical noise. This can impact the sensitivity of scRNA-seq experiments and the ability to capture rare transcripts accurately. Due to the cost, usually the sequencing depth is not very high, which may lead to incomplete transcriptomic profiles, resulting in missed detection of lowly expressed genes.

f. Cost and throughput: Compared to bulk RNA-seq, scRNA-seq is often more expensive and time-consuming due to the need to process and sequence individual cells. Additionally, the throughput of scRNA-seq platforms may be lower, limiting the scale of experiments that can be performed.

Challenges in scRNA-seq application in prokaryotes

ScRNA-seq application on prokaryotes presents several technical challenges (Figure 5-1). Firstly, the small size of bacterial cells makes isolating individual cells challenging, often introducing biases and artifacts. Additionally, one major issue is the relatively low abundance of mRNA in bacterial cells; for instance, an *E. coli* cell contains thousands of mRNA molecules, compared to 10^5–10^6 mRNA molecules in a typical mammalian cell. This disparity necessitates highly sensitive detection methods. Ribosomal RNA (rRNA) also presents a significant noise problem, as it comprises a large portion of total RNA in bacterial cells. Unlike eukaryotic mRNAs, bacterial mRNAs lack poly A tails, which are commonly required in RNA enrichment in the existing scRNA-seq protocols, necessitating alternative strategies for RNA selection. The short half-life of bacterial mRNA further complicates RNA capture and sequencing efforts. Overcoming these obstacles requires robust experimental designs tailored to bacterial systems. Additionally, the structural differences between Gram-positive and Gram-negative bacterial cell walls necessitate strain-specific protocols for effective cell lysis and RNA extraction. Furthermore, the development of specialized computational tools and statistical models is essential to accurately analyze and interpret scRNA-seq data from prokaryotes.

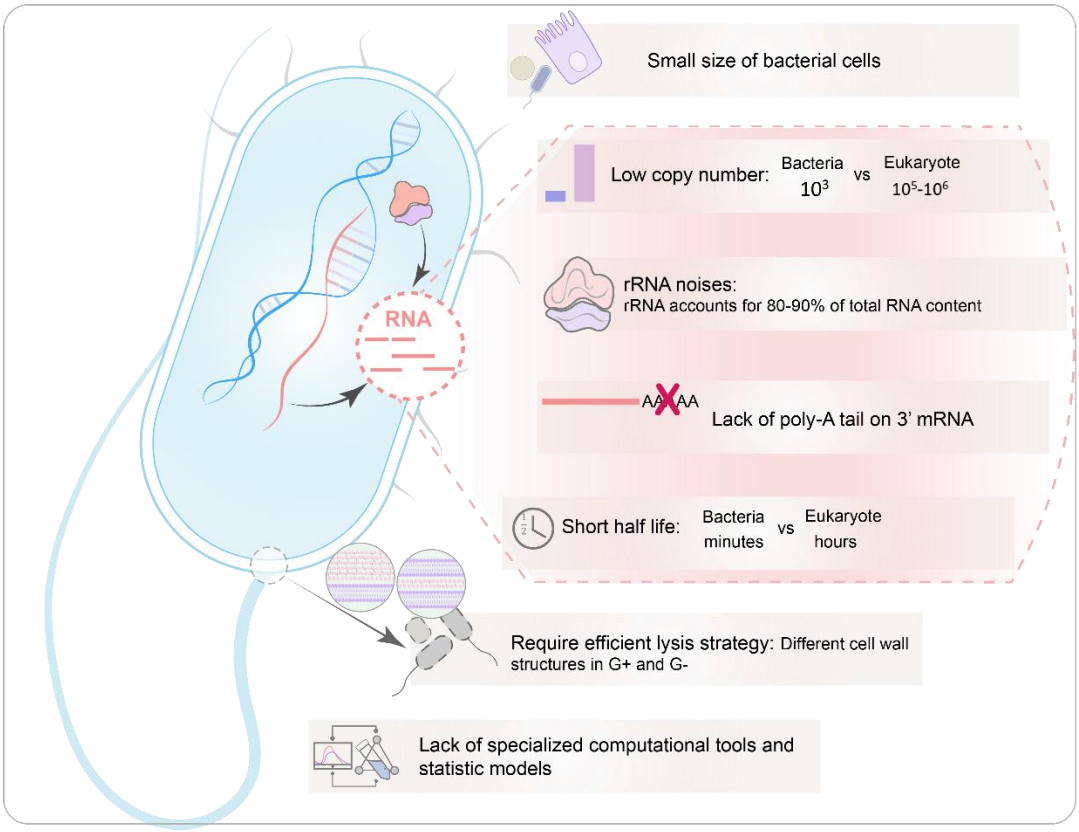


Figure 5-1. Challenges in scRNA-seq application in prokaryotes.

Existing ScRNA-seq applications on bacteria

ScRNA-seq has been successfully applied to bacteria, including both Gram-negative and Gram-positive species. This technology provides unprecedented resolution in studying bacterial heterogeneity, gene expression, and regulatory mechanisms. The following sections will discuss seven published scRNA-seq pipelines on bacteria: MATQ-seq[237], PETRI-seq[248], MicroSPLiT[249] , Par-seqFISH[250], Bacdrop[251], ProBac-seq[252], and M3-seq[253] (Table 5-1).

MATQ-seq: multiple annealing and dC-tailing based scRNA-seq

MATQ-seq (multiple annealing and dC-tailing-based quantitative single-cell RNA-seq), initially developed by Sheng et al. [237] for single-cell RNA sequencing in mammalian cells, has been adapted by Imadhl et al. [254] for bacterial applications. As depicted in Figure 5-2, the MATQ-seq workflow for bacterial cells begins with the isolation of single cells using fluorescence-activated flow cytometry (FACS). These cells are sorted into PCR plates preloaded with lysis buffer. Following cell lysis, the samples undergo lysozyme digestion to break down bacterial cell walls. The key innovation of MATQ-seq lies in its reverse transcription (RT) step, which employs multiple rounds of annealing and looping-based amplification cycles (MALBAC). This process enhances the efficiency of cDNA synthesis from bacterial mRNA. After the first-strand cDNA synthesis, poly dC tails are added using terminal transferase. The second-strand cDNA synthesis then utilizes G-enriched MALBAC primers that include unique molecular identifiers (UMIs). These cDNAs are subsequently amplified with a limited number of PCR cycles and tagged with TN5 transposase to generate the final library for sequencing.

Imadhl et al.[254] demonstrated the effectiveness of MATQ-seq in bacterial systems by applying it to the model bacterial pathogen *Salmonella enterica* serovar Typhimurium. They analyzed 60 samples of 10-pooled bacteria (10 cells each) and 71 single-cell samples. The method captured approximately 5% of mRNAs from total aligned reads, detecting an average of 413 genes in the 10-pooled libraries and 170 genes in the single-cell libraries (Table 5-1). Importantly, MATQ-seq successfully identified distinct gene expression

profiles under different growth conditions, highlighting its utility in studying bacterial responses to environmental changes. The researchers also demonstrated the method's compatibility with *Pseudomonas aeruginosa*, a pathogen with higher GC content, indicating its potential applicability to a broader range of bacterial species.

MATQ-seq presents several benefits for bacterial single-cell RNA sequencing. Unlike many other methods, it does not require the presence of poly-A tails on mRNA, making it particularly suitable for bacterial transcripts. The incorporation of UMIs allows for absolute and unbiased transcript counts, providing a more accurate representation of gene expression levels. The method exhibits high sensitivity and requires only a small amount of input material (hundreds of cells for *Salmonella*), making it valuable for studying rare bacterial populations or limited samples.

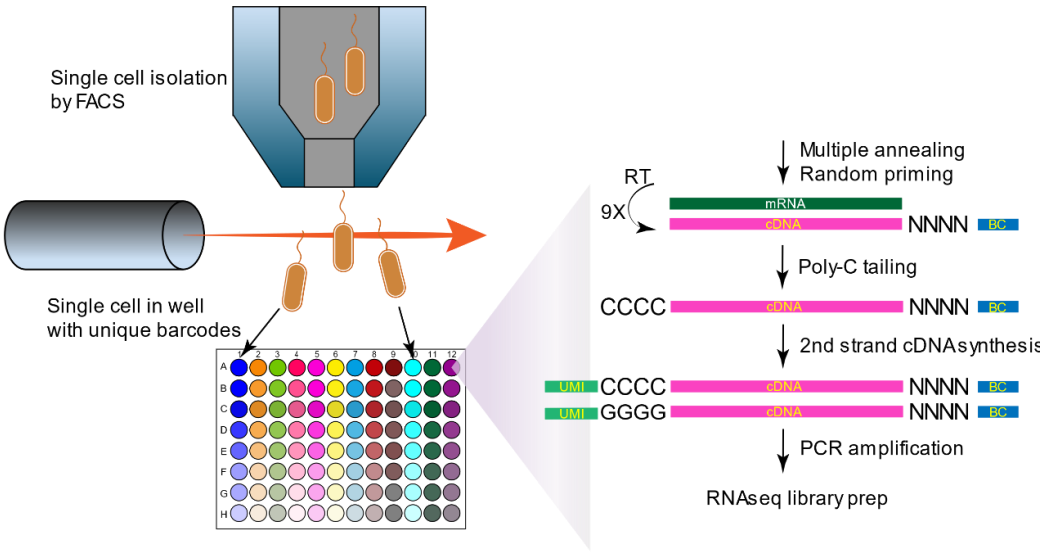


Figure 5-2. The workflow of MATQ-seq. Single cell is sorted by FACS and loaded into a well containing lysis buffer and a unique barcode. After reverse transcription, poly-C tailing, 2nd strand cDNA synthesis and PCR amplification, a scRNA-seq library is generated.

However, MATQ-seq has some drawbacks. A significant drawback is the high level of non-mRNA noise, with approximately 95% of aligned reads corresponding to non-mRNA transcripts (Table 5-1). This necessitates deeper sequencing to obtain sufficient mRNA coverage, potentially increasing the overall cost of the analysis. Additionally, the complexity of the protocol and the specialized equipment required may limit its accessibility to some research laboratories.

PETRI-seq[248] and MicroSPLiT[249] : plate based scRNA-seq

PETRI-seq (Prokaryotic Expression-profiling by Tagging RNA in Situ and Sequencing) [248], developed by Blattman et al. in 2010, and **MicroSPLiT (Microbial split-pool ligation transcriptomics)**[249], developed by Kuchina et al. in 2021, are both based on SPLiT-seq[255], thus they have similar pipelines.

SPLiT-seq was developed for eukaryotic cells and validated in mouse brain and spinal cord tissues, involves fixing cells or nuclei with formaldehyde followed by four rounds of combinatorial barcoding. Initially, as shown in Figure 5-3, cells are distributed into a 96-well plate, where unique barcodes are added during first-strand cDNA synthesis using barcoded RT primers. After pooling and redistributing the cells into a new 96-well plate, the second round of barcoding is performed via ligation. The third round mirrors the second, also using ligation. In the fourth round, unique barcodes are appended to the cDNA during sequence library preparation via 24 PCR reactions. This process ultimately generates up to 21,233,664 unique barcode combinations. They identified 69 types of cells in the brain and

44 types in the spinal cord and identified new molecular markers. One major difference compared to previous methods is SPLiT-seq is compatible with fixed cells. Fixation of cells can reduce the perturbations of the endogenous gene expression and make it possible for storage.

In the **MicroSPLiT** method, as depicted in Figure 5-3, cells are similarly fixed and permeabilized using Tween-20 and lysozyme, which resulted in optimal capture efficiency for both Gram-positive and Gram-negative bacteria. cDNA is synthesized with a mixture of barcoded random hexamers and barcoded poly-T primers, followed by purification according to the SPLiT-seq protocol. A key difference in MicroSPLiT is that mRNAs are enriched by polyadenylation using *E. coli* poly(A) polymerase I (PAP) before three rounds of barcoding. Additionally, mild sonication is applied to separate cell clumps after the reverse transcription step. Library construction utilizes NGS Library Construction Reagents from Enzymatics, and the libraries are sequenced on MiSeq or NextSeq systems (Illumina) using 150-nucleotide kits and paired-end sequencing.

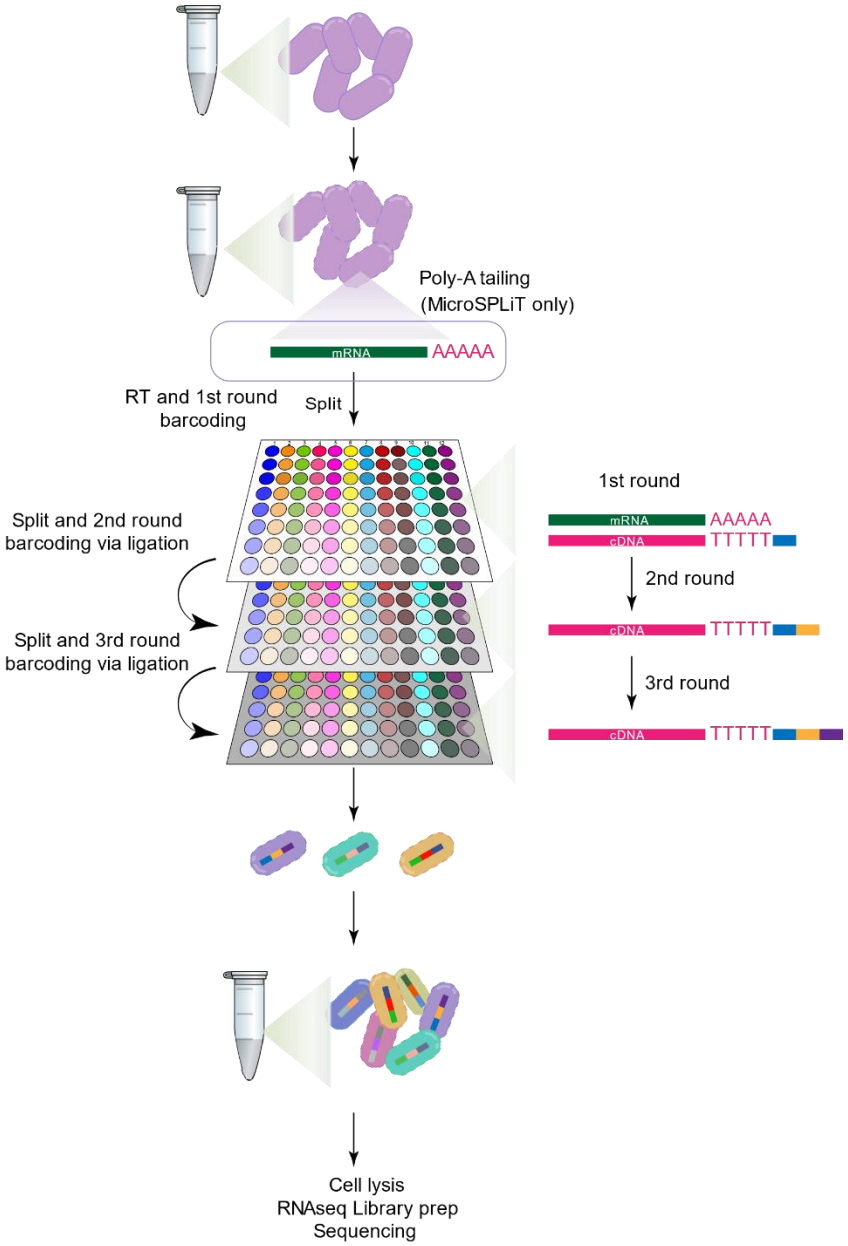


Figure 5-3. The workflow of PETRI-seq/MicroSPLiT. After cell fixation, permeabilization and poly-A tailing (only in MicroSPLiT), and reverse transcription, cells are split into wells containing unique barcodes. After 3 to 4 rounds of barcoding, cDNAs containing unique barcodes combination are generated and ready for sequencing.

The first test, involving a mixture of 2,682 *E. coli* and *Bacillus subtilis* cells subjected to heat shock, revealed a median of 235 mRNA transcripts per cell for *E. coli* and 397 for *B. subtilis*, representing approximately 5-10% of the estimated total mRNA content (Table 5-1). This corresponded to 3.7% and 9.5% of all detected RNA molecules per cell for each respective species, indicating that most RNA molecules were not mRNA. The median number of unique genes detected per cell was 230 for *B. subtilis* and 138 for *E. coli* (Table 5-1). Interestingly, an additional small cluster of *E. coli* cells from both control and heat-treated samples exhibited distinct gene induction phenotypes. In another test, which analyzed over 25,214 *B. subtilis* cells growing in liquid rich medium, the MicroSPLiT method uncovered both rare and unexpected cellular states in *B. subtilis*, although the mRNA abundance was not quantified.

While methods like MicroSPLiT and PETRI-seq offer advantages in terms of simplicity and compatibility with basic pipetting tools, the overall mRNA abundance remains relatively low, even with the enrichment step of polyadenylation. To improve resolution and increase the number of unique barcode combinations to accommodate larger input cell numbers, further optimization of permeabilization techniques, mRNA enrichment strategies (e.g., rRNA depletion), and the incorporation of additional barcoding steps may be necessary.

Par-seqFISH[250]: probe based parallel sequential fluorescence in situ hybridization

Single-molecule RNA fluorescence in situ hybridization (smFISH)[256], developed from the fluorescence in situ hybridization (FISH), enables visualization, spatial resolution and quantitative measurement of transcripts at single cell level. However, this method is restricted by the limited number of genes that can be detected at a time. A modified smFISH approach, called seqFISH[257,258], developed in 2014, overcome this limitation by serial rounds of hybridization, imaging and probe stripping. Shortly, secondary fluorescent probes are designed complementary to the target RNAs, and then hybridize these probes to RNA within fixed cells or tissue samples. The samples are imaged using fluorescence microscopy to detect and record the spatial locations of the fluorescent probes. The fluorescent probes are then stripped from the samples and repeat the hybridization with news sets of probes and imaging as needed. It enables hundreds to thousands of genes to be detected and analyzed consecutively within the same sample in eukaryotes.

Dar et al.[250] successfully adapted the seqFISH approach for bacterial applications, developing a method called **par-seqFISH (parallel sequential fluorescence in situ hybridization)**. A key difference from the original seqFISH is that par-seqFISH utilizes a two-step hybridization process in each round instead of a single hybridization step. Briefly, as illustrated in Figure 5-4, a set of designed primary probes complementary to the target RNAs and flanked by unique secondary sequences are first hybridized to the mRNA. Fluorescence microscopy of the samples at this stage can reveal the spatial context and overall gene expression patterns. Next, a set of three fluorescent readout probes are

introduced to bind to the secondary sequences of the primary probes, effectively "turning on" the signal for specific genes. After imaging, the secondary probes can be stripped and washed away, allowing for the next round of hybridization with a new set of readout probes and the detection of different gene expressions. This approach overcomes the challenge of limited fluorescent probe accessibility in smaller bacterial cells compared to eukaryotes.

In a proof-of-concept study[250] on *P. aeruginosa* (Table 5-1), the authors generated a probe library targeting 105 marker genes that capture various core physiological aspects of this pathogen. By analyzing approximately 600,000 cells collected at different growth stages, they successfully captured diverse metabolic and transient virulence transcriptional states. For instance, they found that the *cdrA* gene, encoding a major adhesive protein component of *P. aeruginosa*, was 186-fold enriched in a metabolically hyperactive subpopulation. Notably, par-seqFISH enables the integration of global cell parameters, such as cell size, shape, and ribosomal levels, with gene expression data. For example, the analysis revealed a transient emergence of two distinct T3SS+ (Type III Secretion System-positive) populations from two growth phases, one expressing all T3SS-related genes, while the other expressed only effector genes. The specific expression of effector genes in the latter population may be related to the need for maintaining appropriate concentrations of effector proteins.

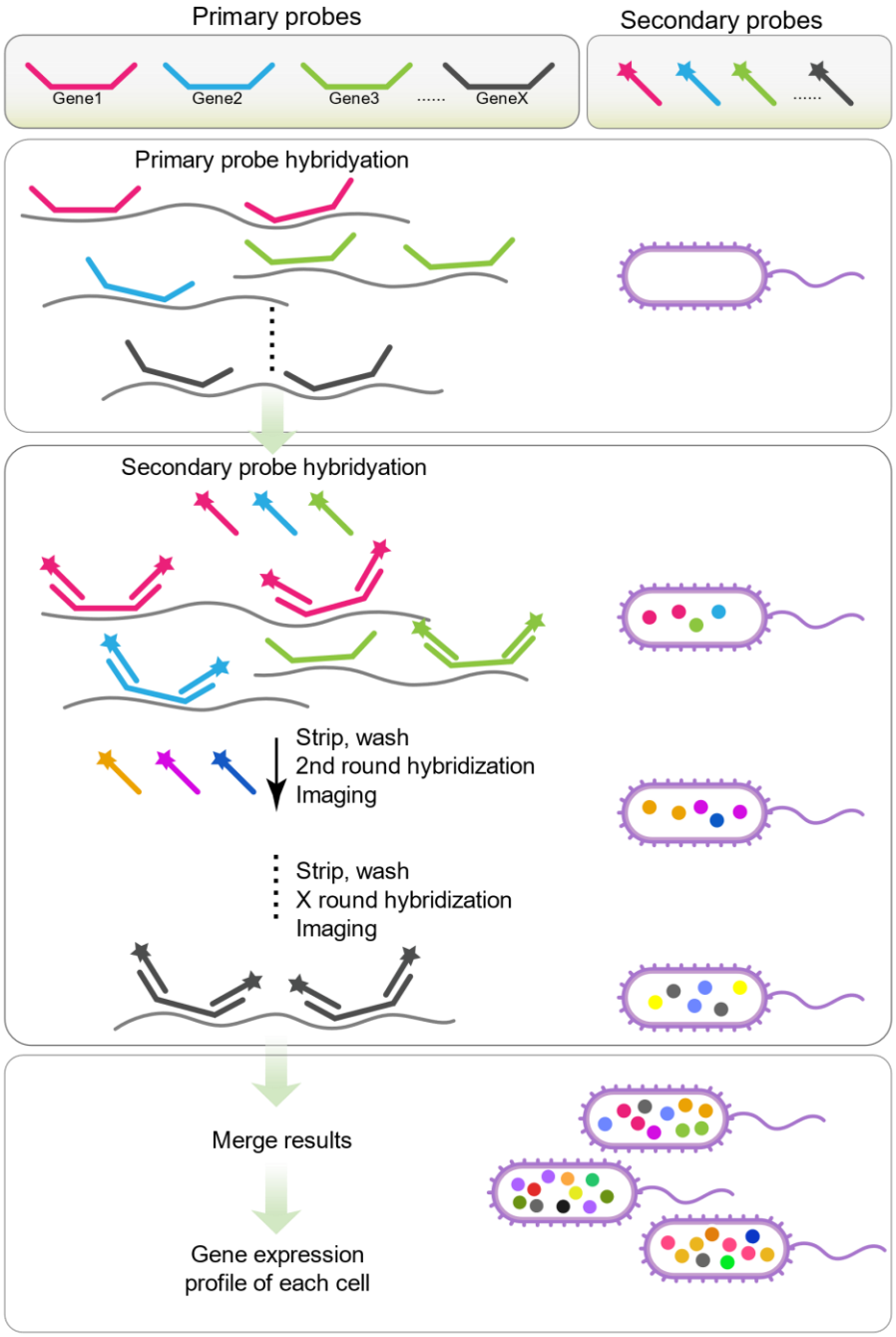


Figure 5-4. The workflow of par-seqFISH. It requires sets of primary and secondary probes to specifically target a selection of genes for high-throughput microscopy. After rounds of hybridization and stripping, with three probes used per cycle, it allows the detection gene expression profiles on a gene-by-gene basis. By combining the images from each microscopy cycle, the overall gene expression profile and spatial information of individual cells can be obtained.

The par-seqFISH method offers several advantages, including the ability to provide novel insights by combining spatial and quantitative gene expression information at the single-cell level, compatibility with large input cell numbers (>600,000), and the avoidance of potential biases introduced by reverse transcription or PCR amplification steps required in traditional RT-PCR and RNA sequencing methods. However, the method also faces challenges, such as increasing costs with a larger number of target genes, the requirement for prior knowledge of gene profiles to design probes, the inability to discover novel genes, the need for further validation across different bacterial species, and the overall complexity of the entire process.

BacDrop[251]: microfluid-based scRNA-seq

Instead of relying on several rounds of barcoding by splitting pools multiple times, **BacDrop (Bacterial droplet-based single-cell RNA-seq)**[251] employs droplet-based microfluidic technology using the 10x Genomics platform and achieves uniquely barcoded cell transcripts via only two rounds of barcoding. As depicted in Figure 5-5, cells are fixed and permeabilized, followed by rRNA and genomic DNA (gDNA) depletion treatments, which were not performed in the previously described split-based methods. Similarly to those methods, cells are then distributed into 384-well plates for the first round of barcoding while generating the first-strand cDNA. During this step, cDNAs are appended with UMIs and round 1 plate barcodes. Afterwards, the cells are pooled together, and cDNA 3' poly-A tailing is performed using terminal deoxynucleotidyl transferase (TdT), followed by droplet generation on the 10x Genomics Chromium Controller, oligo-dT second-strand

cDNA synthesis, and round 2 barcoding within the droplets. The emulsions are combined and broken. Double-stranded cDNAs are tagged, purified, and PCR-enriched for library preparation using the Illumina Nextera XT DNA library preparation kit. Libraries are diluted to desired concentrations and sequenced on the Illumina NovaSeq 6000 platform.

Notably, as summarized in Table 5-1, the rRNA depletion step in BacDrop significantly enriched mRNA representation, boosting the fraction of mRNA reads from just ~5% to encompass 50-90% of total aligned reads, while preserving congruent mRNA profiles relative to undepleted samples. This method also exhibits low cell barcode collision rates. BacDrop has been successfully applied to both Gram-negative species (*E. coli*, *Klebsiella pneumoniae*, *Pseudomonas aeruginosa*) and Gram-positive species (*Enterococcus faecium*), demonstrating its ability to distinguish all four species. Additionally, BacDrop could reproducibly identify population heterogeneity in *K. pneumoniae* MGH66 treated with different antibiotics and identify mobile genetic element (MGE)-driven subpopulations in two *K. pneumoniae* strains, MGH66 and K. BIDMC35.

Compared to previous methods, BacDrop offers several advantages, including significant mRNA enrichment with substantial removal of rRNA, the ability to increase input cell numbers to millions of cells, and the potential for expanded application to a wider range of cell types and studies. However, it also has limitations, such as sequencing depth being constrained by the relatively high expense of the 10x Genomics kit and droplet-generating system, and sequencing costs, even though significantly decreased by rRNA depletion.

Additionally, the need for protocol modifications to accommodate different bacterial strains (e.g., adjusting centrifugation speeds for cells of varying sizes) poses another challenge. Furthermore, additional optimization may be required to adapt BacDrop for more complex microbial communities, such as gut communities.

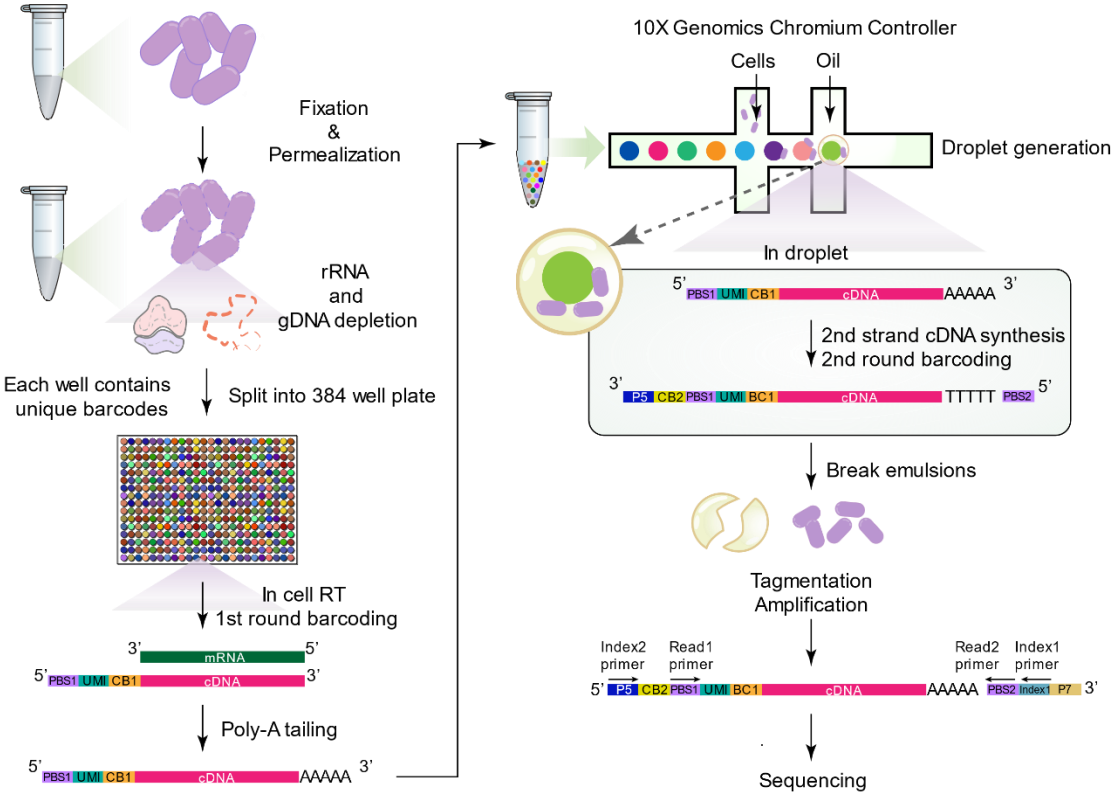


Figure 5-5. The workflow of BacDrop. Bulk cells are first fixed and permeabilized, followed by depletion of rRNA and gDNA. The cells are then divided into multi-well plates containing primers with unique cell barcodes (CB1), unique molecular identifiers (UMIs), and partial primer sequences (PBS1) for Illumina sequencing. The first round of barcoding occurs when mRNAs are reverse transcribed into cDNAs, with PBS1, UMI, and CB1 added to the 5' ends of the cDNAs. Poly-A tails are subsequently added to the 3' ends of the cDNAs. The cells are then loaded into a 10x Genomics Chromium Controller, generating droplets containing multiple cells and one bead harbors unique barcode. The second strand of cDNAs are synthesized, followed by a second round of barcoding where CB2 and adapters for cDNA amplification are attached to the double-stranded cDNAs. Finally, the droplets are broken, and the cDNAs are pooled and amplified via PCR, incorporating the necessary adapters for Illumina sequencing.

ProBac-seq: probed and microfluid based scRNA-seq

ProBac-seq(Probe-based bacterial sequencing)[252], developed by McNulty et al. in 2023, represents a significant advancement in bacterial single-cell RNA sequencing by combining microfluidic droplet encapsulation of single cells with in situ hybridization of DNA probes. The ProBac-seq procedure begins with the design of a library of 50 base pair DNA sequences (Figure 5-6). These sequences contain a 5' PCR handle for library generation, a binding region complementary to target mRNAs, a UMI, and a 3' poly-A tail compatible with the 10X Genomics Single Cell 3′ system. To enhance capture efficiency and minimize noise from poor hybridization or insufficient amplification, multiple probes are used for each gene. As illustrated in Figure 5-6, cells are fixed in 1% paraformaldehyde, permeabilized by mild lysozyme treatment, and incubated with the DNA probe library. Following probe hybridization, the cells are separated via microfluidic encapsulation on a 10X Genomics Chromium Controller, generating droplets containing one or fewer cells and a hydrogel with a unique cell barcode. Within these droplets, barcodes are added to the 3’ of DNA probes. Finally, the droplets are broken, and the cDNAs are pooled, amplified, and purified before sequencing.

McNulty et al.[252] applied ProBac-seq to several bacterial species (Table 5-1), demonstrating its versatility and effectiveness. In *Bacillus subtilis*, using a library of 29,765 probes targeting 2,959 genes, they captured 2,784 cells with an average of 1,073 reads per cell. This resulted in a median of 325 mRNAs per cell, representing 10-20% of total mRNA and a median of 241 genes. For *E. coli*, 21,527 probes targeting 4,181 genes were used,

resolving 3,315 cells with an average of 1,070 reads per cell and detecting a median of 263 transcripts representing 165 distinct genes. In both cases, ProBac-seq successfully identified known cellular states and revealed previously unknown heterogeneity. For instance, competence genes and genes associated with sporulation were found to be overexpressed in some *B. subtilis* subpopulations, while genes related to motility were upregulated in 14.5% of the *E. coli* population. The method was also applied to *Clostridium perfringens*, a Gram-positive, spore-forming, toxin-producing bacterium, uncovering heterogeneous expression of *netB*, which produces the β-barrel pore-forming toxin, NetB, in a subpopulation inducible by acetate.

ProBac-seq offers several advantages over other RNA sequencing methods. Like Par-seqFISH, it provides high sensitivity by directly targeting mRNA, avoiding disturbance from non-mRNA transcripts. The method utilizes commercially available equipment, enhancing its accessibility to researchers.

However, like other probe-based methods, ProBac-seq faces certain limitations. It is restricted to known genome sequences, which can be a drawback when studying novel or poorly characterized organisms. There is potential for probe design bias, and as the number of target genes increases, so do the costs and complexity of the method, particularly when studying complicated microbial communities. Designing effective probes can be challenging, especially for highly similar gene families or organisms with complex genomes, and there is always a risk of non-specific binding or cross-hybridization.

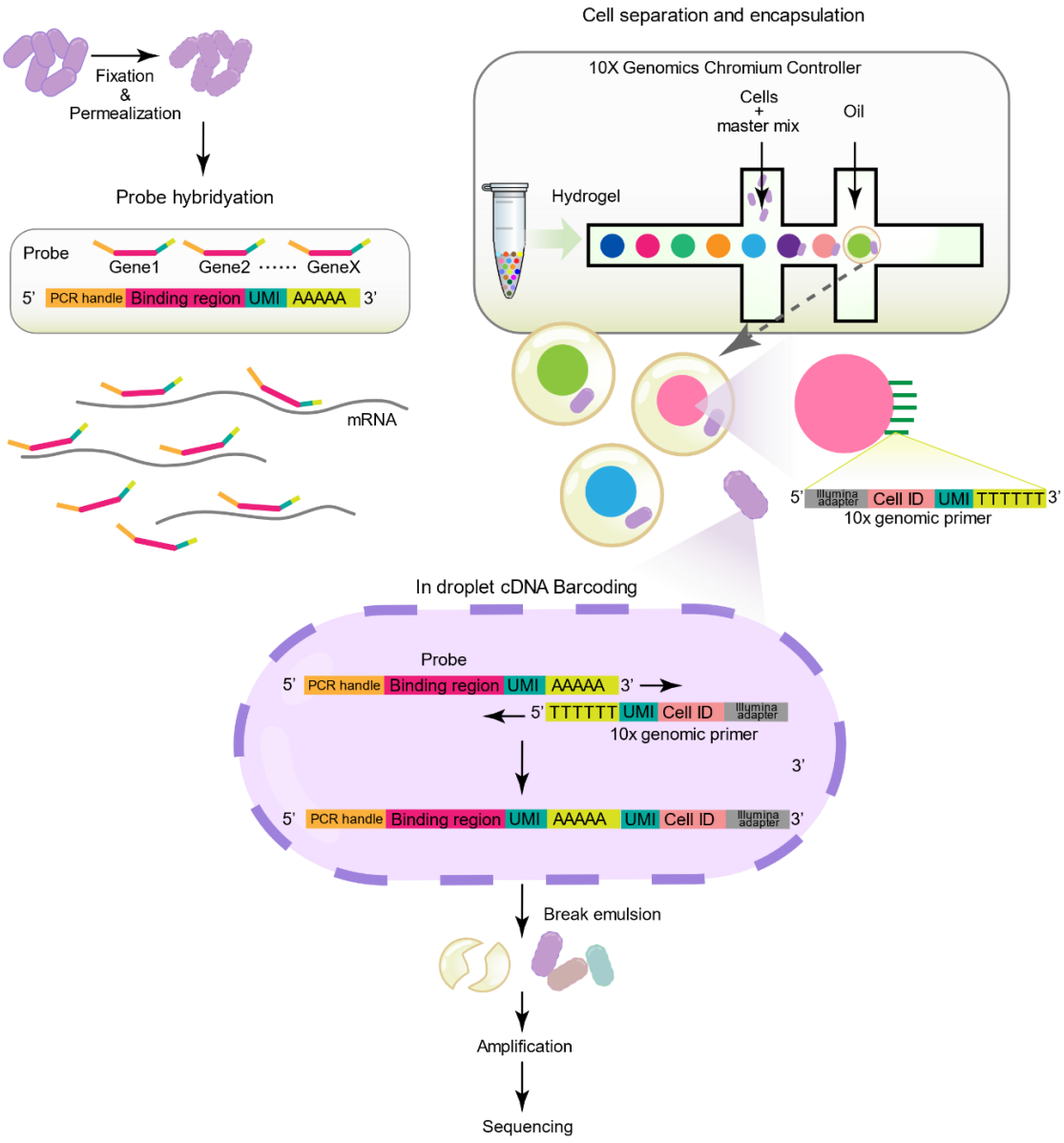


Figure 5-6. The workflow of ProBac-seq. Fixed and permeabilized cells are hybridized with short DNA probes that target mRNAs. These probes contain, in order from 5' to 3', a PCR handle, an mRNA binding region, a UMI, and a poly-A tail. The hybridized cells are then loaded into a 10x Genomics Chromium Controller, creating droplets that each contain one or fewer cells and one hydrogel with a unique barcode. Within the droplets, barcoded cDNAs are synthesized via PCR. Subsequently, the droplets are broken, and the cDNAs are pooled, amplified, and processed for sequencing.

M3-seq[253]: single-cell massively-parallel multiplexed microbial sequencing

Wang et al.[253] introduced **M3-seq (Single-cell massively-parallel multiplexed microbial sequencing)** in 2023 as a novel approach to bacterial single-cell RNA sequencing. The M3-seq procedure begins with cell fixation using 4% formaldehyde, followed by lysozyme permeabilization. Cells are then distributed into 96-well plates for two rounds of cell indexing. As shown in Figure 5-7, the first-round barcoding occurs during in situ reverse transcription, using random primers containing a cell index (BC1) and a UMI. This step can be performed in multiple parallel reactions before pooling. The second indexing round takes place after cells are encapsulated into droplets using a 10x Genomics Chromium Controller, where a second index (BC2) is ligated to the 5' end of first-strand cDNAs. Subsequent steps include cell lysis, second-strand cDNA synthesis, fragmentation using Tn5 transposase, and the addition of a T7 promoter. A key innovation in M3-seq is its approach to rRNA depletion, which occurs after amplification but before final library preparation. This is achieved by transcribing cDNAs to RNA, annealing rRNA-specific DNA probes, and degrading rRNA using RNase H. The resulting RNA is then reverse transcribed back to cDNA and amplified to create the final sequencing library.

Wang et al.[253] demonstrated the effectiveness of M3-seq by generating high-quality mRNA sequences from *B. subtilis* and *E. coli* (Table 5-1), with mRNA reads accounting for approximately 80% and 70% of total reads, respectively. The method successfully identified heterogeneity within bacterial populations, revealing acid-tolerant, bet-hedging subpopulations of *E. coli* in early stationary phase and subpopulations exhibiting strong

gene expression of prophages in antibiotic-treated *B. subtilis*. M3-seq offers several advantages over existing methods. By removing rRNA after amplification using an RNase H-based approach, it efficiently depletes rRNA without significantly altering the total library composition compared to bulk RNA-seq. This strategy differs from methods like BacDrop, which remove rRNA before reverse transcription. Consequently, M3-seq enables single-cell RNA sequencing across massive cell numbers and multiple conditions simultaneously, providing a powerful tool for exploring bacterial population dynamics and heterogeneity.

This method faces challenges in balancing cell recovery across different treatments, which can complicate data interpretation. For instance, significant disparities in recovered cell numbers between different treatment conditions have been observed. Additionally, when applied to mixed-species bacterial communities, M3-seq encounters difficulties in parsing genes with highly conserved sequences and optimizing barcoding for species-specific transcriptome recovery.

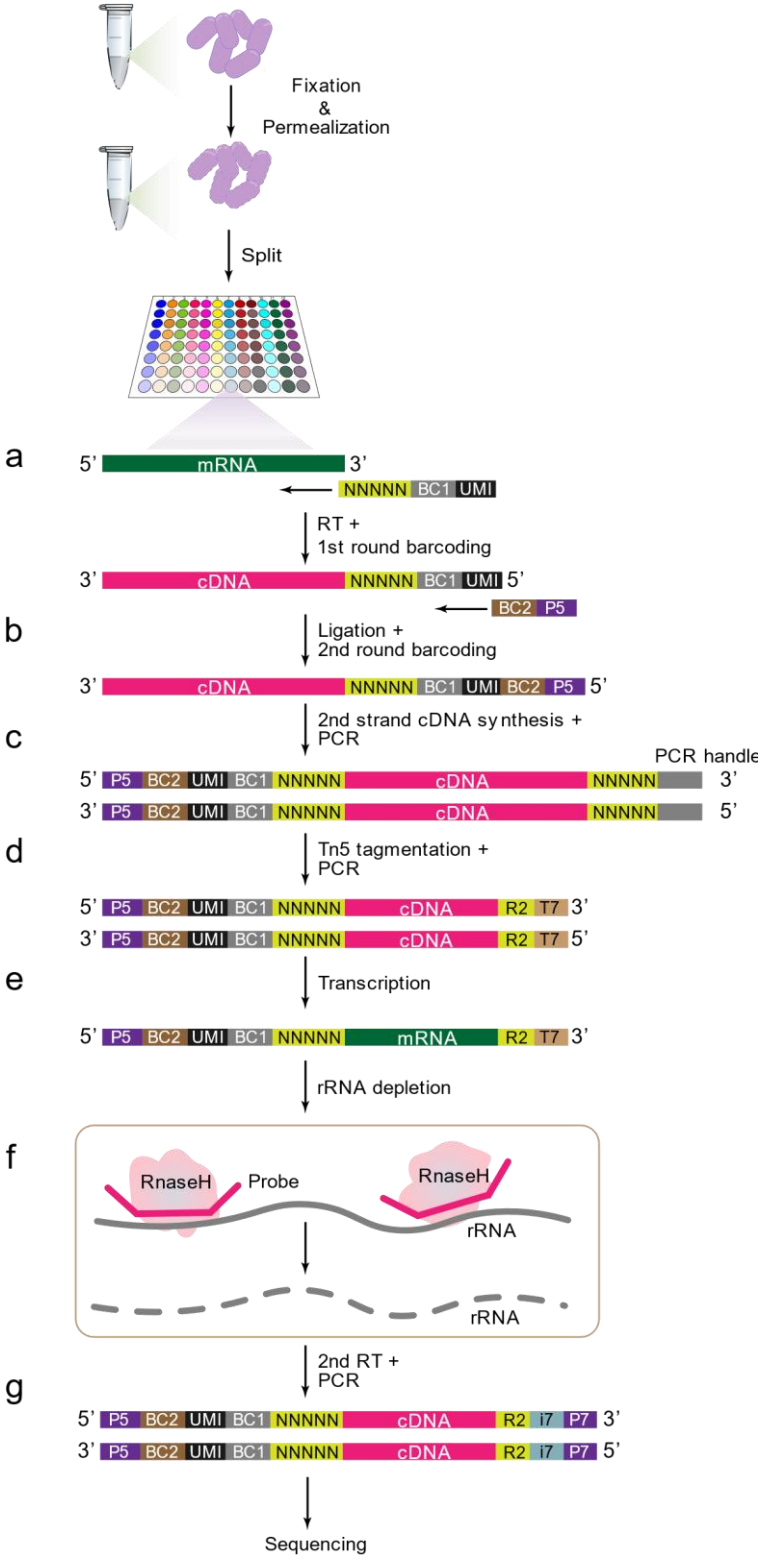

Fixation
&
Permealization
Split
a
5'
mRNA
3'
NNNNN BC1 UMI
RT +
1st round barcoding
3'
cDNA
NNNNN BC1 UMI
5'
BC2 P5
b
Ligation +
2nd round barcoding
3'
cDNA
NNNNN BC1 UMI BC2 P5
5'
c
2nd strand cDNA synthesis +
PCR
PCR handle
5' P5 BC2 UMI BC1 NNNNN cDNA NNNNN 3'
3' P5 BC2 UMI BC1 NNNNN cDNA NNNNN 5'
d
Tn5 tagmentation +
PCR
5' P5 BC2 UMI BC1 NNNNN cDNA R2 T7 3'
3' P5 BC2 UMI BC1 NNNNN cDNA R2 T7 5'
e
Transcription
5' P5 BC2 UMI BC1 NNNNN mRNA R2 T7 3'
rRNA depletion
f
RnaseH
Probe
RnaseH
rRNA
rRNA
g
2nd RT +
PCR
5' P5 BC2 UMI BC1 NNNNN cDNA R2 i7 P7 3'
3' P5 BC2 UMI BC1 NNNNN cDNA R2 i7 P7 5'
Sequencing

Figure 5-7. The workflow of M3-seq. a. After fixation and permeabilization, cells are split into one or more 96 well plates. Each well contains a unique barcoded random hexamer and a UMI. mRNAs are reverse transcribed to cDNAs and barcoded. **b.** cDNAs undergo 2nd round barcoding via ligation. **c.** After 2 rounds of barcoding, 2nd strand cDNAs are synthesized using a Klenow enzyme and a random primer with a PCR handle at 5' end. cDNAs are then PCR amplified and Tn5 fragmented, loaded with Nextera read 2 primers (R2). A T7 promoter is PCR attached to R2. **e.** cDNAs are transcribed back to mRNA. **f.** rRNA specific probes hybrid with rRNA, leading to selective degradation of rRNA by RNaseH. **g.** rRNA depleted RNAs are transcribed back to cDNA, followed by PCR to add required adapters for illumina sequencing.

Table 5-1. Comparisons of existing bacterial scRNA-seq methods.

	MATQ-seq	PETRI-seq	MicroSPLiT	par-seqFISH	BacDrop	ProBac-seq	M3-seq
Publication	Sheng et al., Imadhl et al.	Blattman et al. 2020	Kuchina et al. 2021	Dar et al. 2021	Ma et al. 2023	McNulty et al.	Wang et al. 2023
Probe/plate/microfliud dependent?	FACS	Plate	Plate	Probe	Microfluid	Probe	Microfluid
Strains tested	*Salmonella enterica* , *P. aeruginosa*	*E. coli* , *S. aureus*	*E. coli*, *B. subtilis*	*P. aeruginosa*	*E. coli* , *K. pneumoniae* , *P. aeruginosa* , *E. faecium*	*B. subtilis* , *E. coli*	*B. subtilis* , *E. coli* , *P. aeruginosa*
Cells input in a library prep	N/A	3×10^7 (*E. coli* , *S. aureus*)	1.2×10^7 (*E. coli* + *B. subtilis*)	10^5 (*P. aeruginosa*)	Small: 10,000 (*E. coli*) 12,000 (*K. pneumoniae*) Large: 1 million (*K. pneumoniae*)	N/A	N/A
Cell throughput	71 (*S. enterica*)	~10,000	2,682 (*E. coli* +*B. subtilis*)	50,000 (*P. aeruginosa)*	Small: 4,000 (*E. coli*) 6,000 (*K. pneumoniae*) Large: 60,000 (*K. pneumoniae*)	2,784 (*B. subtilis*) 3,315 (*E. coli*)	Thousnads
Average reads per cell	62.4 ± 20.9 million	Thousands	N/A	N/A	Small: 80,000 per cell (*E. coli*, *K. pneumoniae*) Large: 5,000 (*K. pneumoniae*)	1,073 (*B. subtilis*) 1,070 (*E. coli*)	164 (*B. subtilis*) ~75 (*E. coli*)
Persentage of mRNA reads	~5%	~5%	~10%	100%	~60%	100%	~80%
Median mRNA reads per cell	800,000	227 (exponential *E.coli)* *27 (stationary E. coli*) 43 (*S. aureus*)	235 (*E. coli*) 397 (*B. subtilis*)	~125 (*P. aeruginosa*)	Small: 90 (*E. coli*) 88 (*K. pneumoniae*) Large: 127 (K. pneumoniae) (in top 3,000 high qality cells)	325 (*B. subtilis*) 263 (*E. coli*)	~2,500 (*B. subtilis*) ~1,900 (*E. coli*)
Total genes covered	170	103 operons (exponential *E.coli*) 24 operons (stationary *E. coli*)	138 (*E. coli*) 230 (*B. subtilis*)	105	Small: 70% (*E. coli*) 80% (*K. pneumoniae*) Large: n/a	241 (*B. subtilis*) 165 (*E. coli*)	~160 (*B. subtilis*) , ~60 (*E. coli*)
Barcode collision rate/multiplet rate	N/A	0.19–0.36%	0.80%	N/A	0.07%	0.03%	0.02%
Fixation	Mild fixed by RNAlater /DPBS	4% formaldehyde	4% formaldehyde	2% paraformaldehyde	4% formaldehyde	1% paraformaldehyde	4% formaldehyde
Permeabilization	Lysozyme	Lysozyme/lysostaphin	Lysozyme	70% EtOH	Lysozyme	Mild lysozyme treatment	Lysozyme
rRNA depletion?	No	No	No	No	Yes	No	Yes
mRNA enriched by adding polyA/C tail?	Poly-C tail added to 3' of cDNA	No	Poly-A tail added to mRNA by PAP	No	Poly-A tail added to 3' of cDNA	Poly-A tail added to mRNA from DNA probes	No
Key facilities required beyong standard lab supplies	FACS	No	No	Electron microscopy	10x Genomics Chromium Controller	10x Genomics Chromium Controller	10x Genomics Chromium Controller
Cost	High	Moderate (5.6 cents/cell)	Moderate	Moderate, increase as number of cell types increase	Moderate	High*	Moderate

#: Here we showed two indenpedent experiments: one used a small library size (highlighted in orange) one used a large library size (highlighted in blue).

***:** A one-time cost of US$0.05–0.15 per probe. Need 20000 to 30000 probes per strain. The cost drops to 0.01/cell without rerdering probes.

N/A: Information not found from the publications.

Possible applications on *V. cholerae* and gut microbiota studies

Heterogeneity of genetically identical bacteria has been observed in many bacteria, exhibiting distinct metabolic, virulence and antibiotic resistant profiles. Study of these heterogeneities by scRNA could help us better understand when, how and why individuals in a group react to different stresses/signals/molecules differently.

In the context of *V. cholerae*, the causal agent of the human diarrheal disease cholera, scRNA-seq can be used to identify heterogeneity within populations. ScRNA-seq could help us identify subpopulations of *V. cholerae* with distinct transcriptional profiles missed by traditional bulk transcriptomic analysis. For example, we may identify subpopulations with distinct virulence profiles and solve some questions such as cells primed for biofilm formation or toxin production, which is crucial for understanding how this pathogen transitions between environmental and pathogenic states.

Furthermore, ScRNAseq can uncover spatially dependent gene expression profiles of *V. cholerae* when interacting with complex commensal communities. Here I proposed three specific applications of sc-RNAseq:

a. **Uncovering the heterogeneity in *V. cholerae* responses to AI-2 signals**. ScRNA-seq could potentially uncover the heterogeneity in *V. cholerae* responses to AI-2 signals from *Blautia obeum*, which has been challenging to elucidate using traditional bulk RNA sequencing methods. By combining scRNAseq with cell sorting and fluorescence labeling, we may be able to correlate the gene expression profiles of individual *V.*

cholerae cells with their spatial proximity to signal-producing cells. This could reveal how only a subset of *V. cholerae* cells - those nearest to *B. obeum* - exhibit the AI-2 triggered gene expression profile, a nuance that would be lost in bulk analyses.

b. **Defining heterogeneity of *V. cholerae* in complex commensal communities.** Our preliminary data suggests that TagA, a secreted metalloprotease upregulated by the *V. cholerae* virulence master regulator ToxT, modulates commensal growth. So, we hypothesize that commensal microbes that in close proximal to *V. cholerae* during colonization will exhibit mucin-dependent metabolic variances, resulting in heterogeneity within *V. cholerae* populations. To test this, we can use an appropriate scRNA-seq pipeline to examine how clonal inoculating *V. cholerae* populations behave in the context of close association with diverse microbial communities during infection.

c. **Defining bile acids-triggered heterogeneity of *V. cholerae* in different gut segments.** Previous research has shown that *V. cholerae* reacts differently to various bile acids[149], and bile acid concentration impacts *V. cholerae*'s growth differently (see Chapter 2). Bile acids are unevenly distributed, with most located in the small intestines and only a small amount in the large intestines. Additionally, bile acids compositions differ across different gut segments. Thus, it is reasonable to hypothesize that *V. cholerae* in close proximal to different bile acids in the gut will exhibit bile acid-dependent transcriptomic differences. ScRNA-seq could define subpopulations of *V. cholerae* that react specifically to bile conditions and interactions with gut commensals such as

Clostridium scindens, which converts primary bile acids to secondary bile acids via the *bai* operon and exhibits deconjugation activities[122]. Identifying these bile-acid-dependent heterogeneities in *V. cholerae* can help us understand how these interactions influence the pathogen's pathogenicity, survival, and fitness during infection. Detailed transcriptomic mapping can reveal crucial regulatory pathways and adaptive mechanisms employed by *V. cholerae* in different gut environments with complex communities.

Furthermore, scRNA-seq could simultaneously analyze how proximity to *V. cholerae* affects the signal-producing strain's gene expression, potentially uncovering mutual adaptation responses. Such insights could be crucial in understanding the complex interplay between *V. cholerae* and the gut microbiota during infection, potentially leading to new strategies for managing cholera.

ScRNA-seq methods could also be valuable for studying the effects of antibiotics on gut microbiota at the single-cell level, potentially revealing how different species and subpopulations respond to treatment. This could aid in developing more targeted antimicrobial strategies that preserve beneficial bacteria while eliminating pathogens.
This concept could be applied to study more complex gut microbiota scenarios involving multiple strains. This could provide a more comprehensive understanding of the microbial ecology in the gut during *V. cholerae* infection. However, such multi-strain studies would require overcoming technical challenges in multiplexing and data analysis to distinguish

and integrate information from diverse microbial populations. Starting with *in vitro* samples, scRNA-seq can be applied to *in vivo* samples, offering insights into real bacterial interactions within the gut environment. However, this presents significant challenges, including minimizing interference from host cells, preserving spatial information during sample collection and processing, and adapting scRNAseq methods for *in vivo* samples.

Chapter 6 Conclusion and Future Directions

Conclusion

Bile acids have been recognized as major regulators of the gut microbiota structure and function. Gut microbes can manipulate bile acid pool by enzymatic activities, including deconjugation of bile acids, for example, converting TCA, TDCA to CA, DCA, respectively. Bile acids demonstrated effects on *V. cholerae* in many aspects, including virulent gene expression, biofilm formation, mobility, and fitness during infection. Thus, studying bile acids, bile acids transforming activities and their effects on *V. cholerae* is critical to understand *V. cholerae* pathogenesis and prevent infection.

In **Chapter 2**, we identified a gene *vbh* (*VCA0877*) encodes a functional bile salt hydrolase in *V. cholerae*. This enzyme was shown to deconjugate bile acids such as taurodeoxycholic acid (TDCA) and taurochenodeoxycholic acid (TCDCA), producing secondary bile acids like deoxycholic acid (DCA) and chenodeoxycholic acid (CDCA), and these two bile acids exhibit different effects on *V. cholerae*'s growth and virulence gene expression, demonstrating a complex interaction between the pathogen and its substrates. Our results indicate that DCA negatively impacts *V. cholerae* growth and colonization, and the constitutive expression of *vbh* regulated by AphA led to significant growth inhibition and colonization defects in vivo. In addition, we found that the primary bile acid CDCA exhibits induction on *tcpA* expression. This study highlights that balancing virulence-activating and growth-suppressive bile acids according to host bile availability and

composition is crucial for the relative fitness of commensal and pathogenic bacteria in vivo. Furthermore, the variability in the bile acid pool observed in humans may significantly contribute to individualized infection outcomes.

Given that gut microbiota plays important roles in impacting *V. cholerae* infection in many ways, such as transforming bile acid pool composition, and secreting QS signals to control the behavior of themselves and *V. cholerae*, we broaden our investigation from solely *V. cholerae* to the gut microbiota. In **Chapter 3-1**, we highlighted the role of AI-2 in modulating gut microbiome composition and function, particularly through its impact on bile acid metabolism. Analysis on a in vivo RNAseq results showed that expression of *luxS* from *Blautia obeum* induces the expression of *bai* genes in *Clostridium scindens*, one of the most well studied bacteria that exhibit 7-α dihydroxylation activity on primary bile acids. Our results demonstrate that AI-2 produced by *B. obeum* can significantly downregulate the expression of *bai* genes in *C. scindens* in vitro, leading to a reduction in the conversion of primary bile acid CA to the more toxic secondary bile acid DCA. This finding suggests a novel mechanism by which QS signals can influence microbial community via altering the bile acid metabolism. However, due to the limitation of genome editing in *B. obeum* and *C. scindens*, it will be difficult to study the exact molecular pathways through which AI-2 signals lead to downregulation of *bai* genes in *C. scindens*. In **Chapter 3-2**, we found that AI-2 signals, produced by engineered *E. coli* strains expressing LuxS from different commensal bacteria, can significantly modulate the structure of a defined gut microbial community in a germ-free mice model. We showed

that the probiotic bacterium *Akkermansia muciniphila*, even though lacking a known canonical AI-2 receptor, exhibits increased abundance when LuxS-producing strains are present. This effect is absent when *A. muciniphila* is monocolonized with LuxS-producing strains, indicating the interplay of community effects. These findings suggest that AI-2 signaling plays a crucial role in shaping microbial community dynamics and highlight the importance of considering community context when studying microbial interactions.

In **Chapter 4**, our investigation focused on studying the influences of the metalloprotease TagA's dual activities on *V. cholerae* fitness during colonization with and without defined communities. We showed that TagA impacts *V. cholerae* colonization in a microbiota-specific manner: the mucinase activity of TagA helps the defined community (CR) resist *V. cholerae* colonization, while its mucin-inducing activity aids the defined community (DS) in promoting *V. cholerae* colonization. This expands our understanding of the intricate interactions between *V. cholerae* and the gut microbiota, providing insights into *V. cholerae*'s adaptability and strategies for persistence within diverse gut environments.

In **Chapter 5**, we reviewed the recently developed single-cell RNA sequencing (scRNA-seq) pipelines, with a focus on bacteria. Specifically, seven published scRNA-seq pipelines for bacteria were reviewed, and their applications, advantages, and limitations were discussed. This comprehensive review provided a detailed comparison of these methodologies, highlighting their potential for advancing our understanding of bacterial gene expression at the single-cell level. The discussion covered the technical details of each

pipeline, including their sensitivity, specificity, throughput, cost, and suitability for various bacterial species. Lastly, we proposed possible applications of scRNA-seq for studying *V. cholerae* and gut microbes.

Future directions

The work presented in this thesis has significantly broadened our understanding of the bile salt hydrolase in *V. cholerae* and how it regulates *V. cholerae* fitness during infection when exposed to bile acids. However, this study also highlighted several gaps. For example, we did not explore how *V. cholerae* react to a complex mix of bile acids. Although we found the correlation between CDCA and *tcpA* induction in *V. cholerae*, the underlying mechanisms remain unclear. Additionally, how VBH activity impacts *V. cholerae* in a complex gut community, and how individual as well as combined BSH activities from the gut community affects *V. cholerae* infections remains unexplored.

Several new questions arise and could be explored in the future: **1) What does VBH do except for deconjugating bile acids?** Recent studies have uncovered a previously unknown role of bacterial bile salt hydrolases that they can conjugate amines to bile acids[161,162]. This discovery complicates the manipulation of the bile acid pool and makes its composition more unpredictable. Moreover, since the bile acid pool composition significantly impacts *V. cholerae* and other microbes (such as *B. obeum*), this new role of BSH adds another layer of intricacy to the interactions between bile acids and gut

microbiota. To address this, we can utilize untargeted LC–MS/MS profiling of unconjugated bile acids incubated with BSH producing *E. coli* or vector in media containing various amino acids. To compare the new peaks that show up in the BSH treated samples, we will be able to identify possible new products catalyzed by BSH. **2) What is the role of the gut microbiota in modulating bile acid composition and its subsequent impact on *V. cholerae* colonization and virulence?** Previous study[149] has demonstrated that *B. obeum* produces BSHs that deconjugates TCA to CA, resulting in resistance to *V. cholerae* colonization. However, the BSHs from the other gut members remains unexplored. Understanding how these enzymes from diverse microbial sources affect bile acid composition could provide deeper insights into their collective impact on *V. cholerae*. Future research can start by incubating BSH-producing *E. coli* strains with a variety of bile acids substrates and access their ability to deconjugate these bile acids. Then we can introduce these BSH-producing *E. coli* strains to manipulate a community with specific BSH types and quantities, enabling controlled investigations from simple to complex scenarios. **3) How does *V. cholerae* exhibit spatial and heterogeneous gene expression profiles during colonization across different gut segments?** Bile acids are secreted post-ingestion and are unevenly distributed throughout the gut, potentially causing *V. cholerae* to exhibit segment-specific gene expression patterns. Traditional bulk RNA-seq methods may mask this spatial heterogeneity, but scRNA-seq can provide detailed, single-cell transcriptomic profiles. Utilizing scRNA-seq will enable researchers to uncover novel cell states and bile acid-induced responses that are critical for understanding *V. cholerae* colonization dynamics and developing targeted interventions.

In addition, this thesis highlighted the role of AI-2 signals from *B. obeum* in modulating bile acid metabolism through its impacts on *bai* gene expressions in *C. scindens*. This finding links QS, bile acid metabolism, and gut microbiota together. The detailed mechanisms behind this interaction must be investigated. One possible approach is to develop feasible genome editing methods to genetically modify *B. obeum* and *C. scindens*. Furthermore, future studies should expand to examine the effects of various AI-2 signals on bile acid metabolism and their corresponding impacts on *V. cholerae* colonization and gut microbiota composition. By showing that TagA is a bi-functional protein working on mucin and plays distinct roles in different communities. The mucus layer not only serves as nutrient source but also a structural anchor for gut commensals. It remains unclear how these TagA-related phenotypes might vary under different bile acid conditions. Future research should investigate the influence of various bile acid compositions on TagA's mucinase and mucin-inducing activities and their consequent effects on the microbial community structure and *V. cholerae* colonization.

References

1. Almagro-Moreno, S., and Taylor, R.K. (2013). Cholera: Environmental Reservoirs and Impact on Disease Transmission. Microbiol Spectr *1*, OH-0003-2012. https://doi.org/10.1128/microbiolspec.OH-0003-2012.

2. Smith, A.M., Sekwadi, P., Erasmus, L.K., Lee, C.C., Stroika, S.G., Ndzabandzaba, S., Alex, V., Nel, J., Njamkepo, E., Thomas, J., et al. Imported Cholera Cases, South Africa, 2023 - Volume 29, Number 8—August 2023 - Emerging Infectious Diseases journal - CDC. https://doi.org/10.3201/eid2908.230750.

3. Chatterjee, S.N., and Chaudhuri, K. (2003). Lipopolysaccharides of Vibrio cholerae. I. Physical and chemical characterization. Biochim Biophys Acta *1639*, 65–79. https://doi.org/10.1016/j.bbadis.2003.08.004.

4. Sack, D., Sack, R., Nair, G., and Siddique, A. (2004). Cholera. LANCET *363*, 223–233. https://doi.org/10.1016/S0140-6736(03)15328-7.

5. Barua, D. (1992). History of cholera. In Cholera (Springer), pp. 1–36.

6. CDC (2024). About Cholera. Cholera. https://www.cdc.gov/cholera/about/index.html.

7. Morris, J.G. (2011). Cholera—Modern Pandemic Disease of Ancient Lineage. Emerg Infect Dis *17*, 2099–2104. https://doi.org/10.3201/eid1711.111109.

8. Das, B., Verma, J., Kumar, P., Ghosh, A., and Ramamurthy, T. (2020). Antibiotic resistance in *Vibrio cholerae*: Understanding the ecology of resistance genes and mechanisms. Vaccine *38 Suppl 1*, A83–A92. https://doi.org/10.1016/j.vaccine.2019.06.031.

9. Antibiotic Treatment | Treatment | Cholera | CDC (2022). https://www.cdc.gov/cholera/treatment/antibiotic-treatment.html.

10. Gabutti, G., Rossanese, A., Tomasi, A., Giuffrida, S., Nicosia, V., Barriga, J., Florescu, C., Sandri, F., and Stefanati, A. (2020). Cholera, the Current Status of Cholera Vaccines and Recommendations for Travellers. Vaccines (Basel) *8*, 606. https://doi.org/10.3390/vaccines8040606.

11. Colwell, R. (1996). Global climate and infectious disease: The cholera paradigm. SCIENCE *274*, 2025–2031. https://doi.org/10.1126/science.274.5295.2025.

12. Middlebrook, J.L., and Dorland, R.B. (1984). Bacterial toxins: cellular mechanisms of action. Microbiol Rev *48*, 199–221. https://doi.org/10.1128/mr.48.3.199-221.1984.

13. Bharati, K., and Ganguly, N.K. (2011). Cholera toxin: A paradigm of a multifunctional protein. Indian J Med Res *133*, 179–187.

14. Field, M. (1979). Mechanisms of action of cholera and *Escherichia coli* enterotoxins. Am J Clin Nutr *32*, 189–196. https://doi.org/10.1093/ajcn/32.1.189.

15. Wands, A.M., Fujita, A., McCombs, J.E., Cervin, J., Dedic, B., Rodriguez, A.C., Nischan, N., Bond, M.R., Mettlen, M., Trudgian, D.C., et al. Fucosylation and protein glycosylation create functional receptors for cholera toxin. eLife *4*, e09545. https://doi.org/10.7554/eLife.09545.

16. Taylor, R.K., Miller, V.L., Furlong, D.B., and Mekalanos, J.J. (1987). Use of phoA gene fusions to identify a pilus colonization factor coordinately regulated with cholera toxin. Proc Natl Acad Sci U S A *84*, 2833–2837. https://doi.org/10.1073/pnas.84.9.2833.

17. Ritchie, J.M., Rui, H., Bronson, R.T., and Waldor, M.K. (2010). Back to the Future: Studying Cholera Pathogenesis Using Infant Rabbits. mBio *1*, e00047-10. https://doi.org/10.1128/mBio.00047-10.

18. Herrington, D., Hall, R., Losonsky, G., Mekalanos, J., Taylor, R., And Levine, M. (1988). Toxin, toxin-coregulated pili, and the toxr regulon are essential for vibrio-cholerae pathogenesis in humans. JOURNAL OF EXPERIMENTAL MEDICINE *168*, 1487–1492. https://doi.org/10.1084/jem.168.4.1487.

19. Waldor, M., and Mekalanos, J. (1996). Lysogenic conversion by a filamentous phage encoding cholera toxin. SCIENCE *272*, 1910–1914. https://doi.org/10.1126/science.272.5270.1910.

20. Kirn, T.J., Bose, N., and Taylor, R.K. (2003). Secretion of a soluble colonization factor by the TCP type 4 pilus biogenesis pathway in *Vibrio cholerae*. Mol Microbiol *49*, 81–92. https://doi.org/10.1046/j.1365-2958.2003.03546.x.

21. Krebs, S.J., and Taylor, R.K. (2011). Protection and Attachment of *Vibrio cholerae* Mediated by the Toxin-Coregulated Pilus in the Infant Mouse Model. Journal of Bacteriology *193*, 5260–5270. https://doi.org/10.1128/jb.00378-11.

22. Dirita, V., and Mekalanos, J. (1991). Periplasmic interaction between 2 membrane regulatory proteins, toxr and toxs, results in signal transduction and transcriptional activation. CELL *64*, 29–37. https://doi.org/10.1016/0092-8674(91)90206-E.

23. Miller, V., and Mekalanos, J. (1988). A novel suicide vector and its use in construction of insertion mutations - osmoregulation of outer-membrane proteins and virulence determinants in *Vibrio cholerae* requires toxr. JOURNAL OF

BACTERIOLOGY *170*, 2575–2583. https://doi.org/10.1128/JB.170.6.2575-2583.1988.

24. Provenzano, D., Lauriano, C., and Klose, K. (2001). Characterization of the role of the ToxR-modulated outer membrane porins OmpU and OmpT in *Vibrio cholerae* virulence. JOURNAL OF BACTERIOLOGY *183*, 3652–3662. https://doi.org/10.1128/JB.183.12.3652-3662.2001.

25. Miller, V., Dirita, V., and Mekalanos, J. (1989). Identification of toxs, a regulatory gene whose product enhances toxr-mediated activation of the cholera-toxin promoter. JOURNAL OF BACTERIOLOGY *171*, 1288–1293. https://doi.org/10.1128/jb.171.3.1288-1293.1989.

26. Goss, T., Seaborn, C., Gray, M., and Krukonis, E. (2010). Identification of the TcpP-Binding Site in the toxT Promoter of *Vibrio cholerae* and the Role of ToxR in TcpP-Mediated Activation. INFECTION AND IMMUNITY *78*, 4122–4133. https://doi.org/10.1128/IAI.00566-10.

27. Beck, N., Krukonis, E., and DiRita, V. (2004). TcpH influences virulence gene expression in *Vibrio cholerae* by inhibiting degradation of the transcription activator TcpP. JOURNAL OF BACTERIOLOGY *186*, 8309–8316. https://doi.org/10.1128/JB.186.24.8309-8316.2004.

28. Matson, J., and DiRita, V. (2005). Degradation of the membrane-localized virulence activator TcpP by the YaeL protease in *Vibrio cholerae*. PROCEEDINGS OF THE NATIONAL ACADEMY OF SCIENCES OF THE UNITED STATES OF AMERICA *102*, 16403–16408. https://doi.org/10.1073/pnas.0505818102.

29. Morgan, S., French, E., Thomson, J., Seaborn, C., Shively, C., and Krukonis, E. (2016). Formation of an Intramolecular Periplasmic Disulfide Bond in TcpP Protects TcpP and TcpH from Degradation in *Vibrio cholerae*. JOURNAL OF BACTERIOLOGY *198*, 498–509. https://doi.org/10.1128/JB.00338-15.

30. Kovacikova, G., Lin, W., and Skorupski, K. (2004). *Vibrio cholerae* AphA uses a novel mechanism for virulence gene activation that involves interaction with the LysR-type regulator AphB at the tcpPH promoter. MOLECULAR MICROBIOLOGY *53*, 129–142. https://doi.org/10.1111/j.1365-2958.2004.04121.x.

31. Kovacikova, G., and Skorupski, K. (2001). Overlapping binding sites for the virulence gene regulators AphA, AphB and cAMP-CRP at the *Vibrio cholerae* tcpPH promoter. MOLECULAR MICROBIOLOGY *41*, 393–407. https://doi.org/10.1046/j.1365-2958.2001.02518.x.

32. Kovacikova, G., and Skorupski, K. (1999). A Vibrio cholerae LysR homolog, AphB, cooperates with AphA at the tcpPH promoter to activate expression of the ToxR

virulence cascade. J Bacteriol *181*, 4250–4256. https://doi.org/10.1128/JB.181.14.4250-4256.1999.

33. Xu, X., Stern, A., Liu, Z., Kan, B., and Zhu, J. (2010). Virulence regulator AphB enhances toxR transcription in Vibrio cholerae. BMC MICROBIOLOGY *10*. https://doi.org/10.1186/1471-2180-10-3.

34. Chen, X., Schauder, S., Potier, N., Van Dorsselaer, A., Pelczer, I., Bassler, B., and Hughson, F. (2002). Structural identification of a bacterial quorum-sensing signal containing boron. NATURE *415*, 545–549. https://doi.org/10.1038/415545a.

35. Papenfort, K., and Bassler, B.L. (2016). Quorum sensing signal-response systems in Gram-negative bacteria. Nat Rev Microbiol *14*, 576–588. https://doi.org/10.1038/nrmicro.2016.89.

36. Hammer, B., and Bassler, B. (2003). Quorum sensing controls biofilm formation in *Vibrio cholerae*. MOLECULAR MICROBIOLOGY *50*, 101–114. https://doi.org/10.1046/j.1365-2958.2003.03688.x.

37. Miller, M.B., Skorupski, K., Lenz, D.H., Taylor, R.K., and Bassler, B.L. (2002). Parallel quorum sensing systems converge to regulate virulence in *Vibrio cholerae*. Cell *110*, 303–314. https://doi.org/10.1016/s0092-8674(02)00829-2.

38. Suckow, G., Seitz, P., and Blokesch, M. (2011). Quorum sensing contributes to natural transformation of *Vibrio cholerae* in a species-specific manner. J Bacteriol *193*, 4914–4924. https://doi.org/10.1128/JB.05396-11.

39. Papenfort, K., and Vogel, J. (2010). Regulatory RNA in bacterial pathogens. Cell Host Microbe *8*, 116–127. https://doi.org/10.1016/j.chom.2010.06.008.

40. Cao, J.G., and Meighen, E.A. (1989). Purification and structural identification of an autoinducer for the luminescence system of *Vibrio harveyi*. J Biol Chem *264*, 21670–21676.

41. Defoirdt, T., Boon, N., Sorgeloos, P., Verstraete, W., and Bossier, P. (2008). Quorum sensing and quorum quenching in *Vibrio harveyi*: lessons learned from in vivo work. ISME J *2*, 19–26. https://doi.org/10.1038/ismej.2007.92.

42. Higgins, D., Pomianek, M., Kraml, C., Taylor, R., Semmelhack, M., and Bassler, B. (2007). The major *Vibrio cholerae* autoinducer and its role in virulence factor production. NATURE *450*, 883–886. https://doi.org/10.1038/nature06284.

43. Schauder, S., Shokat, K., Surette, M.G., and Bassler, B.L. (2001). The LuxS family of bacterial autoinducers: biosynthesis of a novel quorum-sensing signal

molecule. Molecular Microbiology *41*, 463–476. https://doi.org/10.1046/j.1365-2958.2001.02532.x.

44. Papenfort, K., Silpe, J., Schramma, K., Cong, J., Seyedsayamdost, M., and Bassler, B. (2017). A *Vibrio cholerae* autoinducer-receptor pair that controls biofilm formation. NATURE CHEMICAL BIOLOGY *13*, 551-+. https://doi.org/10.1038/NCHEMBIO.2336.

45. Liu, Z., Hsiao, A., Joelsson, A., and Zhu, J. (2006). The transcriptional regulator VqmA increases expression of the quorum-sensing activator HapR in *Vibrio cholerae*. JOURNAL OF BACTERIOLOGY *188*, 2446–2453. https://doi.org/10.1128/JB.188.7.2446-2453.2006.

46. Papenfort, K., Forstner, K., Cong, J., Sharma, C., and Bassler, B. (2015). Differential RNA-seq of *Vibrio cholerae* identifies the VqmR small RNA as a regulator of biofilm formation. PROCEEDINGS OF THE NATIONAL ACADEMY OF SCIENCES OF THE UNITED STATES OF AMERICA *112*, E766–E775. https://doi.org/10.1073/pnas.1500203112.

47. Eickhoff, M.J., and Bassler, B.L. (2018). SnapShot: Bacterial Quorum Sensing. Cell *174*, 1328-1328.e1. https://doi.org/10.1016/j.cell.2018.08.003.

48. Pfam: the protein families database - PubMed https://pubmed.ncbi.nlm.nih.gov/24288371/.

49. Hsiao, A., Ahmed, A., Subramanian, S., Griffin, N., Drewry, L., Petri, W., Haque, R., Ahmed, T., and Gordon, J. (2014). Members of the human gut microbiota involved in recovery from *Vibrio cholerae* infection. NATURE *515*, 423-+. https://doi.org/10.1038/nature13738.

50. Huang, X., Duddy, O.P., Silpe, J.E., Paczkowski, J.E., Cong, J., Henke, B.R., and Bassler, B.L. (2020). Mechanism underlying autoinducer recognition in the *Vibrio cholerae* DPO-VqmA quorum-sensing pathway. J Biol Chem *295*, 2916–2931. https://doi.org/10.1074/jbc.RA119.012104.

51. Silpe, J., and Bassler, B. (2019). A Host-Produced Quorum-Sensing Autoinducer Controls a Phage Lysis-Lysogeny Decision. CELL *176*, 268-+. https://doi.org/10.1016/j.cell.2018.10.059.

52. Henry, J.T., and Crosson, S. (2011). Ligand-binding PAS domains in a genomic, cellular, and structural context. Annu Rev Microbiol *65*, 261–286. https://doi.org/10.1146/annurev-micro-121809-151631.

53. Tateda, K., Ishii, Y., Horikawa, M., Matsumoto, T., Miyairi, S., Pechere, J.C., Standiford, T.J., Ishiguro, M., and Yamaguchi, K. (2003). The *Pseudomonas*

aeruginosa autoinducer N-3-oxododecanoyl homoserine lactone accelerates apoptosis in macrophages and neutrophils. Infect Immun *71*, 5785–5793. https://doi.org/10.1128/IAI.71.10.5785-5793.2003.

54. Shiner, E., Terentyev, D., Bryan, A., Sennoune, S., Martinez-Zaguilan, R., Li, G., Gyorke, S., Williams, S., and Rumbaugh, K. (2006). *Pseudomonas aeruginosa* autoinducer modulates host cell responses through calcium signalling. CELLULAR MICROBIOLOGY *8*, 1601–1610. https://doi.org/10.1111/j.1462-5822.2006.00734.x.

55. Bryan, A., Watters, C., Koenig, L., Youn, E., Olmos, A., Li, G., Williams, S.C., and Rumbaugh, K.P. (2010). Human transcriptome analysis reveals a potential role for active transport in the metabolism of *Pseudomonas aeruginosa* autoinducers. Microbes Infect *12*, 1042–1050. https://doi.org/10.1016/j.micinf.2010.07.006.

56. Zargar, A., Quan, D., Carter, K., Guo, M., Sintim, H., Payne, G., and Bentley, W. (2015). Bacterial Secretions of Nonpathogenic *Escherichia coli* Elicit Inflammatory Pathways: a Closer Investigation of Interkingdom Signaling. MBIO *6*. https://doi.org/10.1128/mBio.00025-15.

57. Li, Q., Peng, W., Wu, J., Wang, X., Ren, Y., Li, H., Peng, Y., Tang, X., and Fu, X. (2019). Autoinducer-2 of gut microbiota, a potential novel marker for human colorectal cancer, is associated with the activation of TNFSF9 signaling in macrophages. ONCOIMMUNOLOGY *8*. https://doi.org/10.1080/2162402X.2019.1626192.

58. Bansal, T., Alaniz, R.C., Wood, T.K., and Jayaraman, A. (2010). The bacterial signal indole increases epithelial-cell tight-junction resistance and attenuates indicators of inflammation. Proc Natl Acad Sci U S A *107*, 228–233. https://doi.org/10.1073/pnas.0906112107.

59. Shimada, Y., Kinoshita, M., Harada, K., Mizutani, M., Masahata, K., Kayama, H., and Takeda, K. (2013). Commensal Bacteria-Dependent Indole Production Enhances Epithelial Barrier Function in the Colon. PLoS One *8*, e80604. https://doi.org/10.1371/journal.pone.0080604.

60. Ismail, A.S., Valastyan, J.S., and Bassler, B.L. (2016). A Host-Produced Autoinducer-2 Mimic Activates Bacterial Quorum Sensing. Cell Host Microbe *19*, 470–480. https://doi.org/10.1016/j.chom.2016.02.020.

61. Valastyan, J.S., Kraml, C.M., Pelczer, I., Ferrante, T., and Bassler, B.L. (2021). Saccharomyces cerevisiae Requires CFF1 To Produce 4-Hydroxy-5-Methylfuran-3(2H)-One, a Mimic of the Bacterial Quorum-Sensing Autoinducer AI-2. mBio *12*, e03303-20. https://doi.org/10.1128/mBio.03303-20.

62. Kumar, P., Lee, J., Beyenal, H., and Lee, J. (2020). Fatty Acids as Antibiofilm and Antivirulence Agents. TRENDS IN MICROBIOLOGY *28*, 753–768. https://doi.org/10.1016/j.tim.2020.03.014.

63. Santhakumari, S., Nilofernisha, N.M., Ponraj, J.G., Pandian, S.K., and Ravi, A.V. (2017). In vitro and in vivo exploration of palmitic acid from *Synechococcus elongatus* as an antibiofilm agent on the survival of *Artemia franciscana* against virulent vibrios. Journal of Invertebrate Pathology *150*, 21–31. https://doi.org/10.1016/j.jip.2017.09.001.

64. Watve, S., Barrasso, K., Jung, S., Davis, K., Hawver, L., Khataokar, A., Palaganas, R., Neiditch, M., Perez, L., and Ng, W. (2020). Parallel quorum-sensing system in *Vibrio cholerae* prevents signal interference inside the host. PLOS PATHOGENS *16*. https://doi.org/10.1371/journal.ppat.1008313.

65. Landman, C., Grill, J., Mallet, J., Marteau, P., Humbert, L., Le Balc'h, E., Maubert, M., Perez, K., Chaara, W., Brot, L., et al. (2018). Inter-kingdom effect on epithelial cells of the N-Acyl homoserine lactone 3-oxo-C12:2, a major quorum-sensing molecule from gut microbiota. PLOS ONE *13*. https://doi.org/10.1371/journal.pone.0202587.

66. Thompson, J., Oliveira, R., Djukovic, A., Ubeda, C., and Xavier, K. (2015). Manipulation of the Quorum Sensing Signal AI-2 Affects the Antibiotic-Treated Gut Microbiota. CELL REPORTS *10*, 1861–1871. https://doi.org/10.1016/j.celrep.2015.02.049.

67. Sun, Z., He, X., Brancaccio, V., Yuan, J., and Riedel, C. (2014). Bifidobacteria Exhibit LuxS-Dependent Autoinducer 2 Activity and Biofilm Formation. PLOS ONE *9*. https://doi.org/10.1371/journal.pone.0088260.

68. Kim, J., Kim, J., Kim, Y., Oh, S., Song, M., Choe, J., Whang, K., Kim, K., and Oh, S. (2018). Influences of quorum-quenching probiotic bacteria on the gut microbial community and immune function in weaning pigs. ANIMAL SCIENCE JOURNAL *89*, 412–422. https://doi.org/10.1111/asj.12954.

69. Darkoh, C., Plants-Paris, K., Bishoff, D., and DuPont, H. (2019). *Clostridium difficile* Modulates the Gut Microbiota by Inducing the Production of Indole, an Interkingdom Signaling and Antimicrobial Molecule. MSYSTEMS *4*. https://doi.org/10.1128/mSystems.00346-18.

70. van der Ploeg, J.R. (2005). Regulation of bacteriocin production in *Streptococcus mutans* by the quorum-sensing system required for development of genetic competence. J Bacteriol *187*, 3980–3989. https://doi.org/10.1128/JB.187.12.3980-3989.2005.

71. Fontaine, L., Boutry, C., Guédon, E., Guillot, A., Ibrahim, M., Grossiord, B., and Hols, P. (2007). Quorum-sensing regulation of the production of Blp bacteriocins in *Streptococcus thermophilus*. J Bacteriol *189*, 7195–7205. https://doi.org/10.1128/JB.00966-07.

72. Majerczyk, C., Schneider, E., and Greenberg, E.P. (2016). Quorum sensing control of Type VI secretion factors restricts the proliferation of quorum-sensing mutants. Elife *5*, e14712. https://doi.org/10.7554/eLife.14712.

73. Ishikawa, T., Rompikuntal, P.K., Lindmark, B., Milton, D.L., and Wai, S.N. (2009). Quorum Sensing Regulation of the Two hcp Alleles in *Vibrio cholerae* O1 Strains. PLOS ONE *4*, e6734. https://doi.org/10.1371/journal.pone.0006734.

74. Ackermann, M. (2015). A functional perspective on phenotypic heterogeneity in microorganisms. Nat Rev Microbiol *13*, 497–508. https://doi.org/10.1038/nrmicro3491.

75. Striednig, B., and Hilbi, H. (2022). Bacterial quorum sensing and phenotypic heterogeneity: how the collective shapes the individual. Trends in Microbiology *30*, 379–389. https://doi.org/10.1016/j.tim.2021.09.001.

76. Cárcamo-Oyarce, G., Lumjiaktase, P., Kümmerli, R., and Eberl, L. (2015). Quorum sensing triggers the stochastic escape of individual cells from *Pseudomonas putida* biofilms. NATURE COMMUNICATIONS *6*. https://doi.org/10.1038/ncomms6945.

77. Boedicker, J., Vincent, M., and Ismagilov, R. (2009). Microfluidic Confinement of Single Cells of Bacteria in Small Volumes Initiates High-Density Behavior of Quorum Sensing and Growth and Reveals Its Variability. ANGEWANDTE CHEMIE-INTERNATIONAL EDITION *48*, 5908–5911. https://doi.org/10.1002/anie.200901550.

78. Mukherjee, S., and Bassler, B.L. (2019). Bacterial quorum sensing in complex and dynamically changing environments. Nat Rev Microbiol *17*, 371–382. https://doi.org/10.1038/s41579-019-0186-5.

79. Grimbergen, A.J., Siebring, J., Solopova, A., and Kuipers, O.P. (2015). Microbial bet-hedging: the power of being different. Current Opinion in Microbiology *25*, 67–72. https://doi.org/10.1016/j.mib.2015.04.008.

80. Ackermann, M. (2013). Microbial individuality in the natural environment. ISME J *7*, 465–467. https://doi.org/10.1038/ismej.2012.131.

81. Anetzberger, C., Pirch, T., and Jung, K. (2009). Heterogeneity in quorum sensing-regulated bioluminescence of *Vibrio harveyi*. MOLECULAR MICROBIOLOGY *73*, 267–277. https://doi.org/10.1111/j.1365-2958.2009.06768.x.

82. Šarenac, T.M., and Mikov, M. (2018). Bile Acid Synthesis: From Nature to the Chemical Modification and Synthesis and Their Applications as Drugs and Nutrients. Frontiers in Pharmacology *9*.

83. Bjorkhem, I., Araya, Z., Rudling, M., Angelin, B., Einarsson, C., and Wikvall, K. (2002). Differences in the regulation of the classical and the alternative pathway for bile acid synthesis in human liver - No coordinate regulation of CYP7A1 and CYP27A1. JOURNAL OF BIOLOGICAL CHEMISTRY *277*, 26804–26807. https://doi.org/10.1074/jbc.M202343200.

84. Russell, D. (2003). The enzymes, regulation, and genetics of bile acid synthesis. ANNUAL REVIEW OF BIOCHEMISTRY *72*, 137–174. https://doi.org/10.1146/annurev.biochem.72.121801.161712.

85. Li, T., Francl, J.M., Boehme, S., and Chiang, J.Y.L. (2013). Regulation of cholesterol and bile acid homeostasis by the cholesterol 7α-hydroxylase/steroid response element-binding protein 2/microRNA-33a axis in mice. Hepatology *58*, 1111–1121. https://doi.org/10.1002/hep.26427.

86. Šarenac, T.M., and Mikov, M.M. (2017). Biosynthesis and biotransformation of bile acids. Hospital Pharmacology - International Multidisciplinary Journal *4*, 469–485. https://doi.org/10.5937/hpimj1701469S.

87. Javitt, N. (1990). 26-Hydroxycholesterol: synthesis, metabolism, and biologic activities. Journal of Lipid Research *31*, 1527–1533. https://doi.org/10.1016/S0022-2275(20)42337-5.

88. Li, X., Pandak, W.M., Erickson, S.K., Ma, Y., Yin, L., Hylemon, P., and Ren, S. (2007). Biosynthesis of the regulatory oxysterol, 5-cholesten-3β,25-diol 3-sulfate, in hepatocytes. Journal of Lipid Research *48*, 2587–2596. https://doi.org/10.1194/jlr.M700301-JLR200.

89. Cali, J.J., and Russell, D.W. (1991). Characterization of human sterol 27-hydroxylase. A mitochondrial cytochrome P-450 that catalyzes multiple oxidation reaction in bile acid biosynthesis. Journal of Biological Chemistry *266*, 7774–7778. https://doi.org/10.1016/S0021-9258(20)89517-9.

90. Kakiyama, G., Marques, D., Takei, H., Nittono, H., Erickson, S., Fuchs, M., Rodriguez-Agudo, D., Gil, G., Hylemon, P.B., Zhou, H., et al. (2019). Mitochondrial oxysterol biosynthetic pathway gives evidence for CYP7B1 as controller of regulatory

oxysterols. The Journal of Steroid Biochemistry and Molecular Biology *189*, 36–47. https://doi.org/10.1016/j.jsbmb.2019.01.011.

91. Pandak, W.M., and Kakiyama, G. (2019). The acidic pathway of bile acid synthesis: Not just an alternative pathway☆. Liver Res *3*, 88–98. https://doi.org/10.1016/j.livres.2019.05.001.

92. Javitt, N.B. (2002). 25R,26-Hydroxycholesterol revisited: synthesis, metabolism, and biologic roles. Journal of Lipid Research *43*, 665–670. https://doi.org/10.1016/S0022-2275(20)30106-1.

93. Mertens, K.L., Kalsbeek, A., Soeters, M.R., and Eggink, H.M. (2017). Bile Acid Signaling Pathways from the Enterohepatic Circulation to the Central Nervous System. Frontiers in Neuroscience *11*.

94. Björkhem, I., Andersson, U., Ellis, E., Alvelius, G., Ellegård, L., Diczfalusy, U., Sjövall, J., and Einarsson, C. (2001). From Brain to Bile: evidence that conjugation and ω-hydroxylation are important for elimination of 24s-hydroxycholesterol (cerebrosterol) in humans*. Journal of Biological Chemistry *276*, 37004–37010. https://doi.org/10.1074/jbc.M103828200.

95. Zhang, Y., and Klaassen, C.D. (2010). Effects of feeding bile acids and a bile acid sequestrant on hepatic bile acid composition in mice. J Lipid Res *51*, 3230–3242. https://doi.org/10.1194/jlr.M007641.

96. Xia, X., Francis, H., Glaser, S., Alpini, G., and LeSage, G. (2006). Bile acid interactions with cholangiocytes. World J Gastroenterol *12*, 3553–3563. https://doi.org/10.3748/wjg.v12.i22.3553.

97. Craddock, A.L., Love, M.W., Daniel, R.W., Kirby, L.C., Walters, H.C., Wong, M.H., and Dawson, P.A. (1998). Expression and transport properties of the human ileal and renal sodium-dependent bile acid transporter. Am J Physiol *274*, G157-169. https://doi.org/10.1152/ajpgi.1998.274.1.G157.

98. Niekerk, J. van, Tolenaars, D., María Banales, J., Elferink, R.O., Graaf, S. van de, and Beuers, U. (2019). THU-027-The human apical sodium dependent bile salt transporter (ASBT) activates a bile salt-induced defense in human cholangiocytes. Journal of Hepatology *70*, e172. https://doi.org/10.1016/S0618-8278(19)30311-1.

99. Roberts, M., Magnusson, B., Burczynski, F., and Weiss, M. (2002). Enterohepatic circulation - Physiological, pharmacokinetic and clinical implications. CLINICAL PHARMACOKINETICS *41*, 751–790. https://doi.org/10.2165/00003088-200241100-00005.

100. Hofmann, A.F. (2009). The enterohepatic circulation of bile acids in mammals: form and functions. Front Biosci (Landmark Ed) *14*, 2584–2598. https://doi.org/10.2741/3399.

101. Chiang, J. (2009). Bile acids: regulation of synthesis. JOURNAL OF LIPID RESEARCH *50*, 1955–1966. https://doi.org/10.1194/jlr.R900010-JLR200.

102. Watanabe, M., Houten, S., Wang, L., Moschetta, A., Mangelsdorf, D., Heyman, R., Moore, D., and Auwerx, J. (2004). Bile acids lower triglyceride levels via a pathway involving FXR, SHP, and SREBP-1c. JOURNAL OF CLINICAL INVESTIGATION *113*, 1408–1418. https://doi.org/10.1172/JCI200421025.

103. Kim, K., Choi, S., Zhou, Y., Kim, E., Lee, J., Saha, P., Anakk, S., and Moore, D. (2017). Hepatic FXR/SHP Axis Modulates Systemic Glucose and Fatty Acid Homeostasis in Aged Mice. HEPATOLOGY *66*, 498–509. https://doi.org/10.1002/hep.29199.

104. Bello-Chavolla, O., Antonio-Villa, N., Vargas-Vazquez, A., Avila-Funes, J., and Aguilar-Salinas, C. (2019). Pathophysiological Mechanisms Linking Type 2 Diabetes and Dementia: Review of Evidence from Clinical, Translational and Epidemiological Research. CURRENT DIABETES REVIEWS *15*, 456–470. https://doi.org/10.2174/1573399815666190129155654.

105. Vallim, T., Tarling, E., Ahn, H., Hagey, L., Romanoski, C., Lee, R., Graham, M., Motohashi, H., Yamamoto, M., and Edwards, P. (2015). MAFG Is a Transcriptional Repressor of Bile Acid Synthesis and Metabolism. CELL METABOLISM *21*, 298–310. https://doi.org/10.1016/j.cmet.2015.01.007.

106. Yang, Y.M., Roh, Y.S., and Seki, E. (2015). MafG, A Novel Target of FXR that Regulates Bile Acid Homeostasis. Gastroenterology *149*, 1981–1983. https://doi.org/10.1053/j.gastro.2015.10.014.

107. Hofmann, M., Schumann, C., Zimmer, G., Henzel, K., Locher, U., and Leuschner, U. (2001). LUV's lipid composition modulates diffusion of bile acids. Chemistry and Physics of Lipids *110*, 165–171. https://doi.org/10.1016/S0009-3084(01)00131-1.

108. Cabral, D.J., Small, D.M., Lilly, H.S., and Hamilton, J.A. (1987). Transbilayer movement of bile acids in model membranes. Biochemistry *26*, 1801–1804. https://doi.org/10.1021/bi00381a002.

109. Schubert, R., Jaroni, H., Schoelmerich, J., and Schmidt, K.H. (2009). Studies on the Mechanism of Bile Salt-Induced Liposomal Membrane Damage. Digestion *28*, 181–190. https://doi.org/10.1159/000198984.

110. Coleman, R., Lowe, P.J., and Billington, D. (1980). Membrane lipid composition and susceptibility to bile salt damage. Biochimica et Biophysica Acta (BBA) - Biomembranes *599*, 294–300. https://doi.org/10.1016/0005-2736(80)90075-9.

111. Begley, M., Gahan, C., and Hill, C. (2005). The interaction between bacteria and bile. FEMS MICROBIOLOGY REVIEWS *29*, 625–651. https://doi.org/10.1016/j.femsre.2004.09.003.

112. Kandell, R.L., and Bernstein, C. (1991). Bile salt/acid induction of DNA damage in bacterial and mammalian cells: Implications for colon cancer. Nutrition and Cancer *16*, 227–238. https://doi.org/10.1080/01635589109514161.

113. Prieto, A.I., Ramos-Morales, F., and Casadesús, J. (2004). Bile-Induced DNA Damage in *Salmonella enterica*. Genetics *168*, 1787–1794. https://doi.org/10.1534/genetics.104.031062.

114. García-Quintanilla, M., Ramos-Morales, F., and Casadesús, J. (2008). Conjugal Transfer of the *Salmonella enterica* Virulence Plasmid in the Mouse Intestine. Journal of Bacteriology *190*, 1922–1927. https://doi.org/10.1128/jb.01626-07.

115. Ley, R.E., Turnbaugh, P.J., Klein, S., and Gordon, J.I. (2006). Human gut microbes associated with obesity. Nature *444*, 1022–1023. https://doi.org/10.1038/4441022a.

116. Kübeck, R., Bonet-Ripoll, C., Hoffmann, C., Walker, A., Müller, V.M., Schüppel, V.L., Lagkouvardos, I., Scholz, B., Engel, K.-H., Daniel, H., et al. (2016). Dietary fat and gut microbiota interactions determine diet-induced obesity in mice. Molecular Metabolism *5*, 1162–1174. https://doi.org/10.1016/j.molmet.2016.10.001.

117. Turnbaugh, P.J., Ridaura, V.K., Faith, J.J., Rey, F.E., Knight, R., and Gordon, J.I. (2009). The Effect of Diet on the Human Gut Microbiome: A Metagenomic Analysis in Humanized Gnotobiotic Mice. Sci Transl Med *1*, 6ra14. https://doi.org/10.1126/scitranslmed.3000322.

118. David, L.A., Maurice, C.F., Carmody, R.N., Gootenberg, D.B., Button, J.E., Wolfe, B.E., Ling, A.V., Devlin, A.S., Varma, Y., Fischbach, M.A., et al. (2014). Diet rapidly and reproducibly alters the human gut microbiome. Nature *505*, 559–563. https://doi.org/10.1038/nature12820.

119. Islam, K.B.M.S., Fukiya, S., Hagio, M., Fujii, N., Ishizuka, S., Ooka, T., Ogura, Y., Hayashi, T., and Yokota, A. (2011). Bile acid is a host factor that regulates the composition of the cecal microbiota in rats. Gastroenterology *141*, 1773–1781. https://doi.org/10.1053/j.gastro.2011.07.046.

120. Ridlon, J.M., Alves, J.M., Hylemon, P.B., and Bajaj, J.S. (2013). Cirrhosis, bile acids and gut microbiota: unraveling a complex relationship. Gut Microbes *4*, 382–387. https://doi.org/10.4161/gmic.25723.

121. Song, Z., Cai, Y., Lao, X., Wang, X., Lin, X., Cui, Y., Kalavagunta, P., Liao, J., Jin, L., Shang, J., et al. (2019). Taxonomic profiling and populational patterns of bacterial bile salt hydrolase (BSH) genes based on worldwide human gut microbiome. MICROBIOME *7*. https://doi.org/10.1186/s40168-019-0628-3.

122. Ridlon, J.M., and Hylemon, P.B. (2012). Identification and characterization of two bile acid coenzyme A transferases from *Clostridium scindens*, a bile acid 7α-dehydroxylating intestinal bacterium. J Lipid Res *53*, 66–76. https://doi.org/10.1194/jlr.M020313.

123. Kang, D.-J., Ridlon, J.M., Moore, D.R., Barnes, S., and Hylemon, P.B. (2008). Clostridium scindens baiCD and baiH genes encode stereo-specific 7α/7β-hydroxy-3-oxo-Δ4-cholenoic acid oxidoreductases. Biochimica et Biophysica Acta (BBA) - Molecular and Cell Biology of Lipids *1781*, 16–25. https://doi.org/10.1016/j.bbalip.2007.10.008.

124. Guzior, D.V., and Quinn, R.A. (2021). Review: microbial transformations of human bile acids. Microbiome *9*, 140. https://doi.org/10.1186/s40168-021-01101-1.

125. Ridlon, J.M., and Bajaj, J.S. (2015). The human gut sterolbiome: bile acid-microbiome endocrine aspects and therapeutics. Acta Pharm Sin B *5*, 99–105. https://doi.org/10.1016/j.apsb.2015.01.006.

126. Wahlström, A., Sayin, S.I., Marschall, H.-U., and Bäckhed, F. (2016). Intestinal Crosstalk between Bile Acids and Microbiota and Its Impact on Host Metabolism. Cell Metab *24*, 41–50. https://doi.org/10.1016/j.cmet.2016.05.005.

127. Odermatt, A., Da Cunha, T., Penno, C.A., Chandsawangbhuwana, C., Reichert, C., Wolf, A., Dong, M., and Baker, M.E. (2011). Hepatic reduction of the secondary bile acid 7-oxolithocholic acid is mediated by 11β-hydroxysteroid dehydrogenase 1. Biochem J *436*, 621–629. https://doi.org/10.1042/BJ20110022.

128. Sayin, S., Wahlstrom, A., Felin, J., Jantti, S., Marschall, H., Bamberg, K., Angelin, B., Hyotylainen, T., Oresic, M., and Backhed, F. (2013). Gut Microbiota Regulates Bile Acid Metabolism by Reducing the Levels of Tauro-beta-muricholic Acid, a Naturally Occurring FXR Antagonist. CELL METABOLISM *17*, 225–235. https://doi.org/10.1016/j.cmet.2013.01.003.

129. Wahlström, A., Kovatcheva-Datchary, P., Ståhlman, M., Khan, M.-T., Bäckhed, F., and Marschall, H.-U. (2017). Induction of farnesoid X receptor signaling in germ-free

mice colonized with a human microbiota. Journal of Lipid Research *58*, 412–419. https://doi.org/10.1194/jlr.M072819.

130. Li, J., and Dawson, P. (2019). Animal models to study bile acid metabolism. BIOCHIMICA ET BIOPHYSICA ACTA-MOLECULAR BASIS OF DISEASE *1865*, 895–911. https://doi.org/10.1016/j.bbadis.2018.05.011.

131. Hardison, W.G.M., and Grundy, S.M. (1983). Effect of bile acid conjugation pattern on bile acid metabolism in normal humans. Gastroenterology *84*, 617–620. https://doi.org/10.1016/0016-5085(83)90088-4.

132. Falany, C.N., Fortinberry, H., Leiter, E.H., and Barnes, S. (1997). Cloning, expression, and chromosomal localization of mouse liver bile acid CoA:amino acid N-acyltransferase. Journal of Lipid Research *38*, 1139–1148. https://doi.org/10.1016/S0022-2275(20)37196-0.

133. Hofmann, A.F., and Hagey, L.R. (2008). Bile Acids: Chemistry, Pathochemistry, Biology, Pathobiology, and Therapeutics. Cell. Mol. Life Sci. *65*, 2461–2483. https://doi.org/10.1007/s00018-008-7568-6.

134. Sharma, R., Majer, F., Peta, V.K., Wang, J., Keaveney, R., Kelleher, D., Long, A., and Gilmer, J.F. (2010). Bile acid toxicity structure–activity relationships: Correlations between cell viability and lipophilicity in a panel of new and known bile acids using an oesophageal cell line (HET-1A). Bioorganic & Medicinal Chemistry *18*, 6886–6895. https://doi.org/10.1016/j.bmc.2010.07.030.

135. Woolbright, B.L., McGill, M.R., Yan, H., and Jaeschke, H. (2016). Bile Acid-Induced Toxicity in HepaRG Cells Recapitulates the Response in Primary Human Hepatocytes. Basic & Clinical Pharmacology & Toxicology *118*, 160–167. https://doi.org/10.1111/bcpt.12449.

136. Truong, J.K., and Dawson, P.A. (2021). Chapter 12 - Bile acid metabolism. In Biochemistry of Lipids, Lipoproteins and Membranes (Seventh Edition), N. D. Ridgway and R. S. McLeod, eds. (Elsevier), pp. 395–428. https://doi.org/10.1016/B978-0-12-824048-9.00016-X.

137. Inagaki, T., Choi, M., Moschetta, A., Peng, L., Cummins, C., McDonald, J., Luo, G., Jones, S., Goodwin, B., Richardson, J., et al. (2005). Fibroblast growth factor 15 functions as an enterohepatic signal to regulate bile acid homeostasis. CELL METABOLISM *2*, 217–225. https://doi.org/10.1016/j.cmet.2005.09.001.

138. Björkhem, I., Blomstrand, R., Lewenhaupt, A., and Svensson, L. (1978). Effect of lymphatic drainage on 7α-hydroxylation of cholesterol in rat liver. Biochemical and Biophysical Research Communications *85*, 532–540. https://doi.org/10.1016/0006-291X(78)91196-8.

139. Stellaard, F., and Paumgartner, G. (1987). A new model to assess deoxycholic acid metabolism in health using stable isotope dilution technique. Eur J Clin Invest *17*, 63–67. https://doi.org/10.1111/j.1365-2362.1987.tb01227.x.

140. Ahmad, T.R., and Haeusler, R.A. (2019). Bile acids in glucose metabolism and insulin signalling — mechanisms and research needs. Nat Rev Endocrinol *15*, 701–712. https://doi.org/10.1038/s41574-019-0266-7.

141. Honda, A., Miyazaki, T., Iwamoto, J., Hirayama, T., Morishita, Y., Monma, T., Ueda, H., Mizuno, S., Sugiyama, F., Takahashi, S., et al. (2020). Regulation of bile acid metabolism in mouse models with hydrophobic bile acid composition. J Lipid Res *61*, 54–69. https://doi.org/10.1194/jlr.RA119000395.

142. Hung, D.T., Zhu, J., Sturtevant, D., and Mekalanos, J.J. (2006). Bile acids stimulate biofilm formation in *Vibrio cholerae*. Mol Microbiol *59*, 193–201. https://doi.org/10.1111/j.1365-2958.2005.04846.x.

143. Gupta, S., and Chowdhury, R. (1997). Bile affects production of virulence factors and motility of *Vibrio cholerae*. INFECTION AND IMMUNITY *65*, 1131–1134. https://doi.org/10.1128/IAI.65.3.1131-1134.1997.

144. Butler, S., and Camilli, A. (2005). Going against the grain: Chemotaxis and infection in *Vibrio cholerae*. NATURE REVIEWS MICROBIOLOGY *3*, 611–620. https://doi.org/10.1038/nrmicro1207.

145. Xue, Y., Tu, F., Shi, M., Wu, C., Ren, G., Wang, X., Fang, W., Song, H., and Yang, M. (2016). Redox pathway sensing bile salts activates virulence gene expression in *Vibrio cholerae*. MOLECULAR MICROBIOLOGY *102*, 909–924. https://doi.org/10.1111/mmi.13497.

146. Almagro-Moreno, S., Kim, T., Skorupski, K., and Taylor, R. (2015). Proteolysis of Virulence Regulator ToxR Is Associated with Entry of *Vibrio cholerae* into a Dormant State. PLOS GENETICS *11*. https://doi.org/10.1371/journal.pgen.1005145.

147. Lembke, M., Hofler, T., Walter, A., Tutz, S., Fengler, V., Schild, S., and Reidl, J. (2020). Host stimuli and operator binding sites controlling protein interactions between virulence master regulator ToxR and ToxS in *Vibrio cholerae*. MOLECULAR MICROBIOLOGY *114*, 262–278. https://doi.org/10.1111/mmi.14510.

148. Hung, D., and Mekalanos, J. (2005). Bile acids induce cholera toxin expression in *Vibrio cholerae* in a ToxT-independent manner. PROCEEDINGS OF THE NATIONAL ACADEMY OF SCIENCES OF THE UNITED STATES OF AMERICA *102*, 3028–3033. https://doi.org/10.1073/pnas.0409559102.

149. Alavi, S., Mitchell, J.D., Cho, J.Y., Liu, R., Macbeth, J.C., and Hsiao, A. (2020). Interpersonal Gut Microbiome Variation Drives Susceptibility and Resistance to Cholera Infection. Cell *181*, 1533-1546.e13. https://doi.org/10.1016/j.cell.2020.05.036.

150. Lowden, M., Skorupski, K., Pellegrini, M., Chiorazzo, M., Taylor, R., and Kull, F. (2010). Structure of *Vibrio cholerae* ToxT reveals a mechanism for fatty acid regulation of virulence genes. PROCEEDINGS OF THE NATIONAL ACADEMY OF SCIENCES OF THE UNITED STATES OF AMERICA *107*, 2860–2865. https://doi.org/10.1073/pnas.0915021107.

151. Deen, J., Mengel, M.A., and Clemens, J.D. (2020). Epidemiology of cholera. Vaccine *38 Suppl 1*, A31–A40. https://doi.org/10.1016/j.vaccine.2019.07.078.

152. Miller, V., Taylor, R., and Mekalanos, J. (1987). Cholera-toxin transcriptional activator toxr is a transmembrane dna-binding protein. CELL *48*, 271–279. https://doi.org/10.1016/0092-8674(87)90430-2.

153. Higgins, D., and Dirita, V. (1994). Transcriptional control of toxt, a regulatory gene in the toxr regulon of *Vibrio cholerae*. MOLECULAR MICROBIOLOGY *14*, 17–29. https://doi.org/10.1111/j.1365-2958.1994.tb01263.x.

154. Hase, C., and Mekalanos, J. (1998). TcpP protein is a positive regulator of virulence gene expression in *Vibrio cholerae*. PROCEEDINGS OF THE NATIONAL ACADEMY OF SCIENCES OF THE UNITED STATES OF AMERICA *95*, 730–734. https://doi.org/10.1073/pnas.95.2.730.

155. Childers, B., and Klose, K. (2007). Regulation of virulence in *Vibrio cholerae*: the ToxR regulon. FUTURE MICROBIOLOGY *2*, 335–344. https://doi.org/10.2217/17460913.2.3.335.

156. Louis, P., and O'Byrne, C.P. (2010). Life in the Gut: Microbial responses to Stress in the Gastrointestinal Tract. Sci Prog *93*, 7–36. https://doi.org/10.3184/003685009X12605525292307.

157. Yang, M., Liu, Z., Hughes, C., Stern, A., Wang, H., Zhong, Z., Kan, B., Fenical, W., and Zhu, J. (2013). Bile salt-induced intermolecular disulfide bond formation activates *Vibrio cholerae* virulence. PROCEEDINGS OF THE NATIONAL ACADEMY OF SCIENCES OF THE UNITED STATES OF AMERICA *110*, 2348–2353. https://doi.org/10.1073/pnas.1218039110.

158. Frommherz, L., Bub, A., Hummel, E., Rist, M.J., Roth, A., Watzl, B., and Kulling, S.E. (2016). Age-Related Changes of Plasma Bile Acid Concentrations in Healthy Adults—Results from the Cross-Sectional KarMeN Study. PLoS One *11*, e0153959. https://doi.org/10.1371/journal.pone.0153959.

159. Uchida, K., Chikai, T., Takase, H., Nomura, Y., Seo, S., Nakao, H., and Takeuchi, N. (1990). Age–related changes of bile acid metabolism in rats. Archives of Gerontology and Geriatrics *10*, 37–48. https://doi.org/10.1016/0167-4943(90)90042-5.

160. Niijima, S. (1985). Studies on the conjugating activity of bile acids in children. Pediatr Res *19*, 302–307. https://doi.org/10.1203/00006450-198503000-00010.

161. Rimal, B., Collins, S.L., Tanes, C.E., Rocha, E.R., Granda, M.A., Solanki, S., Hoque, N.J., Gentry, E.C., Koo, I., Reilly, E.R., et al. (2024). Bile salt hydrolase catalyses formation of amine-conjugated bile acids. Nature *626*, 859–863. https://doi.org/10.1038/s41586-023-06990-w.

162. Guzior, D.V., Okros, M., Shivel, M., Armwald, B., Bridges, C., Fu, Y., Martin, C., Schilmiller, A.L., Miller, W.M., Ziegler, K.M., et al. (2024). Bile salt hydrolase acyltransferase activity expands bile acid diversity. Nature *626*, 852–858. https://doi.org/10.1038/s41586-024-07017-8.

163. Bina, T.F., Kunkle, D.E., Bina, X.R., Mullett, S.J., Wendell, S.G., and Bina, J.E. (2021). Bile Salts Promote ToxR Regulon Activation during Growth under Virulence-Inducing Conditions. Infection and Immunity *89*. https://doi.org/10.1128/iai.00441-21.

164. Ridlon, J., Kang, D., and Hylemon, P. (2006). Bile salt biotransformations by human intestinal bacteria. JOURNAL OF LIPID RESEARCH *47*, 241–259. https://doi.org/10.1194/jlr.R500013-JLR200.

165. Jones, B., Begley, M., Hill, C., Gahan, C., and Marchesi, J. (2008). Functional and comparative metagenomic analysis of bile salt hydrolase activity in the human gut microbiome. PROCEEDINGS OF THE NATIONAL ACADEMY OF SCIENCES OF THE UNITED STATES OF AMERICA *105*, 13580–13585. https://doi.org/10.1073/pnas.0804437105.

166. Provenzano, D., and Klose, K. (2000). Altered expression of the ToxR-regulated porins OmpU and OmpT diminishes *Vibrio cholerae* bile resistance, virulence factor expression, and intestinal colonization. PROCEEDINGS OF THE NATIONAL ACADEMY OF SCIENCES OF THE UNITED STATES OF AMERICA *97*, 10220–10224. https://doi.org/10.1073/pnas.170219997.

167. Kovacikova, G., Lin, W., and Skorupski, K. (2003). The virulence activator AphA links quorum sensing to pathogenesis and physiology in *Vibrio cholerae* by repressing the expression of a penicillin amidase gene on the small chromosome. J Bacteriol *185*, 4825–4836. https://doi.org/10.1128/JB.185.16.4825-4836.2003.

168. Dalia, A., McDonough, E., and Camilli, A. (2014). Multiplex genome editing by natural transformation. PROCEEDINGS OF THE NATIONAL ACADEMY OF

SCIENCES OF THE UNITED STATES OF AMERICA *111*, 8937–8942. https://doi.org/10.1073/pnas.1406478111.

169. Kelley, L., Mezulis, S., Yates, C., Wass, M., and Sternberg, M. (2015). The Phyre2 web portal for protein modeling, prediction and analysis. NATURE PROTOCOLS *10*, 845–858. https://doi.org/10.1038/nprot.2015.053.

170. DuPont, H.L., Formal, S.B., Hornick, R.B., Snyder, M.J., Libonati, J.P., Sheahan, D.G., LaBrec, E.H., and Kalas, J.P. (1971). Pathogenesis of *Escherichia coli* Diarrhea. New England Journal of Medicine *285*, 1–9. https://doi.org/10.1056/NEJM197107012850101.

171. Darling, A.C.E., Mau, B., Blattner, F.R., and Perna, N.T. (2004). Mauve: multiple alignment of conserved genomic sequence with rearrangements. Genome Res *14*, 1394–1403. https://doi.org/10.1101/gr.2289704.

172. Lee, I., Ha, S.-M., Baek, M., Kim, D.W., Yi, H., and Chun, J. (2021). VicPred: A *Vibrio cholerae* Genotype Prediction Tool. Front. Microbiol. *12*. https://doi.org/10.3389/fmicb.2021.691895.

173. Lassalle, F., Al-Shalali, S., Al-Hakimi, M., Njamkepo, E., Bashir, I.M., Dorman, M.J., Rauzier, J., Blackwell, G.A., Taylor-Brown, A., Beale, M.A., et al. (2023). Genomic epidemiology reveals multidrug resistant plasmid spread between *Vibrio cholerae* lineages in Yemen. Nat Microbiol *8*, 1787–1798. https://doi.org/10.1038/s41564-023-01472-1.

174. Edgar, R.C. (2004). MUSCLE: multiple sequence alignment with high accuracy and high throughput. Nucleic Acids Research *32*, 1792–1797. https://doi.org/10.1093/nar/gkh340.

175. Price, M.N., Dehal, P.S., and Arkin, A.P. (2010). FastTree 2--approximately maximum-likelihood trees for large alignments. PLoS One *5*, e9490. https://doi.org/10.1371/journal.pone.0009490.

176. Stamatakis, A. (2014). RAxML version 8: a tool for phylogenetic analysis and post-analysis of large phylogenies. Bioinformatics *30*, 1312–1313. https://doi.org/10.1093/bioinformatics/btu033.

177. Miller, M.A., Pfeiffer, W., and Schwartz, T. (2010). Creating the CIPRES Science Gateway for inference of large phylogenetic trees. In 2010 Gateway Computing Environments Workshop (GCE), pp. 1–8. https://doi.org/10.1109/GCE.2010.5676129.

178. Yang, Z. (2007). PAML 4: phylogenetic analysis by maximum likelihood. Mol Biol Evol *24*, 1586–1591. https://doi.org/10.1093/molbev/msm088.

179. Dawson, P.A., and Karpen, S.J. (2015). Intestinal transport and metabolism of bile acids. J Lipid Res *56*, 1085–1099. https://doi.org/10.1194/jlr.R054114.

180. Godlewska, U., Bulanda, E., and Wypych, T.P. (2022). Bile acids in immunity: Bidirectional mediators between the host and the microbiota. Front Immunol *13*, 949033. https://doi.org/10.3389/fimmu.2022.949033.

181. Staley, C., Weingarden, A., Khoruts, A., and Sadowsky, M. (2017). Interaction of gut microbiota with bile acid metabolism and its influence on disease states. APPLIED MICROBIOLOGY AND BIOTECHNOLOGY *101*, 47–64. https://doi.org/10.1007/s00253-016-8006-6.

182. Urdaneta, V., and Casadesús, J. (2017). Interactions between Bacteria and Bile Salts in the Gastrointestinal and Hepatobiliary Tracts. Frontiers in Medicine *4*.

183. Tian, Y., Gui, W., Koo, I., Smith, P.B., Allman, E.L., Nichols, R.G., Rimal, B., Cai, J., Liu, Q., and Patterson, A.D. (2020). The microbiome modulating activity of bile acids. Gut Microbes *11*, 979–996. https://doi.org/10.1080/19490976.2020.1732268.

184. Pandak, W.M., Bohdan, P., Franklund, C., Mallonee, D.H., Eggertsen, G., Björkhem, I., Gil, G., Vlahcevic, Z.R., and Hylemon, P.B. (2001). Expression of sterol 12α-hydroxylase alters bile acid pool composition in primary rat hepatocytes and in vivo. Gastroenterology *120*, 1801–1809. https://doi.org/10.1053/gast.2001.24833.

185. Vlahcevic*, Z.R., Eggertsen‡, G., Björkhem‡, I., Hylemon§, P.B., Redford*, K., and Pandak*, W.M. (2000). Regulation of sterol 12α-hydroxylase and cholic acid biosynthesis in the rat. Gastroenterology *118*, 599–607. https://doi.org/10.1016/S0016-5085(00)70267-8.

186. Krukonis, E., Yu, R., and DiRita, V. (2000). The *Vibrio cholerae* ToxR/TcpP/ToxT virulence cascade: distinct roles for two membrane-localized transcriptional activators on a single promoter. MOLECULAR MICROBIOLOGY *38*, 67–84. https://doi.org/10.1046/j.1365-2958.2000.02111.x.

187. Cho, J.Y., Liu, R., and Hsiao, A. (2022). Microbiota-Associated Biofilm Regulation Leads to *Vibrio cholerae* Resistance Against Intestinal Environmental Stress. Frontiers in Cellular and Infection Microbiology *12*.

188. Ribet, D., and Cossart, P. (2015). How bacterial pathogens colonize their hosts and invade deeper tissues. Microbes Infect *17*, 173–183. https://doi.org/10.1016/j.micinf.2015.01.004.

189. David, L., Weil, A., Ryan, E., Calderwood, S., Harris, J., Chowdhury, F., Begum, Y., Qadri, F., LaRocque, R., and Turnbaugh, P. (2015). Gut Microbial Succession

Follows Acute Secretory Diarrhea in Humans. MBIO *6*. https://doi.org/10.1128/mBio.00381-15.

190. Bachmann, V., Kostiuk, B., Unterweger, D., Diaz-Satizabal, L., Ogg, S., and Pukatzki, S. (2015). Bile Salts Modulate the Mucin-Activated Type VI Secretion System of Pandemic *Vibrio cholerae*. PLOS NEGLECTED TROPICAL DISEASES *9*. https://doi.org/10.1371/journal.pntd.0004031.

191. Wibbenmeyer, J.A., Provenzano, D., Landry, C.F., Klose, K.E., and Delcour, A.H. (2002). *Vibrio cholerae* OmpU and OmpT porins are differentially affected by bile. Infect Immun *70*, 121–126. https://doi.org/10.1128/IAI.70.1.121-126.2002.

192. Simonet, V., Basle, A., Klose, K., and Delcour, A. (2003). The *Vibrio cholerae* Porins OmpU and OmpT have distinct channel properties. JOURNAL OF BIOLOGICAL CHEMISTRY *278*, 17539–17545. https://doi.org/10.1074/jbc.M301202200.

193. Taylor, D., Bina, X., and Bina, J. (2012). *Vibrio cholerae* vexH Encodes a Multiple Drug Efflux Pump That Contributes to the Production of Cholera Toxin and the Toxin Co-Regulated Pilus. PLOS ONE *7*. https://doi.org/10.1371/journal.pone.0038208.

194. Bina, J.E., Provenzano, D., Wang, C., Bina, X.R., and Mekalanos, J.J. (2006). Characterization of the *Vibrio cholerae* vexAB and vexCD efflux systems. Arch Microbiol *186*, 171–181. https://doi.org/10.1007/s00203-006-0133-5.

195. Kunkle, D., Bina, X., and Bina, J. (2017). The *Vibrio cholerae* VexGH RND Efflux System Maintains Cellular Homeostasis by Effluxing Vibriobactin. MBIO *8*. https://doi.org/10.1128/mBio.00126-17.

196. Chen, S., Wang, H., Katzianer, D., Zhong, Z., and Zhu, J. (2013). LysR family activator-regulated major facilitator superfamily transporters are involved in *Vibrio cholerae* antimicrobial compound resistance and intestinal colonisation. INTERNATIONAL JOURNAL OF ANTIMICROBIAL AGENTS *41*, 188–192. https://doi.org/10.1016/j.ijantimicag.2012.10.008.

197. Marciani, L., Cox, E., Hoad, C., Totman, J., Costigan, C., Singh, G., Shepherd, V., Chalkley, L., Robinson, M., Ison, R., et al. (2013). Effects of various food ingredients on gall bladder emptying. EUROPEAN JOURNAL OF CLINICAL NUTRITION *67*, 1182–1187. https://doi.org/10.1038/ejcn.2013.168.

198. Faith, J., McNulty, N., Rey, F., and Gordon, J. (2011). Predicting a Human Gut Microbiota's Response to Diet in Gnotobiotic Mice. SCIENCE *333*, 101–104. https://doi.org/10.1126/science.1206025.

199. Kovacikova, G., Lin, W., Taylor, R.K., and Skorupski, K. (2017). The Fatty Acid Regulator FadR Influences the Expression of the Virulence Cascade in the El Tor Biotype of *Vibrio cholerae* by Modulating the Levels of ToxT via Two Different Mechanisms. J Bacteriol *199*, e00762-16. https://doi.org/10.1128/JB.00762-16.

200. Schneierson, S.S., and Amsterdam, D. (1958). Effect of Bile Salts upon the Activity of Antibiotics. Nature *182*, 56–57. https://doi.org/10.1038/182056a0.

201. Buffie, C., Bucci, V., Stein, R., McKenney, P., Ling, L., Gobourne, A., No, D., Liu, H., Kinnebrew, M., Viale, A., et al. (2015). Precision microbiome reconstitution restores bile acid mediated resistance to Clostridium difficile. NATURE *517*, 205-U207. https://doi.org/10.1038/nature13828.

202. Reed, A.D., Nethery, M.A., Stewart, A., Barrangou, R., and Theriot, C.M. (2020). Strain-Dependent Inhibition of *Clostridioides difficile* by Commensal Clostridia Carrying the Bile Acid-Inducible (bai) Operon. J Bacteriol *202*, e00039-20. https://doi.org/10.1128/JB.00039-20.

203. Bassler, B., Wright, M., and Silverman, M. (1994). Multiple signaling systems controlling expression of luminescence in *Vibrio harveyi* - sequence and function of genes encoding a 2nd sensory pathway. MOLECULAR MICROBIOLOGY *13*, 273–286. https://doi.org/10.1111/j.1365-2958.1994.tb00422.x.

204. Greenberg, E.P., Hastings, J.W., and Ulitzur, S. (1979). Induction of luciferase synthesis in *Beneckea harveyi* by other marine bacteria. Arch. Microbiol. *120*, 87–91. https://doi.org/10.1007/BF00409093.

205. Schauder, S., and Bassler, B.L. (2001). The languages of bacteria. Genes Dev. *15*, 1468–1480. https://doi.org/10.1101/gad.899601.

206. Winzer, K., Hardie, K.R., Burgess, N., Doherty, N., Kirke, D., Holden, M.T.G., Linforth, R., Cornell, K.A., Taylor, A.J., Hill, P.J., et al. (2002). LuxS: its role in central metabolism and the in vitro synthesis of 4-hydroxy-5-methyl-3(2H)-furanone. Microbiology *148*, 909–922. https://doi.org/10.1099/00221287-148-4-909.

207. Winzer, K., Hardie, K.R., and Williams, P. (2003). LuxS and Autoinducer-2: Their Contribution to Quorum Sensing and Metabolism in Bacteria. In Advances in Applied Microbiology (Academic Press), pp. 291–396. https://doi.org/10.1016/S0065-2164(03)53009-X.

208. Xue, C., Li, G., Gu, X., Su, Y., Zheng, Q., Yuan, X., Bao, Z., Lu, J., and Li, L. Health and Disease: *Akkermansia muciniphila*, the Shining Star of the Gut Flora. Research (Wash D C) *6*, 0107. https://doi.org/10.34133/research.0107.

209. Desai, M.S., Seekatz, A.M., Koropatkin, N.M., Kamada, N., Hickey, C.A., Wolter, M., Pudlo, N.A., Kitamoto, S., Terrapon, N., Muller, A., et al. (2016). A dietary fiber-deprived gut microbiota degrades the colonic mucus barrier and enhances pathogen susceptibility. Cell *167*, 1339-1353.e21. https://doi.org/10.1016/j.cell.2016.10.043.

210. Everard, A., Belzer, C., Geurts, L., Ouwerkerk, J.P., Druart, C., Bindels, L.B., Guiot, Y., Derrien, M., Muccioli, G.G., Delzenne, N.M., et al. (2013). Cross-talk between *Akkermansia muciniphila* and intestinal epithelium controls diet-induced obesity. Proc Natl Acad Sci U S A *110*, 9066–9071. https://doi.org/10.1073/pnas.1219451110.

211. Raba, G., and Luis, A.S. (2023). Mucin utilization by gut microbiota: recent advances on characterization of key enzymes. Essays Biochem *67*, 345–353. https://doi.org/10.1042/EBC20220121.

212. Millet, Y.A., Alvarez, D., Ringgaard, S., von Andrian, U.H., Davis, B.M., and Waldor, M.K. (2014). Insights into *Vibrio cholerae* intestinal colonization from monitoring fluorescently labeled bacteria. PLoS Pathog *10*, e1004405. https://doi.org/10.1371/journal.ppat.1004405.

213. Wang, B.X., Takagi, J., McShane, A., Park, J.H., Aoki, K., Griffin, C., Teschler, J., Kitts, G., Minzer, G., Tiemeyer, M., et al. (2023). Host-derived O-glycans inhibit toxigenic conversion by a virulence-encoding phage in *Vibrio cholerae*. The EMBO Journal *42*, e111562. https://doi.org/10.15252/embj.2022111562.

214. Szabady, R.L., Yanta, J.H., Halladin, D.K., Schofield, M.J., and Welch, R.A. (2011). TagA is a secreted protease of *Vibrio cholerae* that specifically cleaves mucin glycoproteins. Microbiology (Reading) *157*, 516–525. https://doi.org/10.1099/mic.0.044529-0.

215. Bolyen, E., Rideout, J.R., Dillon, M.R., Bokulich, N.A., Abnet, C.C., Al-Ghalith, G.A., Alexander, H., Alm, E.J., Arumugam, M., Asnicar, F., et al. (2019). Reproducible, interactive, scalable and extensible microbiome data science using QIIME 2. Nat Biotechnol *37*, 852–857. https://doi.org/10.1038/s41587-019-0209-9.

216. Bina, J., Zhu, J., Dziejman, M., Faruque, S., Calderwood, S., and Mekalanos, J. (2003). ToxR regulon of *Vibrio cholerae* and its expression in vibrios shed by cholera patients. PROCEEDINGS OF THE NATIONAL ACADEMY OF SCIENCES OF THE UNITED STATES OF AMERICA *100*, 2801–2806. https://doi.org/10.1073/pnas.2628026100.

217. Wagner, C.E., Wheeler, K.M., and Ribbeck, K. (2018). Mucins and Their Role in Shaping the Functions of Mucus Barriers. Annu Rev Cell Dev Biol *34*, 189–215. https://doi.org/10.1146/annurev-cellbio-100617-062818.

218. Shin, J., Noh, J.-R., Chang, D.-H., Kim, Y.-H., Kim, M.H., Lee, E.S., Cho, S., Ku, B.J., Rhee, M.-S., Kim, B.-C., et al. (2019). Elucidation of *Akkermansia muciniphila* Probiotic Traits Driven by Mucin Depletion. Front Microbiol *10*, 1137. https://doi.org/10.3389/fmicb.2019.01137.

219. Xu, Y., Wang, N., Tan, H.-Y., Li, S., Zhang, C., and Feng, Y. (2020). Function of *Akkermansia muciniphila* in Obesity: Interactions With Lipid Metabolism, Immune Response and Gut Systems. Front Microbiol *11*, 219. https://doi.org/10.3389/fmicb.2020.00219.

220. Valle Arevalo, A., and Nobile, C.J. (2020). Interactions of microorganisms with host mucins: a focus on *Candida albicans*. FEMS Microbiol Rev *44*, 645–654. https://doi.org/10.1093/femsre/fuaa027.

221. Ottman, N., Huuskonen, L., Reunanen, J., Boeren, S., Klievink, J., Smidt, H., Belzer, C., and de Vos, W.M. (2016). Characterization of Outer Membrane Proteome of *Akkermansia muciniphila* Reveals Sets of Novel Proteins Exposed to the Human Intestine. Front Microbiol *7*, 1157. https://doi.org/10.3389/fmicb.2016.01157.

222. Linden, S.K., Sutton, P., Karlsson, N.G., Korolik, V., and McGuckin, M.A. (2008). Mucins in the mucosal barrier to infection. Mucosal Immunol *1*, 183–197. https://doi.org/10.1038/mi.2008.5.

223. van Putten, J.P.M., and Strijbis, K. (2017). Transmembrane Mucins: Signaling Receptors at the Intersection of Inflammation and Cancer. J Innate Immun *9*, 281–299. https://doi.org/10.1159/000453594.

224. Lindén, S.K., Sheng, Y.H., Every, A.L., Miles, K.M., Skoog, E.C., Florin, T.H.J., Sutton, P., and McGuckin, M.A. (2009). MUC1 Limits *Helicobacter pylori* Infection both by Steric Hindrance and by Acting as a Releasable Decoy. PLoS Pathog *5*, e1000617. https://doi.org/10.1371/journal.ppat.1000617.

225. Bhowmick, R., Ghosal, A., Das, B., Koley, H., Saha, D.R., Ganguly, S., Nandy, R.K., Bhadra, R.K., and Chatterjee, N.S. (2008). Intestinal Adherence of *Vibrio cholerae* Involves a Coordinated Interaction between Colonization Factor GbpA and Mucin. Infection and Immunity *76*, 4968–4977. https://doi.org/10.1128/iai.01615-07.

226. Silva, S.H., Vieira, E.C., Dias, R.S., and Nicoli, J.R. (2001). Antagonism against *Vibrio cholerae* by diffusible substances produced by bacterial components of the human faecal microbiota. J Med Microbiol *50*, 161–164. https://doi.org/10.1099/0022-1317-50-2-161.

227. Kaur, S., Sharma, P., Kalia, N., Singh, J., and Kaur, S. (2018). Anti-biofilm Properties of the Fecal Probiotic Lactobacilli Against *Vibrio* spp. Front Cell Infect Microbiol *8*, 120. https://doi.org/10.3389/fcimb.2018.00120.

228. Sengupta, C., Ekka, M., Arora, S., Dhaware, P.D., Chowdhury, R., and Raychaudhuri, S. (2017). Cross feeding of glucose metabolism byproducts of *Escherichia coli* human gut isolates and probiotic strains affect survival of Vibrio cholerae. Gut Pathog *9*, 3. https://doi.org/10.1186/s13099-016-0153-x.

229. Nag, D., Breen, P., Raychaudhuri, S., and Withey, J.H. (2018). Glucose Metabolism by *Escherichia coli* Inhibits *Vibrio cholerae* Intestinal Colonization of Zebrafish. Infect Immun *86*, e00486-18. https://doi.org/10.1128/IAI.00486-18.

230. Chen, J., Byun, H., Liu, R., Jung, I.-J., Pu, Q., Zhu, C.Y., Tanchoco, E., Alavi, S., Degnan, P.H., Ma, A.T., et al. (2022). A commensal-encoded genotoxin drives restriction of *Vibrio cholerae* colonization and host gut microbiome remodeling. Proc Natl Acad Sci U S A *119*, e2121180119. https://doi.org/10.1073/pnas.2121180119.

231. Afzaal, M., Saeed, F., Shah, Y.A., Hussain, M., Rabail, R., Socol, C.T., Hassoun, A., Pateiro, M., Lorenzo, J.M., Rusu, A.V., et al. (2022). Human gut microbiota in health and disease: Unveiling the relationship. Front. Microbiol. *13*. https://doi.org/10.3389/fmicb.2022.999001.

232. Tang, F., Barbacioru, C., Wang, Y., Nordman, E., Lee, C., Xu, N., Wang, X., Bodeau, J., Tuch, B., Siddiqui, A., et al. (2009). mRNA-Seq whole-transcriptome analysis of a single cell. NATURE METHODS *6*, 377-U86. https://doi.org/10.1038/NMETH.1315.

233. Goetz, J., and Trimarchi, J. (2012). Transcriptome sequencing of single cells with Smart-Seq. NATURE BIOTECHNOLOGY *30*, 763–765. https://doi.org/10.1038/nbt.2325.

234. Picelli, S., Björklund, Å., Faridani, O., Sagasser, S., Winberg, G., and Sandberg, R. (2013). Smart-seq2 for sensitive full-length transcriptome profiling in single cells. NATURE METHODS *10*, 1096–1098. https://doi.org/10.1038/NMETH.2639.

235. Macosko, E., Basu, A., Satija, R., Nemesh, J., Shekhar, K., Goldman, M., Tirosh, I., Bialas, A., Kamitaki, N., Martersteck, E., et al. (2015). Highly Parallel Genome-wide Expression Profiling of Individual Cells Using Nanoliter Droplets. CELL *161*, 1202–1214. https://doi.org/10.1016/j.cell.2015.05.002.

236. Zheng, G., Terry, J., Belgrader, P., Ryvkin, P., Bent, Z., Wilson, R., Ziraldo, S., Wheeler, T., McDermott, G., Zhu, J., et al. (2017). Massively parallel digital transcriptional profiling of single cells. NATURE COMMUNICATIONS *8*. https://doi.org/10.1038/ncomms14049.

237. Sheng, K., Cao, W., Niu, Y., Deng, Q., and Zong, C. (2017). Effective detection of variation in single-cell transcriptomes using MATQ-seq. NATURE METHODS *14*, 267-+. https://doi.org/10.1038/NMETH.4145.

238. Gierahn, T., Wadsworth, M., Hughes, T., Bryson, B., Butler, A., Satija, R., Fortune, S., Love, J., and Shalek, A. (2017). Seq-Well: portable, low-cost RNA sequencing of single cells at high throughput. NATURE METHODS *14*, 395-+. https://doi.org/10.1038/nmeth.4179.

239. Hashimshony, T., Wagner, F., Sher, N., and Yanai, I. (2012). CEL-Seq: Single-Cell RNA-Seq by Multiplexed Linear Amplification. CELL REPORTS *2*, 666–673. https://doi.org/10.1016/j.celrep.2012.08.003.

240. Jaitin, D., Kenigsberg, E., Keren-Shaul, H., Elefant, N., Paul, F., Zaretsky, I., Mildner, A., Cohen, N., Jung, S., Tanay, A., et al. (2014). Massively Parallel Single-Cell RNA-Seq for Marker-Free Decomposition of Tissues into Cell Types. SCIENCE *343*, 776–779. https://doi.org/10.1126/science.1247651.

241. Klein, A., Mazutis, L., Akartuna, I., Tallapragada, N., Veres, A., Li, V., Peshkin, L., Weitz, D., and Kirschner, M. (2015). Droplet Barcoding for Single-Cell Transcriptomics Applied to Embryonic Stem Cells. CELL *161*, 1187–1201. https://doi.org/10.1016/j.cell.2015.04.044.

242. Xie, Z., Li, J., Huang, P., Zhang, Y., Yang, J., Liu, K., and Jiang, Y. (2022). Applications and Achievements of Single-Cell Sequencing in Gastrointestinal Cancer. Front Oncol *12*, 905571. https://doi.org/10.3389/fonc.2022.905571.

243. Vieira Braga, F.A., Kar, G., Berg, M., Carpaij, O.A., Polanski, K., Simon, L.M., Brouwer, S., Gomes, T., Hesse, L., Jiang, J., et al. (2019). A cellular census of human lungs identifies novel cell states in health and in asthma. Nat Med *25*, 1153–1163. https://doi.org/10.1038/s41591-019-0468-5.

244. Jovic, D., Liang, X., Zeng, H., Lin, L., Xu, F., and Luo, Y. (2022). Single-cell RNA sequencing technologies and applications: A brief overview. Clin Transl Med *12*, e694. https://doi.org/10.1002/ctm2.694.

245. Chong, S., Chen, C., Ge, H., and Xie, X.S. (2014). Mechanism of Transcriptional Bursting in Bacteria. Cell *158*, 314–326. https://doi.org/10.1016/j.cell.2014.05.038.

246. Liu, Y., Beyer, A., and Aebersold, R. (2016). On the Dependency of Cellular Protein Levels on mRNA Abundance. Cell *165*, 535–550. https://doi.org/10.1016/j.cell.2016.03.014.

247. van den Brink, S., Sage, F., Vértesy, A., Spanjaard, B., Peterson-Maduro, J., Baron, C., Robin, C., and van Oudenaarden, A. (2017). Single-cell sequencing reveals dissociation-induced gene expression in tissue subpopulations. NATURE METHODS *14*, 935–936. https://doi.org/10.1038/nmeth.4437.

248. Blattman, S.B., Jiang, W., Oikonomou, P., and Tavazoie, S. (2020). Prokaryotic Single-Cell RNA Sequencing by In Situ Combinatorial Indexing. Nat Microbiol *5*, 1192–1201. https://doi.org/10.1038/s41564-020-0729-6.

249. Kuchina, A., Brettner, L.M., Paleologu, L., Roco, C.M., Rosenberg, A.B., Carignano, A., Kibler, R., Hirano, M., DePaolo, R.W., and Seelig, G. (2021). Microbial single-cell RNA sequencing by split-pool barcoding. Science *371*, eaba5257. https://doi.org/10.1126/science.aba5257.

250. Dar, D., Dar, N., Cai, L., and Newman, D.K. (2021). Spatial transcriptomics of planktonic and sessile bacterial populations at single-cell resolution. Science *373*, eabi4882. https://doi.org/10.1126/science.abi4882.

251. Ma, P., Amemiya, H.M., He, L.L., Gandhi, S.J., Nicol, R., Bhattacharyya, R.P., Smillie, C.S., and Hung, D.T. (2023). Bacterial droplet-based single-cell RNA-seq reveals antibiotic-associated heterogeneous cellular states. Cell *186*, 877-891.e14. https://doi.org/10.1016/j.cell.2023.01.002.

252. McNulty, R., Sritharan, D., Pahng, S.H., Meisch, J.P., Liu, S., Brennan, M.A., Saxer, G., Hormoz, S., and Rosenthal, A.Z. (2023). Probe-based bacterial single-cell RNA sequencing predicts toxin regulation. Nat Microbiol *8*, 934–945. https://doi.org/10.1038/s41564-023-01348-4.

253. Wang, B., Lin, A.E., Yuan, J., Novak, K.E., Koch, M.D., Wingreen, N.S., Adamson, B., and Gitai, Z. (2023). Single-cell massively-parallel multiplexed microbial sequencing (M3-seq) identifies rare bacterial populations and profiles phage infection. Nat Microbiol *8*, 1846–1862. https://doi.org/10.1038/s41564-023-01462-3.

254. Imdahl, F., Vafadarnejad, E., Homberger, C., Saliba, A.-E., and Vogel, J. (2020). Single-cell RNA-sequencing reports growth-condition-specific global transcriptomes of individual bacteria. Nat Microbiol *5*, 1202–1206. https://doi.org/10.1038/s41564-020-0774-1.

255. Rosenberg, A.B., Roco, C.M., Muscat, R.A., Kuchina, A., Sample, P., Yao, Z., Graybuck, L.T., Peeler, D.J., Mukherjee, S., Chen, W., et al. (2018). Single-cell profiling of the developing mouse brain and spinal cord with split-pool barcoding. Science *360*, 176–182. https://doi.org/10.1126/science.aam8999.

256. Femino, A.M., Fay, F.S., Fogarty, K., and Singer, R.H. (1998). Visualization of single RNA transcripts in situ. Science *280*, 585–590. https://doi.org/10.1126/science.280.5363.585.

257. Lubeck, E., Coskun, A.F., Zhiyentayev, T., Ahmad, M., and Cai, L. (2014). Single-cell in situ RNA profiling by sequential hybridization. Nat Methods *11*, 360–361. https://doi.org/10.1038/nmeth.2892.

258. Shah, S., Lubeck, E., Zhou, W., and Cai, L. (2016). In Situ Transcription Profiling of Single Cells Reveals Spatial Organization of Cells in the Mouse Hippocampus. Neuron *92*, 342–357. https://doi.org/10.1016/j.neuron.2016.10.001.